JOURNAL OF THE

AERO/SPACE SCIENCES

VOLUME 26 JUNE, 1959 NUMBER 6

MECHANICAL ENGINEERING
JUN 11 1959
LIBRARY

PURDUE UNIVERSITY
JUN 8 1959
LIBRARY

CONTENTS

A Theory for the Ablation of Glassy Materials..HANS A. BETHE AND MAC C. ADAMS 321

Comparison of Approximate Solutions of the Thermoelastic Problem of the Thick-Walled Tube.....J. H. BALTRUKONIS 329

The Axisymmetric Free-Convection Temperature Field Along a Vertical Thin Cylinder .....FRANCIS R. HAMA, JOHN V. RECESSO, AND JEAN CHRISTIAENS 335

Relaxation Characteristics of Pneumatic Tires.....JOHN ERWIN STEVENS 343

A Simple Method of Matric Structural Analysis: Part IV—Nonlinear Problems.... .....BERTRAM KLEIN 351

Nose Drag in Free-Molecule Flow and Its Minimization.....H. S. TAN 360

Further Developments of New Methods in Heat-Flow Analysis.....M. A. BIOT 367

Readers' Forum..... 382

Published by
INSTITUTE OF THE AERONAUTICAL SCIENCES, INC.

JOURNAL OF THE AERO/SPACE SCIENCES

Editor: W. R. SEARS

Director, Graduate School of Aeronautical Engineering, Cornell University

Associate Editor: ROBERT R. DEXTER *Managing Editor:* RITA J. TURINO

Editorial Assistant: CAROLINE TAYLOR

Editorial Committee

Aerodynamics and Fluid Mechanics

H. Julian Allen
Holt Ashley
Dean R. Chapman
Francis H. Clauser
Hugh L. Dryden
John C. Evvard
Antonio Ferri
Alexander Flax
Wallace D. Hayes
R. T. Jones
Carl Kaplan
H. W. Liepmann
C. C. Lin
H. F. Ludloff
Harold Luskin
Clark B. Millikan
Henry T. Nagamatsu
H. J. E. Reid
George S. Schairer
G. B. Schubauer
John Stack
Theodore Theodorsen
Arthur N. Tifford
Th. von Kármán

Flight Testing

R. R. Gilruth
Melvin N. Gough
W. L. Howland
W. F. Milliken, Jr.

Rotating Wing Aircraft

F. B. Gustafson
K. H. Hohenemser
Bartram Kelley
R. B. Maloy
Ralph McClarren
R. H. Miller
R. H. Prewitt
Igor I. Sikorsky

Structures

John E. Duberg
R. R. Heldenfels
N. J. Hoff
Samuel Levy
J. F. McBrearty
W. Ramberg
E. E. Sechler
F. R. Shanley
C. R. Strang
S. Timoshenko

Meteorology

C. F. Brooks
D. M. Little
F. W. Reichelderfer
K. C. Spengler

Vibration and Flutter

Lee Arnold
M. A. Biot
R. L. Bisplinghoff
Harold A. Cheilek
I. E. Garrick
Martin Goland

Aircraft Design

W. E. Beall
E. H. Heinemann
Hall L. Hibbard
Richard Hutton
C. L. Johnson
A. A. Kartveli
F. K. Teichmann

Electronics

K. C. Black
M. V. Kiebert, Jr.
David S. Little
Paul Rosenberg
Giles J. Strickroth

Physiologic Problems

H. G. Armstrong
Louis H. Bauer
Robert J. Benford
W. Randolph Lovelace, II
Ross A. MacFarland

Flight Propulsion

William Bollay
George W. Brady
R. P. Kroon
Frank E. Marble
Abe Silverstein
E. S. Taylor

Instruments

Alan G. Binnie
Charles H. Colvin
Frank R. Cook
C. S. Draper
S. G. Eskin
C. F. Savage
R. C. Sylvander

SUBSCRIPTION RATES

JOURNAL OF THE AERO/SPACE SCIENCES (formerly Journal of the Aeronautical Sciences), Published Monthly. United States and Possessions: 1 Year, $15.00; Single Copies, $1.50. Foreign Countries Including Canada (American Currency Rates): 1 Year, $16.00; Single Copies, $1.50.

AERO/SPACE ENGINEERING, Published Monthly. United States and Possessions: 1 Year, $5.00; Single Copies, $0.50. Foreign Countries Including Canada (American Currency Rates): 1 Year, $6.00; Single Copies, $0.50.

Notices of change of address should be sent to the Institute at least 30 days prior to actual change of address.

Manuscripts for publication, proofs, and all correspondence should be addressed to the Editorial Office of the JOURNAL.

Publication Office, 20th and Northampton Sts., Easton, Pa. Correspondence regarding subscriptions may be addressed to the Editorial Office of the JOURNAL OF THE AERO/SPACE SCIENCES, 2 East 64th Street, New York 21, N.Y.

© *Copyright, 1959, by the Institute of the Aeronautical Sciences, Inc.*

Second-Class Mail Privileges Authorized at Easton, Penna. Acceptance for mailing at a special rate of postage provided for in Section 1103, Act of October 3, 1917, authorized April 29, 1937.

JOURNAL OF THE AERO/SPACE SCIENCES

VOLUME 26 JUNE, 1959 NUMBER 6

A Theory for the Ablation of Glassy Materials†

HANS A. BETHE* AND MAC C. ADAMS**

Avco Research Laboratory

SUMMARY

The ablation of glassy materials, when subjected to aerodynamic heating, is treated theoretically. Glasses possess a viscosity which increases exponentially as the temperature decreases, and, therefore, no distinct solid state exists. This behavior allows important simplifications to be made, and approximate analytical equations are derived for the significant ablation parameters. By a second-order analysis the approximate equations are shown to be extremely accurate for determining the energy absorbed per unit mass of ablated material.

For simplicity, the analysis is restricted to the stagnation region of a blunted body and only steady-state ablation is considered. A procedure is suggested for ablation calculations along an arbitrary body contour. The theory treats two physical cases of interest: (1) the ablated material flows without evaporation, and (2) partial evaporation occurs. As an example, numerical results are presented for Pyrex.

SYMBOLS

C_p = heat capacity per unit mass
h = enthalpy (energy per unit mass)
h_{bl} = see Eq. (36)
h_{eff} = effective energy absorbed per unit mass of ablated material
h_T = energy absorbed by heat capacity, C_pT
K = thermal conductivity
°K. = degrees Kelvin
M = molecular weight ratio (air to glass vapor)
p = pressure
q = heat-transfer rate per unit area
q_0 = heat-transfer rate to nonablating surface
r = body radius measured normal to axis
R = body nose radius
T = temperature
T_{Ls} = temperature at which glass vapor pressure equals stagnation pressure
u = velocity tangent to body surface
v = velocity normal to body surface
v_w = ablation velocity
x = coordinate tangent to body surface
y = coordinate normal to body surface
δ = thickness of liquid layer
k = thermal diffusivity ($K/\rho C_p$)
μ = viscosity
μ_{Ls} = viscosity of glass at a temperature such that its vapor pressure equals the stagnation pressure
ρ = density
σ = Prandtl Number ($C_p\mu/K$)
τ = shear stress
τ_0 = shear stress on nonablating surface
ψ = ratio of heat transfer with and without mass injection

Subscripts

i = gas-liquid interface
L = liquid property
s = gas property at stagnation point
v = property of glass vapor
∞ = free stream

Received December 22, 1958.

† This work was sponsored by the Ballistic Missile Division, ARDC, USAF, under Contract AF04(645)-18.

The authors wish to acknowledge the contributions of others who assisted greatly in the formulation of this paper. They are Steven Georgiev, for his most able assistance in the preparation of the paper, James A. Fay, for his stimulating discussions and many valuable suggestions, Richard Fleddermann, who pointed out the importance of the pressure gradient on the liquid layer flow, and M. Zlotnick for his valuable discussions on the effect of mass injection into the gas boundary layer.

* Consultant, Avco Research Laboratory, and Professor, Cornell University.

** Deputy Director, Avco Research Laboratory.

INTRODUCTION

MATERIAL ABLATION is recognized as a powerful heat protection method for high-speed flight application. In the ablation process, energy is transferred from the gas stream to the material surface by the mechanism of aerodynamic heating from the gas boundary layer. This energy is absorbed in the form of heat capacity and latent heat of vaporization (for that fraction of ablated material which vaporizes). Some materials may in addition possess a latent heat of fusion, though in general the glasses do not.

Of particular interest to the designer is the energy absorbed per unit mass of ablated material, or the energy of ablation. The quantities which influence the energy of ablation may be seen by writing an energy balance for the case of steady-state ablation:

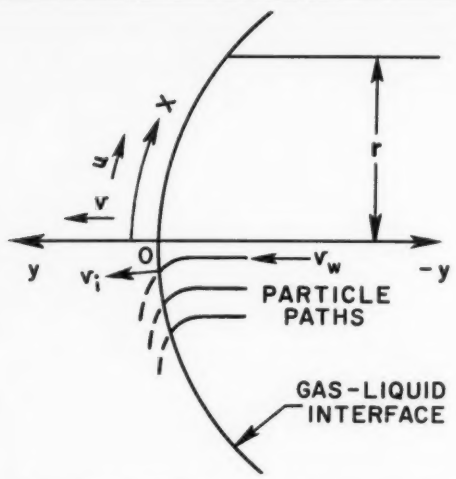

FIG. 1. Coordinate system, stationary with respect to the gas-liquid interface.

$$q_t = \dot{m}[h_T + f h_v]$$

where q_t is the aerodynamic heat-transfer rate per unit surface area, $\dot{m}$ the mass rate of material loss, h_T the heat capacity ($C_p T$), f the fraction of material vaporized, and h_v the latent heat of evaporation. The aerodynamic heat transfer q_t is dependent upon the mass flow of vapor into the boundary layer. As will be seen in Section (3), the injected vapor, in diffusing through the boundary layer at the stagnation point, effectively absorbs an energy per unit mass of about two-thirds the enthalpy difference across the boundary layer. The heat transfer to the surface is therefore reduced by the mass injection effect and is given approximately by the formula

$$q_t = q_0 - (2/3)\, \dot{m}_v\, \Delta h$$

where q_0 is the heat-transfer rate to a nonablating surface, $\dot{m}_v$ the mass flow of vapor from the surface, and Δh the enthalpy difference across the gas boundary layer. The fraction of material vaporized $f = \dot{m}_v/\dot{m}$. Thus, we may write

$$q_0 = \dot{m}[h_T + f\, h_v + (2/3)\, f\, \Delta h]$$

Now for a given body at specified flight conditions, q_0 and Δh are essentially known. Thus, for a low ablation rate, or a large energy of ablation, it is clear that the fraction of material vaporized should be near unity and, in addition, both a high surface temperature and large energy of evaporation are desired.

In analyzing a given material, subjected to given aerodynamic heating, it is thus necessary to determine the surface temperature and the fraction of material vaporized. The determination of these quantities, in the case of glassy materials, is one of the principal objectives of this paper.

The glasses appear promising as ablating materials because, relative to most high-temperature materials, they possess many desirable properties—e.g., (1) high liquid viscosity at elevated temperature (this favors energy storage as heat capacity and latent heat of vaporization before the liquid flows away due to aerodynamic shear), (2) a large energy of vaporization, (3) a low thermal conductivity (a necessary property to ensure a large fraction of energy absorbed by the ablation process rather than by storage within the solid material), and (4) good thermal stress characteristics.

Sutton[1] has investigated the ablation problem and obtained numerical solutions for Pyrex for a range of heat-transfer conditions. His analysis was restricted to the case of no vaporization, and he pointed out the important influence of viscosity on the surface temperature (or the energy stored in the form of heat capacity). All other properties being equal, the greater the viscosity the higher the surface temperature. It will be seen that the viscosity has an equally important effect on the energy absorbed by vaporization—namely, as the viscosity is increased so is the fraction of ablated material which vaporizes.

(1) The Liquid Layer Equations

When subjected to aerodynamic heat transfer and shear forces, a glassy material will form a flowing liquid layer. Since the liquid glass viscosity is much greater than that of the gas, the tangential velocity of the liquid will be small compared to the gas velocity. Hence the liquid motion produces a negligible change in the gas boundary layer—i.e., in the heat transfer and shear forces. On the other hand, when some of the flowing liquid vaporizes, the injected vapor does bring about an important interaction between the liquid layer and gas boundary layer. The effect of vapor injection is to reduce the aerodynamic heating and shear forces; this is discussed in Section (3). For the present the liquid layer will be treated independently as if the external heating and shear were known boundary conditions.

The equations governing the liquid layer are nearly the same as for the case of an incompressible gas boundary layer, the difference being a variation of viscosity with temperature. These equations are well known (see, for example, reference 2) and are therefore written without further discussion. For the coordinate system defined in Fig. 1, the three basic equations for the steady-state* liquid layer are

Continuity: $$[\partial(ru)/\partial x] + [\partial(rv)/\partial y] = 0 \qquad (1)$$

Energy:

$$u(\partial T/\partial x) + v(\partial T/\partial y) = (K/\rho C_p)\, (\partial^2 T/\partial y^2) \qquad (2)$$

Momentum:

$$\rho u(\partial u/\partial x) + \rho v(\partial u/\partial y) = (\partial/\partial y)\, [\mu(\partial u/\partial y)] - (\partial p/\partial x) \qquad (3)$$

The thermal conductivity K, density ρ, and heat capacity C_p are assumed constant.

* The present theory can be easily extended, in principle, to the nonstationary case. The calculation involved, however, is considerably more complicated.

(2) Solutions for the Stagnation Point of a Blunted Body

In the stagnation region of a blunted body, approximate analytical solutions of the above equations can be obtained. Since such solutions allow much physical insight into the ablation problem to be gained, the present report will be devoted to the stagnation region. A method for treating an arbitrary body of revolution will be indicated later.

The inertia forces in Eq. (3) can be neglected, as will be seen later; hence, to a good approximation the momentum equation can be integrated to give for the tangential velocity,

$$u(x, y) = \tau_i(x) \int_{-\infty}^{y} (d\eta/\mu) + [\partial p(x)/\partial x] \int_{-\infty}^{y} (\eta/\mu)\, d\eta \quad (4)$$

where τ_i and p represent, respectively, the aerodynamic shear at the gas-liquid interface and the pressure. The evaluation of the above integrals requires a knowledge of the viscosity, μ, as a function of y. Then, knowing these integrals, the ablation velocity $v_w = v(-\infty)$ is easily obtained from the continuity equation and the mathematical solution is completed.

The viscosity distribution can be determined by combining a given viscosity-temperature law with the temperature distribution through the liquid and solid. The temperature distribution can be found from the energy equation [Eq. (2)]. For the stagnation region $\partial T/\partial x = 0$ and the energy equation reduces to

$$v(\partial T/\partial y) = (K/\rho C_p)(\partial^2 T/\partial y^2) = k(\partial^2 T/\partial y^2) \quad (5)$$

A first integral of this equation gives

$$\partial T/\partial y = (\partial T/\partial y)_i \exp\left[(1/k)\int_0^y v\, d\, y\right] \quad (6)$$

A coupling exists between the energy and momentum equations through the integral in Eq. (6). This coupling in general leads to much difficulty; however, in the case of glassy materials, an important simplification can be made.

Now for glassy materials the viscosity increases exponentially with a decrease in temperature—i.e.,

$$\mu = \exp\,[(a/T) - b] \quad (7a)$$

or, approximately,

$$\mu/\mu_i = (T/T_i)^{-n} \quad (7b)$$

where $n = a/T_i$. At a given interface temperature, the exponent n varies between about 10 and 20 for different glasses (see, for example, reference 3) and therefore the liquid "freezes" beneath the surface after a relatively small temperature drop. The result is that the thickness of the liquid layer is thin in comparison with the thermal thickness; consequently, the temperature gradient is nearly constant through the liquid layer.

Beneath the gas-liquid interface at depths larger than the liquid layer thickness the temperature gradient approaches exactly the value obtained by replacing the velocity v in Eq. (6) by v_w; thus,

$$\partial T/\partial y = (\partial T/\partial y)_i \exp\left[(1/k)\int_0^y v dy\right] \approx (\partial T/\partial y)_i \exp\,(v_w y/k) \quad (8)$$

Eq. (8) therefore represents a good approximation for the temperature distribution through the solid *and* liquid regions of the glass. This is true because the choice of v is not critical for the liquid region where the temperature gradient is constant. A discussion of the accuracy of Eq. (8) is given in the Appendix.

Integration of Eq. (8) now leads to the desired temperature distribution:

$$T(y) = (k/v_w)(\partial T/\partial y)_i \exp\,(y/\delta_T) = T_i \exp\,(y/\delta_T) \quad (9)$$

where $\delta_T = k/v_w$, and it should be noted that $y < 0$.

Eq. (9) gives $T = 0$ for $y = -\infty$; if the actual temperature in the material before heating is T_0, we should write instead of Eq. (9):

$$T(y) - T_0 = (k/v_w)(\partial T/\partial y)_i \exp\,(y/\delta_T) \quad (9a)$$

Accordingly, we should also write instead of Eq. (7b):

$$\mu/\mu_i = [(T - T_0)/(T_i - T_0)]^{-n'} \quad (7c)$$

For a given fundamental viscosity law [Eq. (7a)] the exponent n' required in Eq. (7c) will be slightly lower than n required in Eq. (7b). For simplicity we shall, in the following, denote $T - T_0$ simply by T, thus implying that the temperature is measured from a zero-point equal to the initial temperature, T_0. We also write n for n', the exponent in Eq. (7c). All formulas should be read with this understanding.

Combination of Eqs. (7b) and (9) then yields the viscosity distribution,

$$\mu(y) = \mu_i \exp\,[-n(y/\delta_T)] = \mu_i \exp\,[-(y/\delta)] \quad (10)$$

Notice that the liquid layer thickness* is $1/n$ of the thermal thickness—i.e.,

$$\delta = \delta_T/n = k/v_w n \quad (11)$$

The viscosity relation given by Eq. (10) now allows the determination of the liquid flow and the ablation velocity.

Inserting Eq. (10) into Eq. (4) gives, for the tangential velocity,

$$u(x, y) = [\tau_i(x)/\mu_i]\,\delta e^{y/\delta} + [(\partial p/\partial x)/\mu_i]\,\delta^2[(y/\delta) - 1]e^{y/\delta} \quad (12)$$

The ablation velocity or normal velocity is now readily determined by use of the continuity equation. This leads to

$$v_i - v_w = -(1/r)\int_{-\infty}^{0} (\partial/\partial x)\,(ru)dy \quad (13)$$

* The liquid layer thickness is defined as the distance at which the viscosity increases by one exponential factor; the tangential velocity decreases by nearly the same factor.

Here v_i represents the velocity of the liquid at the gas-liquid interface (i.e., ρv_i gives the mass rate of vaporization) and v_w denotes the rate of ablation of the material.

Now use of Eqs. (12) and (13), noting that $r = x$ at the stagnation point and that τ_i and p' are linear in x, yields the relation,

$$v_i = v_w - (2\delta^2/\mu_i)\ (\tau_i' - 2p''\delta) \tag{14}$$

This is the fundamental equation of the liquid layer theory.* The second derivative of the pressure p'' (which is negative) is determined for the particular nose radius and flight conditions while the shear gradient τ_i' is related to the mass injection into the gas boundary. In the absence of vaporization the liquid layer has a negligible influence on the shear and τ_i' is determined from a knowledge of the gas boundary layer alone.

Having obtained a solution for the liquid layer, neglecting the inertia forces in Eq. (3), we can go back and check the validity of the approximation. By use of Eq. (3) it follows that the change in shear stress across the liquid layer, due to the inertia terms, is of order $\rho v_w u_i$. The magnitude of the error is then obtained by comparing this quantity with the shear stress τ_i. The ratio of the two quantities, making use of Eq. (12), gives

$$\rho v_w u_i/\tau_i = \rho v_w \delta/\mu_i = K/c_p\mu_i n = 1/\sigma_L n$$

The liquid Prandtl Number σ_L is greater than unity and $n > 10$, consequently the neglect of inertia terms is justified.

It is now necessary to consider the coupling between the liquid layer and the gas boundary layer in order to determine the ablation velocity v_w.

(3) Coupling of Liquid and Gas Boundary Layers

(a) No Evaporation

For the case of no evaporation, Eq. (14) reduces to

$$v_w = (2\delta^2/\mu_{Li})\ [\tau_i' - 2p''\delta] \tag{15}$$

where $\delta = k/v_w n$ as before and $\mu_{Li} = f(T_i)$. It is noted that the temperature is still unknown. The solution of Eq. (15) requires a knowledge of the heat transfer and shear due to the gas boundary layer.

Consider now a gas boundary layer with no mass injection. The following relations are obtained from reference 4:

Heat transfer:†

$$q_i/(h_s - h_i) \equiv q_0/(h_s - h_i) \approx 0.7\ \sqrt{(\rho\mu)_s(du_e/dx)}\ \sigma_s^{-2/3} \tag{16}$$

Shear stress:

$$\tau_i \equiv \tau_0 \approx [q_0(du_e/dx)x/(h_s - h_i)]\sigma_s^{2/3} \tag{17}$$

where

$$du_e/dx = (1/R)\ \sqrt{2(p_s/\rho_s)}$$

assuming a Newtonian pressure distribution given by

$$p = p_s[1 - (x^2/R^2)] \tag{18}$$

In the absence of vaporization the aerodynamic heat transfer q_0 must be balanced by the energy absorbed by the solid and liquid in the form of heat capacity only; thus,

$$q_0 = \rho_L v_w C_{pL} T_i \equiv \rho_L v_w h_T \tag{19}$$

where h_T represents the energy absorbed per unit of mass of ablated material.‡

Now the combination of Eqs. (15)–(19) yields the following relation:

$$[h_T/(h_s - h_i)]^3 \left\{1 + (4/\sigma_s^{1/3}n)\ (C_{ps}K_L/C_{pL}K_s) \times [h_T/(h_s - h_i)]\right\} = (1/4)\ (\rho_s/\rho_L)\ (n^2\mu_{Li}/\mu_s) \times [(K_s/K_L)\ (C_{pL}/C_{ps})]^2 \tag{20}$$

Eq. (20) together with a given viscosity law allows the determination of the energy absorbed by the ablated material, and therefore the surface temperature, ablation velocity, etc. It should be noted that μ_{Li} is a very sensitive function of the interface temperature T_i while all other quantities, including h_T, are relatively insensitive. It is therefore possible to make a rough estimate of the surface temperature; calculate all quantities in terms of this first estimate and solve Eq. (20) for μ_{Li}; the viscosity law then gives a better value of T_i, etc. We may say that the surface temperature adjusts itself so as to give the right liquid viscosity.

Several observations can be drawn from Eq. (20) regarding the energy of ablation.

(1) The energy of ablation is independent of the heat-transfer rate—i.e., body dimension—and depends primarily upon the enthalpy difference across the gas boundary layer. The ablation rate, on the other hand, is directly proportional to the heat-transfer rate and, therefore, is dependent on the body dimension.

(2) As is to be expected, a low thermal conductivity and high viscosity are desirable. The conductivity appears to be the more important since roughly $h_T \sim \mu_{Li}^{1/3}/K_L^{2/3}$. However, the viscosity varies far more

* For an arbitrary position on a body of revolution, Eqs. (12) and (13) lead to

$$v_i = v_w - (1/r)\,(d/dx)\,\{r[(\tau_i\delta^2/\mu_i) - (2p'\delta^3/\mu_i)]\} \tag{14a}$$

This differential equation is best solved numerically by a stepwise process, starting at the stagnation point and proceeding by increments of Δx along the body contour. The aerodynamic shear and pressure gradient must of course be known.

† In many practical situations the radiation emission from the surface may be important; however, this effect is neglected in the present analysis.

‡ Note that the heat capacity is taken for the full interface temperature. The correct temperature is a mean value within the liquid layer; however, since the temperature difference across the liquid layer is T_w/n, the approximation used in Eq. (19) is good for large n.

between glasses, as well as with temperature, so that large changes in h_T are caused primarily by viscosity variations.

(3) For large flight velocities, where $h_s \gg h_i$ and also $h_s \gg h_T$, Eq. (20) may be simplified to

$$h_T^3 \approx C_1 n^2 \rho_s \mu_{Ls} \mu_s h_s^3 \tag{20a}$$

where C_1 is nearly constant for glassy materials and a constant gas Prandtl Number $\sigma_s = C_{ps}\mu_s/K_s$ is assumed.

If we choose air as the gas, the following approximate empirical relations may be used:*

$$\rho_s \sim \rho_\infty h_s^{0.34} \quad \text{and} \quad \mu_s \sim h_s^{0.3}$$

In addition, for a given glass the liquid viscosity may be written

$$\mu_{Li} \sim T_{Li}^{-n} \sim h_T^{-n}$$

Eq. (20a) now takes the proportional form

$$h_T^{3+n} \sim \rho_\infty h_s^{3.64}$$

or

$$h_T \sim \rho_\infty^{1/(3+n)} h_s^{3.64/(3+n)} \tag{20b}$$

Eq. (20b) shows that h_T is insensitive to both ρ_∞ and h_s (since n is of order 10); however, the more sensitive parameter is h_s. Numerical results for Pyrex glass are presented in Section (5).

The above expressions apply only in cases where the ablated material flows without vaporization. In the next section we treat the case of partial vaporization.

(b) *Partial Evaporation of the Ablating Liquid*

The energy absorbed by a material will further depend upon the fraction of ablated material which vaporizes. In this section we derive the equations necessary to determine the fraction of material vaporized and the resulting energy absorbed.

One effect of evaporation, or mass injection, is to reduce the heat transfer and shear due to the gas boundary layer. This effect is represented as follows (where use is made of the well known Reynolds analogy which relates heat-transfer rate to shear):

$$q_i/q_0 = \tau_i/\tau_0 = \psi \tag{21}$$

where ψ is a function of the mass injection into the boundary layer. The determination of the ψ function has been the subject of several investigations (see, for example, references 5 and 6) and the results of these investigations will simply be written down here with a minimum of discussion.

The following approximate empirical relation can be derived from the numerical results of references 5 and 6:

$$\psi \approx 1 - 0.68M^{0.26}(h_s - h_i)\ (\rho_L v_i/q_0) \tag{22}$$

where M is the ratio of the molecular weights† of air to the injected vapor, $\rho_L v_i$ the mass rate of injection, and q_0 the aerodynamic heat-transfer rate to a non-ablating surface, defined by Eq. (16). It is now necessary to relate the mass injection rate to the concentration and vapor pressure of the injected material at the gas-liquid interface. To do this in a simple way the following assumptions are made: (1) the injected vapor does not react chemically with the other gas present (i.e., the air), and (2) energy is transported equally efficiently by diffusion and by conduction (i.e., the Lewis Number is unity).

The first assumption can be shown to be quite good for silicates, while the second is not critical.[7] With these two assumptions the following relation may be derived,[5, 10] for the mass flow of vapor (which equals the mass flow of liquid at the interface):

$$\rho_L v_i = [\psi q_0/(h_s - h_i)]\ [C_{vi}/(1 - C_{vi})] \tag{23}$$

where C_{vi} denotes the mass fraction of the injected vapor at the interface and is related to the vapor pressure by

$$C_{vi} = 1/\{1 + M[(p_s/p_{vi}) - 1]\} \tag{24}$$

A knowledge of the vapor pressure as a function of temperature is, of course, required.

The aerodynamic heat flux is balanced by the energy of vaporization in addition to heat capacity. In place of Eq. (19) the energy balance is now written

$$\psi q_0 = \rho_L(v_w C_{pL} T_i + v_i h_v) = \rho_L(v_w h_T + v_i h_v) \tag{25}$$

Given a flight condition, Eqs. (14) and (21)–(25), combined with given viscosity and vapor pressure laws, must be solved simultaneously in order to yield the desired quantities, T_w, v_i, and v_w.

The equations can be combined and considerably simplified. In order to simplify writing let

$$h_g = h_s - h_i \tag{26}$$

Then Eq. (22) and (23) combine to give

$$(1 - C_{vi})/C_{vi} = q_0/\rho_L v_i h_g - 0.68M^{0.26} \tag{27}$$

From Eq. (24)

$$(1 - C_{vi})/C_{vi} = M[(p_s/p_{vi}) - 1] \tag{28}$$

Combining Eqs. (27) and (28),

$$p_s/p_{vi} = 1 - 0.68M^{-0.74} + (q_0/M\rho_L h_g v_i) \tag{29}$$

It is easily shown that v_i is always such that $p_s/p_{vi} > 1$, as it must be.

Now, the vapor pressure, as well as the viscosity, is a rapidly varying function of the interface temperature. We may write

$$\mu \propto p_v^{-\alpha} \tag{30}$$

$$\mu_{Li}/\mu_{Ls} = (p_{vi}/p_s)^{-\alpha}$$

where μ_{Ls} denotes the viscosity at *that* temperature T_{Ls} at which the vapor pressure is equal to the stagnation pressure p_s; hence, μ_{Ls} is determined by the flight conditions. Since α is a known constant, Eqs. (29) and (30) determine μ_{Li}. Eqs. (11), (29), and (30)

* These empirical relations were obtained by the use of equilibrium properties for air and Sutherland's viscosity law.

† The results of reference 9 indicate that upon vaporizing SiO_2 forms mostly SiO and O_2; thus, $M = 0.72$.

can now be inserted into Eq. (14):

$$v_w = v_i + (2D^2/\mu_{Ls}v_w^2)\,[\tau_i' - 2p''(D/v_w)] \times [1 - 0.68M^{-0.74} + (q_0/M\rho_L h_g v_i)]^{-\alpha} \quad (31)$$

where

$$D = K_L/\rho_L C_{pL} n \quad (32)$$

is a known constant.

For the energy balance, we insert Eq. (22) into Eq. (25) and obtain

$$q_0/\rho_L = v_w h_T + v_i(h_v + 0.68M^{0.26}h_g) \quad (33)$$

The effective energy of ablation is defined as follows:

$$h_{eff} = q_0/\rho_L v_w = h_T + (v_i/v_w)\,(h_v + 0.68M^{0.26}h_g) \quad (34)$$

Since the vapor pressure is a very steep function of the temperature (about 10th to 20th power), the interface temperature T_i may be considered as equal to T_{Ls} for the purpose of calculating* $h_T = C_{pL}T_i$ so h_T may be considered as given by the flight conditions. So, of course, are h_g and q_0. Hence, Eq. (33) gives one relation between the two remaining unknowns, v_i and v_w; the other equation is (31).

It is convenient to eliminate v_i and v_w in terms of h_{eff} by means of Eq. (34); we have

$$v_i/v_w = (h_{eff} - h_T)/h_{bl} \quad (35)$$

where

$$h_{bl} = h_v + 0.68M^{0.26}h_g \quad (36)$$

and h_{bl} is determined by flight conditions.

A simple calculation starting from Eq. (29) yields

$$p_s/p_{vi} = 1 - 0.68M^{-0.74} + (q_0/M\rho_L h_g v_i) = 1 + (1/M)\,[h_{eff}/(h_{eff} - h_T)] \times [(h_v/h_g) + 0.68M^{0.26}(h_T/h_{eff})] \quad (37)$$

If there is strong evaporation, $h_T \ll h_{eff}$, and then we have simply

$$p_s/p_{vi} \approx 1 + (h_v/Mh_g) \quad (38)$$

After considerable algebra, utilizing the above relations, Eq. (31) can be rewritten as follows:†

$$1 = \{(h_{eff} - h_T)/[h_v + 0.68M^{0.26}(h_s - h_i)]\} + 4(C_{ps}K_L/C_{pL}K_s n)^2\,(\rho_L\mu_s/\rho_s\mu_{Ls})\,[h_{eff}/(h_s - h_i)]^3 \times \{\psi + (4/\sigma_s^{1/3})\,(C_{ps}K_L/C_{pL}K_s n) \times [h_{eff}/(h_s - h_i)]\}\,(p_s/p_{vi})^{-\alpha} \quad (39)$$

where

$$\psi = 1 - 0.68M^{0.26}[(h_s - h_i)/h_{eff}] \times \{(h_{eff} - h_T)/[h_v + 0.68M^{0.26}\,(h_s - h_i)]\} \quad (39a)$$

and p_s/p_{vi} is given by Eq. (37).

For strong evaporation, $h_{eff} \gg h_T$, and

$$\psi \approx h_v/[h_v + 0.68M^{0.26}(h_s - h_i)] \quad (40)$$

Eq. (39) is a somewhat complicated equation for h_{eff} and is most easily solved in reverse—i.e., for given h_{eff} (and other quantities), the required liquid viscosity μ_{Ls} can be calculated.

(4) Discussion of Results

An examination of Eq. (39) leads to a very important result for glassy materials—namely, that h_{eff} is dependent principally on flight velocity (i.e., h_s) and is insensitive to the altitude. A similar behavior was noted previously in the case of no evaporation. The insensitivity to altitude can be seen by examining the density dependent quantities h_i, h_T, and $\rho_s\mu_{Ls}$. The two quantities h_i and h_T are linear with T_i. Hence,

$$T_i \approx T_{Ls} \sim (\mu_{Ls})^{-1/n} \sim p_s^{\alpha/n} \sim (\rho_\infty h_s)^{\alpha/n}$$

For glasses $\alpha \approx 1$ and $n > 10$, therefore the interface temperature has only a weak dependence on both free-stream density and stagnation enthalpy.

Consider next the quantity $\rho_s\mu_{Ls}$, at constant flight velocity. Then

$$\rho_s\mu_{Ls} \sim \rho_\infty p_s^{-\alpha} \sim \rho_\infty^{1-\alpha}$$

which again is insensitive to ρ_∞ because $1 - \alpha \ll 1$.

In three limiting cases, Eq. (39) gives simple results:

(a) *Very High Viscosity*—If μ_{Ls} is very large, the second term of Eq. (39) will give a small contribution. This means physically that there is very little flow of the liquid, essentially all the liquid evaporates. Accordingly, v_i/v_w is nearly one, or mathematically, the first term in Eq. (39) is nearly one. Then

$$h_{eff} = h_v + h_T + 0.68M^{0.26}(h_s - h_i) \quad (41)$$

Eq. (41) is an upper limit to h_{eff}, and is independent of the viscosity; and if μ_{Ls} is not quite so large h_{eff} will depend only slightly on its value. The third term in Eq. (41) represents the maximum effect due to mass injection. This quantity can be interpreted as additional energy absorbed by the vapor as it diffuses through the gas boundary layer.

(b) *Moderate Viscosity but Still a Large Effect Due to Evaporation*—For flight situations where the fraction of material vaporized is less than unity, Eq. (41) becomes instead

$$h_{eff} = h_T + (v_i/v_w)\,[h_v + 0.68M^{0.26}(h_s - h_i)] \quad (42)$$

Now in general h_v and $h_s - h_i$ are $\gg h_T$ so that under certain conditions $h_{eff} \gg h_T$ even though $v_i/v_w \ll 1$. For such conditions the second (viscosity) term in Eq. (39) is much larger than the first. In addition p_s/p_{vi} may be replaced by the simple expression (38) and ψ is given by Eq. (40). Eq. (39) then reduces to an equation of the type

$$A\,[h_{eff}/(h_s - h_i)]^3 + B[h_{eff}/(h_s - h_i)]^4 = \rho_s\mu_{Ls} \quad (43)$$

where A and B are expressions depending only slightly on the temperature T_i; i.e., on the stagnation pressure p_s. Thus, $h_{eff}/(h_s - h_i)$ will depend only weakly, as the third or fourth root, on the liquid viscosity.

(c) *Low Viscosity, Weak Evaporation*—In this case,

$$h_{eff} - h_T \ll h_T \quad (44)$$

---

* This approximation may not be made, of course, for calculating the viscosity, μ_{Li}; see Eq. (30).

† Away from the stagnation point Eq. (14a) can be utilized to obtain a differential equation with the same parameters as in Eq. (39).

Then the first term in Eq. (39), due to evaporation, is negligible. and Eq. (39) reduces to an equation quite similar to Eq. (20). The form of the two equations is still different—Eq. (20) is best solved for μ_{Li}, in terms of the other variables which are not sensitive to temperature. Eq. (39) may be solved for the small quantity $h_{eff} - h_T$, with h_{eff} replaced by h_T in all places where h_{eff} occurs alone. In the limit Eq. (39) becomes

$$h_{eff} - h_T \sim \mu_{Ls}^{1/\alpha} \tag{45}$$

i.e., the viscosity only enters the small correction term $h_{eff} - h_T$.

In every case, therefore, h_{eff} changes much less than proportionately with the liquid viscosity. This does not mean, however, that viscosity is unimportant. On the contrary, the variation of viscosity between different glasses is great enough to produce large differences in h_{eff}.

(5) Numerical Results for Pyrex

For the purpose of illustration the present theory is applied to Pyrex. The physical properties used are as follows:

C_{pL} = 0.25(cal./gm.°K.), $K_L = 7 \times 10^{-3}$(cal./cm. sec.°K.), ρ_L = 2.25(gm./cm.^{3})

$\mu_L = \exp\{[38{,}000/T(°K.)] - 17\}$ (gm./cm. sec.)

$p_v = \exp\{-[46{,}400/T(°K.)] + 14.5\}$ (atm.)

h_v = 2,470 (cal./gm.)

The viscosity law is an approximate fit to the results of reference 3, while the vapor pressure* and energy of vaporization were determined from data for silica in references 8 and 9. The latter two quantities are at best only approximate; however, for illustration purposes they will suffice.

It follows that

$$\mu_{Li} = (2/3) \times 10^{-2} p_{vi}^{-0.825}$$

hence, $\alpha = 0.825$.

In the calculations a constant value of $n = 11$ has been taken. A more correct calculation, with variable n, would not appreciably change the results.

Fig. 2 shows the results of the calculations. In this Figure, lines of constant h_{eff} and T_i are drawn on a velocity versus altitude scale. These two parameters combined with the flight conditions are sufficient for the determination of other parameters of interest. As discussed in the previous section, it is observed that h_{eff} is primarily a function of flight velocity and is weakly dependent on altitude. For the flight velocities considered only a small fraction of the ablated Pyrex vaporizes, at most about 2 per cent. Thus, h_{eff} varies according to the zero evaporation result,

$$h_T \sim \rho_\infty^{1/(3+n)} h_s^{3.64/(3+n)}$$

The onset of evaporation is detected by the departure

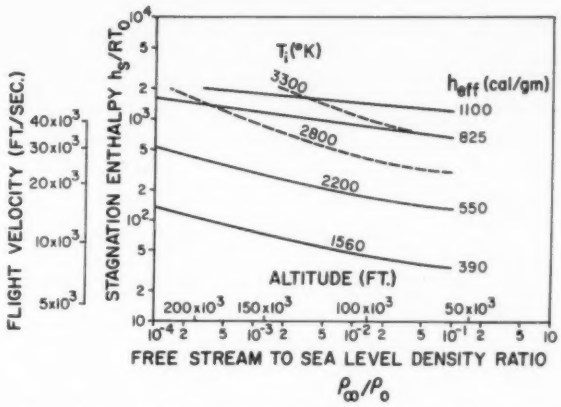

Fig. 2. Effective energy absorbed by Pyrex glass at the stagnation point for different flight conditions (RT_0 = 18.8 cal./gm.).

of the constant interface temperature lines from constant h_{eff} lines.

Other glasses may be evaluated by making graphs similar to Fig. 2. Such graphs are generally useful in conjunction with given flight trajectories. In particular if a trajectory is plotted on the same graph the effective energy of absorption h_{eff} (at the stagnation point) can be read directly for points along the flight path. Then dividing the stagnation point heat-transfer rate by h_{eff} gives the mass rate of ablation for quasi-steady-state conditions.

Appendix

The approximation given by Eq. (8) for the temperature distribution is discussed in this Appendix. The exact integral before the approximation is given by

$$\partial T/\partial y = (\partial T/\partial y)_i \exp\left[(1/k)\int_0^y v\, d\, y\right] \tag{A-1}$$

Now since the temperature distribution is utilized to determine the viscosity and, therefore, the liquid layer flow characteristics, a good approximation must be made for the temperature distribution through the liquid layer.

The results in Section (2) are now used as the initial approximation in the solution of Eq. (A-1) by means of the small perturbation method of successive approximations. Eq. (14), when expressed for any point in the liquid layer, becomes

$$v(y) = v_w - (2\delta^2/\mu_i)\{\tau_i' + p''\delta[(y/\delta) - 2]\}e^{y/\delta} \tag{A-2}$$

Integrating again,

$$\int v dy = v_w y - (2\delta^3/\mu_i)e^{y/\delta}\{\tau_i' + p''\delta[(y/\delta) - 3]\} + \text{const.} \tag{A-3}$$

Insert into Eq. (A-1), noting Eq. (11):

$$\partial T/\partial y = (\partial T/\partial y)_0 \exp(y/n\delta) \exp\left(-(2\delta^2 e^{y/\delta}/n v_w \mu_i) \times \{\tau_i' + p''\delta[(y/\delta) - 3]\}\right) \tag{A-4}$$

where the constant of Eq. (A-3) has been absorbed in the definition of $(\partial T/\partial y)_0$; in fact, we have clearly

* The vapor pressure is weakly influenced by the O_2 present in the gas boundary layer; however, this effect is neglected here.

$$(\partial T/\partial y)_0 = (\partial T/\partial y)_i \exp\left\{(2\delta^2/nv_w\mu_i) \times (\tau_i' - 3p''\delta)\right\} \quad \text{(A-5)}$$

Now the exponent of the second exponential in Eq. (A-4) is largest for $y = 0$ (note that $y \leq 0$ by definition), and there its absolute value is equal to the exponent in Eq. (A-5). However, we know from Eq. (14) that

$$(2\delta^2/v_w\mu_i)\ (\tau_i' - 2p''\delta) = 1 - (v_i/v_w) \leq 1 \quad \text{(A-6)}$$

Since p'' is negative, the exponent in Eq. (A-5) satisfies the relation

$$(2\delta^2/nv_w\mu_i)\ (\tau_i' - 3p''\delta) < 3/2n \quad \text{(A-7)}$$

Our fundamental assumption being $n \gg 1$, we therefore see that the exponential in Eq. (A-5) and the second exponential in Eq. (A-4) can be expanded and only the first two terms retained in the expansion. This is the fundamental point in our proof. Eq. (A-4) becomes then,

$$dT/dy = (dT/dy)_0 e^{y/n\delta}\left(1 - (2\delta^2/nv_w u_i)e^{y/\delta} \times \left\{\tau_i' + p''\delta[(y/\delta) - 3]\right\}\right) \quad \text{(A-8)}$$

which may be integrated once more to give

$$T = \left(\frac{dT}{dy}\right)_0 \left\{n\delta e^{y/n\delta} - \frac{2\delta^3 e^{(y/\delta)[1+(1/n)]}}{(n+1)v_w\mu_i}\left[\tau_i' + p''\delta\left(\frac{y}{\delta} - 4 + \frac{1}{n+1}\right)\right]\right\} \quad \text{(A-9)}$$

$$= T_0 e^{y/n\delta}\left\{1 - \frac{2\delta^2 e^{y/\delta}}{n(n+1)v_w\mu_i}\left[\tau_i' + p''\delta\left(\frac{y}{\delta} - \bar{4}\right)\right]\right\} \quad \text{(A-10)}$$

where we define

$$\bar{4} = 4 - [1/(n+1)] \quad \text{(similarly, } \bar{5}, \bar{6}, \text{ etc.)} \quad \text{(A-11)}$$

and

$$T_0 = n\delta(dT/dy)_0 \quad \text{(A-12)}$$

According to Eq. (A-10), T_0 is related to the surface temperature, T_i, by

$$T_0 = T_i\left\{1 + [2\delta^2/n(n+1)v_w\mu_i]\ [\tau_i' - \bar{4}p''\delta]\right\} \quad \text{(A-13)}$$

We require the viscosity,

$$\mu(y) = \mu_0(T/T_0)^{-n} = \mu_0 e^{-y/\delta}\left(1 + [2\delta^2 e^{y/\delta}/(n+1)v_w\mu_i] \times \left\{\tau_i' + p'\delta[(y/\delta) - \bar{4}]\right\}\right) \quad \text{(A-14)}$$

using Eq. (A-10) and defining $\mu_0 = \mu(T_0)$. In particular, the interface viscosity is

$$\mu_i = \mu_0\left\{1 + [2\delta^2/(n+1)v_w\mu_i]\ [\tau_i' - \bar{4}p''\delta]\right\} \quad \text{(A-15)}$$
$$\approx \mu_0 + [2\delta^2/(n+1)v_w]\ [\tau_i' - \bar{4}p''\delta]$$

We have neglected in Eq. (A-14) the deviation of the viscosity-temperature relation from the simple law Eq. (7b) which gives a correction of the same order $(1/n)$ as the one we are calculating.

We insert Eq. (A-14) into Eq. (4) and obtain by integration a second approximation to u, which near the stagnation point reduces to

$$u = u_1 - [\delta^3 x e^{2y/\delta}/(n+1)v_w\mu_0^2]\left\{\tau_i'^2 + p''\tau_1'\delta \times [(2y/\delta) - \bar{5}] + p''^2\delta^2[(y^2/\delta^2) - \bar{5}(y/\delta) + (\bar{5}/2)]\right\} \quad \text{(A-16)}$$

where u_1 is the first-order result, Eq. (12). Using the continuity equation, Eq. (13), and integrating once more,

$$v_i/v_w = 1 - (2\delta^2/\mu_0 v_w)\ [\tau_i' - 2p''\delta] + [1/2(n+1)]\ (\delta^2/\mu_0 v_w)^2\left\{\tau_i'^2 - \bar{6}\tau_i' p''\delta + [\bar{5} + (1/2)]p''^2\delta^2\right\} \quad \text{(A-17)}$$

where the first two terms are identical with Eq. (14) except for the replacement of μ_i by μ_0, and the third is the result of our present, second-order calculation. If, in the second term, μ_0 is expressed in terms of μ_i using Eq. (A-15), we obtain to second order:

$$v_i/v_w = 1 - (2\delta^2/\mu_i v_w)\ [\tau_i' - 2p''\delta] - [1/(n+1)] \times (\delta^2/\mu_i v_w)^2\left(4[\tau_i' - 2p''\delta]\ [\tau_i' - \bar{4}p''\delta] - (1/2)\left\{\tau_i'^2 - \bar{6}\tau_i' p''\delta + [\bar{5} + (1/2)]p''^2\delta^2\right\}\right) \quad \text{(A-18)}$$

The first term in the heavy parentheses, arising from the difference between μ_0 and μ_i, is roughly eight times larger than the second term, which arises from the integration of Eq. (A-16); i.e., the change of μ inside the liquid. Thus the main correction is to substitute μ_0 for μ_i in Eq. (14), and Eq. (A-15) shows that to our approximation, μ_0 is less than μ_i by an amount independent of μ_i but dependent on flight conditions.

The main feature of the third term—i.e., the correction term—in Eq. (A-18) is that it is proportional to the square of the second term but is divided by $n + 1$. Now for all glassy materials, n is large, of order 10, therefore, the correction term is of order 10 per cent. This establishes the validity of the theory given in the main part of this report. It is clear that further correction terms can be calculated, and that the final result for v_i/v_w will be a series which progresses essentially in inverse powers of n.

Since the main effect is a change of the effective μ from the interface value, μ_i, to the slightly smaller μ_0, we may use the result of Section (4)—namely, for *any* value of μ, the effective heat of ablation h_{eff} is rather insensitive to μ. Thus a change of 10 per cent in the effective value of μ will change h_{eff} by much less, in general by 3 per cent or less.

References

[1] Sutton, George W., *The Hydrodynamics and Heat Conduction of a Melting Surface*, Journal of the Aeronautical Sciences, Vol. 25, No. 1, pp. 29–32, January 1958.

[2] Howarth, L., *Modern Developments in Fluid Dynamics*, Vol. I, Chap. X, Oxford at the Clarendon Press, 1953.

[3] Corning Glass Works, *Properties of Selected Commercial Glasses*, Bulletin B-83, Corning Glass Works, Corning, N.Y., 1957.

(*Continued on page 350*)

Comparison of Approximate Solutions of the Thermoelastic Problem of the Thick-Walled Tube

J. H. BALTRUKONIS**

Space Technology Laboratories, Inc.

SUMMARY

The stress distribution in a thick-walled, circular cylindrical tube subjected to a steady-state temperature gradient across the tube wall is calculated, taking into account the variation with temperature of the elastic and thermal properties of the material. The calculations are made by five different methods: (I) by electronic digital computer, (II) by assuming an incompressible material, (III) by assuming a temperature-independent material and using the average properties of the material, (IV) by using the weighted-average properties of the material, and (V) by using a higher order approximation. Good agreement is found when high temperature levels do not persist over large portions of the tube. When the latter is the case, only Method (V) gives much better than a qualitative picture of the stress distribution.

SYMBOLS

r	= radius
a	= inner radius of thick-walled tube
b	= outer radius
T_0	= 68°F. = initial uniform temperature before heating
T	= $T(r)$ = temperature at any point r
T_a	= temperature at $r = a$
T_b	= temperature at $r = b$
$u(r)$	= radial displacement at any point r
ϵ_r, ϵ_θ, ϵ_z	= radial, circumferential, and axial components of strain
σ_r, σ_θ, σ_z	= radial, circumferential, and axial components of stress, and the components of stress for temperature-dependent material
σ_{ri}, $\sigma_{\theta i}$, σ_{zi}	= stress components for incompressible material
σ_{r_0}, σ_{θ_0}, σ_{z_0}	= stress components for temperature-independent material with arithmetic-average properties of the material
σ_r', σ_θ', σ_z'	= stress components for temperature-independent material with weighted-average properties of the material
σ_r^*, σ_θ^*, σ_z^*	= higher order approximations to stress components
E	= $E(r)$ = elastic modulus (assumed a function of position)
ν	= $\nu(r)$ = Poisson's ratio (assumed a function of position)
$\bar{\alpha}$	= $\bar{\alpha}(r) = [1/(T - T_0)] \int_{T_0}^{T} \alpha \, dT$, mean coefficient of linear expansion (assumed a function of position)
$\bar{E}$, $\bar{\nu}$, $\bar{\alpha}$	= arithmetic-average properties of the material
E', ν', $\bar{\alpha}'$	= weighted-average properties of the material

Presented at the Structures Session, National Summer Meeting, IAS, Los Angeles, July 8–11, 1958.

** Member, Technical Staff, Engineering Mechanics Department.

The author wishes to acknowledge the contributions of Dr. Y. C. Fung for his invaluable suggestions throughout the study and in particular in connection with Method (IV), Dr. Samuel D. Conte for his direction of the digital computer work in Methods (I) and (II), and Mrs. Irene Sagey, who performed most of the hand computations in Methods (III), (IV), and (V).

INTRODUCTION

A RECENT TREND throughout the field of engineering has been to use all types of structures and machines at high temperatures accompanied by unavoidably large temperature gradients. This makes the solution of the associated stress problems much more difficult since, under these conditions, the assumption of the homogeneity of the properties of the material becomes invalid. For a short presentation of the history of the problem, together with a bibliography of the early work in the field, the reader is referred to Love.[1]

Assuming that the elastic and thermal properties of the material are known functions of position, one can formulate the thermoelastic boundary value problem, but it will ordinarily be so complex that it will require a numerical solution, usually on a large-scale automatic computer. Such a solution will be subsequently referred to as a "temperature-dependent material solution," implying that, by this method, one can calculate stresses as accurately as desired. While it is comforting to know that one can always obtain a computer solution, this approach is not always feasible or economical.

The primary objective of the present investigation is to formulate the thermoelastic boundary value problem for a thick-walled, circular, cylindrical tube subjected to an axially symmetric, steady-state, temperature difference, to obtain the "temperature-dependent material solution" in several specific cases, and to compare it with four approximate methods.

A solution, referred to here as the "temperature-independent material solution," one where the elastic and thermal properties of the material are considered homogeneous, has been presented by Timoshenko,[2] among others. In this method the Neumann-Duhamel generalization of Hooke's law is used. In applying this method, one is faced with the problem of deciding what magnitudes to select for the properties of the material, thus giving rise to many different approximate solutions. Two methods of evaluating the properties of the material will be used: (a) one using

arithmetic averages, and (b) one using a weighted average based on conservation of energy.

Hilton[3] went a step further by taking into account the variation with temperature of the elastic shear modulus and the coefficient of thermal expansion. However, Poisson's ratio was assumed to have a constant value of 0.5, thereby resulting in a solution which will be referred to as the "incompressible material solution." This assumption was introduced because it allowed a closed-form solution for the thick-walled tube problem and seems intuitively reasonable since, in general, Poisson's ratio tends to 0.5 as the temperature increases. Substantial differences were found between the stresses corresponding to the temperature-independent material solution and the incompressible material solution. In the specific problems solved, the stresses for the incompressible material were markedly lower than those for the temperature-independent material. This stress relationship cannot be considered typical since it must depend on the values selected for the properties of the material and on the temperature distribution. This observation will be demonstrated subsequently.

Finally, higher order approximations should be considered. The logical approach would be to select any of the previous solutions, add to it an arbitrary correction which does not violate either the differential equations or the boundary conditions, and evaluate it by any of several different methods—e.g., collocation, least squares, Galerkin's method, minimum complementary energy, etc. Only the nature of the particular problem under consideration can determine which of these approaches is the best. In the present case a correction term, satisfying the boundary conditions and having an arbitrary constant as a factor, was added to the temperature-independent solution using weighted-average properties of the material. The arbitrary constant was evaluated by minimizing the integral of the square of the error in satisfaction of the differential equation.

It was not the intention of this study to select an optimum approach from among the several methods considered, since the author believes that such a method does not exist. Rather it is believed instead that many methods are available with varying accuracies and involving different amounts of computational labor. Comparing the results obtained here using each of the methods provides some evidence to support a choice of method in other, more complex problems.

Theory

The problem to be considered is that of a long, thick-walled circular cylindrical tube subjected to an axially symmetric steady-state temperature distribution. For the sake of simplicity, it will be assumed that the conditions at the ends are such that the problem can be considered one of axially symmetric, plane strain for which the only nonvanishing stress equilibrium equation is

$$r(d\sigma_r/dr) + \sigma_r - \sigma_\theta = 0 \tag{1}$$

The only nonvanishing strain compatibility condition is

$$r(de_\theta/dr) + e_\theta - e_r = 0 \tag{2}$$

The Neumann-Duhamel thermoelastic stress-strain relations for axially symmetric plane strain,

$$\left.\begin{aligned} e_r &= [(1-\nu^2)/E]\{\sigma_r - [\nu/(1-\nu)]\sigma_\theta\} + (1+\nu)\,\bar{\alpha}(T-T_0) \\ e_\theta &= [(1-\nu^2)/E]\{\sigma_\theta - [\nu/(1-\nu)]\sigma_r\} + (1+\nu)\,\bar{\alpha}(T-T_0) \end{aligned}\right\} \tag{3}$$

$$\sigma_z = \nu(\sigma_r + \sigma_\theta) - E\,\bar{\alpha}(T - T_0) \tag{4}$$

will be used, except that the properties of the material, E, ν, and $\bar{\alpha}$, will be assumed functions of position.

Eqs. (1)–(3) constitute a system of four equations in the four unknowns: σ_r, σ_θ, e_r, and e_θ. Elimination of the latter three results in

$$\begin{aligned} r^2(d^2\sigma_r/dr^2) + \{3 + [E/(1-\nu^2)]\}\, r(d/dr) \times \\ [(1-\nu^2)/E]\}\, r(d\sigma_r/dr) + \{[E/(1-\nu^2)] \times \\ r(d/dr)\,[(1+\nu)(1-2\nu)/E]\}\sigma_r = \\ -[E/(1-\nu^2)]r(d/dr)\,[(1+\nu)\,\bar{\alpha}(T-T_0)] \end{aligned} \tag{5}$$

while Eq. (1) results in

$$\sigma_\theta = \sigma_r + r(d\sigma_r/dr) \tag{6}$$

Thus, we have seen that solution of Eq. (5), subject to the boundary conditions

$$\sigma_r(a) = \sigma_r(b) = 0 \tag{7}$$

yields a complete solution to the boundary value problem since the remaining stress components can be calculated by means of Eqs. (4) and (6). Eq. (5) is a nonhomogeneous, second-order, ordinary differential equation with variable coefficients. A closed-form solution is not possible, so that approximate solutions must be attempted. The various solutions attempted in the present study are described in the following Section.

Methods of Solution

As stated in the Introduction, it is the objective of this study to solve several different problems by each of five different methods which are described in detail below.

(*I*) *Temperature-Dependent Material*

Eq. (5), as it stands, defines the solution of the temperature-dependent material problem. As previously mentioned, it cannot be solved in closed form, so that a numerical method must be used. The first method of solution was by means of a Sperry-Rand ERA 1103 electronic digital computer. The properties of the material were approximated by second-degree polynominals. While the resulting program was reasonably simple, and the programing, coding, and running times were not large in the present case, it is expected that the time involved will increase very rapidly as the

complexity of the problem increases. Furthermore, the usual practical difficulties such as scheduling, allocation of computing personnel, etc., add immeasurably to the time required to obtain a solution.

(II) *Incompressible Material*

For the incompressible material problem it is assumed that Poisson's ratio has the constant value of 0.5, and E and $\bar{a}$ remain functions of position. Under these conditions Eq. (5) reduces to

$$r^2(d^2\sigma_{r_i}/dr^2) + [3 + Er(d/dr)\ (1/E)]\ r(d\sigma_{r_i}/dr) = -2Er(d/dr)\ [\bar{a}(T - T_0)] \quad (8)$$

which can be solved in closed form as shown by Hilton.[3] In the present study, however, Eq. (8) was solved on the digital computer since Eq. (5) had already been programed and very little additional effort was required to solve Eq. (8). It appears that this method has very little advantage over Method (I), even if the approximation is very good, since one rarely encounters a problem for which a closed-form solution exists, as in the present case.

(III) *Temperature-Independent Material With Average Properties*

If it is assumed that the properties of the material are independent of temperature, Eq. (5) reduces to

$$r^2(d^2\sigma_{r_0}/dr^2) + 3r(d\sigma_{r_0}/dr) = -[\bar{E}\bar{a}/(1 - \bar{\nu})]r(dT/dr) \quad (9)$$

This equation also can be solved in closed form—for example, see Timoshenko.[2] The average properties of the material are merely arithmetic averages over the cross section. Calculation of the stresses by this method is routine and can be accomplished in a minimum of time on an ordinary desk calculator.

It is suggested that, due to its relative simplicity, this solution should be (and usually is) calculated for every thermal stress problem. It is an extremely important solution since it represents a first approximation to the actual solution, and since it can serve as a point of departure for more accurate approximations, as will be shown in subsequent sections.

(IV) *Temperature-Independent Material With Weighted-Average Properties*

As suggested above, the first step in any thermal stress problem should be to obtain a solution by means of Method (III). In some cases this solution may be sufficiently accurate since, as will be subsequently pointed out, Method (III) yields a solution which is not unreasonably inaccurate, at least in the case of the present problem.

If greater accuracy is desired, another method must be used. Methods (I) and (II) are available but their use may not always be feasible or economical. Another simple method is required, one such that an ordinary desk calculator can be used in the computations. Such a method can be used when a temperature-independent material is assumed. In this case, however, it is proposed that weighted-average properties of the material be used rather than mere arithmetic averages. We must now devise a method whereby these weighted-average properties of the material can be calculated.

We begin by assuming that the total complementary energy for the temperature-dependent material is equal to that for the temperature-independent material with weighted-average properties—i.e.,

$$\int [(1/2E)\ (\sigma_r^2 + \sigma_\theta^2 + \sigma_z^2) - (\nu/E) \times (\sigma_r\sigma_\theta + \sigma_\theta\sigma_z + \sigma_z\sigma_r) + \bar{a}(T - T_0)\ (\sigma_r + \sigma_\theta + \sigma_z)] \times dV = (1/2E')\int (\sigma_r'^2 + \sigma_\theta'^2 + \sigma_z'^2)\ dV - (\nu'/E')\int (\sigma_r'\sigma_\theta' + \sigma_\theta'\sigma_z' + \sigma_z'\sigma_r')\ dV + \bar{a}'\int (T - T_0)\ (\sigma_r' + \sigma_\theta' + \sigma_z')\ dV$$

This equality can be rearranged as follows:

$$[(1/2E')\int (\sigma_r'^2 + \sigma_\theta'^2 + \sigma_z'^2)\ dV - \int (1/2E) \times (\sigma_r^2 + \sigma_\theta^2 + \sigma_z^2)\ dV] - [(\nu'/E')\int (\sigma_r'\sigma_\theta' + \sigma_\theta'\sigma_z' + \sigma_r'\sigma_r')dV - \int (\nu/E)\ (\sigma_r\sigma_\theta + \sigma_\theta\sigma_z + \sigma_z\sigma_r)\ dV] + [\bar{a}'\int (T - T_0)\ (\sigma_r' + \sigma_\theta' + \sigma_z') \times dV - \int \bar{a}(T - T_0)\ (\sigma_r + \sigma_\theta + \sigma_z)dV] = 0 \quad (10)$$

Assuming that the quantity within each of the three pairs of brackets vanishes, Eq. (10) is not violated and the weighted-average properties of the material can be obtained. Before doing so, however, let us examine the implications more carefully. If we consider the quantity within the second pair of brackets as typical, we get

$$(\nu'/E')\int (\sigma_r'\sigma_\theta' + \sigma_\theta'\sigma_z' + \sigma_z'\sigma_r')dV = \int (\nu/E)\ (\sigma_r\sigma_\theta + \sigma_\theta\sigma_z + \sigma_z\sigma_r)\ dV$$

Fundamentally, this relation expresses the equality of the mean values of the respective integrands. We anticipate no difficulty with the use of this equation except when the integrand of the left-hand integral, which can be either positive or negative, has equal positive and negative parts. Under these conditions fictitiously large values for ν'/E' can be obtained. To avoid this difficulty, we argue that since the integrands of both integrals have essentially the same shape, we can replace the above relation by one expressing the equality of the mean amplitudes—i.e.,

$$(\nu'/E')\int [|\sigma_r'\sigma_\theta'| + |\sigma_\theta'\sigma_z'| + |\sigma_z'\sigma_r'|]dV = \int (\nu/E)[|\sigma_r\sigma_\theta| + |\sigma_\theta\sigma_z| + |\sigma_z\sigma_r|]dV$$

This argument is essential for the second and third pair of brackets of Eq. (10), but is not required for the first pair since the integrands of both integrals there are positive definite. Now, we note that at this point we have neither of the solutions, $(\sigma_r, \sigma_\theta, \sigma_z)$ and $(\sigma_r', \sigma_\theta', \sigma_z')$, required for the calculation of ν'/E'. It is suggested, therefore, that a reasonable approximation can be obtained by replacing both solutions by $(\sigma_{r_0}, \sigma_{\theta_0}, \sigma_{z_0})$ which can be obtained quite readily.

By means of these arguments we obtain the following expressions for the weighted-average properties of the material:

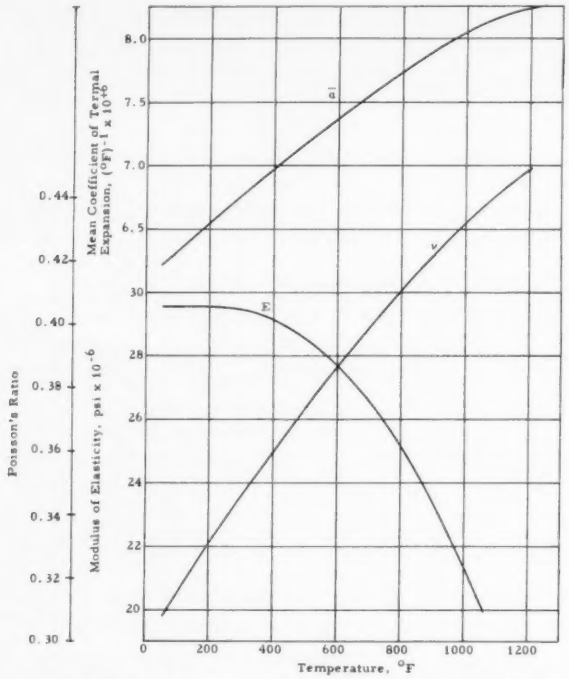

FIG. 1. Variation of the elastic and thermal properties of mild steel with temperature, from Everett and Miklowitz[5] and Lucks and Deem.[6]

$$E' = \frac{\int(\sigma_{r_0}^2 + \sigma_{\theta_0}^2 + \sigma_{z_0}^2)dV}{\int(1/E)\,(\sigma_{r_0}^2 + \sigma_{\theta_0}^2 + \sigma_{z_0}^2)dV} \tag{11a}$$

$$\nu' = \frac{E'\int(\nu/E)\left[|\sigma_{r_0}\sigma_{\theta_0}| + |\sigma_{\theta_0}\sigma_{z_0}| + |\sigma_{z_0}\sigma_{r_0}|\right]dV}{\int\left[|\sigma_{r_0}\sigma_{\theta_0}| + |\sigma_{\theta_0}\sigma_{z_0}| + |\sigma_{z_0}\sigma_{r_0}|\right]dV} \tag{11b}$$

$$\bar{a}' = \frac{\int\bar{a}|T - T_0|\cdot\left[|\sigma_{r_0}| + |\sigma_{\theta_0}| + |\sigma_{z_0}|\right]dV}{\int|T - T_0|\cdot\left[|\sigma_{r_0}| + |\sigma_{\theta_0}| + |\sigma_{z_0}|\right]dV} \tag{11c}$$

In the present study the integrals involved in Eqs. (11) were evaluated numerically by means of Simpson's rule.

The procedure required to obtain this solution is now clear. The solution must first be calculated by Method (III); then, the weighted-average properties of the material are calculated by means of Eqs. (11), and finally, the solution is obtained from Method (III) by merely exchanging the weighted-average properties of the material and the arithmetic-average properties.

(V) *Higher Order Approximations*

If the solution found by Method (IV) does not have the desired accuracy, higher order approximations can be obtained by any one of several different methods—e.g., collocation, Galerkin's method, minimum complementary energy theorem, etc. The proper method to use can only be determined by the specific problem under consideration.

In the present problem the governing differential equation, Eq. (5), had already been derived so that the least squares method [see, for example, reference 7] was reasonably simple and reliable. In this application the following radial stress, satisfying the boundary conditions identically, was assumed:

$$\sigma_r^* = \sigma_r' + [(r/a) - 1]\,[(b/a) - (r/a)]A_0 \tag{12}$$

Theoretically, one could achieve any desired accuracy by replacing A_0 by $\sum_{n=0}^{N} A_n r^n$ and using any desired number of constants. In the present case, only one constant was required to obtain a reasonable correction to the solution of Method (IV).

TABLE 1
Problems Solved

Problem	a	b	T_a, °F.	T_b, °F.
1	1	3	68	408
2	1	3	68	816
3	1	3	544	680
4	1	8	68	680
5	1	10	952	857

THE PROBLEMS

In the present investigation, the five specific problems listed in Table 1 were solved by each of the five methods outlined in the previous Section. In selecting the problems, attention was given to choosing cases at high- and low-temperature levels with large and small temperature gradients for cylinders of varying thicknesses. Problem 5 is very nearly identical to one of the numerical examples presented by Hilton.[3]

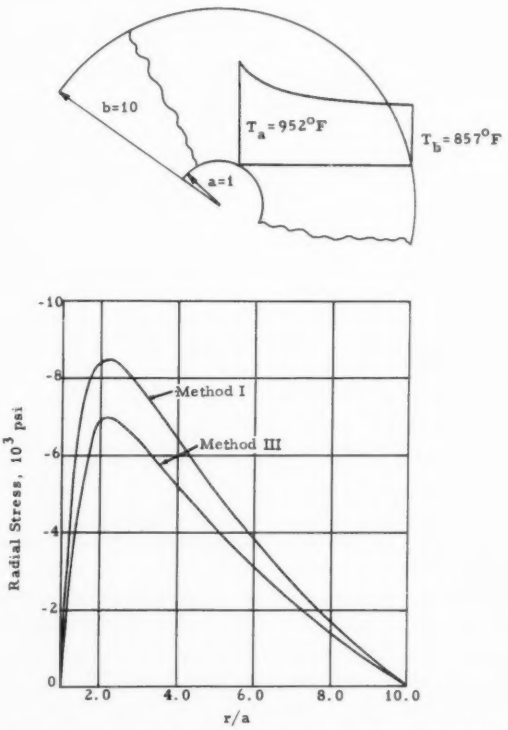

FIG. 2. Comparison of radial stresses as calculated by Methods (I) and (III) for Problem 5.

Temperature Distribution

If, in the stress problem, we assume that the thermal properties are temperature dependent, we should retain the same assumption for the heat-transfer problem. However, in the case of the thick-walled cylinder problem presently under consideration, we need not make this assumption since the steady-state solution of the heat-transfer problem is independent of the thermal properties of the material. See, for example, reference 4.

Thus, the solution of the heat-transfer problem, for which the boundary conditions are $T(a) = T_a$, $T(b) = T_b$, is

$$T = T(r) = T_a + [(T_b - T_a)/\log_e (b/a)]\log_e (r/a) \quad (13)$$

This is the temperature distribution used in the problems solved. By varying T_a and T_b different problems are obtained.

Properties of the Material

The properties of the material constitute one of the major stumbling blocks in any thermal stress problem, since comprehensive and reliable data on material elastic and thermal properties seems to be practically nonexistent in unclassified literature, especially when one is interested in short-time phenomena. However, by restricting consideration to the steady-state problem—i.e., long time—the properties of the material data for mild steel, shown in Fig. 1, becomes useful and will be applied in the following Sections.

Since the properties of the material are known as functions of temperature, and since the temperature distribution is known, the properties of the material become known functions of position.

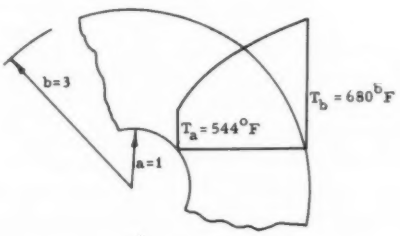

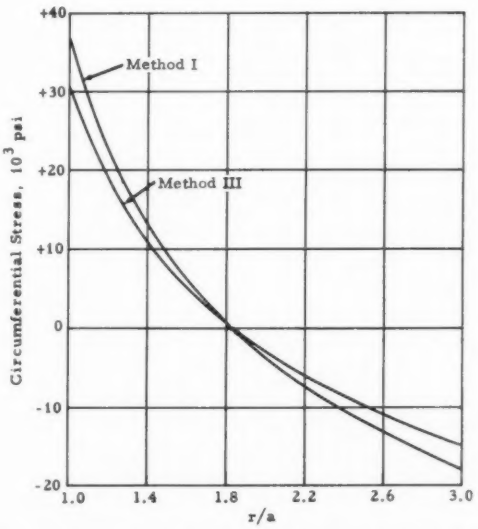

FIG. 3. Comparison of circumferential stresses as calculated by Methods (I) and (III) for Problem 3.

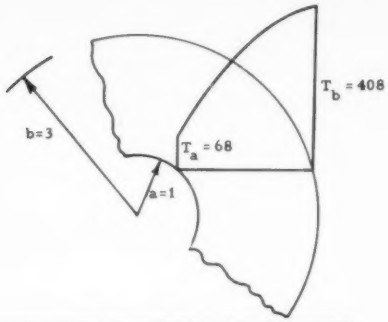

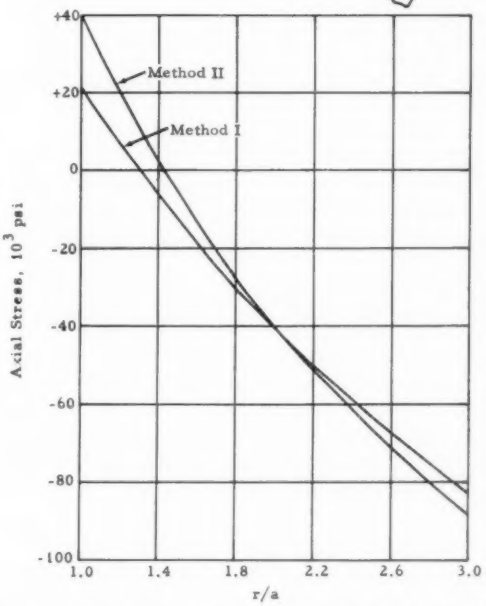

FIG. 4. Comparison of axial stresses as calculated by Methods (I) and (II) for Problem 1.

Results and Conclusions

Figs. 2, 3, and 4 show a few typical results. Complete results are shown in Table 2, where an effort is made to compare Method (I) with the other methods in the neighborhood of maximum stress and throughout the cylinder cross section.

It should be noted that the resulting stress magnitudes indicate that local yielding will have occurred in the cylinder in each of the problems considered. Consequently, the numerical results have no significance in the region of yielding and can be used there only to compare the approximate methods considered.

Several interesting observations can be made concerning the results, of which the most important is un-

TABLE 2
Comparison of Results

Problem	b/a	T_a, °F.	T_b, °F.	Method	σ_r (a)†	σ_r (b)‡	σ_θ (a)†	σ_θ (b)‡	σ_z (a)†	σ_z b)†
1	3	68	408	Max. stress in kips per Method (I)	14.2 at r/a = 1.60		68.7 at r/a = 1.0		−83.5 at r/a = 3.0	
				(II)	−8.3	5.7	−16.0	5.5	−6.5	9.3
				(III)	+7.6	6.3	+0.9	4.0	+6.1	2.7
				(IV)	+3.6	3.6	−3.3	2.9	+3.0	1.9
				(V)	+0.5	1.0	−4.8	1.7	+1.7	1.7
2	3	68	816	Max. stress in kips per Method (I)	34.2 at r/a = 1.6		165.0 at r/a = 1.0		−181.0 at r/a = 3.0	
				(II)	+1.3	2.0	−6.5	2.6	−3.4	7.8
				(III)	+10.8	8.3	+3.7	5.0	+1.6	6.9
				(IV)	+2.7	2.8	−5.1	2.6	−2.9	4.2
				(V)	−1.0	1.2	−6.9	2.3	−4.9	4.9
3	3	544	680	Max. stress in kips per Method (I)	7.0 at r/a = 1.6		36.3 at r/a = 1.0		−130.0 at r/a = 3.0	
				(II)	+11.7	8.5	+11.8	5.1	−0.6	0.8
				(III)	+16.5	12.0	+16.5	7.4	0	0.4
				(IV)	+16.7	12.2	+16.8	7.5	+0.3	0.3
				(V)	+12.7	8.8	+15.0	5.8	−0.3	0.3
4	8	68	680	Max. stress in kips per Method (I)	45.3 at r/a = 2.1		154.0 at r/a = 1.0		−143.0 at r/a = 8	
				(II)	−1.5	1.6	−8.1	3.2	−2.6	9.7
				(III)	+8.4	7.3	+2.4	3.4	+3.4	2.6
				(IV)	+4.2	4.7	−1.9	2.6	+0.8	3.1
				(V)	+2.9	2.7	−2.4	1.6	−0.6	3.2
5	10	952	857	Max. stress in kips per Method (I)	−8.5 at r/a = 2.2		−28.9 at r/a = 1.0		−169.0 at r/a = 1.0	
				(II)	+12.3	8.3	+10.9	4.4	−0.3	0.1
				(III)	+17.6	11.5	+16.8	6.4	−2.6	1.1
				(IV)	+16.8	10.9	+15.8	6.0	−3.4	1.3
				(V)	+13.8	6.8	+14.8	5.5	−3.4	1.5

† (a) = Difference between maximum stresses as calculated by Method (I) and those as calculated by the indicated methods as a percentage of the maximum stress by Method (I). Negative sign means indicated maximum stress was higher than that per Method (I).
‡ (b) = Root mean square deviation of the stress as calculated by the indicated method from that calculated by Method (I) as a percentage of the maximum stress per Method (I).

doubtedly the fact that, unless one accounts for the variation in the properties of the material, not much better than a qualitative picture of the stress distribution will be obtained.

Another interesting feature of the results is the notably poor agreement between Method (I) and other methods for Problems 3 and 5 to be contrasted with the agreement in Problems 1, 2, and 4. This is probably accounted for by the fact that in Problems 3 and 5 the entire cylinder cross section is at high temperatures so that the properties of the material will vary rapidly as functions of position. (It is reasonable to expect poorer agreement under these circumstances.) Good agreement, for example, results in Problem 4 where the high temperatures are restricted to relatively small portions of the cross section. It is evident that considerable care must be exercised in calculating the stress distribution in a body where high temperatures persist over large portions of the body. Even Method (V) yielded only marginal results for Problems 3 and 5. However, by using additional undetermined constants, as previously suggested, much better approximations can be obtained.

Further, we note that in no case did we get better than about 5 per cent agreement for Method (III), which makes its use somewhat questionable for other than qualitative purposes or as a point of departure for more accurate methods.

Methods (II) and (IV) were essentially in agreement. However, Method (IV) has the advantage of simplicity which will be far more evident in problems that are more complex than the present one, where Method (II) resulted in a closed-form solution.

Finally, Method (V) was the most satisfactory of all the methods considered and resulted in reasonably good agreement despite the fact that only a single undetermined constant was used.

REFERENCES

[1] Love, A. E. H., *A Treatise on the Mathematical Theory of Elasticity*, 4th Ed., pp. 108–109; Dover Publications, Inc., New York, 1944.

[2] Timoshenko, S., *Theory of Elasticity*, pp. 366–376; McGraw-Hill Book Co., New York, 1934.

[3] Hilton, H. H., *Thermal Stresses in Bodies Exhibiting Temperature-Dependent Elastic Properties*, J. Appl. Mech., Vol. 19, pp. 350–354, 1952.

[4] Carslaw, H. S., and Jaeger, J. C., *Conduction of Heat in Solids*, p. 167; Oxford University Press, London, 1947.

[5] Everett, F. L., and Miklowitz, J., *Poisson's Ratio at Elevated Temperatures*, J. Appl. Phys., Vol. 15, p. 592, 1944.

[6] Lucks, C. F., and Deem, H. W., *Thermal Properties of Thirteen Metals*, ASTM Special Tech. Pub. No. 226, 1958.

[7] Frazer, R. A., Jones, W. P., and Skan, S. W., *Approximations to Functions and to the Solutions of Differential Equations*, British ARC R&M No. 1799, March 19, 1937.

The Axisymmetric Free-Convection Temperature Field Along a Vertical Thin Cylinder†

FRANCIS R. HAMA,* JOHN V. RECESSO,** AND JEAN CHRISTIAENS***
University of Maryland

SUMMARY

With a view to studying the effect of strong transverse curvature on boundary-layer problems, the axisymmetric free-convection problem along a vertical thin cylinder is investigated theoretically as well as experimentally. A theory is developed as an extension of the Pohlhausen solution of a thick axisymmetric laminar boundary layer by Mark and by Glauert and Lighthill. Experiments consist of a thermocouple survey of the temperature field over an electrically-heated brass cylinder of 1/4-in. diameter and 10 ft. height and an interferometric study of the density field over a bare tungsten wire of 0.02-in. diameter and 5 ft. height. The thermal-layer thicknesses are about five and fifty times the radii of the cylinders, respectively. Experimental results of the local heat-transfer coefficient are in excellent agreement with the theory. This, in turn, justifies the theories of laminar boundary layer along a thin cylinder, at least indirectly.

SYMBOLS

a	= radius of cylinder
c_p	= specific heat at constant pressure
f	= dimensionless stream function, Eq. (7)
g	= gravitational acceleration
k	= heat conductivity
Nu_x	= local Nusselt Number at x
q	= rate of heat transfer per unit area
r	= radial distance from axis
T	= absolute temperature
T_a	= ambient temperature
T_w	= wall temperature
U	= velocity outside of boundary layer
u	= velocity parallel to surface
v	= velocity normal to surface
x	= distance from nose or leading edge
y	= normal distance from surface
α	= constant of logarithmic temperature profile
$1/\alpha$	= local heat-transfer coefficient, Eq. (21)
β	= coefficient of volumetric expansion
γ	= Euler's constant
δ	= thermal-layer thickness, Eq. (20)
η	= dimensionless y coordinate in two dimension, Eq. (9)
η^*	= dimensionless y coordinate in axisymmetry, Eq. (5)
θ	= dimensionless temperature, Eq. (8)
Θ	= integrated thermal area, Eq. (31)
μ	= viscosity
ν	= kinematic viscosity
ξ	= dimensionless x parameter, Eq. (6)
ρ	= density
σ	= Prandtl Number
τ	= shearing stress on surface
ψ	= stream function

Received July 8, 1958.

† This research was supported by the Air Force Office of Scientific Research under Contract AF 18(600)-1014 and was originally reported in references 1 and 2 in more detail.

* Associate Research Professor, Institute for Fluid Dynamics and Applied Mathematics.

** Formerly, Graduate Assistant. Now with AVCO.

*** Formerly, Graduate Assistant. Now serving in the Belgian Army.

INTRODUCTION

THE THICK AXISYMMETRIC BOUNDARY LAYER over slender bodies of revolution is drawing an increasing amount of attention in connection with some practical applications. When the boundary-layer thickness is small compared with the radius of a cylinder, the effect of the transverse curvature on the flow is negligible and the boundary layer can be described sufficiently by the Blasius solution. Such an approximation is permissible near the well-shaped leading nose of the circular cylinder. As the distance from the nose increases, the boundary-layer thickness also increases so that the effect of the transverse curvature becomes no longer negligible.

The boundary layer near the nose of a circular cylinder has been considered by Seban and Bond,[3] by expanding the stream function in an ascending power series of the x parameter $\sqrt{(\nu x/Ua^2)}$, which is essentially the ratio of the boundary-layer thickness to the radius of a cylinder and hence is a measure of the transverse-curvature effect. Kelly[4] has made important corrections to their theory. Due to the nature of the analysis, however, such theoretical results are not expected to hold when the parameter $\sqrt{(\nu x/Ua^2)}$ ceases to be small.

Cooper and Tulin[5] have developed a linearized theory in order to estimate the asymptotic behavior of a thick axisymmetric boundary layer. Glauert and Lighthill[6] and Stewartson,[7] on the other hand, have considered more rigorously the asymptotic behavior of the boundary layer over a thin cylinder for which $\sqrt{(\nu x/Ua^2)}$ is large.

The Pohlhausen solution obtained by Glauert and Lighthill[6] and by Mark[8] may be considered most attractive for practical purposes since it can be applied to any value of the x parameter. It is, however, an approximate solution using the modified Pohlhausen method and is subject to experimental confirmation. Typical theoretical results are plotted in Fig. 1, in which the recommended curve is the adjusted Pohlhausen solution following the procedure suggested in reference 2.

To perform an experiment compatible with the theory in a low-speed wind tunnel is a rather difficult

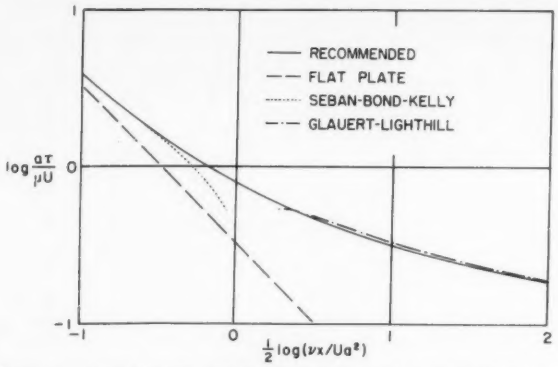

FIG. 1. Skin-friction coefficient of a circular cylinder vs. x parameter.

task. Indeed, Richmond[9] has encountered insurmountable difficulties in achieving a steady laminar boundary layer along a thin cylinder, but he has had better success in high supersonic flow. In order to obtain "subsonic" data, which are always needed as a basis of comparison, we consider here a slightly different problem which would just as well provide sufficient experimental information on the behavior of a thick axisymmetric boundary layer and in which the technical difficulty can be easily avoided.

The free-convection problem along a heated solid boundary is a boundary-layer problem; the temperature profile in the free-convection field has a close similarity to the velocity profile in the ordinary boundary layer, and the heat-transfer coefficient corresponds to the skin-friction coefficient. The theory of free convection along a vertical flat plate has been developed by Pohlhausen[10] and by Ostrach[11] under the boundary-layer assumption. Experiments performed by Schmidt and Beckmann[10] and by Eckert and Soehngen[12] confirm the theoretical results.

The free-convection field along a vertical hot cylinder presents an axisymmetric "boundary-layer" problem through which the effect of the transverse curvature may be experimentally investigated. Vertical suspension of a thin cylinder, or even a wire, is no technical problem. Moreover, since the thickness of the free-convection layer can be much thicker than the boundary-layer thickness under ordinary conditions, the curvature effect would appear more conspicuously.

We are primarily concerned with the measurement of the mean temperature distribution and the local heat-transfer coefficient. In order to make direct comparison with a theory possible, however, it is necessary to develop a theory comparable to the Pohlhausen solution by Mark and by Glauert and Lighthill, for theoretical investigations of the axisymmetric free convection are limited to the Sparrow-Gregg solution[13] which is a counterpart of the Seban-Bond-Kelly solution.

THEORY

The Sparrow-Gregg Solution

Under the assumptions of boundary-layer approximation and incompressibility other than the buoyancy term, the basic equations of axisymmetric free-convection field are

$$u(\partial u/\partial x) + v(\partial u/\partial r) = (\nu/r)\,(\partial/\partial r)\,[r(\partial u/\partial r)] + g\beta(T - T_a) \quad (1)$$

$$u(\partial T/\partial x) + v(\partial T/\partial r) = (k/\rho c_p r)\,(\partial/\partial r)\,[r(\partial T/\partial r)] \quad (2)$$

$$[\partial(ru)/\partial x] + [\partial(rv)/\partial r] = 0 \quad (3)$$

It is characteristic of these equations that there is no similar solution for either temperature or velocity distribution satisfying pertinent boundary conditions at the solid boundary. The only solution of the axisymmetric free-convection problem so far obtained is that by Sparrow and Gregg[13] who have applied the Seban-Bond-Kelly method[3] to the present problem.

By introducing the stream function defined by

$$ru = \partial\psi/\partial r, \quad rv = -(\partial\psi/\partial x) \quad (4)$$

the continuity equation (3) is satisfied. The following transformations are introduced:

$$\eta^* = [g\beta(T_w - T_a)/4\nu^2]^{1/4} \times [(r^2 - a^2)/2a]\,(1/x^{1/4}) \quad (5)$$

$$\xi = (2/a)\,[g\beta(T_w - T_a)/4\nu^2]^{-(1/4)}\,x^{1/4} \quad (6)$$

$$\psi = [g\beta(T_w - T_a)/4\nu^2]^{3/4}\,\nu a^3 x^{1/4} f(\xi, \eta^*) \quad (7)$$

$$\theta = \theta(\xi, \eta^*) = (T - T_a)/(T_w - T_a) \quad (8)$$

The axisymmetric dimensionless y coordinate η^* is related to the two-dimensional dimensionless y coordinate η used by Pohlhausen[10] and Ostrach[11] by the following equation:

$$\eta^* = \eta[1 + (1/2)\,(y/a)] \quad (9)$$

It is noted that the x parameter ξ is essentially the ratio of the thermal-layer thickness to the radius of a cylinder. The basic equations are converted into

$$\xi[(\partial f/\partial\eta^*)\,(\partial^2 f/\partial\xi\partial\eta^*) - (\partial f/\partial\xi)\,(\partial^2 f/\partial\eta^{*2})] - f(\partial^2 f/\partial\eta^{*2}) = \xi^2(\partial/\partial\eta^*)\{(1 + \xi\eta^*) \times (\partial^2 f/\partial\eta^{*2})\} + \xi^4\theta \quad (10)$$

$$\xi[(\partial f/\partial\eta^*)\,(\partial\theta/\partial\xi) - (\partial f/\partial\xi)\,(\partial\theta/\partial\eta^*)] - f(\partial\theta/\partial\eta^*) = (\xi^2/\sigma)\,(\partial/\partial\eta^*)\{(1 + \xi\eta^*)\,(\partial\theta/\partial\eta^*)\} \quad (11)$$

Assuming that f and θ can be expanded in power series of ξ; i.e.,

$$f(\xi, \eta^*) = \xi^2\{f_0(\eta^*) + \xi f_1(\eta^*) + \xi^2 f_2(\eta^*) + \ldots\} \quad (12)$$

$$\theta(\xi, \eta^*) = \theta_0(\eta^*) + \xi\theta_1(\eta^*) + \xi^2\theta_2(\eta^*) + \ldots \quad (13)$$

they obtained sets of ordinary differential equations

$$\left.\begin{aligned} &f_0''' + 3f_0f_0'' - 2f_0'^2 + \theta_0 = 0 \\ &\theta_0'' + 3\sigma f_0\theta_0' = 0 \end{aligned}\right\} \quad (14)$$

$$\left.\begin{aligned} &f_1''' + f_0'' + \eta f_0''' - 5f_0'f_1' + 4f_0''f_1 + 3f_0f_1'' + \theta_1 = 0 \\ &\theta_1'' + \theta_0' + \eta\theta_0'' - \sigma(f_0'\theta_1 - 4f_1\theta_0' - f_0\theta_1') = 0 \end{aligned}\right\} \quad (15)$$

. . . . . .

in which the primes indicate differentiations with respect to η^*. The boundary conditions are

$$f_0(0) = f_1(0) = \ldots = 0, \quad f_0'(0) = f_1'(0) = \ldots = 0,$$

$$\theta_0(0) = 1, \quad \theta_1(0) = \theta_2(0) = \ldots = 0,$$

$$f_0'(\infty) = f_1'(\infty) = \ldots = 0, \quad \theta_0(\infty) = \theta_1(\infty) = \ldots = 0$$

Note that Eq. (14) for the zeroth approximation is formally identical with that for a vertical plate, and its solution is known. The solutions for Eq. (15) have been obtained using an IBM machine, and a rough estimation on $\theta_2'(0)$ has been made.† These results will be referred to later in connection with our theoretical and experimental results.

The "Pohlhausen" Solution

The Sparrow-Gregg solution should provide good approximation near the nose where the thermal-layer thickness is still small compared with the radius of the cylinder. It is not expected to be applicable in the region far from the nose where the thickness is comparable with or much larger than the radius of a cylinder. We will therefore seek an approximate solution, which is nevertheless valid for any value of the x parameter ξ, as an extension of the Pohlhausen solution by Glauert and Lighthill[6] and by Mark.[8]

In applying the Pohlhausen method to axisymmetric problems, Glauert and Lighthill emphasize the importance of a proper profile whose behavior near the solid boundary is realistic. In Eq. (2), $u = v = 0$ at $r = a$ $(y = 0)$; therefore, we have

$$(\partial^2\theta/\partial y^2) + (1/a)\,(\partial\theta/\partial y) = 0 \quad \text{at } y = 0 \tag{16}$$

Differentiating Eq. (2) with respect to r and considering the boundary conditions again, we obtain

$$(\partial^3\theta/\partial y^3) + (1/a)\,(\partial^2\theta/\partial y^2) - (1/a^2)\,(\partial\theta/\partial y) = 0 \quad \text{at } y = 0 \tag{17}$$

In obtaining this relation, the wall temperature is assumed uniform along x. Eqs. (16) and (17) show that, as $y \to 0$,

$$\theta = 1 - (1/\alpha)\{(y/a) - (1/2)\,(y/a)^2 + (1/3)\,(y/a)^3 + 0(y/a)^4\} \tag{18}$$

Therefore,

$$\theta = 1 - (1/\alpha)\ln[(y + a)/a] \tag{19}$$

is correct, the order of error being $0(y/a)^4$. One may notice the analogy between the temperature field in the free-convection problem and the velocity field in the boundary-layer problem; Eq. (19) is essentially identical with the velocity profile assumed by Glauert and Lighthill. The logarithmic profile in either case is expected to become increasingly accurate as the layer thickness increases.

The parameter α is related to the thickness of the thermal layer δ by

$$\delta = a(e^\alpha - 1) \tag{20}$$

and to the rate of heat transfer from the wall by

$$1/\alpha = aq/k(T_w - T_a) \tag{21}$$

In this respect, the dimensionless factor $1/\alpha$ may be called a local heat-transfer coefficient and is related to the conventional local Nusselt Number by

$$Nu_x = (x/a)\,(1/\alpha) \tag{22}$$

In a similar manner to the above procedure, it is possible to obtain a velocity distribution:

$$u = K\{(y/a) - (1/2)\,(y/a)^2 + (1/3)\,(y/a)^3 - [g\beta(T_w - T_a)a^2/2\nu]\{(y/a)^2 - (1/3)\,[(1/\alpha) + 1]\,(y/a)^3\} + 0(y/a)^4 \tag{23}$$

Neglecting a part of the third-order term, Eq. (23) can be approximated by

$$u = \{K - [g\beta(T_w - T_a)a^2/2\nu]\,(y/a)\} \times \ln[(y + a)/a] \tag{24}$$

Although it is conventional and more correct to solve the problem for both K and α, a further simplification will be used. It is known that the inertia terms in the momentum equation (1) are rather insignificant in the free-convection problem unless the Prandtl Number is extremely small, such as in the case of mercury; the inertia terms affect essentially the Prandtl Number effect only. Therefore, for the present purpose the inertia terms may be omitted entirely. Then, putting Eqs. (19) and (24) into the integral relation of Eq. (1), we obtain K and the velocity distribution becomes

$$u = [g\beta(T_w - T_a)a^2/2\nu]\{(1/2\alpha) \times (e^{2\alpha} - 1) - [(y + a)/a]\}\ln[(y + a)/a] \tag{25}$$

Now, the temperature distribution (19) and the velocity distribution (25), which are indeed realistic near the wall, are substituted into the integral relation of the energy equation (2)

$$(d/dx)\int_0^\delta (y + a)u\theta dy = [aq/\rho c_p(T_w - T_a)] \tag{26}$$

The solution is

$$(1/8)e^{4\alpha} - (\alpha/9)e^{3\alpha} + (1/9)e^{3\alpha} - [(e^{4\alpha} - 1)/4\alpha] + [(e^{2\alpha} - 1)/2\alpha] + (3/8)\int_0^{4\alpha}[(e^t - 1)/t]dt - (2/27)\int_0^{3\alpha}[(e^t - 1)/t]dt - (1/2)\int_0^{2\alpha}[(e^t - 1)/t]dt - (17/27) = (1/\sigma)[2\nu^2/g\beta(T_w - T_a)a^3](x/a) \equiv (1/32\sigma)\xi^4 \tag{27}$$

in which the last integral, for example, is $\mathrm{Ei}(2\alpha) - \ln(2\alpha) - \gamma$ in the usual notation. This solution gives the variation of the local heat-transfer coefficient $1/\alpha$ with the x parameter ξ.

Eq. (27) may be expanded as

$$(1/32\sigma)\xi^4 = (1/16)\alpha^4 + (11/90)\alpha^5 + (29/216)\alpha^6 + 0(\alpha^7) \tag{28}$$

† Note added in proof: Exact numerical values have recently been obtained for the second approximation.

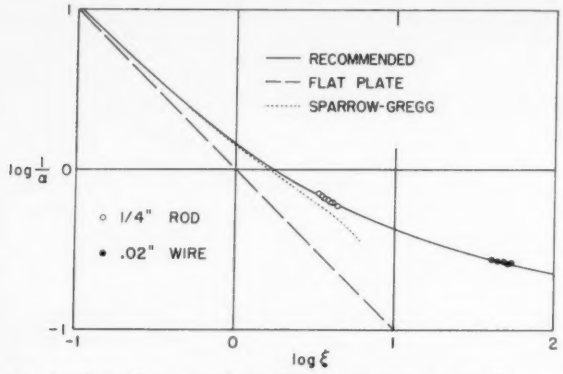

FIG. 2. Local heat-transfer coefficient of a circular cylinder vs. x parameter.

and it is easy to invert to give

$$1/\alpha = 1.095\xi^{-1} + 0.489 - 0.0552\xi + \ldots \quad (29)$$

for which $\sigma = 0.72$ (air). On the other hand, the Sparrow-Gregg solution is

$$1.009\xi^{-1} + 0.441 - 0.0403\xi + \ldots \quad (30)$$

in which the first term (the zeroth approximation) is identical with the flat-plate solution by Ostrach. It must be remembered that the third term is guessed from their chart and their value itself is a rough estimate.

The Pohlhausen solution is seen to predict a heat-transfer coefficient slightly larger than the exact solution. This is due to the fact that the assumed profiles are not quite accurate for small values of ξ. It is indeed expected that the error involved in the approximate Pohlhausen solution is largest when ξ is very small. In order to make the Pohlhausen solution compatible with the exact solutions, Glauert and Lighthill have suggested a fixed-percentage adjustment of $a\tau/\mu U$ for given values of $\sqrt{(\nu x/Ua^2)}$. The same procedure may be applied to the present case—i.e., a fixed-percentage adjustment of $1/\alpha$ for given values of ξ. As discussed in reference 2, however, this procedure does not appear to be reasonable in either case. Instead, we propose a fixed-percentage adjustment of the x parameter for given values of $a\tau/\mu U$ or $1/\alpha$. The recommended curve in Fig. 1 is thus obtained by increasing the values of $\sqrt{(\nu x/Ua^2)}$ calculated by the Pohlhausen solution by 14.9 per cent, since the Pohlhausen solution falls short of the exact solution in that case.

The values of ξ obtained by the Pohlhausen solution (27) are then decreased by 8.5 per cent. The adjusted numerical values are listed in Table 1 and plotted in Fig. 2 as a recommended curve in comparison with other solutions. It can be seen that the recommended curve is in good agreement with the Sparrow-Gregg solution for small ξ.

The logarithmic temperature profile provides the integrated thermal area Θ in the following form:

$$\Theta/\pi a^2 \equiv (1/\pi a^2)\int_0^\infty 2\pi(y + a)\theta\, dy = [(e^{2\alpha} - 1)/2\alpha] - 1 \quad (31)$$

which may be expanded into

$$\alpha + (2/3)\alpha^2 + \ldots \quad (32)$$

On the other hand, from the Sparrow-Gregg solution we obtain

$$\Theta/\pi a^2 = 1.253\xi + 0.507\xi^2 + \ldots \quad (33)$$

By combining Eqs. (30) and (33), we have

$$1.264\alpha + \ldots \quad (34)$$

Therefore, the integrated thermal area obtained by Eq. (31) falls short of the exact solution by 26.4 per cent. In a similar manner, $\Theta/\pi a^2$ obtained by Eq. (31) is increased by 26.4 per cent in its relation to $1/\alpha$, and the adjusted values are listed in Table 1 and plotted in Fig. 3.

TABLE 1
Recommended Values For Axisymmetric Free-Convection Layer

α	$1/\alpha$	ξ	$\Theta/\pi a^2$
.1	10	0.107	0.135
.2	5	.223	.290
.3	3.33	.353	.468
.4	2.50	.496	.673
.6	1.67	.828	1.18
.8	1.25	1.24	1.86
1.0	1.00	1.74	2.77
1.2	0.833	2.36	4.02
1.5	.667	3.57	6.78
1.7	.588	4.62	9.51
2.0	.500	6.65	15.7
2.5	.400	11.8	36.0
3.0	.333	20.5	83.5
3.3	.303	28.2	139
3.7	.270	43.1	278
4.0	.250	—	468
4.4	.227		1,047
4.5	.222		1,135

EXPERIMENTAL EQUIPMENT

In order to cover a wide range of the x parameter, two different series of experiments are performed—one over a 1/4-in. rod by use of a thermocouple and the other over a 0.02-in. bare wire by use of an interferometer.

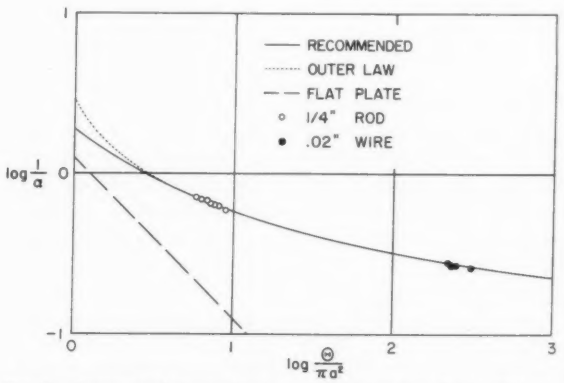

FIG. 3. Integrated thermal area vs. local heat-transfer coefficient.

1/4-In. Rod

General arrangement of the experimental equipment is shown in Fig. 4. The vertical cylinder is a brass tubing, 1/4 in. outside diameter, 10 ft. long, and 0.032 in. thick. The bottom tip is smoothly tapered to make a sharp nose through which a piano wire is fixed to hang a weight in an oil damper. The entire brass tubing is heated internally by two sets of No. 22 Nichrome wires; the wires pass through a four-hole Stoupakoff insulating tubing which is fitted tightly in the brass tubing. By means of two Variacs the a.c. current through Nichrome wires is controlled to 0.5 ampere. The temperature of the cylinder is determined by extrapolating the result of the temperature-field survey.

The brass tubing is suspended vertically on the axis of a 6-in. Lucite tubing which is also suspended vertically but fixed at the bottom end to the floor by four turnbuckles. The Lucite tubing protects the cylinder from draft. The bottom end of the tubing is enclosed by a 60-mesh brass screen in order to achieve a steady laminar convection flow. The nose of the cylinder is located $4^1/_2$ in. above the wire screen.

The Lucite tubing has holes through which a thermocouple probe can be inserted every 6 in. along the cylinder, the lowest location being 3 in. above the nose. The thermocouple is a copper-constantan junction of approximately 1/64-in. length, each strand of the wire being 0.005 in. in diameter. One strand of each wire is glued to the sides of two narrowly-spaced sewing needles and brought to form a sharp V-shaped junction. This type of thermojunction is adopted because, when the needles are placed parallel to the cylinder, the conduction effect along the thermocouple wires due to the concentric temperature field is believed to be best avoided. The thermocouple probe is attached to a vernier caliper, accurate to 0.001 in., which is used to measure the normal distance from the cylinder. The electromotive force is measured by K-2 potentiometer along with Electronik null indicator. The reference junction for the thermocouple is the melting point of ice.

0.02-In. Wire

It is technically difficult to extend the range of the x parameter ξ considerably for a given size of a cylinder while satisfying the requirements of laminar flow, steadiness, uniform wall temperature, and experimental accuracy. Since ξ is inversely proportional to the radius of a cylinder, and since the effect of the other quantities involved in ξ is proportional to their fourth root, the most effective way of changing ξ is to use a cylinder of considerably different size. In the second series of the present investigation, therefore, a bare wire is chosen as a cylinder so as to be able to increase ξ about ten times.

As will be discussed in the next Section, the thermocouple appears to disturb the convection field when it is located very close to the cylinder surface, giving an unduly high temperature reading near the cylinder. The disturbance would be even more severe for the smaller cylinder. Therefore, the precision thermocouple technique is abandoned and an interferometric study is used in the second series of experiments. The latter method is less accurate than the former but does not require any probe protruding into the field, thereby the disturbance is entirely avoided.

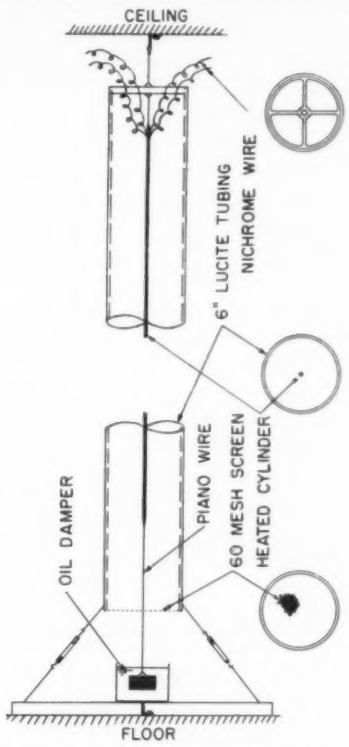

FIG. 4. General arrangement of 1/4-in. rod experiment.

The general arrangement is sketched in Fig. 5. A tungsten wire of 0.020-in. diameter and 5-ft. length is chosen as a heated cylinder. Both ends of the wire are copper-plated and soldered to flexible copper lead wires of a larger diameter than the tungsten wire itself. The Joule heating in the lead wire is considered negligible compared with that in the tungsten wire. The lower junction is covered by a small piece of cork fairing in order to assure smooth air flow and to make the lowest end of the heated body well defined.

Any section of the tungsten wire can be located at the horizontal level of the interferometer by a pulley system. A weight is hung on the lowest pulley and is put in an oil damper to prevent oscillation of the wire and to keep the wire straight and vertical. The wire is always enclosed in a vertical square box approximately 11 in. square and 7 ft. high to protect the wire from draft. The bottom of the box is enclosed by a 60-mesh screen but the top is kept open. The wire is located at approximately one-third the distance between two optical-flat windows so as to achieve the best optical condition.

A 60 cycle a.c. current is applied to the wire through a step-down transformer and a Variac. The current is nominally kept at 4 amperes, and no other current is used because changing the current does not extend the range of ξ significantly.

The interferometer is a conventional Mach-Zehnder type and a detailed description is given elsewhere.[14] The light source is a mercury lamp and a monochromatic light beam is obtained by using a 5460 Å filter. Royal Pan film is used to take interferograms. Exposure time is 1/5 sec. throughout the investigation except in the turbulent region where a faster exposure (1/25 sec.) is necessary because of rapid fluctuations. The original negative film has the same size as the density field and is enlarged about ten times. The enlarged picture is then split into 35 or more zones, each zone being about 3 mm. in width. Following the procedure given by Gooderum and Wood,[15] the fringe shifts are converted into the axisymmetric density distribution which is further transformed into temperature by use of the perfect gas law, assuming a constant pressure.

Experimental Results

A typical result of the temperature-profile measurements over the 1/4-in. rod is shown in Fig. 6. A marked sharp temperature rise is always observed in the region very near the cylinder up to approximately $y = 0.005$ in. It may be suspected that the field is already turbulent and that the sharp temperature rise is the manifestation of a laminar sublayer. Examination by a hot-wire anemometer has clearly ruled out this possibility; the flow is indeed laminar. If the flow is laminar, the temperature distribution near the cylinder has to be logarithmic [Eq. (19)], and the temperature rise is unlikely. A possible explanation of the temperature rise is the interference of the thermocouple probe. It is quite possible that, when the probe is very close to the cylinder surface, the flow field near the cylinder is disturbed causing a less effective heat transfer and a local temperature rise of the cylinder surface. This would result in the higher temperature readings. Indeed, the least indication of such a temperature rise is detected in the second series of experiments for which the optical method is used and no probe is inserted into the field. Therefore, the narrow portion of the temperature profile over the 1/4-in. rod, in which the sharp rise which deviates from the logarithmic distribution appears, is excluded from further analyses.

Interferograms taken at the distances 0, 2, and 4 ft. from the lower end of the 0.02-in. wire are reproduced in Fig. 7. Fig. 7(a) is a typical interferogram of an axisymmetric free-convection density field at 2 ft. and may be compared with the turbulent field, Fig. 7(c). Fig. 7(b), which is that near the lower end, indicates negligible overheating in the lead wire. The result of the analysis of Fig. 7(a) is plotted in Fig. 8.

The logarithmic temperature distribution, Eq. (19), is shown to agree with the experimental results very well both in Fig. 6 (rod) and Fig. 8 (wire). This is particularly true for the free-convection field over the thin wire; the entire profile is approximately logarithmic. The expectation that the approximate logarithmic expression of temperature distribution would be increasingly accurate with increasing thermal-layer thickness is thus confirmed. A similar expectation indicated by Glauert and Lighthill must also be true in the axisymmetric laminar boundary layer along a thin cylinder.

It is then easy to estimate the wall temperature by extrapolation. The wall-temperature distribution along the cylinder is fairly uniform. The ambient temperature is determined as the minimum reading of the temperature profile.

Temperature readings are then converted into the dimensionless quantity $\theta = (T - T_a)/(T_w - T_a)$. Some of the results are plotted against the two-dimensional y parameter η in Fig. 9 in comparison with the flat-plate solution. It is seen that the thermal layer in the axisymmetric case is much narrower than that along a flat plate. Consequently, the local heat transfer must be far larger than that in the two-dimensional case. The effect of strong transverse curvature on the temperature distribution is more clearly shown in Fig. 10, in which the dimensionless temperature profile is plotted against the axisymmetric y parameter η^*. In the thick axisymmetric free-convection layers with which we are concerned, the zeroth or even the first approximation of the Sparrow-Gregg solution is not sufficient.

The local heat-transfer coefficient $1/\alpha$ is obtained from the slope of the logarithmic profile. Experimental results are shown in Fig. 2 in comparison with the theories, demonstrating excellent agreement with the Pohlhausen solution (recommended curve). Since the theory developed is analogous to that by Mark and by Glauert and Lighthill, the validity of the Pohlhausen solution of the axisymmetric laminar boundary layer may also be justified.

The temperature profile over the 1/4-in. rod deviates from the logarithmic distribution as it approaches the outer edge of the thermal layer (Fig. 6), although the deviation is hardly discernible in the thermal layer over thinner wire. On the other hand, the logarithmic formula

$$(T_w - T)/(aq/k) = \ln [(y + a)/a] \qquad (35)$$

which is equivalent to Eq. (19), reminds us of the law of the wall in turbulent boundary-layer flow. In fact, Glauert and Lighthill have noted the resemblance of the axisymmetric laminar boundary layer to the turbulent boundary layer. Since the inner law Eq. (35) is the counterpart of the law of the wall, a pertinent counterpart of the velocity-defect law, if it exists, might be expressed by the following form:

$$\frac{(T_w - T_a) - (T_w - T)}{aq/k} = \frac{T - T_a}{aq/k} = fn\left(\frac{y + a}{\delta + a}\right) \qquad (36)$$

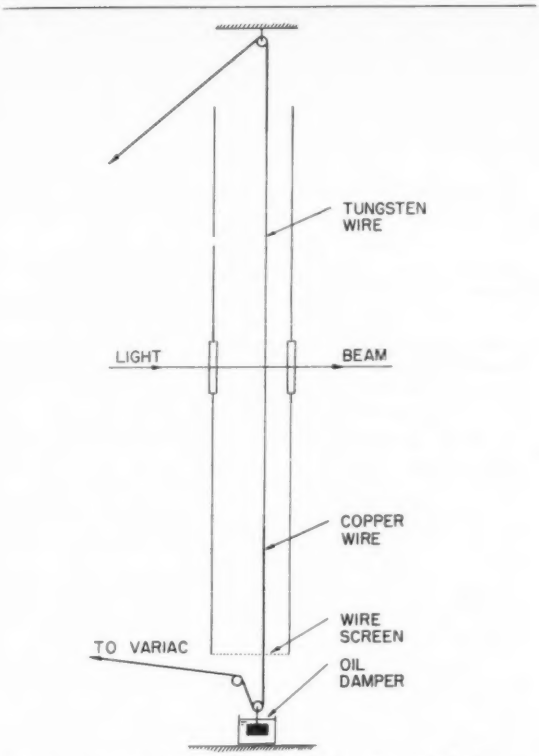

FIG. 5. General arrangement of 0.02-in. wire experiment.

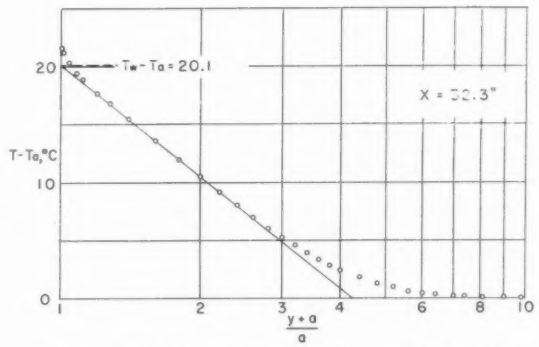

FIG. 6. Typical temperature profile near 1/4-in. rod.

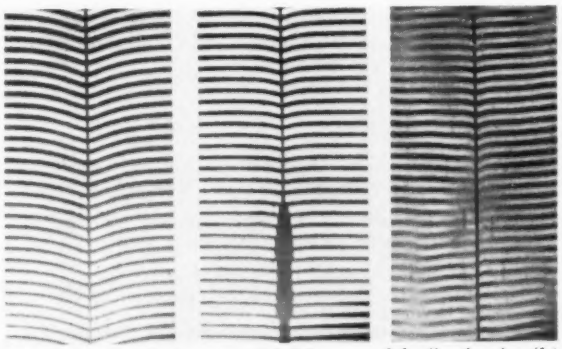

FIG. 7. Interferograms. (a) *left*, $x = 2$ ft. (laminar). (b) *center*, near the lower end of wire. (c) *right*, $x = 4$ ft. (turbulent).

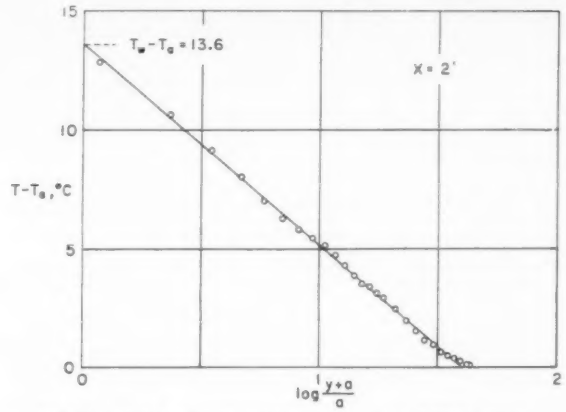

FIG. 8. Typical temperature profile near 0.02-in. wire.

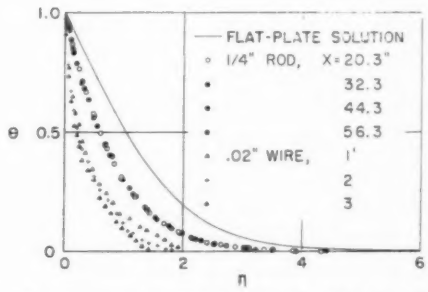

FIG. 9. Temperature profiles compared with the flat-plate solution.

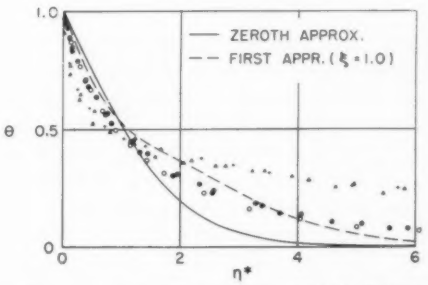

FIG. 10. Temperature profiles compared with the Sparrow-Gregg zeroth and first approximation (for symbols, see Fig. 9).

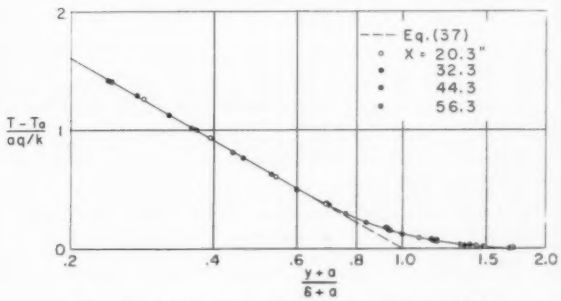

FIG. 11. Outer law of the temperature profile.

which should approach, for small values of y,

$$(T - T_a)/(aq/k) = -\ln [(y + a)/(\delta + a)] + \text{const.} \quad (37)$$

so as to yield Eq. (35). By use of the thermal-layer thickness defined by Eq. (20) the temperature distribution is rearranged in Fig. 11. The universal relation Eq. (36) is indeed found to exist. Therefore, an outer law of the velocity distribution similar to Eq. (36) might be expected in thick axisymmetric laminar boundary layers.

Unlike the turbulent boundary layer, however, the merit of establishing the two laws is not significant. The already known relation Eq. (21) is re-established. Nevertheless, the outer law renders a semiempirical formula of the integrated thermal area

$$\Theta/\pi a^2 = (1/2\alpha)\,(e^{2\alpha} - 1) - 1 + 0.100(e^{2\alpha}/\alpha) \quad (38)$$

This formula should be quite accurate for thick thermal layers and can be looked upon as a higher-order asymptotic solution. It is, therefore, particularly useful in examining the validity of the adjustment procedure applied to the Pohlhausen solution. Fig. 3 shows perfect agreement between the adjusted Pohlhausen approximation and the semiempirical formula. Thus the adjustment procedure proposed in the Section entitled "THEORY" appears to be justified. Experimental results of the integrated thermal area agree with the recommended curve and, of course, with the semiempirical formula. Consequently, the displacement area and the momentum area calculated by Glauert and Lighthill may also be trusted, although their adjustment procedure seems to require a revision.

CONCLUSION

Through the study of the axisymmetric free-convection temperature field along a vertical thin cylinder, the behavior of thick axisymmetric laminar boundary layers is investigated experimentally. Although the approach taken in the present investigation is indirect, the existing theories of thick axisymmetric boundary layers, both the exact and the approximate, are verified.

REFERENCES

[1] Hama, F. R., and Recesso, J. V., *The Axisymmetric Free-Convection Temperature Field Along a Vertical Thin Cylinder*, Univ. of Maryland, Inst. Fluid Dynamics & Appl. Math., TN BN-116, January, 1958.

[2] Hama, F. R., and Christiaens, J., *Experiment on the Axisymmetric Free-Convection Field Along a Vertically-Suspended Wire*, Univ. of Maryland, Inst. Fluid Dynamics & Appl. Math., TN BN-138, May, 1958.

[3] Seban, R. A., and Bond, R., *Skin-Friction and Heat-Transfer Characteristics of a Laminar Boundary Layer on a Cylinder in Axial Incompressible Flow*, Journal of the Aeronautical Sciences, Vol. 18, No. 10, pp. 671–675, October, 1951.

[4] Kelly, H. R., *A Note on the Laminar Boundary Layer on a Circular Cylinder in Axial Incompressible Flow*, Journal of the Aeronautical Sciences, Vol. 21, No. 9, p. 634, September, 1954.

[5] Cooper, R. D., and Tulin, M. P., *The Laminar Flow About Very Slender Cylinders in Axial Motion, Including the Effect of Pressure Gradients and Unsteady Motions*, David Taylor Model Basin, Rep. 838, NS 715-102, April, 1953.

[6] Glauert, M. B., and Lighthill, M. J., *The Axisymmetric Boundary Layer on a Long Thin Cylinder*, Proc. Roy. Soc. (London) Series A, Vol. 230, No. 1181, pp. 188–203, June, 1955.

[7] Stewartson, K., *The Asymptotic Boundary Layer on a Circular Cylinder in Axial Incompressible Flow*, Quart. Appl. Math., Vol. 13, No. 2, pp. 113–122, July, 1955.

[8] Mark, R. M., *Laminar Boundary Layers on Slender Bodies of Revolution in Axial Flow*, GALCIT, Hypersonic Res. Proj. Memo. 21, July, 1954.

[9] Richmond, R. L., *Experimental Investigation of Thick Axially Symmetric Boundary Layers on Cylinders at Subsonic and Hypersonic Speeds*, GALCIT, Hypersonic Res. Proj. Memo. 39, June, 1957.

[10] Schmidt, E., and Beckmann, W., *Das Temperatur- und Geschwindigkeitsfeld vor einer Waerme abgebenden senkrechten Platte bei natuerlicher Konvektion*, Tech. Mech. Thermodyn., Vol. 1, No. 10, pp. 341–349; No. 11, pp. 391–406, 1930.

[11] Ostrach, S., *An Analysis of Laminar Free-Convection Flow and Heat Transfer About a Flat Plate Parallel to the Direction of the Generating Body Force*, NACA TN 2635, February, 1952 (superseded by Rep. 1111, 1953).

[12] Eckert, E. R. G., and Soehngen, E. E., *Studies on Heat Transfer in Laminar Free Convection with the Zehnder-Mach Interferometer*, Air Material Command, Tech. Rep. 5747, December, 1948.

[13] Sparrow, E. M., and Gregg, J. L., *Laminar Free-Convection Heat Transfer from the Outer Surface of a Vertical Circular Cylinder*, Trans. ASME, Vol. 78, No. 8, pp. 1823–1829, November, 1956.

[14] Carey, B. B., *Optical Study of Two-Dimensional Jet Mixing of Compressible Fluid*, Univ. of Maryland, Ph.D. thesis, 1954.

[15] Gooderum, P. B., and Wood, G. P., *Density Fields Around a Sphere at Mach Numbers 1.30 and 1.62*, NACA TN 2173, August, 1950.

Tenth International Congress of Applied Mechanics

Stresa, Italy, August 31–September 7, 1960

Apart from a number of invited general lectures, the technical sessions of the Congress will be held in two sections: Fluid dynamics (hydrodynamics and aerodynamics); and Mechanics of solids (rigid body dynamics, vibrations, elasticity, plasticity, and theory of structures).

It should be noted that thermodynamics and computational methods as such are not included, although specific applications of computational methods to pertinent problems of one of the two sections stated above are acceptable subjects for presentation.

Abstracts should be submitted before January 1, 1960 to: *The Secretary of the International Committee, Prof. Mekelweg 2, Delft, Netherlands.* Abstracts, in four copies, should not exceed two typewritten pages (double-spaced). It is recommended that abstracts be in two of the official Congress languages (English, French, German, and Italian).

All correspondence, apart from submission of papers, should be addressed to: *The Italian Organizing Committee, Consiglio Nazionale delle Ricerche, Ufficio relazioni internazionali, Piazza delle Scienza 7, Roma.*

Relaxation Characteristics of Pneumatic Tires

JOHN ERWIN STEVENS*
Chance Vought Aircraft, Inc.

SUMMARY

The behavior of a pneumatic tire as it is rolled forward after the wheel has been initially moved laterally a given distance, or is initially turned to a given angle around the vertical axis, demonstrates the relaxation characteristics of a tire. These characteristics result in the initial side force and/or torque on the wheel, which have been imposed by the initial displacements of the tire to be relieved if the wheel is rolled a sufficient distance. In the present paper, a differential equation is developed which describes the relaxation behavior of a tire in terms of simple tire parameters. The derivation of the differential equation is believed to be original in this paper. The cornering behavior of a tire, which allows a wheel to move sideways without skidding as it moves forward under the influence of a constant side load, is described with the same differential equations. The lateral spring rate and the torsional spring rate of the tire are derived.

Tire relaxation and cornering characteristics are important in the wheel shimmy problem and for determining the motion, and hence the forces, on a wheeled vehicle during ground handling.

SYMBOLS

T' = total tension in the tire walls normal to a section through the tire
T = tension in the running band
k = $k(0)$ = lateral spring rate of the tire per unit length along the running band except above the footprint
$k(\delta/W)$ = lateral spring rate per unit length along the tire above the footprint
R = radius of the tire
r = minor radius of the toroid assumed for the tire
h = semilength of the footprint
K_1 = lateral spring rate of the tire
K_t = part of the lateral spring rate due to the tension in the running band
K_k = part of the lateral spring rate due to the tire walls above the footprint
δ = vertical deflection of the tire wall along the footprint
δ_0 = maximum vertical deflection of the tire wall above the footprint
Δ = average lateral displacement of the footprint relative to the wheel center plane
Δ_F = lateral displacement of the footprint at its leading edge relative to its undeflected position
Δ_R = lateral displacement of the running band other than above the footprint
S = lateral slope of the running band at the footprint leading edge
K = lateral slope of the running band at the footprint leading edge per unit lateral displacement of the footprint leading edge
p = pressure in the tire
p_0 = pressure in the tire with no load on the footprint
T_t = transverse tension in the tire wall
D = diameter of the running band
W = width of the tire
W_r = width of the wheel rim
$B[(W_r)/W]$ = Lateral nondimensional slope coefficient for running band at the footprint leading edge
$E[(W_r)/W] = k/p$
$G[(W_r)/W] = K_t/2pw$

$$F\left(\frac{W_r}{W}, \frac{\delta_0}{W}\right) = \int_0^{1.0} \frac{k(\delta/W)}{p}\, d\left(\frac{s}{h}\right)$$

$$H\left(\frac{W_r}{W}, \frac{\delta_0}{W}\right) = \int_0^{1.0} \frac{k(\delta/W)}{p}\left(\frac{s}{h}\right)^2 d\left(\frac{s}{h}\right)$$

σ = cornering angle
y = lateral displacement of the wheel plane

Received June 9, 1958. Revised and received February 9, 1959.

* Assistant Chief of Structures.

INTRODUCTION

IT IS THE PURPOSE of this paper to develop the differential equations required to define the relaxation behavior of pneumatic tires and, in addition, equations which will define the forces and moments applied to the wheel through the tire during the relaxation process. A simplified model will be used which results in defining the force and relaxation coefficients required in terms of readily available tire parameters. Relaxation is defined as the characteristics of a pneumatic tire which allows a tire initially subjected to a lateral displacement, or an initial twist, to unload the portion of the tire in contact with the ground without skidding, if the wheel is rolled sufficiently far. Relaxation is related to the cornering characteristics of a tire. Cornering can be described as the behavior of a wheel subjected to a constant side force which allows the wheel to move laterally as the wheel moves forward without skidding the tire. An understanding of the relaxation behavior of tires, as well as their cornering behavior, is necessary to assess properly the effects of pneumatic tires on shimmy of castering wheels and for defining the ground handling behavior of airplanes when being steered by power steering systems, or when being towed by a catapult. A knowledge of cornering characteristics is necessary to define the side load on a landing gear during a side drift landing after spin-up has been accomplished.

The relaxation characteristics of tires have been studied most often by investigators studying shimmy of castering wheels. In most cases, these investigators have relied largely on experimental data to define the behavior of tires. Kantrowitz[1] used experimental data to establish the differential equations that he used to define the behavior of tires. In reference 2, de Carbon assumed that the portion of the tire which could contact the ground, or the running band, was made up of a series of independent springs which deflected when a side load was applied to a tire. He used this model to explain the relaxation behavior of tires. However, like Kantrowitz, he used experimental data to obtain the coefficients for the differential equation to define the

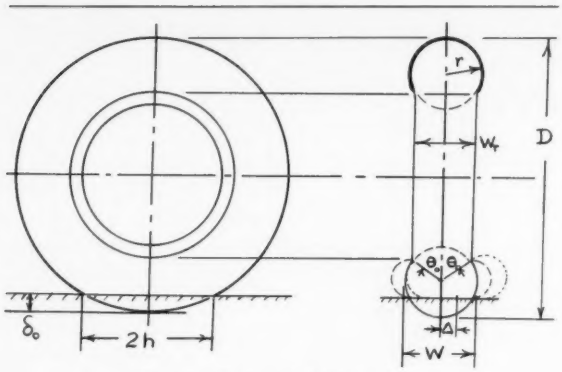

FIG. 1. Geometric information.

behavior of the tire. Rotta's model was similar to that used by de Carbon in his work as described in reference 5, but, unlike de Carbon, he derived an expression for the lateral running spring rate in terms of the tire dimensions and servicing pressure. Thorson, in reference 3, set out to define the cornering characteristics as well as the lateral stiffness and torsional stiffness of the tire. He was primarily concerned with the asymptotic behavior of tires subjected to side loads and torsional moments and did not define all the parameters of interest for relaxation. His model was essentially complete, as he assumed that, for lateral motion of the running band of the tire, the running band could be assumed to be a beam under tension restrained against lateral motion by a continuous spring. He solved the differential equation in the running band for appropriate boundary conditions and defined the tension in the running band and the lateral continuous spring rate of the tire in terms of the tire pressure and the tire geometry. With his theory, he was able to show a good correlation between theory and experimentally determined equilibrium cornering and stiffness parameters. Thorson's theory requires a knowledge of the section properties of the tire running band.

The present theory makes use of a model of the tire simpler than that of Thorson and basically the same as that used by Temple and Von Schlippe to describe the behavior of a relaxing tire.[5] These authors used experimental results to define the coefficients required and did not attempt to derive analytical expressions for the coefficients as is done here. The tire running band away from the footprint is assumed to be under tension, T, and restrained from lateral displacement by a continuous spring of spring rate, k, per unit of arc length along the running band. In this theory, k is derived using assumptions similar to those used by Rotta in his derivation as described in reference 5. The bending stiffness of the running band is neglected. Fig. 1 and Fig. 2 can help in visualizing the model.

A differential equation for the relaxation behavior of a tire is derived, making use of the simple model defined above. The relaxation coefficients and stiffness coefficients resulting from this theory are in a form useful for shimmy analysis and in terms of tire parameters which are easily available to the analyst.

Lateral Spring Rate of the Tire

It will be assumed that lateral spring rate and the torsional stiffness of the tire can be evaluated with the tire and that no skidding occurs between the ground and the tire. The model for the tire used in this theory assumes that the running band is a string under tension, T, with no lateral bending stiffness. The string is restrained against lateral motion by a continuous spring with a spring rate, k, per unit arc length along the running band. The model is used for the entire running band with the exception of the portion of the arc defined by ground contact. The footprint is assumed to be of length $2h$. Fig. 2 gives a sketch of this model.

When a side force is applied to a wheel-tire combination, it is reacted by an equal force through friction between the tire and the ground. Forces are transferred to the ground in two ways: first, by the lateral deflection of the tire walls adjacent to and above the footprint, and, second, by reacting the component of tension of the running band which results from the lateral displacement of the footprint with respect to the wheel centerline. The total spring rate K_1 can then be written as the sum of the spring rate K_t due to the running band and the lateral spring rate of tire wall above the footprint K_k. We can then write the total spring rate as

$$K_1 = K_t + K_k \tag{1}$$

K_k and K_t will be derived in terms of tire parameters.

The differential equation for the lateral displacement of the running band, except along the footprint, can be written as

$$T(d^2\Delta_R/ds^2) - k\Delta_R = 0 \tag{2}$$

where s is measured along the running band. The

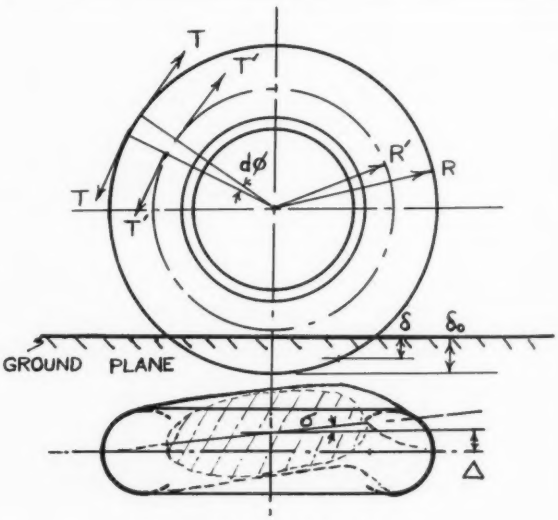

FIG. 2. Sketch of deflected tire.

solution to this differential equation has the form

$$\Delta_R = A \cosh \sqrt{k/T}s + B \sinh \sqrt{k/T}s \qquad (3)$$

The boundary conditions are: at $s = h$, $\Delta_R = \Delta_F$ while at $s = \pi R$, $\Delta_R = 0$ if the displacements are antisymmetric, or if the displacements are symmetric at $s = \pi R$, $d\Delta_R/ds = 0$. It can be shown that, for the range of tire dimensions usually found, the boundary conditions at $s = \pi R$ are of no importance since

$$\cosh \sqrt{k/T}\,\pi R \approx \sinh \sqrt{k/T}\,\pi R$$

The slope at the leading edge of the footprint is

$$\frac{d\Delta_R}{ds} = -S = \Delta_F \sqrt{\frac{k}{T}} \left\{ - \frac{\cosh \sqrt{k/T}\,(\pi R - h)}{\sinh \sqrt{k/T}\,(\pi R - h)} \right\} \qquad (4)$$

If we simplify, assuming that $\sqrt{k/T}(\pi R - h)$ is large,

$$S \approx \sqrt{k/T}\,\Delta_F = K\,\Delta_F \qquad (5)$$

Our next step is to define k and T in terms of the dimensions of the tire and the servicing pressure. If we assume that the tire is a toroid of major radius R' and minor radius r, the total tension normal to the radius vector R' can be written as

$$T' = 2p \int_0^{\pi} (R'r \cos\theta + r^2 \cos^2\theta) d\theta = \pi r^2 p \qquad (6)$$

The total tension T' is assumed not to be the force which takes part in the differential equation for the lateral behavior of the running band since the rim of the wheel will restrict the lateral motion of the tire at the wheel rim to zero. To obtain an effective tension, T, we will assume that the lateral displacement of the tire varies linearly from zero at the rim to Δ_R at the running band and this linear displacement will be used to weigh the contribution of the tension in the toroid.

The rim is defined by the angle θ_0 as indicated in Fig. 1. The effective tension can then be expressed as

$$T = pr^2 \int_{\theta_0}^{\pi} \frac{(\cos\theta - \cos\theta_0)^2}{(1 + \cos\theta_0)^2}\, d\theta$$

or

$$T = pr^2 \frac{[(\pi - \theta_0)\,(1 + 2\cos^2\theta_0) + 3\cos\theta_0 \sin\theta_0]}{2(1 + \cos\theta_0)^2} \qquad (7)$$

The lateral spring rate of the tire, k, per unit arc length, s, along the running band and the spring rate per unit length along the footprint can be derived simultaneously. In the case of the lateral running spring rate on the running band, the vertical deflection of the tire, δ, is zero. To derive k, we will assume that the tire section is a cylinder with no wall stiffness so that the only stresses are membrane stresses. The transverse tension in the cylinder wall, per unit length of cylinder, will then be $T_t = pr$. If we apply a side load at the running band, the tire will deflect laterally an amount Δ and a resisting force equal to the applied side force will be developed as a consequence of the changes in tension on the two sides of the cylinder as the radius of curvature of each side of the cylinder changes—i.e., to a smaller value on the side of the cylinder towards the displacement and to a larger value on the side away from the displacement. If the tire is deflected an amount, δ, due to contact with the ground, the radius, r, is reduced and, hence, the transverse tension, T_t, is reduced. If we consider small motions,

$$k = 2(dT_t/d\Delta) \qquad (8)$$

If we note that, at a given servicing pressure, the radius of curvature of the cylinder must change if the tension is to change, and note that the cylinder is restrained at θ_0, we can derive an expression for $k(\delta/W)$. The assumptions used in this derivation for k are similar to the ones used by Rotta in his derivation of the lateral spring rate of a tire described in reference 5.

$$k\left(\frac{\delta}{W}\right) = \frac{p[\sin\theta_0 - 2\sqrt{(\delta/W) - (\delta/W)^2}]}{\left[\sin\frac{(\pi - \theta_0)}{2} - \frac{(\pi - \theta_0)}{2}\cos\frac{(\pi - \theta_0)}{2}\right]\sqrt{(2 + 2\cos\theta_0) - 4\cos\theta_0\,\frac{\delta}{W} - 4\sin\theta_0\sqrt{\frac{\delta}{W} - \left(\frac{\delta}{W}\right)^2}}} \qquad (9)$$

In evaluating Eq. (9), use can be made of reference 4, which shows that

$$p = p_0[1 + 1.5(W/D)\,(\delta_0/W)^2] \qquad (10)$$

θ_0 can be defined in terms of the tire width, W, and width of the wheel rim, W_r.

$$W_r/W = \sin\theta_0 \qquad (11)$$

When δ/W is allowed to go to zero, $k(\delta/W)$ becomes $k(0)$ which is by definition equal to k. Eq. (12) defines k.

$$k(0) = k = \frac{p \sin\theta_0}{\sqrt{2 + 2\cos\theta_0}\,\{\sin[(\pi - \theta_0)/2] - [(\pi - \theta_0)/2]\cos[(\pi - \theta_0)/2]\}} = pE\left(\frac{W_r}{W}\right) \qquad (12)$$

From Eq. (9) it is interesting to note that the running lateral spring rate reduces as δ/W increases.

The slope coefficient, K, which defines the slope of the running band at the leading edge of the footprint in terms of the deflection at the footprint leading edge, Δ_F, can now be expressed in terms of the tire parameters θ_0 and W, by substituting the values of T and k from Eqs. (7) and (12), respectively, into $K = \sqrt{k/T}$.

$$K = \left.\sqrt{\frac{8 \sin\theta_0(1+\cos\theta_0)^2}{W^2\sqrt{2+2\cos\theta_0}\left[\sin\frac{(\pi-\theta_0)}{2} - \frac{(\pi-\theta_0)}{2}\cos\frac{(\pi-\theta_0)}{2}\right][(\pi-\theta_0)(1+2\cos^2\theta_0)+3\cos\theta_0\sin\theta_0]}}\right\} = B(W_r/W)/W \quad (13)$$

We now have sufficient information to define K_t, which is the contribution to the lateral spring rate due to the part of the tire away from the footprint. The tension in the running band is known from Eq. (7) and the slope of the running band is defined by Eq. (13).

$$K_t = 2p\left.\sqrt{\frac{W^2\sin\theta_0[(\pi-\theta_0)(1+2\cos^2\theta_0)+3\sin\theta_0\cos\theta_0]}{8(1+\cos\theta_0)^2\sqrt{2+2\cos\theta_0}\{\sin[(\pi-\theta_0)/2]-[(\pi-\theta_0)/2]\cos[(\pi-\theta_0)/2]\}}}\right\} = 2p_0[1+1.5(W/D)(\delta_0/W)^2]WG(W_r/W) \quad (14)$$

K_k, which is the contribution to the tire lateral spring rate due to lateral deflection of the tire wall above the footprint, can be calculated making use of the relationship between $k(\delta/W)$ and (δ/W) defined in Eq. (9).

We can then define an integral for K_k.

$$K_k = 2phF[(\delta_0/W), (W_r/W)] = 2ph\int_0^{1.0}[k(\delta/W)/p]d(s/h) \quad (15)$$

If we assume that $\delta/W = (\delta_0/W)[1-(s/h)^2]$, it is possible to evaluate the function $F[(\delta_0/W), (W_r/W)]$ for any value of W_r/W. Making use of the experimental data given in reference 4,

$$h \leftrightarrows 0.85\sqrt{(\delta_0/D)-(\delta_0/D)^2} \quad (16)$$

The lateral spring rate of a tire can then be written as follows in terms of the parameters W_r/W, W/D, δ_0/W, and p by adding Eqs. (14) and (15).

$$K_1 = 2p_0D[1+1.5(D/W)(\delta_0/D)^2]\{(W/D)G(W_r/W)+0.85\sqrt{(\delta_0/D)-(\delta_0/D)^2}\,F[(\delta_0/W),(W_r/W)]\} \quad (17)$$

The function $F[(\delta_0/W), (W_r/W)]$ is plotted in Fig. 3 for the values of W_r/W equal to 0.90 and 0.95. It should be noted that, for a given W/D, δ_0/D and δ_0/W are proportional. For $W_r/W = 0.90$ for various values of W/D, K_1/p_0W is plotted vs. δ_0/D in Fig. 4. The value of $W_r/W = 0.90$ gives results which seem to check with experimental results for type VII tires when the service pressure is near the rated pressure. For type I or type III tires a larger value of W_r/W is necessary. On Fig. 4 the results of Eq. (17) are compared with the best fit curve of experimental data presented as Eq. (33) in reference 4. Eq. (33) of reference 4, for type VII tires, is $K_1 = K_\lambda = 2W(p+0.24\,p_r)\times[1-0.7(\delta_0/W)]$. In the comparison on Fig. 4, p_r is assumed to be equal to p. p_r is defined as the rated pressure of the tire and would be a constant for any particular tire. This term is included to allow for the effects of tire wall stiffness. Naturally, as service pressure is increased this term becomes less important. Eq. (33) of reference 4 is a best fit straight line to measured values and it cannot be expected to be correct over the entire range of tire vertical deflections. Eq. (17) gives values for K_1 which compare with these test data as well as the best fit curve.

Torsional Stiffness of the Tire at Rest

Using the same reasoning used in developing the lateral spring rate in the previous section, the torsional stiffness can be developed. As in the lateral stiffness case, the torsional stiffness can be considered to come from two effects—i.e., the tension in the running band and the deflection of the tire wall above the footprint. We can then write

$$K_2 = 2ph^3\int_0^{1.0}[k(\delta/W)/p](s/h)^2d(s/h) + 2ph^2WG(W_r/W) = 2p_0[1+1.5(D/W)(\delta_0/D)^2]D^3\{0.614[(\delta_0/D)-(\delta_0/D)^2]^{3/2}H[(\delta_0/W),(W_r/W)] + 0.72(W/D)[(\delta_0/D)-(\delta_0/D)^2]G\} \quad (18)$$

here

$$H[(\delta_0/W), (W_r/W)] = \int_0^{1.0}[k(\delta/W)/p](s/h)^2\,d(s/h) \quad (19)$$

$H[(\delta_0/W), (W_r/W)]$ can be evaluated similarly to $F[(\delta_0/W), (W_r/W)]$ if we assume that $\delta/W \approx (\delta_0/W)\times[1-(s/h)^2]$. For values of W_r/W equal to 0.90 and 0.95, $H[(\delta_0/W), (W_r/W)]$ is plotted vs. δ_0/W in Fig. 5. In Fig. 6, K_2/p_0W^3 is plotted vs. δ_0/D for various values of W/D for a value of $W_r/W = 0.90$. A comparison with the best fit of experimental data given as Eq. (45) in reference 4 is also presented. Eq. (45) of reference 4 is

$K_2 = K_\alpha = 19W^3(p+0.8pr)[(\delta_0/D) - 0.01]$ for $\delta_0/D \geqq 0.02$

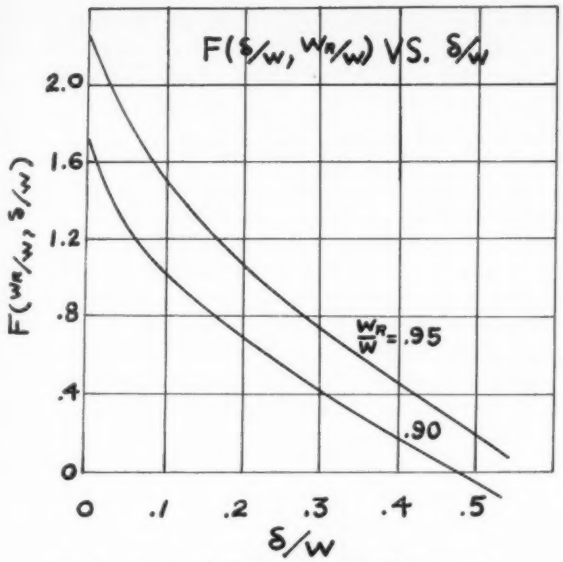

FIG. 3. NOTE: δ/W should read δ_0/W in all cases.

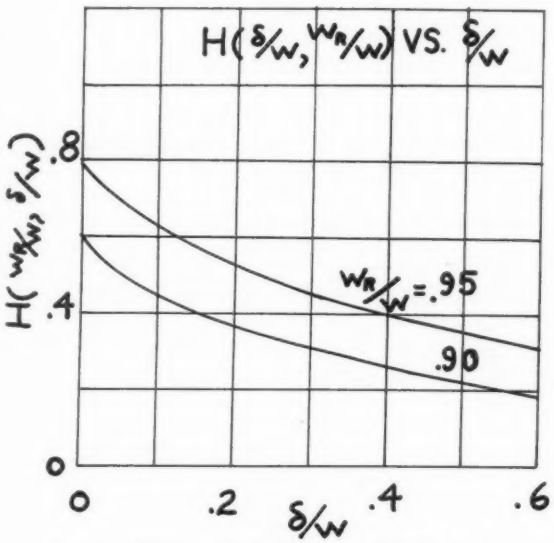

FIG. 5. NOTE: δ/W should read δ_0/W in all cases.

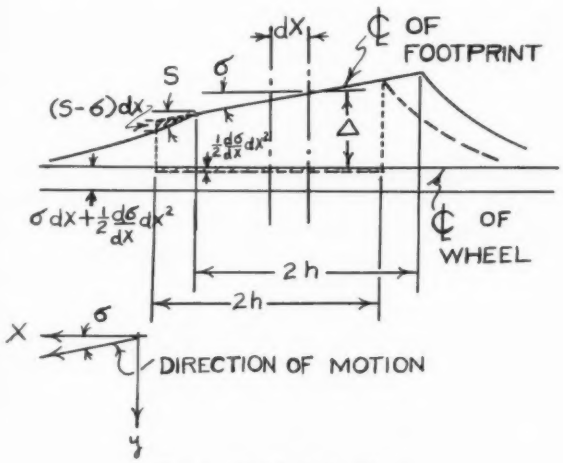

Fig. 7. Model of relaxation.

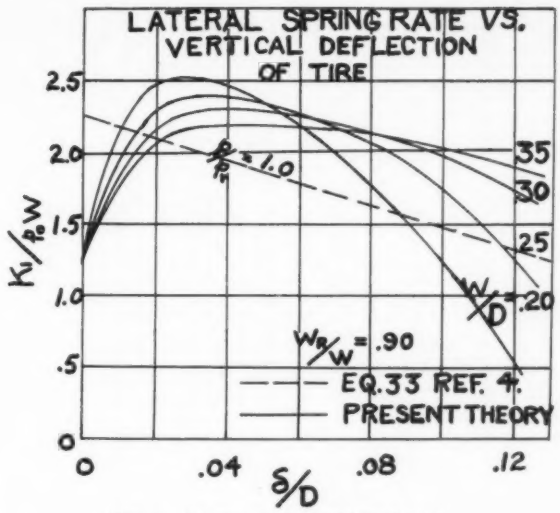

FIG. 4. NOTE: δ/D should read δ_0/D

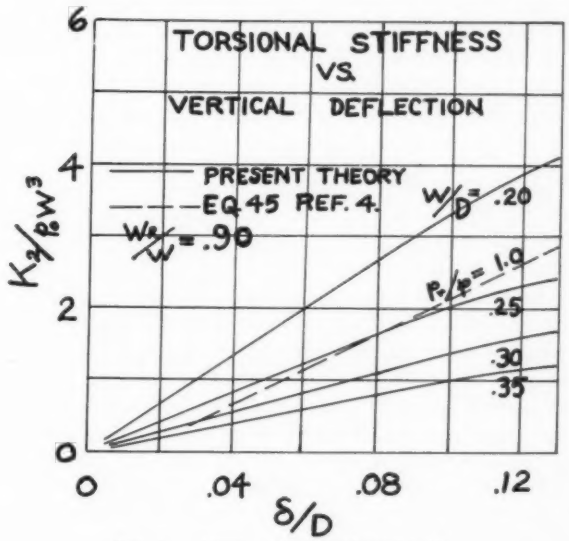

FIG. 6. NOTE: δ/D should read δ_0/D.

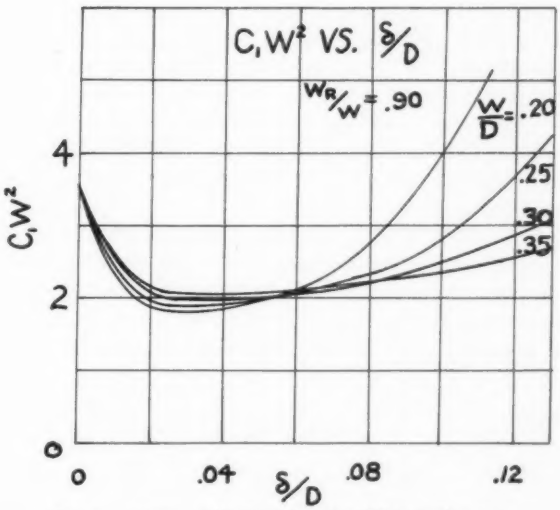

FIG. 8. NOTE: δ/D should read δ_0/W in both cases.

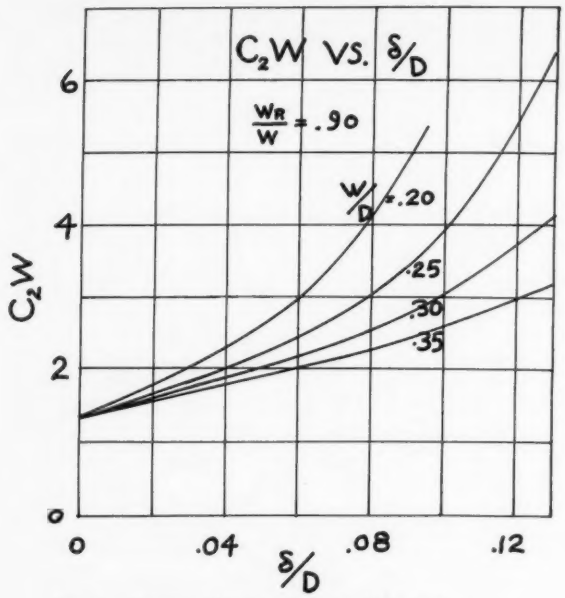

FIG. 9. NOTE: δ/D should read δ_0/D in both cases.

DEVELOPMENT OF DIFFERENTIAL EQUATIONS FOR RELAXATION

As a first step in developing the differential equation for the relaxation of a tire, it is convenient to first define the differential equation for cornering, which is in a sense the reverse of relaxation. In the relaxation situation, the wheel is initially displaced either laterally or twisted so the footprint of the tire is deformed. The wheel is then held securely as it is allowed to roll forward. Under these conditions the side force and torque transmitted to the wheel from the ground, as a result of the deformed tire, will reduce to zero if the wheel is rolled forward far enough. In the cornering situation, a constant side force is applied to the wheel and the wheel is restrained against torsion. The side force is resisted by the tire so the wheel will shift laterally as the tire deforms. If the wheel is then allowed to roll forward, the wheel will move sideways as it rolls forward without skidding the tire. The angle between the path the wheel takes under the action of the side load and the path which it would have taken under no side load is called the cornering angle. When a side force is applied, the cornering does not take place immediately but comes on exponentially to the asymptotic cornering path for a given side load.

To define the change in cornering angle with forward progress as a wheel is subjected to a side load, up until the asymptotic cornering angle is reached, the following reasoning will be used. If a wheel-tire combination is subjected to a side load, the wheel is pulled laterally with respect to the footprint of the tire by an amount Δ. The lateral displacement of the centerline of the wheel relative to the footprint leading edge results in giving the running band a slope of magnitude S at the footprint leading edge which will be proportional to the leading-edge lateral deflection Δ_F. As the wheel progresses forward, the side force tends to be relieved as the deflection at the footprint leading edge is reduced by an amount determined by the slope of the running band at the footprint leading edge. Since the side force is a constant in the cornering situation, the differential relieving of the side force at the leading edge is accompanied by a differential lateral displacement of the wheel plane such that the side force remains constant as the wheel progresses forward a differential amount. When the cornering angle of the wheel equals the running band slope, S, an equilibrium cornering angle is reached. The differential equation for cornering is derived by equating the differential side force change at the leading edge due to a differential forward motion to the side force resulting from a differential cornering angle change. This can be visualized by looking at Fig. 7.

$$(S - \sigma)k(dx^2/2) = K_1(d\sigma/dx)\ (dx^2/2)$$

or
$$d\sigma/dx = (S - \sigma)k/K_1 \tag{20}$$

By making use of Eq. (5), S can be defined in terms of Δ_F and Eq. (20) can be rewritten

$$(d\sigma/dx) + (k/K_1)\,\sigma = (k/K_1)\,S = (kK/K_1)\,\Delta_F \tag{21}$$

Δ_F can be written in terms of the lateral deflection of center of the footprint, Δ, and the cornering angle. It will be assumed that the footprint lateral displacement can be defined by use of a Taylor series where only the first term is used.

$$\Delta_F \backsimeq \Delta - h\sigma \ldots \tag{22}$$

Then, when Eq. (22) is introduced into Eq. (21),

$$(d\sigma/dx) + (k/K_1)\,(1 + hK)\sigma = (kK/K_1)\Delta \tag{23}$$

Eq. (23) is the basic equation for cornering of a tire. When Eq. (23) is combined with an equation defining the lateral motion of the wheel without skidding, the behavior of a relaxing tire is defined. The no skid equation is

$$dy/dx = (d\Delta/dx) + \sigma \tag{24}$$

In Eq. (24), dy/dx defines the lateral motion of the wheel, $d\Delta/dx$ defines the lateral motion of the wheel with respect to the tire footprint, and σ defines the lateral motion due to cornering.

For convenience Eq. (23) is rewritten as follows:

$$(d\sigma/dx) + C_2\sigma = C_1\Delta \tag{25}$$

where
$$C_1 = \frac{E(W_r/W)B(W_r/W)}{2W^2(D/W)\left\{(W/D)G(W_r/W) + 0.85\sqrt{(\delta_0/D) - (\delta_0/D)^2}\,F[(\delta_0/W),\ (W_r/W)]\right\}} \tag{26}$$

$$C_2 = \frac{E(W_r/W)\left[1 + (D/W)B(W_r/W)\,0.85\sqrt{(\delta_0/D) - (\delta_0/D)^2}\right]}{2W(D/W)\left\{(W/D)G(W_r/W) + 0.85\sqrt{(\delta_0/D) - (\delta_0/D)^2}\,F[(\delta_0/W),\ (W_r/W)]\right\}} \tag{27}$$

Figs. 8 and 9 show how $W^2 C_1$ and $W C_2$ vary with δ_0/D for various values of D/W for the value of $W_r/W = 0.90$, which seems to approximate a type VII tire.

Relaxation of a Tire

Now that the differential equations defining the rolling behavior of tires have been derived, the differential equation which defines the relaxation behavior of a tire-wheel combination where the wheel is initially displaced laterally with respect to the footprint can be defined. In this case, the wheel is initially displaced relative to the footprint, then held rigidly and allowed to roll forward. The side force on the wheel will then reduce to zero if the wheel is allowed to roll forward far enough. This behavior gives rise to the term *relaxation*. If the tire is initially twisted, the tire will also relax. From this initial condition where the side force is initially zero, but the initial torque is finite, the side force will initially build up and then reduce to zero if the wheel is allowed to roll far enough.

For the relaxation situation as used here, $dy/dx = 0$; then, from Eq. (24),

$$d\Delta/dx = d(\Delta/W)/d(x/W) = -\sigma \tag{28}$$

If this equation is combined with Eq. (25), the homogeneous differential equation for relaxation becomes

$$[d^2\sigma/d(x/W)^2] + WC_2[d\sigma/d(x/W)] + W^2C_1\sigma = 0 \tag{29}$$

For the relaxation which begins initially with a lateral displacement, the initial conditions are, at $x/W = 0$: $\sigma = 0$, $[d\sigma/d(x/W)] = W^2C_1\Delta_0/W$.
The relaxation equation is then

$$\Delta/\Delta_0 = e^{-\lambda_R(x/W)} [\cos \lambda_I(x/W) + (\lambda_R/\lambda_I)\sin \lambda_I(x/W)] \tag{30}$$

where
$$\lambda_R = WC_2/2$$
$$\lambda_I = \sqrt{W^2C_1 - (WC_2/2)^2}$$

if the roots are complex. If the roots are real,

$$\frac{\Delta}{\Delta_0} = \frac{\lambda_2 e^{\lambda_1 x/W} - \lambda_1 e^{\lambda_2 x/W}}{\lambda_2 - \lambda_1} \tag{31}$$

where

$$\lambda_1 = -(C_2W/2) - \sqrt{(C_2W/2)^2 - C_1W^2}$$
$$\lambda_2 = -(C_2W/2) + \sqrt{(C_2W/2)^2 - C_1W^2}$$

During relaxation the side force obtained from this solution does not follow a simple exponential expression as is usually assumed after examining experimental data. These solutions when plotted, however, look like simple exponential expressions. If the relaxation length is defined as the distance rolled until the amplitude reaches a value equal to $1/e$ of the initial value (even though the solution is not of the type $e^{-\lambda x}$), this theory gives values of relaxation length of magnitude about equal to those found from experimental data.

For the torsional relaxation the initial conditions are, at $x/W = 0$: $\sigma = \sigma_0$, $(d\sigma/d(x/W)) = -C_2W\sigma_0$. This results in the following solution for relaxation for the case of real roots:

$$\frac{\sigma}{\sigma_0} = \frac{(\lambda_2 + WC_2)e^{\lambda_1 x/W} - (\lambda_1 + WC_2)\, e^{\lambda_2 x/W}}{\lambda_2 - \lambda_1} \tag{32}$$

and

$$\sigma/\sigma_0 = e^{-\lambda_R x/W} [\cos \lambda_I(x/W) - (\lambda_R/\lambda_I) \sin \lambda_I(x/W)] \tag{33}$$

for the complex case. If these equations are integrated again, the lateral displacement and, hence, the side force, is defined and can be seen to build up from zero to a finite value before it decays away, as the experimental data also shows.

Cornering Power Coefficient

The cornering behavior of a wheel-tire combination can be determined by putting a side force on a wheel-tire combination and keeping it at a constant level without letting relaxation occur or allowing the wheel to twist. In this case, if the wheel is allowed to roll, the wheel will move laterally as well as forward such that the angle between the path followed by the footprint and the line determined by the wheel plane intersection with the ground varies exponentially to an asymptotic value σ. The differential equation for cornering can be defined by noting that for this case Δ is a constant. This means Eq. (25) can be solved directly. The solution is

$$\sigma = (WC_1/C_2)\ (\Delta/W)\ (1 - e^{-C_1W(x/W)}) \tag{34}$$

After a sufficient distance has been rolled, σ reaches the asymptotic value,

$$\sigma = (WC_1/C_2)\ (\Delta/W) \tag{35}$$

If we note that $P = K_1\Delta$, where P is the side force on the wheel, we can write

$$\sigma = C_1P/C_2K_1 \tag{36}$$

The reciprocal of C_1/C_2K_1 is the parameter usually called the cornering power coefficient. This coefficient defines the magnitude of the side force required for a wheel to assume an asymptotic path with an angle σ with the direction defined by the wheel. The cornering power coefficient from the present theory is plotted in nondimensional form in Fig. 10. A comparison is made with the best fit to experimental data for tires serviced to pressures near their rated pressure as given in Eq. (82) of reference 4. Eq. (82) of reference 4 for type VII tires is

$$C_2K_1/C_1 = N = 57W^2(p + .44p_r) \times [1.2(\delta_0/D) - 8.8(\delta_0/D)^2]; \quad \delta_0/D \leqq 0.0875$$

and

$$C_2K_1/C_1 = N = 57W^2(p + 0.44p_r) \times [0.0674 - 0.34(\delta_0/D)]; \quad \delta_0/D \geqq 0.0875$$

It can be seen in Fig. 10 that the elementary theory

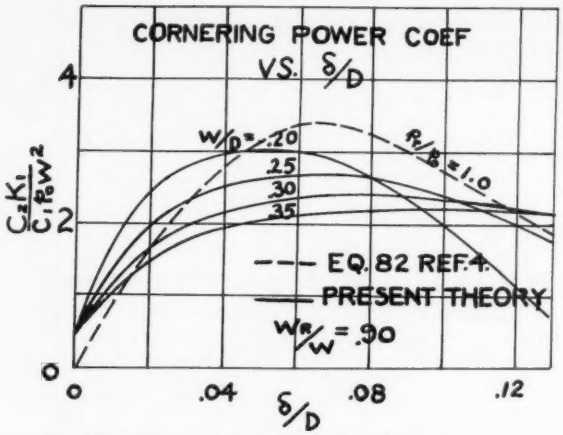

FIG. 10. NOTE: δ/D should read δ_0/D in both cases.

developed gives cornering power coefficients which follow the trends measured in experiments where cornering power is measured as a function of tire vertical deflection.

CONCLUSION

It has been shown that the theory developed for the lateral and torsional spring rates of tires and for the relaxation behavior of tires follows the trends found in experimental data.[4] The theory permits the calculation of the stiffness and relaxation coefficients needed for shimmy analysis and for the behavior of wheels during ground handling situations on airplanes in terms of easily measured tire parameters. A value of W_r/W equal to 0.90 gives results which approximate test data for type VII tires. For type III or type I tires, larger values of W_r/W are required to check experiments.

REFERENCES

[1] Kantrowitz, Arthur, *Stability of Castering Wheels for Aircraft Landing Gears*, NACA Report 686, 1940.

[2] Bourcier de Carbon, Christian, *Analytical Study of Shimmy of Airplane Wheels*, NACA TM 1337, 1952.

[3] Thorson, K. R., *A Rational Method for Predicting Tire Cornering Forces and Lateral Stiffness*, Boeing Doc. No. D-11719, Boeing Airplane Co., March 28, 1951.

[4] Smiley, R. F., and Horne, W. B., *Mechanical Properties of Pneumatic Tires with Special Reference to Modern Aircraft Tires*, NACA TN 4110, January, 1958.

[5] Hadekel, R., *The Mechanical Characteristics of Pneumatic Types*, S and T Memo. No. 5/50, British Ministry of Supply, TPA 3/TIB, March, 1950.

A Theory for the Ablation of Glassy Materials

(*Continued from page 328*)

[4] Fay, J. A., Riddell, F. R., and Kemp, N. H., *Stagnation Point Heat Transfer in Dissociated Air Flow*, Jet Propulsion, Vol. 27, No. 6, June, 1957.

[5] Baron, Judson R., *The Binary-Mixture Boundary Layer Associated with Mass Transfer Cooling at High Speeds*, Massachusetts Institute of Technology, Naval Supersonic Laboratory, Tech. Rept. 160, May, 1956.

[6] Reshotko, E., and Cohen, C. B., *Heat Transfer at the Forward Stagnation Point of Blunt Bodies*, NACA TR 3513, July, 1955.

[7] Fay, J. A., and Riddell, F. R., *Theory of Stagnation Point Heat Transfer in Dissociated Air*, Journal of the Aeronautical Sciences, Vol. 25, No. 2, pp. 73–85, 121, February, 1958.

[8] *Data on Chemicals for Ceramic Use*, NRC Bulletin No. 118, p. 102, June, 1949.

[9] Porter, R. F., Chupka, W. A., and Inghram, M. G., *Mass Spectrometric Study of Gaseous Species in the Si-SiO_2 System*, J. Chem. Phys., Vol. 23, p. 216, 1955.

[10] Lees, Lester, *Convective Heat Transfer with Mass Addition and Chemical Reactions*, Paper presented at Third Combustion and Propulsion Colloquium, AGARD, NATO, Palermo, Sicily, March, 1958.

Notice to Contributors

To expedite review, an additional copy of both the manuscript and figures should be submitted. The manuscript submitted for publication *must* be a double- or triple-spaced original. There should be wide margins on all sides of the sheets and triple spacing around formulas to allow for the marking of directions to the printer.

Original drawings (jet black India ink on white paper or tracing cloth) should accompany the manuscript. *(Blueprints are not acceptable.)* Photographs *must* be on glossy white paper. The smallest lettering on 8- by 10-in. figures should be no less than 1/4 in. high.

Formulas should be typewritten or carefully written in pen and ink. The difference between capital and lower-case letters and Greek symbols should be clearly distinguished.

See Inside Back Cover of this issue for further details

A Simple Method of Matric Structural Analysis: Part IV—Nonlinear Problems

BERTRAM KLEIN*

Convair Astronautics, A Division of General Dynamics Corporation

SUMMARY

The method presented in the previous parts is employed to solve various kinds of nonlinear problems, such as problems concerning large deflections or buckling, or thermal creep, or inelastic stress redistribution involving thermal gradients, or design. The procedure used in each case is one of direct iteration—i. e., after one assumes a starting point all subsequent cycles are self-generating. Simple numerical examples are worked out.

SYMBOLS

A	= cross-sectional area
A, B, C	= matrices or joints
a, b, c	= dimensions
E	= Young's modulus
F	= force
$f, \mathfrak{F}$	= function and flexibility
g	= function
h	= beam depth
I	= moment of inertia
$\mathcal{I}$	= integral
j	= beam column parameter
k	= spring constant
L	= length
M	= bending moment
P	= axial load
p	= pressure
R	= shear force
r	= radius
S	= stiffness
T	= tensile force or transpose
t	= time
u, v	= deflections
W	= load
w	= loading
x, z	= coordinates
y	= deflections
α	= coefficient of thermal expansion
β	= angle
γ	= parameter
δ	= deflection
Δ	= determinant
ΔT	= temperature change
ϵ	= strain
θ	= rotation or angle
ξ	= shear area parameter
ρ	= radius of curvature
σ	= axial stress
k, λ	= parameters
φ, ϕ	= angle

Subscripts

0, 1, 2, 3	= numerical index
c	= centroidal
C	= due to creep
D	= at point D
F	= force
mm, rr, etc.	= stiffnesses
P	= related to P
p	= pressure
δ	= deflection
ΔT	= due to temperature change
sec	= secant
superscript $'$ and $-$	= modified

Received July 14, 1958. Revised and received January 23, 1959.

* Specialist in Theoretical Studies.

INTRODUCTION

THE PREVIOUS PARTS of this series of articles[1-3] concern the solutions of certain types of linear problems. Many problems are or can be treated as linear in nature. However, there are a sufficient number of important nonlinear problems which warrant special attention. The purpose of the present part is to discuss such problems. Furthermore, some of the illustrations are tailored to include the treatment of thermal loadings. Before proceeding with this subject, let us retrace some of the philosophy behind the method of analysis being pursued here.

The basic approach structural engineers use with problems is the principle of equilibrium. Being close to physical reality, this principle is easy to grasp. On the other hand, there is another fundamental principle which is equally important but not as simple to grasp. This second principle relates force and displacement—the quantities used here in their general sense—and may be called the force displacement principle. Whereas an equation of equilibrium involves forces in certain directions on an element, a force displacement equation involves both forces and deflections in certain directions on an element. It should be noted that, whereas equations of equilibrium are written symbolically as $\Sigma F = 0$—at least, in the linear case—there are two ways of writing symbolically force displacement equations—i. e., either as $F = \delta S$ or $\delta = \mathfrak{F}F$. Here S represents stiffness and $\mathfrak{F}$ flexibility. In the method proposed in this series of articles, either form of representation is permissible. It appears, however, that the second way may be better on several accounts. For example, by comparing Eqs. (3) and (4) of reference 3, it appears to be simpler to incorporate thermal effects and nonuniform flexibility effects into the form: $\delta = \mathfrak{F}F$. However, it should be realized that sometimes the first way is to be preferred, such as in cases where a stiffness has to vanish.

Let us return to the discussion of nonlinear problems. There are various kinds of nonlinear problems.

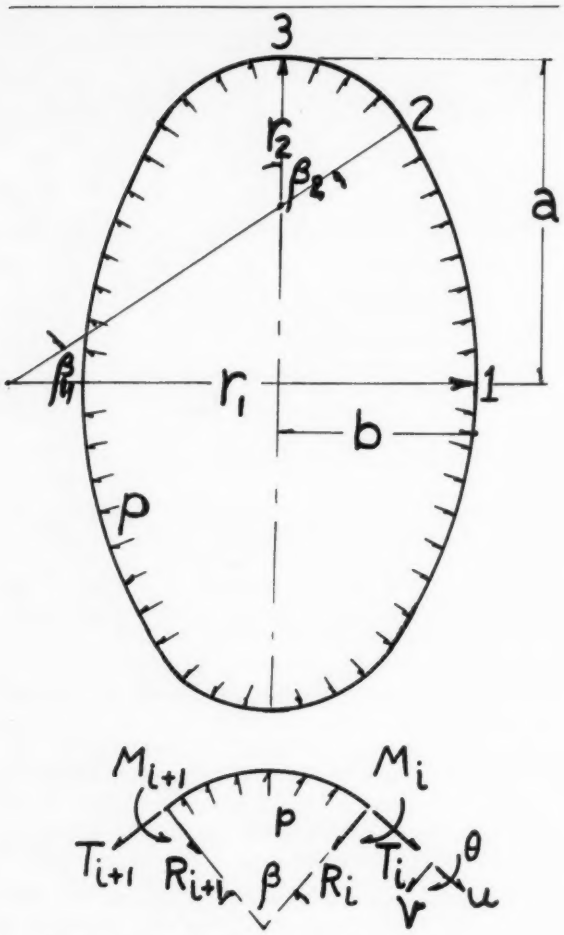

FIG. 1. Pressure loaded frame and element therein.

These problems may be considered to fall into the following categories:

(1) Problems in which equilibrium is a function of deflection—the so-called large deflection problem—in which one must take account of the fact that the structure has deflected under load. Notice that in reality all problems fall into this type. Fortunately, in most cases the deflections are small so that the effect upon the stresses is small.

(2) Stiffness (or flexibility) is a function of (a) deflection, such as in the case of a nonlinear spring where $F = (k\delta)\delta$, (b) internal force, such as the beam column effect.

(3) Stiffness (or flexibility) is a nonlinear function of material properties, such as in cases of yielding, creep, etc.

(4) In design, for a given geometry, stiffness (or flexibility) is a function of external loadings. This problem is the important one of efficient distribution of mass.

(5) Combinations of the above.

In reference to the solution of nonlinear problems, all such problems may be replaced by linear problems in which certain iterations are performed. This concept is fundamental and has been known for a long time. Also, this technique is particularly suited to automatic machine calculations, provided the iteration scheme is direct—i. e., after one assumes a starting point, all subsequent cycles are self-generating. Simple illustrations are given below of most of the above type of nonlinear problems solved by direct iteration. It is to be remembered that the aim here is simply to illustrate the method and not to solve large, complicated problems.

LARGE DEFLECTION PROBLEM

We consider the pressure loaded frame shown in Fig. 1. In reality, the structure is an ellipse before the pressure loading is applied. For purposes of anal-

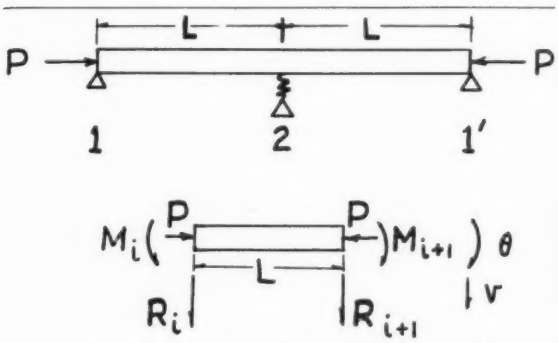

FIG. 2. Spring supported strut and element therein.

TABLE 1
Results for Pressure-Loaded Frame

Quantity	Iteration Cycle 1	2	3	5	10	19	20	Reference 4
a	27.74	26.720273	27.284629	27.138273	27.070515	27.073950	27.073922	27.08
b	23.24	24.572300	23.838827	24.013484	24.097712	24.093389	24.093424	24.07
T_1	234.17679	247.65968	240.23693	242.00445	242.85684	242.81310	242.81345	...
T_2	254.11537	257.88530	256.01447	256.45244	256.66537	256.65442	256.65450	...
R_2	54.84692	26.226003	42.037822	38.130565	36.279715	36.374196	36.73443	...
M_1	568.82784	286.09530	444.03082	405.29082	386.88097	387.82173	387.81424	385
M_2	−62.811942	−4.3204315	−31.697347	−23.804121	−20.324110	−20.497727	−20.496343	−39
T_3	279.71679	269.39716	275.10844	273.62732	272.94161	272.97637	272.97609	...
M_3	−591.98672	−271.39041	−447.34535	−403.49167	−382.1115	−383.86546	−383.85706	−350
v_1	−1.3323006	−0.59882733	−0.99906543	−0.89828353	−0.85101829	−0.85342407	−0.85340492	−0.83
θ_2	−0.074650776	−0.037703423	−0.058291628	−0.053212609	−0.050806054	−0.050928925	−0.050927946	...
v_2	0.001372348	0.035206848	0.018391452	0.022958859	0.025027780	0.024923639	0.024924469	0.05
u_2	0.58870787	0.27286772	0.45033840	0.40679512	0.38611342	0.38717017	0.38716176	0.387
v_3	1.0197267	0.45537077	0.77931674	0.70149566	0.66416381	0.66607717	0.66696195	0.66

ysis by the present method, it is assumed that the structure under load may be approximated by an ellipse which, in turn, is approximated by arcs of circles. Only two circular arcs need to be considered because of double symmetry. The centroidal radii of these arcs are:

$$\left.\begin{aligned} r_{c_1} &= \frac{\{\sqrt{a^2+b^2}\,[\sqrt{a^2+b^2}+(a-b)]\}}{2b}; \\ r_{c_2} &= \frac{\{\sqrt{a^2+b^2}\,[\sqrt{a^2+b^2}-(a-b)]\}}{2a} \end{aligned}\right\} \quad (1)$$

$$\begin{bmatrix} 1 & 1 & \cot\varphi_1 & & & & & & & & & \\ 1 & -1 & \tan\varphi_1 & & & & & & & & & \\ r_{c_1} & -r_{c_1} & 0 & 1 & -1 & & & & & & & \\ & 1 & -\cot\varphi_2 & 0 & 0 & 1 & & & & & & \\ & 1 & \tan\varphi_2 & 0 & 0 & -1 & & & & & & \\ & r_{c_2} & 0 & 0 & 1 & -r_{c_2} & -1 & & & & & \\ & & & -1 & -1 & & & S_{mr_1} & -S_{mm_1} & S_{mr_1} & -S_{mt_1} & \\ & & 1 & & & & & S_{rr_1} & S_{rm_1} & -S_{rr_1} & S_{rt_1} & \\ -1 & -1 & & & & & & S_{tr_1} & -S_{tm_1} & S_{tr_1} & -S_{tt_1} & \\ & & & & & 1 & 1 & S_{mm_2} & S_{mr_2} & S_{mt_2} & S_{mr_2} & \\ & & 1 & & & & & S_{rm_2} & S_{rr_2} & S_{rt_2} & -S_{rr_2} & \\ & -1 & & & & -1 & & S_{tm_2} & S_{tr_2} & S_{tt_2} & S_{tr_2} & \end{bmatrix} \begin{bmatrix} T_1 \\ T_2 \\ R_2 \\ M_1 \\ M_2 \\ T_3 \\ M_3 \\ v_1 \\ \theta_2 \\ v_2 \\ u_2 \\ v_3 \end{bmatrix} = \begin{bmatrix} 2p(r_p)_1 \\ 0 \\ 0 \\ 2p(r_p)_2 \\ 0 \\ 0 \\ 2p(fr_pr_c)_1 \\ 0 \\ -2p(gr_p)_1 \\ 2p(fr_pr_c)_2 \\ 0 \\ -2p(gr_p)_2 \end{bmatrix}$$

The twelve equations represent the equations of equilibrium and force displacement for each element including the effects of internal pressure. The functions f and g are defined as:

$$f = (1/\Delta)\,(1/\gamma)\,[(4/\beta)\,(1-\cos\beta) - 2\sin\beta]; \qquad g = [1-(1/\Delta)\,(2/\gamma)\sin\beta] \quad (4)$$

where $\Delta = k\beta - \lambda\sin\beta - (4/\beta)\,(1-\cos\beta)$; $(1/\gamma) = I/Ar_c^2$ (4a)

The stiffnesses S, as well as k and λ, have already been defined in previous parts.[2, 3]

The problem is solved by direct iteration, as follows: assume initially that $a = a_0$ and $b = b_0$. Solve the matric equation to obtain, among other things, values of v_1 and v_3. Calculate new values of a and b, using Eq. (3). Repeat as before until all unknowns have converged to the desired accuracy. The results of such calculations are shown in Table 1 for a structure having the following properties:[4]

$a_0 = 27.74$ $\quad A = 0.3$ $\quad r_c - r_p = 0.1$ $\quad p = 10.12$

$b_0 = 23.24$ $\quad I = 0.010$ $\quad E = 10.5 \times 10^6$ $\quad \xi = 0.32$

Total computing time is less than 1 minute on the IBM 704 machine. The problem has been solved by a more exact method in reference 4. The results of this accurate solution are shown in Table 1 for comparison purposes. The quantities which are omitted do not have values reported directly in reference 4. The agreement between the solutions is considered good enough to substantiate the validity of the use of the present method for solving large deflection problems. Greater accuracy may be obtained, if desired, by using more arcs of circles.

where a and b are the semiaxes of an ellipse. The angles subtended by the arcs are:

$$2\varphi_1 = \beta_1 = \arctan(b/a);\ 2\varphi_2 = \beta_2 = (\pi/2) - \beta_1 \quad (2)$$

One may write:

$$a = a_0 - v_3; \quad b = b_0 - v_1 \quad (3)$$

where a_0 and b_0 are the semiaxes of the ellipse before the pressure loading is applied and the v's are the radial deflections positive when inward. The matric equation defining the problem may be written as:

Buckling Problem

Let it be required to determine the elastic buckling load of the spring supported uniform strut pictured in Fig. 2. Only one half of the strut needs to be considered. Furthermore, assume the spring is weak enough so that the deflected shape at buckling is symmetric. One proceeds to solve the problem by the present method by writing the following equations:

$$\left.\begin{aligned} R_1 + R_2 = 0;\ \ 2R_2 + kv_2 = 0; \qquad \theta_1 + \mathfrak{F}_1(P)M_2 = 0 \\ Pv_2 + M_2 - (R_1 - R_2)\,(L/2) = 0; \qquad v_2 - (L/2)\theta_1 + \mathfrak{F}_2(P)\,M_2 = 0 \end{aligned}\right\} \quad (5)$$

These equations represent the equations of equilibrium and force displacement for element 1–2 and the force displacement equation for the spring. Here, the functions $\mathfrak{F}$ are flexibility terms defined as

$$\mathfrak{F}_1(P) = [1-\cos(L/j)]/Pj\sin(L/j); \quad j = \sqrt{EI/P};\ \ \mathfrak{F}_2(P) = 1/2P\,(2 - \{[1+\cos(L/j)]/(j/L)\sin(L/j)\}) \quad (5a)$$

The solution is continued by writing Eq. (5) matrically as

$$\left[\begin{array}{ccc:cc} 1 & 1 & & & \\ -(1/2) & 1/2L & 1 & P & \\ & 1 & & k & \\ \hdashline & & & & \\ & & \mathfrak{F}_1(P) & 1 & \\ & & \mathfrak{F}_2(P) & 1 & -(1/2)L \end{array}\right] \left[\begin{array}{c} R_1 \\ R_2 \\ M_2 \\ \hdashline \\ v_2 \\ \theta_1 \end{array}\right] = 0 \quad (6)$$

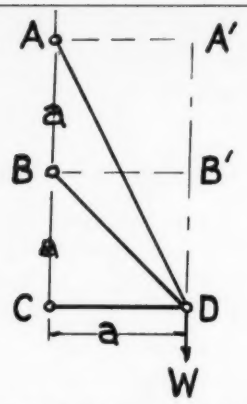

FIG. 3(a). Pin-jointed framework subjected to creep.

Notice that the matrix has been partitioned into four parts. The main diagonal submatrices are square matrices associated with either forces alone (upper left) or displacements alone (lower right). Notice also that these diagonal matrices do not contain any terms involving the buckling load, P. On the other hand, the remaining two submatrices contain terms involving P. However, the functions of P appearing in the upper right matrix are linear. Therefore, the following method of solution is suggested. First write Eq. (6) as

$$\begin{bmatrix} A_F & L(P) \\ \mathfrak{F}(P) & A_\delta \end{bmatrix} \quad \begin{bmatrix} F \\ \delta \end{bmatrix} = 0 \tag{6a}$$

which may be written as the two matric relations after one eliminates δ or F:

$$[A_F - L(P)A_\delta^{-1}\,\mathfrak{F}(P)]\,[F] = 0\,; \qquad [A_\delta - \mathfrak{F}(P)A_F^{-1}\,L(P)]\,[\delta] = 0 \tag{6b}$$

If the matrix $\mathfrak{F}(P)$ is assumed to be known, Eq. (6b) can be put in the form of a standard eigenvalue problem

$$Bx = PCx \text{ or } (B^{-1}C)x = (1/P)x \tag{7}$$

The following overall direct iterative procedure may be used: assume a value of P and hence calculate the matrix, $\mathfrak{F}(P)$. Then determine the matrices B and C. Proceed to solve Eq. (7) for P by direct iteration. Use this determined value of P to carry out the second cycle of the overall iteration, and so on. Notice that there are two choices in setting up Eq. (6b) and hence Eq. (7).

In the present illustrative example, the eigenvalue problem defined by Eq. (7) is so trivial that one can solve for P directly instead of iterating using that equation. The solution for P is

$$P = -(M_2/v_2) + (Lk/2) \text{ where } -(M_2/v_2) = 1/[(L/2)\mathfrak{F}_1(P) + \mathfrak{F}_2(P)] \tag{8}$$

Let $EI = 10^6$, $L = 10$, and $k = 2000$. Then the results of the iterative solution of Eq. (8) are shown in Table 2 starting with $P = 100$.

In general, it is necessary in solving buckling problems first to solve the stress distribution problem for the structure under a set of loads proportional to the set at buckling. Then one proceeds with the method shown here where P is the value assigned to one of the loads. The remaining loads are expressed as percentages of the load P. The deflections at buckling in general will be associated with a mode distinct from the deflected shape prior to buckling. The initially assumed value of P should be taken low enough that convergence is to the first eigenvalue in Eq. (7).

TABLE 2
Buckling of Spring-Supported Strut

	Iterative Cycle					
Quantity	1	2	3	4	5	6
P	100	39980	30874	33196	32620	32767
(L/j)	0.10	2.00	1.757	1.822	1.806	1.8101
$-(M_2/v_2)$	29980	20874	23196	22620	22767	22729
P	39980	30874	33196	32620	32767	32729

CREEP PROBLEM

The pin-jointed framework shown in Fig. 3(a) is assumed to be brought rapidly to an equilibrium temperature of 500°F. How will the stresses in the members and the deflection of joint D vary with time thereafter? For purposes of simplicity, it is assumed that member CD is infinitely rigid. Therefore, for small deflections, point D can move only downward. Also, let the cross-sectional areas of the remaining two bars be equal to each other and designated A. The problem can be solved by the present method by writing three equations as

$$\left.\begin{aligned} &\sigma_1 \cos\theta_1 + \sigma_2 \cos\theta_2 - (W/A) = 0 \\ &(\sigma_1/E_{\text{sec}_1}) - (1/A'D)v_D + (\epsilon_C)_1 = 0 \\ &(\sigma_2/E_{\text{sec}_2}) - (1/B'D)v_D + (\epsilon_C)_2 = 0 \end{aligned}\right\} \tag{9}$$

The first equation represents the equilibrium equation of joint D; the last two—the stress-displacement equations for the two deformable bars. Notice that in the present instance each term in the latter equations has

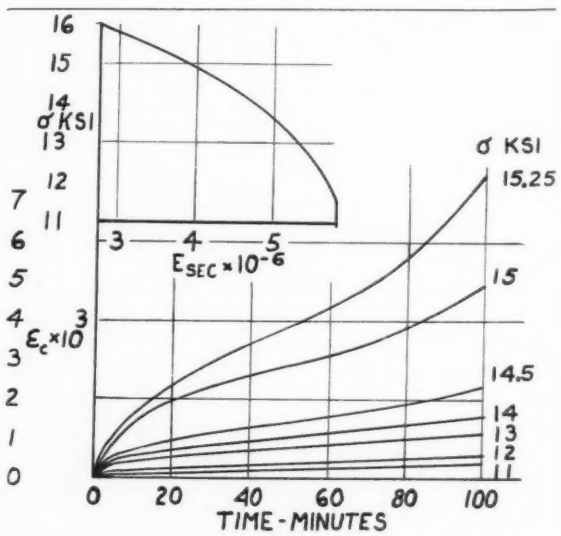

FIG. 3(b). Creep curves and secant modulus for HM 21XA at 500°F.

the significance of a strain. The equations are written matrically in the form:

$$\begin{bmatrix} \cos\theta_1 & \cos\theta_2 & 0 \\ E_{\text{sec}_1}^{-1} & 0 & -\bar{A}'\bar{D}^{-1} \\ 0 & E_{\text{sec}_2}^{-1} & -\bar{B}'\bar{D}^{-1} \end{bmatrix} \begin{bmatrix} \sigma_1 \\ \sigma_2 \\ v_D \end{bmatrix} = \begin{bmatrix} W/A \\ -(\epsilon_C)_1 \\ -(\epsilon_C)_2 \end{bmatrix} \quad (9a)$$

Notice that the creep strains are considered as thermal loads and appear on the right-hand side. The matric equation is solved by direct iteration as a time dependent equation, as follows:

Assume $t = 0$. Therefore, $\epsilon_C = 0$. Next assume the structure is elastic—i. e. $E_{\text{sec}} = E$, and solve the matric Eq. (9). Correct for plasticity and solve again. Repeat this direct iteration procedure until proper convergence is obtained. Next, assume $t = t_1$. Read the values of ϵ_C from an appropriate creep-strain-stress-time curve family using the values of σ found for $t = 0$. Solve the matric equation using in addition the values of E_{sec} at $t = 0$. Correct the values of both ϵ_C and E_{sec}. Repeat this direct iteration procedure until proper convergence is obtained. Notice that E_{sec} is the secant modulus of the instantaneous stress-strain curve of the material at the elevated temperature. This modulus is shown in Fig. 3(b), together with the creep curves for a magnesium alloy at 500°F. The final results of calculations carried out for three times is shown below for a value of $W/A = 20600$

	time		
quantity	0	10 min.	60 min.
σ_1	15000	14600	14600
σ_2	11000	11600	11600
v_D/a	0.00384	0.00418	0.00465

It is seen that there is a small redistribution of stress with time due to creep in this problem.

Inelastic Stress Redistribution Problem Involving Thermal Gradients

Many times one has to consider the fact that the stresses in a structure are larger than the proportional limit stress of the material. This situation occurs, for example, in the previous creep problem. The steps

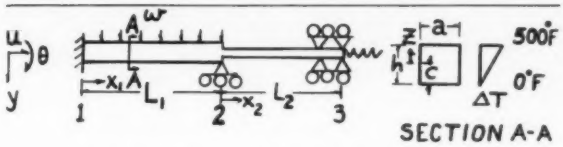

Fig. 4(a). Beam subjected to heat and load.

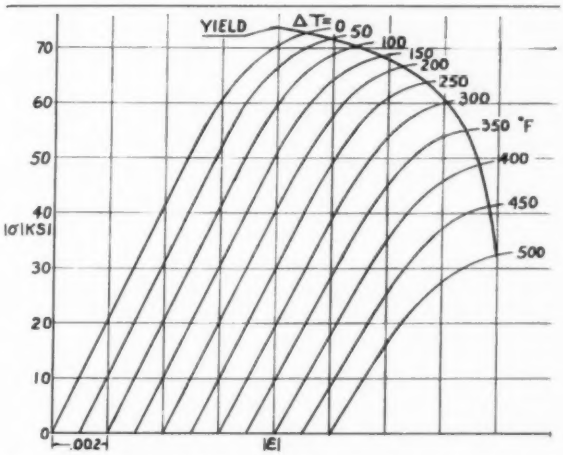

Fig. 4(b). Stress-strain temperature family of curves for 2024S-T86.

in the solution already have been given—i.e., first assume all stresses are elastic; solve the problem. Next, correct all terms that are functions of stress and solve again, and so on. This procedure is a direct iteration pattern.

When the structure is subjected to thermal gradients, one has to consider, in general, the stress-strain-temperature family of curves. Such a situation arises for the beam problem shown in Fig. 4(a). This structure is subjected to simultaneous heat and load applied only to the left span. The temperature profile through the depth of the left span of the beam is assumed to be the linear one depicted in Fig. 4. No creep strains are considered in the analysis. Also, plane sections of the beam are assumed to remain plane. The problem is solved by first writing the matric equation:

$$\begin{bmatrix} 1 & 1 & & & & & & & & & \\ L_1 & -L_1 & & & 2 & -2 & & & & & \\ & & 1 & 1 & & & & & & & \\ & & L_2 & -L_2 & & 2 & -2 & & & & \\ & & & & f_{1_1} & f_{2_1} & & -1 & -\theta_{P_1} & & \\ & & & & -g_{1_1} & g_{2_1} & & -0.5 & -I_{P_1} & & \\ & & & & & f_{1_2} & f_{2_2} & 1 & -\theta_{P_2} & & \\ & & & & & -g_{1_2} & g_{2_2} & -0.5 & -I_{P_2} & & \\ & & & & & & & u_{P_1} & 1 & & \\ & & & & & & & u_{P_2} & -1 & 1 & \\ & & & & & & & 1 & & -k & \end{bmatrix} \begin{bmatrix} R_1 \\ R_2 \\ R_2' \\ R_3 \\ M_1 \\ M_2 \\ M_3 \\ \theta_2 \\ P \\ u_2 \\ u_3 \end{bmatrix} = \begin{bmatrix} -wL_1 \\ \\ \\ \\ \theta_w - (\theta_{\Delta T})_1 \\ I_w \\ \\ \\ (u_{\Delta T})_1 \\ \\ \\ \end{bmatrix}$$

The first four equations represent equilibrium relations; the next four bending force-displacement relations, and the last three, axial force-displacement relations. One must consider two conditions, as follows: (a) Elastic state of stress—the entries are defined as

$$\left.\begin{aligned} f_1 &= f_2 = (L/2E_0I_0)\ (\tan\phi/\phi);\\ \theta_w &= (wL^3/12E_0I)\{(3/\phi^2)[(\tan\phi/\phi) - 1]\};\\ \phi &= (L/2j);\quad j = \sqrt{E_0I/P}\\ g_1 &= g_2 = (L/12E_0I) \times\\ &\quad \{(3/\phi^2)\ [1 - (\tan\phi/\phi)^{-1}]\};\\ \theta_{\Delta T} &\approx (L/c)\ (\alpha\Delta T)_0;\quad u_{\Delta T} \approx L(\alpha\Delta T)_0\\ u_P &\approx (L/E_0A);\quad \theta_P = I_P = I_w = 0 \end{aligned}\right\} \quad (10)$$

Here the subscript 0 refers to values taken at the neutral axis of a cross section which is assumed to coincide with the axis of symmetry in this elastic case for the sake of simplicity.

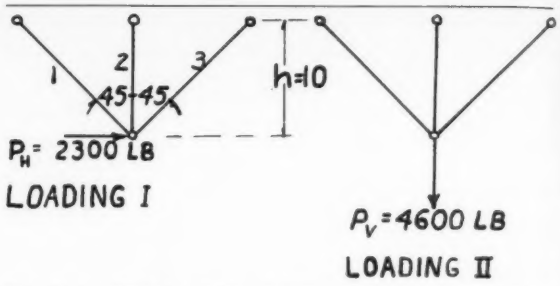

FIG. 5(a). Pin-jointed planar truss subjected to two distinct loading conditions.

(b) Plastic state of stress—one writes:

$$\left.\begin{aligned} f_1 &= L\int_0^1 \overline{EI}^{-1}\ [1 - (x/L)]\ d(x/L);\ f_2 = L\int_0^1 \overline{EI}^{-1}\ (x/L)\ d(x/L);\ \theta_w = +\ (wL^3/2) \times\\ &\qquad \int_0^1 \overline{EI}^{-1}\ (x/L)[1-(x/L)]d(x/L)\\ g_1 &= -L\int_0^1 \overline{EI}^{-1}[1 - (x/L)][(x/L) - 0.5]d(x/L);\ g_2 = L\int_0^1 \overline{EI}^{-1}(x/L)[(x/L)-0.5]d(x/L)\\ \theta_{\Delta T} &= L\int_0^1 \overline{EI}^{-1}M_{\Delta T}d(x/L);\ u_{\Delta T} = L\int_0^1 \overline{EA}^{-1}P_{\Delta T}d(x/L);\ u_P = L\int_0^1 \overline{EA}^{-1}d(x/L)\\ \theta_P &= L\int_0^1 \overline{EI}^{-1}yd(x/L);\ I_P = L\int_0^1 \overline{EI}^{-1}y[(x/L)-0.5]d(x/L);\ I_w = -(wL^3/2) \times\\ &\qquad \int_0^1 (x/L)[(x/L)-1]\overline{EI}^{-1}[(x/L)-0.5]d(x/L) \end{aligned}\right\} \quad (11)$$

where

$$\left.\begin{aligned} \overline{EI} &= \int_{-c}^{c} E_{sec}(z')^2adz;\quad \overline{EA} = \int_{-c}^{c} E_{sec}adz;\quad M_{\Delta T} = \int_{-c}^{c} E_{sec}\alpha\Delta Tz'adz;\quad P_{\Delta T} = \int_{-c}^{c} E_{sec}\alpha\Delta Tadz\\ z' &= z - z_0;\ z_0 = \left(\int_{-c}^{c} E_{sec}zadz\right)\Big/\overline{EA} \end{aligned}\right\} \quad (11a)$$

E_{sec} is defined as the secant modulus of the stress-strain curve corresponding to the temperature existing in a fiber whose actual stress is $E_{sec}\epsilon$, where

$$\epsilon = \epsilon_P + z'(1/\rho) - \alpha\Delta T \quad (12)$$

and

$$\left.\begin{aligned} \epsilon_P &= (-P + P_{\Delta T})/\overline{EA};\\ (1/\rho) &= (M + M_{\Delta T})/\overline{EI};\quad P > 0\\ M &= M_1 + (M_2 - M_1)\ (x/L) +\\ &\quad (wL^2/2)\ (x/L)\ [(x/L) - 1] -\\ &\quad Py \text{ for the left span, 1–2} \end{aligned}\right\} \quad (12a)$$

where, finally,

$$\left.\begin{aligned} y &= L\int_0^{(x/L)} (dy/dx)d(x/L);\ (dy/dx) =\\ &\quad L\int_0^{(x/L)} (1/\rho)d(x/L) \text{ for the left span, 1–2} \end{aligned}\right\} \quad (13)$$

For the right span, 2–3, one must add θ_2 to the above expression for (dy/dx).

The iterative scheme to be followed in the solution is as follows: First assume all the stresses are elastic and the neutral axis at any section corresponds to $z = 0$—i. e., $z' = 0$. Hence, calculate $u_{\Delta T}$ and u_P according to the approximate equations given in Eq. (10). Solve the three by three matrix in the lower right-hand corner. Thus, we establish an approximation to P (compression is assumed plus). Calculate the functions of P appearing in the remaining part of the matrix and invert this eight by eight. Calculate ϵ according to Eq. (12). One must use the following expression for M in this first iteration:

$$M = (M_1 - wj^2)\cos(x/j) + [-(M_1 - wj^2)\cos(L/j) + (M_2 - wj^2)] \times \sin(x/j)/\sin(L/j) + wj^2 \quad (14)$$

This expression is valid for the left span, 1–2; for the right span, replace M_1 and M_2 by M_2 and M_3, respectively. Also, we let $P_{\Delta T}$ and $M_{\Delta T}$ be $(\alpha\Delta T)_0E_0A$ and $(\alpha\Delta T)_0(1/c)\ (E_0I)$, and $\overline{EA}$ and $\overline{EI}$ be simply E_0A and E_0I, respectively, in this first iteration.

Next, enter the stress-strain curves in Fig. 4(b) to obtain values of E_{sec}, thereby forming the basis for the evaluation of the quantities $\overline{EI}$, $\overline{EA}$, etc., appearing in Eq. (11a) and, thus, the entries in the matrix de-

pendent upon such quantities. Solve the entire matric equation. Use the new-found values of P, M_1, M_2, M_3 to calculate new M, ϵ_P, and $(1/\rho)$ and, hence, new values for ϵ and E_{sec}. Repeat the cycle until the desired degree of convergence is obtained. Notice that the curves in Fig. 4(b) are assumed valid for both tension and compression.

A structure is analyzed with the following dimensions and load:

$L_1 = 60$ in. $L_2 = 30$ in. $k = 10{,}000$ lb./in.
$h_1 = 3$ in. $h_2 = 1.5$ in. $w = -50$ lb./in.
$a_1 = 1$ in. $a_2 = 1$ in.

Results are shown in Table 3.

The positive sign convention for R, M, θ, and P is shown in Fig. 2. If one wishes, one may include the effects of lateral deflections in the axial force displacement equations. Then one adds the integrals

$$-(L_1/2)\int_0^1 (dy/dx)^2\, d(x/L_1)$$

$$-(L_2/2)\int_0^1 (dy/dx)^2\, d(x/L_2)$$

to the right-hand side of Eqs. (9) and (10), respectively, in the matrix. These integrals represent the axial shortening due to lateral deflections. This refinement has not been done in the present problem because this shortening is small compared to the axial deflection of 0.18 found above.

Efficient Structural Design Problem

Perhaps the most important nonlinear problem is the one of efficient structural design. One is required to determine the optimum (or near-optimum) distribution of mass in the structure—i. e., to use the least weight of material and still enable the structure to operate properly under all operating conditions. For example, let us consider the simple pin-jointed planar truss shown in Fig. 5(a). Notice that the truss is subjected to two independent, known loading conditions, designated loading condition I and loading condition II. The geometry defining the length and orientation of the three members is assumed to be known. Also, the bars are assumed to be uniform (untapered) hollow tubes made of a known material. The problem at hand is one of determining the least areas of the members, such that for each loading condition (a) no tensile stress exceeds, σ_{max}, a specified stress, and (b) no bar fails in compression.

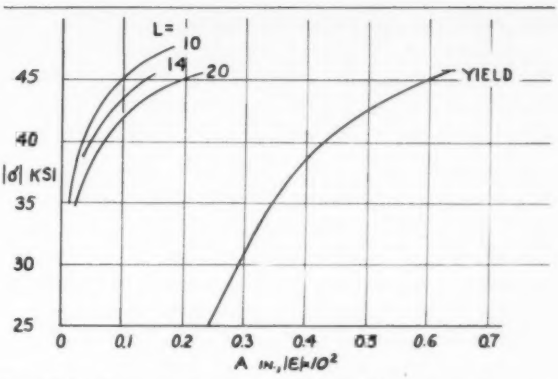

FIG. 5(b). Stress-strain curve and allowable compressive area for 2024S-T3 tubing.

In general, the method of solution consists of a semi-inverse iterative technique. First we write the matric equation defining the physical behavior of the structure under load as

$$\begin{bmatrix} (1/\sqrt{2})A_1 & 0 & -(1/\sqrt{2})A_3 & 0 & 0 \\ (1/\sqrt{2})A_1 & A_2 & (1/\sqrt{2})A_3 & 0 & 0 \\ 2h/E_{sec_1} & 0 & 0 & (1/\sqrt{2}) & (1/\sqrt{2}) \\ 0 & h/E_{sec_2} & 0 & 0 & 1 \\ 0 & 0 & 2h/E_{sec_3} & -(1/\sqrt{2}) & (1/\sqrt{2}) \end{bmatrix} \begin{bmatrix} (\sigma_1)_I & (\sigma_1)_{II} \\ (\sigma_2)_I & (\sigma_2)_{II} \\ (\sigma_3)_I & (\sigma_3)_{II} \\ (u)_I & (u)_{II} \\ (v)_I & (v)_{II} \end{bmatrix} = \begin{bmatrix} P_H & 0 \\ 0 & P_V \\ 0 & 0 \\ 0 & 0 \\ 0 & 0 \end{bmatrix} \tag{15}$$

The last three force displacement equations may be used to obtain a strain compatibility equation which is for each loading condition

$$\epsilon_1 - \epsilon_2 + \epsilon_3 = 0, \quad \text{or} \quad (E_{sec_1})^{-1}\sigma_1 - (E_{sec_2})^{-1}\sigma_2 + (E_{sec_3})^{-1}\sigma_3 = 0 \tag{16}$$

TABLE 3
Iterative Solution for Beam Under Simultaneous Heat and Load

Quantity	Linear	Nonlinear 1	2	3	4	5
R_1	2746.2	2629.9	2734.7	2698.7	2701.9	2701.6
R_2	253.8	370.1	265.3	301.3	298.1	298.4
R_2'	651.2	1005.5	598.9	696.7	688.3	690.0
R_3	− 651.2	−1005.5	− 598.9	− 696.7	− 688.3	− 690.0
M_1	−87667	−84750	−86650	−85826	−85922	−85914
M_2	−12898	−17009	−12567	−13906	−13810	−13816
M_3	6638.8	13158	5399.5	6995.6	6839.4	6853.2
θ_2	0.033398	0.033293	0.036520	0.035602	0.035670	0.035667
P	1871.6	1820.0	1834.7	1834.7	1834.5	1834.5
u_2	0.19085	0.18702	0.18703	0.18712	0.18710	0.18710
u_3	0.18716	0.18200	0.18347	0.18347	0.18345	0.18345
y_{max}		−0.36	−0.40	−0.39	−0.39	−0.39

Therefore, we may rewrite Eq. (15) as

$$\begin{bmatrix} (1/2)\ (L_1A_1) & 0 & -(1/2)\ (L_3A_3) \\ (1/2)\ (L_1A_1) & L_2A_2 & (1/2)\ (L_3A_3) \\ (E_{\text{sec}_1})^{-1} & (E_{\text{sec}_2})^{-1} & (E_{\text{sec}_3})^{-1} \end{bmatrix} \begin{bmatrix} (\sigma_1)_{\text{I}} & (\sigma_2)_{\text{II}} \\ (\sigma_2)_{\text{I}} & (\sigma_2)_{\text{II}} \\ (\sigma_3)_{\text{I}} & (\sigma_3)_{\text{II}} \end{bmatrix} = \begin{bmatrix} hP_H & 0 \\ 0 & hP_V \\ 0 & 0 \end{bmatrix} \tag{17}$$

The change of variable to L_iA_i is made so that the sum ΣL_iA_i is directly proportional to the weight of the three bars. For a given set of values of L_1A_1, L_2A_2, and L_3A_3, one solves Eq. (17) for the sets of stresses σ_{I} and σ_{II} by direct iteration using the stress-strain curves of the material such as shown in Fig. 5(b) (here assumed valid for both tension and compression).

However, in general, one would like to determine a set of values of L_iA_i, such that the stresses σ_{I} and σ_{II} conform to the conditions (a) and (b) above. Since the structure considered is one time redundant, there are three unknown areas but only two equations of equilibrium for each loading condition, and, thus, four equations of equilibrium all together. Thus, there are more equations than unknowns. One may still obtain a solution for L_iA_i in the least squares sense. We write:

$$(B^TB)V = B^TC \tag{18}$$

where

$$B = \begin{bmatrix} 1/2(\sigma_1)_{\text{I}} & 0 & -(1/2)(\sigma_3)_{\text{I}} \\ 1/2(\sigma_1)_{\text{I}} & (\sigma_2)_{\text{I}} & 1/2(\sigma_3)_{\text{I}} \\ 1/2(\sigma_1)_{\text{II}} & 0 & -(1/2)(\sigma_3)_{\text{II}} \\ 1/2(\sigma_1)_{\text{II}} & (\sigma_2)_{\text{II}} & 1/2(\sigma_3)_{\text{II}} \end{bmatrix} \quad V = \begin{bmatrix} L_1A_1 \\ L_2A_2 \\ L_3A_3 \end{bmatrix} \quad C = \begin{bmatrix} hP_H \\ 0 \\ hP_V \end{bmatrix}$$

$$B^T = \begin{bmatrix} 1/2(\sigma_1)_{\text{I}} & 1/2(\sigma_1)_{\text{I}} & 1/2(\sigma_1)_{\text{II}} & 1/2(\sigma_1)_{\text{II}} \\ 0 & (\sigma_2)_{\text{I}} & 0 & (\sigma_2)_{\text{II}} \\ -(1/2)\ (\sigma_3)_{\text{I}} & 1/2(\sigma_3)_{\text{I}} & -(1/2)\ (\sigma_3)_{\text{II}} & 1/2(\sigma_3)_{\text{II}} \end{bmatrix} \tag{18a}$$

B^T is the transpose of matrix B. One may solve Eq. (18) for values of L_iA_i for given sets of stresses, σ_{I}, σ_{II}. However, in general, when these values of L_iA_i are used to solve Eq. (17), one does not obtain the same values of stresses that are used to solve Eq. (18).

A simple relation exists between change in stress and change in area, as follows:

$$B^TB\,dV = -B^TdBV \tag{19}$$

where

$$dV = \begin{bmatrix} d(L_1A_1) \\ d(L_2A_2) \\ d(L_3A_3) \end{bmatrix} \quad dB = \begin{bmatrix} (1/2)d(\sigma_1)_{\text{I}} & 0 & -(1/2)d(\sigma_3)_{\text{I}} \\ (1/2)d(\sigma_1)_{\text{I}} & d(\sigma_2)_{\text{I}} & (1/2)d(\sigma_3)_{\text{I}} \\ (1/2)d(\sigma_1)_{\text{II}} & 0 & -(1/2)d(\sigma_3)_{\text{II}} \\ (1/2)d(\sigma_1)_{\text{II}} & d(\sigma_2)_{\text{II}} & (1/2)d(\sigma_3)_{\text{II}} \end{bmatrix} \tag{19a}$$

The semi-inverse method of solution works out as follows: initially one assumes all the stresses for both loading conditions, such that Eq. (16) is satisfied in each case, and solves Eq. (18) for V. If any area turns out to be negative, reverse the signs of certain stresses in that member. Naturally, one should try to assume the stresses as large as possible. However, by the use of physical intuition and judgment one may see that certain bars cannot or should not be highly stressed, or not stressed at all under certain loading conditions. *It appears, for example, that for each loading condition the most highly stressed bars are the bars which would comprise the least weight statically determinate structure.* In the present example, these are bars one and three for loading condition I and bar 2 for loading condition II. If one decides to take a bar out of the structure, then Eq. (16) does not have to be satisfied. The present structure becomes statically determinate and Eqs. (17) and (18) reduce to order two.

Once a set of areas is known, one can proceed to solve Eq. (17) to obtain a set of compatible stresses for all loading conditions. Naturally, all stresses exceeding tensile and compressive allowable values must be knocked down. One way to accomplish this reduction is by the use of Eq. (19) which gives the least square solution for the changes in area due to changes in the stresses. Eq. (16) should be satisfied in changing the stresses. Now that a new set of areas is known, solve Eq. (17) for new sets of stresses to see that all margins are plus. Eq. (19) may be used to raise certain stresses when necessary.

In general, the solution obtained is not necessarily the optimum one sought but is a relative optimum. One must start over again with different states of assumed stresses and derive other sets of areas before deciding that the optimum (or near-optimum) condition has been attained. However, in each case, once the initial guess for the stresses has been made, the semi-inverse iterative procedure can be made to be a direct iterative procedure.

In the present illustrative example, the steps in the solution are so simple that one is not required to carry out the above procedure in every detail. Examination

of the loading conditions reveals that bar 2 is not in a position to take load in loading condition I. However, this bar can take load efficiently in loading condition II. Therefore, we make

$$(\sigma_2)_I = 0 \text{ and } (\sigma_2)_{II} = 46{,}000$$

The latter value is the yield strength of the material, as shown in Fig. 5(b). Also shown is the relation between allowable compressive stress and cross-sectional area of a tube. Since we have assumed $(\sigma_2)_I = 0$, it follows from Eq. (17) that $(\sigma_1)_I = -(\sigma_3)_I$. Therefore, one must solve the equation

$$L_1A_1(\sigma_1)_I = hP_H$$

so that the solution lies on the upper curve in Fig. 5(b). The solution is obtained by iteration and is

$$L_1A_1 = 0.581 \text{ with } (\sigma_1)_I = 39{,}600$$

In order to satisfy Eq. (16) for loading condition II, we determine the solution with the aid of the stress-strain curve in Fig. 5(b) by iteration to be

$$(\sigma_1)_{II} = (\sigma_3)_{II} = 32{,}800$$

Thus, we may solve for L_2A_2 from the second equation in Eq. (17)

$$46{,}000(L_2A_2) = hP_V - 32{,}800(0.581)$$

to obtain $L_2A_2 = 0.585$. The total volume of the three bars is 1.747. Additional solutions are carried out in which the structure is made statically determinate. In these cases, total volume is found to be 2. Therefore, the above solution represents a weight saving of about 13 per cent when compared to the statically determinate structure.

In actual practice, one may desire to include limiting deflections as well as stresses in the design. Then the force displacement equations in Eq. (15) must be considered. Various other limiting factors may be imposed on the design, such as fatigue, minimum sizes, joint and other attachment weight, probability considerations, etc. Furthermore, when the problems become large, one may have to resort to one of the sophisticated mathematical minimizing procedures being developed for solving nonlinear constrained systems.

References

[1] Klein, B., *A Simple Method of Matric Structural Analysis*, Journal of the Aeronautical Sciences, Vol. 24, No. 1, pp. 39–46, January, 1957.

[2] Klein, B., *A Simple Method of Matric Structural Analysis: Part II—Effects of Taper and a Consideration of Curvature*, Journal of the Aeronautical Sciences, Vol. 24, No. 11, pp. 813–820, November, 1957.

[3] Klein, B., *A Simple Method of Matric Structural Analysis: Part III—Flexible Frame and Stiffened Cylindrical Shell Analysis*, Journal of the Aeronautical Sciences, Vol. 25, No. 6, pp. 385–394, June, 1958.

[4] Steinbacher, F. R., and Lo, Hsu, *Determination of Bending Moments in Pressure—Loaded Rings of Arbitrary Shape When Deflections are Considered*, NACA TN 1692, September, 1948.

[5] Hoff, N. J., *Notes on Thermal Effects in Structures;* Polytechnic Institute of Brooklyn, N.Y., 1953–54.

[6] Sprague, G. H., and Huang, P. C., *Behavior of Aircraft Structures under Thermal Stress*, SAE Paper No. 212, Los Angeles, Calif., October, 1957.

[7] Gatewood, B. E., *Inelastic Combined Thermal and Applied Stresses in Skin-Stringer Structures*, Journal of the Aeronautical Sciences, Readers' Forum, Vol. 25, No. 3, p. 212, March, 1958.

[8] Barta, J., *On the Minimum Weight of Certain Redundant Structures*, Acta Technica, Academiae Scientiarum Hungaricae, Tomus XVIII, Fasciculi 1–2, Budapest, 1957.

[9] Pearson, C. E., *Limit Analysis;* A Service of Arthur D. Little, Los Angeles, Calif., December, 1957.

IAS Twenty-Eighth Annual Meeting

Hotel Astor, New York City, January 25–28, 1960

The scope of the meeting will be broad to cover the many interests of IAS members. The Meetings Committee invites papers to be submitted in any of the scientific fields relating to aeronautics and space.

Members or organizations wishing to have papers considered for presentation at this meeting should submit outlines or summaries to the *Meetings Committee, 2 East 64th St., New York 21, N.Y., no later than August 1, 1959.*

Nose Drag in Free-Molecule Flow and Its Minimization

H. S. TAN*
THERM, Incorporated

SUMMARY

The superaerodynamic nose drag of a body in a free-molecule flow involves two parameters: the speed ratio S between ordered and random molecular motions (modified Mach Number), and the temperature ratio T_r/T between the solid surface and undisturbed gas. Simplifications of the drag formula are obtained at hypersonic as well as low-subsonic extremes. To minimize the drag on a nose of specified length and base radius, the ordinary method of calculus of variation was found inadequate. A generalized approach has, accordingly, been developed, and the specification of end conditions is discussed at length.

Results of the present investigation indicate that in all cases an optimum nose requires a flat tip. The optimum nose curve for the hypersonic extreme does not depend on the temperature ratio, but that for the low-subsonic extreme varies in the following manner: for a hot body the curve is convex; for a cold body, concave. An optimum solution exists in a restricted range of specification only. With prescribed tip and base radii the admissible nose length is bounded below for the cases of hypersonic and low-subsonic hot body and bounded above for the case of low-subsonic cold body. A vanishing tip radius leads to an infinitely long nose in the former and a vanishing nose in the latter case.

Optimum nose curves for several temperature ratios at the low-subsonic extreme, as well as the one for hypersonic extreme, are presented. It is observed that at the low-subsonic extreme, with $T_r/T \to \infty$, the hot-body solution asymptotically approaches the hypersonic solution—i.e., a slender conventional warhead with a flat tip; whereas with $T_r/T \to 0$, the cold-body solution asymptotically approaches the minimal-surface solution—i.e., (a) with prescribed tip radius, a catenoid; (b) with unspecified tip radius, a flat disc.

(1) Drag Formula in Free-Molecule Flow

To make our discussion self-contained, we first present in a brief digression the physical picture, the assumptions involved, and the consequent derivation and simplification of the free-molecule drag formula. For detailed mathematical analysis, the readers are referred to references 4–6.

In a highly rarefied gas where the mean free path of molecules λ is much greater than the body linear dimension l, the aerodynamic force acting on a moving body is determined by the discontinuous collisions between gas molecules and the solid surface, and the intercollision of gas molecules can be ignored. This flow relative to the body is called free-molecule flow. Since there exists no mechanism for intermolecular momentum transfer in a free-molecule flow, the incoming and the reflected flows do not interact. The aerodynamic force can then be separated into two contributions: impact momentum of incoming molecules and reactive momentum of reflected molecules.

Upon colliding with a solid surface, a fraction f of these gas molecules will be absorbed and later on re-evaporated after reaching thermal equilibrium with the solid surface.† For $f = 0$, we have perfect "regular reflection"; for $f = 1$, we have total absorption and "random re-emission."[1] Theoretical determination of f is lacking at present. Experimental results, however, do indicate $f \sim 1$.[2, 3] In the following, we shall, as most investigators do,[4–6] assume $f = 1$.

According to classical kinetic theory of gases, the mean free path λ is independent of temperature T. It depends on density ρ alone and is given by $\lambda = (\sqrt{2}\pi N\sigma^2)^{-1}$, where N is the number of molecules per unit volume, and σ the molecular diameter. Denoting by subscript r all the quantities referring to reflected molecules, and plain letters for incoming molecules, it can be expected that within the superaerodynamic regime the gas temperature T and T_r, (or speeds V_m, V_{mr} of random molecular motion) must appear in the parameters of the drag formula. That this is so will subsequently be seen. Let us here first introduce the two following parameters: the modified Mach Number S and temperature ratio T_r/T:

$$S = V/V_m = \beta V = V/\sqrt{2RT} \tag{1}$$

where V denotes magnitude of body velocity, V_m the most probable molecular speed $\sqrt{2RT}$ for equilibrium temperature T of undisturbed gas, and R the specific gas constant. The corresponding modified Mach Number for re-emitted gas can be expressed as:

$$S_r = V/V_{mr} = S\beta_r/\beta = S\sqrt{T/T_r} \tag{2}$$

Before proceeding to determine the drag force—i.e., to carry out the momentum-transfer analysis between the gas and solid surface, let us observe that appropriate distribution laws for incoming and reflected molecules relative to a surface element at incident angle α and velocity $\boldsymbol{V}$ must first be decided upon as the basis of analysis. It is physically clear that the velocity distribution for the re-emitted molecules in relation to the body, as well as that for the gas at rest, are Maxwellian. This gives the distribution laws referred to the body coordinates as follows:

$$n(q) = \mathcal{A}Ne^{-\beta^2|\boldsymbol{q}-\boldsymbol{V}|^2} \tag{3}$$

$$n_r(q) = \mathcal{A}_rN_re^{-\beta_r^2\boldsymbol{q}^2} \tag{4}$$

Received June 20, 1958. Revised and received November 3, 1958.

* Scientific Adviser, Therm Advanced Research.

† Assuming perfect thermal accommodation.[7]

where $\boldsymbol{q}$ is the molecular velocity vector, $\mathfrak{A} = (2\pi RT)^{-3/2}$, and

$$|\boldsymbol{q} - \boldsymbol{V}|^2 = (q_x - V\sin\alpha)^2 + (q_y + V\cos\alpha)^2 + q_z^2$$

The collision rate per unit area is then obtained as follows:

$$n = \mathfrak{A}N\boldsymbol{f}_{\mathcal{I}} q_n e^{-\beta^2|\boldsymbol{q}-\boldsymbol{V}|^2} d\boldsymbol{q} = (NV_m/2\sqrt{\pi})\chi \quad (5)$$

where q_n denotes the component of molecular velocity normal to its surface element, and the following abbreviations have been adopted:

$$\chi = \exp(-S^2\sin^2\alpha) + \sqrt{\pi}S\sin\alpha[1 + \operatorname{erf}(S\sin\alpha)] \quad (6)$$

$$\operatorname{erf}(\eta) = (2/\sqrt{\pi})\int_0^\eta e^{-\xi^2}d\xi \quad (7)$$

$$\boldsymbol{f}_{\mathcal{I}} F(\boldsymbol{q})d\boldsymbol{q} = \int_{-\infty}^{\infty}\int_{-\infty}^{\infty}\int_0^{\infty} F(\boldsymbol{q})dq_x dq_y dq_z = 2\pi\int_0^{\infty}\int_0^{\pi/2} F(\boldsymbol{q})q^2\sin\theta d\theta dq \quad (8)$$

The drag force experienced by a small surface element dA, at temperature T_r, incident angle α, velocity $\boldsymbol{V}$, in a rarefied gas at rest (with T and T_m), can then be obtained as the sum of the two following contributions.

Impact drag:

$$dD_i = dA\,\boldsymbol{f}_{\mathcal{I}}\{\boldsymbol{q}\cdot\boldsymbol{V}/|\boldsymbol{V}|\}q_n mn(q)d\boldsymbol{q} = dA(\rho V^2/2)\{(1/\sqrt{\pi}S)e^{-S^2\sin^2\alpha} + \sin\alpha[1 + (1/2S^2)][1 + \operatorname{erf}(S\sin\alpha)]\} \quad (9)$$

Reactive drag: The rate of re-emission per unit area is easily obtained as follows.

$$n_r = \boldsymbol{f}_{\mathcal{I}} n_r(q)d\boldsymbol{q} = N_r/2\sqrt{\pi}\beta_r \quad (10)$$

Since there is neither accumulation nor net loss of molecules on the solid surface, n_r must equal n, and so the following relation exists:

$$N_r = N\chi\beta_r/\beta = N\chi S_r/S \quad (11)$$

Thereupon we have:

$$dD_r = dA\sin\alpha\,\boldsymbol{f}_{\mathcal{I}} q_n^2 mn_r(q)d\boldsymbol{q} = dA(\rho V^2/2)(1/2SS_r)\chi\sin\alpha \quad (12)$$

Combining Eqs. (9) and (12), following expression for total differential drag is obtained:

$$dD = (\rho V^2/2)\{[(1/\sqrt{\pi}S) + (1/2S^2)\sqrt{T_r/T}\times\sin\alpha]e^{-S^2\sin^2\alpha} + \sin\alpha[1 + (1/2S^2) + (\sqrt{\pi}/2S)\sqrt{T_r/T}\sin\alpha][1 + \operatorname{erf}(S\sin\alpha)]\}\,dA \quad (13)$$

We notice, as expected, two parameters for free-molecule drag: S and T_r/T. Hypothetically, there are nine cases according to the scheme:

Low subsonic $S \ll 1$		$T_r/T \gg 1$ Very hot body
Compressible $S \sim 0(1)$		$T_r/T \sim 0(1)$
Hypersonic $S \gg 1$		$T_r/T \ll 1$ Very cold body

Physical considerations, however, impose the following upper bound on the ratio T_r/T: $T_r/T \not> 0(10)$ or $\sqrt{T_r/T} \sim 0(1)$. Hence, for practical considerations the six extreme cases corresponding to very hot and very cold bodies can be disregarded as unrealistic. We are left with essentially three main cases covering the entire Mach Number spectrum. It must not be inferred at this point, however, that T_r/T will not play a parametric role; indeed, we shall later see that it does.

Now it can easily be shown that simplifications are possible at the two following speed extremes:

(a) Hypersonic Extreme, $S \gg 1$: In this case, Eq. (13) simplifies to

$$dD = \rho V^2[1 + (\sqrt{\pi}/2S)\sqrt{T_r/T}\sin\alpha]\sin\alpha\,dA \quad (14)$$

This formula is readily identifiable with the random-reflection law adopted in reference 8.

(b) Low-Subsonic Extreme, $S \ll 1$: In this case, Eq. (13) reduces to

$$dD = (\rho V_m^2/2)\{(S/\sqrt{\pi})[1 + (\pi/2)\sqrt{T_r/T}\times\sin^2\alpha] + (1/2)(1 + \sqrt{T_r/T})\sin\alpha\}\,dA \quad (15)$$

It can easily be shown that Eq. (15) provides correct evaluation of the free-molecule viscosity. Indeed, on putting $\alpha = 0$ and $S \neq 0$ in Eq. (15), we obtain, in agreement with reference 9.

$$dD = (\rho V V_m/2\sqrt{\pi})\,dA \quad (16)$$

On the other hand, when $\alpha \neq 0$ and S is negligible, we have

$$dD = (\rho V_m^2/4)(1 + \sqrt{T_r/T})\sin\alpha\,dA$$

which, for $T_r/T = 1$, gives the following expected result:

$$dD = (\rho V_m^2/2)\sin\alpha\,dA \quad (17)$$

(2) A Generalized Variational Problem

The total nose drag for a moving body is obtained by integrating Eq. (13). For an axial symmetric nose, upon introducing meridianial coordinates, x axial and y radial, we can write $dA = 2\pi y\sqrt{1 + y'^2}\,dx$, and $\sin\alpha = y'/\sqrt{1 + y'^2}$. Thus, for such a body traveling along its axial path in a highly rarefied gas, the nose drag is obtained from the following integration:

$$D = \pi\rho V^2\int_0^l \{[(1/\sqrt{\pi}S) + (1/2S^2)\sqrt{T_r/T}\,(y'/\sqrt{1 + y'^2})]e^{-S^2y'^2(1+y'^2)^{-1}} + (y'/\sqrt{1 + y'^2})[1 + (1/2S)^2 + (\sqrt{\pi}/2S)\sqrt{T_r/T}\,(y'/\sqrt{1 + y'^2})][1 + \operatorname{erf}(Sy'/\sqrt{1 + y'^2})]\}\,y\sqrt{1 + y'^2}\,dx \quad (19)$$

Now to obtain an optimum nose curve that gives least drag, the integral (19) must be minimized by the method of variational calculus.[12–14] On account of the unusual form of the integral which we will have to encounter in the investigation, let us first briefly introduce the following statement and procedure of solution for a generalized variational problem.[15]

For the minimization of expression

$$D = G(y_0) + H(y_l) + \int_0^l F(y, y', x)dx \qquad (20)$$

we must have a vanishing first variation and a positive second variation—i.e.:

$$\delta D = G_{y_0}\delta y_0 + H_{y_l}\delta y_l + [F_{y'}\delta y]_0^l + \int_0^l [F_y - (F_{y'})']\delta y dx = 0 \qquad (21)$$

$$\delta^2 D > 0 \qquad (22)$$

The minimizing solution y is accordingly determined by the following conditions.

(a) Euler's variational equation:

$$\varphi = (F_{y'})' - F_y = 0, \quad 0 < x < l \qquad (23)$$

(b) First end conditions—$\delta D_i = 0$, $(i = 0, l)$—i.e.:

$$\left.\begin{aligned} \psi_0\delta y_0 &= [G_{y_0} - (F_{y'})_0]\,\delta y_0 = 0 \\ \psi_l\delta y_l &= [H_{y_l} + (F_{y'})_l]\,\delta y_l = 0 \end{aligned}\right\} \qquad (24)$$

(c) Legendre's second variational inequality:

$$F_{y'y'} > 0, \quad 0 < x < l \qquad (25)$$

(d) Second end conditions:

$$\delta^2 D_i \geq 0, \quad (i = 0, l) \qquad (26)$$

It is easy to see that (a) and (b) are conditions for extremization, while (c) and (d) are conditions for minimization.

The variational equation is itself an ordinary differential equation of second order, with a condition specified at each end point—i.e., a two-point problem. If the terminal points y_0, y_l are both specified, then $\delta y_0 = \delta y_l = 0$, condition (24) is met. If, on the other hand, y_0 and/or y_l are not specified—i.e., $\delta y_0 \neq 0$ and/or $\delta y_l \neq 0$, then the first end conditions are furnished by Eq. (24), which requires: $\psi_0 = G_{y_0} - (F_{y'})_0 = 0$ and/or $\psi_l = H_{y_l} + (F_{y'})_l = 0$.

A nose problem is usually so formulated that the nose length l and base radius y_l are both specified; whereas the tip radius y_0 may or may not be specified, as the situation demands. Hence it is evident that our optimum nose curve must necessarily be: (a) a solution of the variational Eq. (23), which satisfies (b) the second variational inequality (25) in the interval $0 < x < l$, (c) the first end condition $\delta y_0 = 0$ or $\psi_0 = G_{y_0} - (F_{y'})_0 = 0$, and (d) the second end condition (26). To ensure satisfaction of the second end condition, however, on account of the extreme complication of a second variation, an alternative procedure of graphing the characteristic curves will be adopted.[15]

(3) Drag Minimization for Axially Symmetric Nose

From the complex nature of integral (19), it is evident that analytical optimization for the entire range of S is out of the question. For the two speed extremes discussed above, however, optimization can be easily carried out.

(a) *Hypersonic Solution, $S \gg 1$:* We obtain, from Eq. (14),

$$\begin{aligned} D &= 2\pi\rho V^2 \int_0^l [1 + cy'(1 + y'^2)^{-1/2}]yy'dx \\ &= \rho V^2(1 + c)\pi y_0^2 + 2\pi\rho V^2 \int_0^l [yy' + cyy'^2(1 + y'^2)^{-1/2}]dx \\ &= \pi\rho V^2 \left\{ y_l^2 + c\left[y_0^2 + 2\int_0^l yy'^2(1 + y'^2)^{-1/2}\,dx \right] \right\} \end{aligned} \qquad (27)$$

where we have put $c = (\sqrt{\pi}/2S)\,(T_\tau/T)^{1/2}$. It is easy to see that this drag formula is of type (20), with

$$G = y_0^2, \quad F = 2yy'^2(1 + y'^2)^{-1/2} \qquad (28)$$

and the end conditions are

$$\delta y_l = 0; \quad \delta y_0 = 0, \quad \text{or} \quad \psi_0 = G_{y_0} - (F_{y'})_0 = 0 \qquad (29)$$

Substituting Eq. (28) into Eq. (23), the following variational equations are obtained:

$$y'' = -y'^2(1 + y'^2)/y(2 - y'^2) \qquad (30)$$

$$y' = \infty \qquad (31)$$

The solution of Eq. (30) in parametric form has been given as follows:[11]

$$\begin{aligned} y &= C_1(1 + y'^2)^{3/2}/y'^2 \\ x &= (C_1/3)[(2\sqrt{1 + y'^2}/y'^3) - (\sqrt{1 + y'^2}/y') + 3\ln(y' + \sqrt{1 + y'^2})] + C_2 \end{aligned} \qquad (32)$$

whereas the solution of Eq. (31) is simply:

$$x = C \qquad (33)$$

On putting Eq. (28) into Eq. (25), the second variational inequality requires:

$$F_{y'y'} = 2 - y'^2 > 0; \quad \text{i.e., } y' < \sqrt{2} \qquad (34)$$

Now differential Eq. (30) indicates there are two branch curves merging at the cuspidal point $y' = \sqrt{2}$; solution (32) shows that the axis $y = 0$ cannot be reached, and y grows indefinitely, both as y' approaches zero and infinity. Thus the correct branch is specified by the requirement (34), which, together with Eq. (32), imposes the following limitations on the admissible values of y':

$$0 < y' < \sqrt{2}, \quad y'' < 0 \qquad (35)$$

The first end conditions require $\psi_0\delta y_0 = 0$:

(a) For specified y_0: $\delta y_0 = 0$. In this case, the second end condition is automatically satisfied. In

view of the limitations on the admissible values of y', it is evident that with prescribed nose length l and base radius y_l, there is a lower bound for admissible tip radius y_0, below which no solution exists. Within its admissible range, it is easy to see that specification of x_0, y_0, x_l, and y_l uniquely determines the four unknowns C_1, C_2, y_0', and y_l', by the four independent equations from parametric solution (32).

(b) For unspecified y_0:

$$\psi_0 = G_{y_0} - (F_{y'})_0 = y_0[1 - y_0'(2 + y_0'^2) \times (1 + y_0'^2)^{-3/2}] = 0 \quad (36)$$

Although both $y_0 = 0$ and $y_0' = \infty$ satisfy Eq. (36), neither of them is admissible for our solution (32). However, ψ_0 does vanish at

$$y_0' = [(\sqrt{5} - 1)/2]^{1/2} = 0.7862 < \sqrt{2} \quad (37)$$

and, furthermore, the characteristic curve $\psi_0(y_0')$ does lead to $\delta D_0(y_0' \pm \epsilon) > 0$ at this value of y_0'—i.e., satisfies the second end condition. Thus, with unspecified y_0, the value of y_0' (= 0.7862) is fixed by the condition (36). Actual construction of the optimum curve then amounts to specifying x_0, x_l, y_0'(= 0.7862), and y_l, from which four unknowns y_0, y_l', C_1, and C_2 are determined by the four independent equations from parametric solution (32).

It is interesting to note that in references 8 and 11 the drag integral was formulated without considering the tip contribution; hence, the analysis remains valid only for the case of prescribed y_0—i.e., $\delta y_0 = 0$. With the other end condition $\psi_0 = 0$ lost, that analysis is entirely helpless in handling the case of unspecified y_0. To remedy this situation, a tip slope $y_0' = \sqrt{2}$—i.e., the critical value, was arbitrarily introduced. From the present analysis, it is now clear that this step cannot be justified, and the result obtained by taking $y_0' = \sqrt{2}$ is in general erroneous. Indeed, y_0' does not assume its critical value $\sqrt{2}$ at all, unless: (a) in case of specified y_0, y_0 happens to be such that it leads to $y_0' = \sqrt{2}$; or (b) in case of unspecified y_0, the nose length l is made infinite, thereby allowing $y_0 \to 0$, in which case the end condition (36) is again satisfied.

On the other hand, it will not be difficult to show that the solution (33) and the other branch of solution (32) with $y' > \sqrt{2}$ both give maximum values of the drag.

(b) Low-Subsonic Solution, $S \ll 1$: We have, from Eq. (15),

$$D = \pi\rho V_m^2 \int_{0-}^{l} [ay(1 + y'^2)^{1/2} + byy' + cyy'^2(1 + y'^2)^{-1/2}]dx$$

$$= \pi\rho V_m^2 \left\{(b/2)y_l^2 + [(a + c)/2]y_0^2 + \int_0^l [ay\sqrt{1+y'^2} + cyy'^2(1 + y'^2)^{-1/2}]dx\right\} \quad (38)$$

where we have put $a = S/\sqrt{\pi}$, $b = [1 + \sqrt{T_r/T}]/2$, $c = S\sqrt{\pi T_r/T}/2$; and $k = c/a = (\pi/2)(T_r/T)^{1/2}$. It is easy to see that this expression corresponds to Eq. (20), with

$$G = [(1 + k)/2]y_0^2, \quad F = y\sqrt{1 + y'^2} + kyy'^2(1 + y'^2)^{-1/2} \quad (39)$$

Substituting Eq. (39) into Eq. (23), the following variational equations are obtained:

$$y'' = (1 + y'^2)[1 + (1 - k)y'^2] \div y[1 + 2k + (1 - k)y'^2] \quad (40)$$

and

$$y' = \infty \quad (41)$$

The solution of Eq. (40) in parametric form can easily be obtained by quadrature, in the same manner as for Eq. (30),[11] and, after simplification, it takes the following form:

$$\left.\begin{aligned} y &= C_1(1 + y'^2)^{3/2}/[1 + (1 - k)y'^2] \\ x &= C_1 \int (1 + y'^2)^{1/2}[1 + 2k + (1 - k)y'^2][1 + (1 - k)y'^2]^{-2}\,dy' \\ &= C_1\left\{\frac{1}{2(1 - k)} \ln\left(\frac{\sqrt{1 + y'^2} + y'}{\sqrt{1 + y'^2} - y'}\right)\left(\frac{\sqrt{1 + y'^2} - \sqrt{k}y'}{\sqrt{1 + y'^2} + \sqrt{k}y'}\right)^{k^{3/2}} + \frac{ky'\sqrt{1 + y'^2})}{1 + (1 - k)y'^2}\right\} + C_2 \end{aligned}\right\} \quad (42)$$

while the solution of Eq. (41) is simply

$$x = C \quad (43)$$

On putting Eq. (39) into Eq. (25), the second variational inequality requires:

$$\left.\begin{aligned} &F_{y'y'} = 3k + (1 - k)(1 + y'^2) > 0; \\ \text{i.e.,} \quad &\text{for } k > 1: \quad y' < \sqrt{(2k + 1)/(k - 1)} \end{aligned}\right\} \quad (44)$$

for $k < 1$, inequality is identically satisfied for all y', $y'' > 0$.

Differential Eq. (40) indicates that the one-parameter family of solutions changes character at $k = 1$: for $k < 1$, there is no singular curvature; for $k > 1$, all curves branch at a cuspidal point $y' = \sqrt{(2k + 1)/(k - 1)}$. Solution (42) shows that the axis $y = 0$ cannot be reached unless $y \equiv 0$, and y grows indefinitely as y' approaches $(k - 1)^{-1/2}$ and infinity. Taking Eq. (44) into consideration, it is now clear that: (a) for $k < 1$, both solutions (42) and (43) give minimum values of drag, (b) for $k > 1$, Eqs. (44) and (42) together impose the following limitations on the admissible values of y':

$$1/\sqrt{k - 1} < y' < \sqrt{(2k + 1)/(k - 1)}, \quad y'' < 0 \quad (45)$$

while solution (43) and the other branch of solution (42) with $y' > \sqrt{(2k + 1)/(k - 1)}$ both lead to maximum values of the drag.

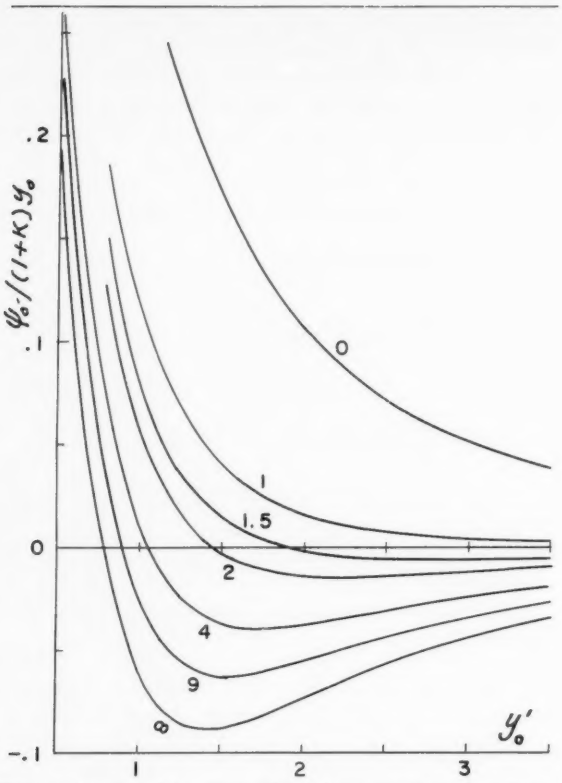

FIG. 1. Characteristic curves, Eq. (43). Low-subsonic solution ($S \ll 1$).

Now the first end conditions require $\psi_0 \delta y_0 = 0$:

(a) For specified y_0: $\delta y_0 = 0$. In this case, the second end condition is automatically satisfied. For specified nose length l and base radius y_l, the nature of solution (42) imposes a lower bound on the admissible values of tip radius y_0, below which no solution exists. Within its admissible range, specification of x_0, y_0, x_l, and y_l uniquely determines the four unknowns C_1, C_2, y_0', and y_l', from which the optimum nose curve can be constructed. Stated in an alternative way, with prescribed y_0 and y_l, the admissible nose length l is bounded below for $k > l$, bounded above for $k < l$.

(b) For unspecified y_0:

$$\psi_0 = G_{y_0} - (F_{y'})_0 = y_0 \{1 + k - y_0'[1 + 2k + (1 + k)y_0'^2] (1 + y_0'^2)^{-3/2}\} = 0 \quad (46)$$

It can easily be seen that both $y_0 = 0$ and $y_0' = \infty$ satisfy Eq. (46).

However, for $k > 1$, neither of these conditions $y_0 = 0$ or $y_0' = \infty$ can be met by our solution (42). On the other hand, $\psi_0(y_0', k)$ does vanish at

$$y_0' = \left(\{k\sqrt{5k^2 + 4k} - [k^2 - 2(1 + k)]\} \div 2(k^2 - 1)\right)^{1/2} < \sqrt{(2k + 1)/(k - 1)} \quad (47)$$

for all $k > 1$, and the characteristic curve does give $\delta D_0(y_0' \neq \epsilon) > 0$ at the corresponding value of y_0'—i.e., satisfies the second end condition $\delta^2 D_0 > 0$. Indeed, for $k > 1$; we have

y_0'	$0 \rightarrow \sqrt{(2k + 1)/(k - 1)} \rightarrow \infty$
ψ_0/y_0	$1 + k \rightarrow (-) \qquad \rightarrow 0-$

Thus, the roots y_0' of $\psi_0 = 0$ must lie at $0 < y_0' < \sqrt{(2k + 1)/(k - 1)}$. To find for what value of k the characteristic curves cease to cross axis $\psi_0 = 0$, we need the limiting value of k that gives $d\psi_0/dy_0' = 0$ at $y_0' = \infty$. Now from

$$d\psi_0/dy_0' = (1 + k)(1 + y_0'^2) + k(1 - 2y_0'^2) = 0 \quad (48)$$

it is clear that characteristic curves $\psi_0(y_0', k)$ have their minimum at $y_0' = \sqrt{(2k + 1)/(k - 1)}$. Furthermore, on putting $y_0' = \infty$ in Eq. (48), it is then obtained: $k = 1$.

Thus, for $k > 1$, the proper value of y_0' for optimum nose curve is given by expression (47), through the end condition $\psi_0 = 0$, Eq. (46).

For $k < 1$, while end condition (46) fails to give a proper value of finite y_0', it must be pointed out that in this case, both end conditions $y_0' = \infty$ and $y_0 = 0$—i.e., $y \equiv 0$—are now compatible with the other minimum solution (43), $y' = \infty$. Hence, in this case, if choice of y_0 is entirely free, the optimum nose curve will simply be a flat tip: $y \equiv 0$, $0 < x < l$; $y = y_l$, $x = l$.

It might be interesting to point out here that the curve for $k = \infty$ is precisely that for the hypersonic solution. This is not surprising if we note that on putting $k = \infty$ we reduce Eq. (40) to Eq. (30). On the other hand, it can also be shown that the curve for $k = 0$ is precisely the minimal-surface solution. However, as already mentioned, these two extreme cases $k = \infty$ (infinitely hot body) and $k = 0$ (infinitely cold body) are rather hypothetical, and not of much practical interest.

(4) Discussion of Results and Concluding Remarks

Nose drag in free-molecule flow was briefly discussed in Part (1). It was pointed out that this drag involves two parameters: the speed ratio S between the ordered and random molecular motions (modified Mach Number), and the temperature ratio T_r/T between the solid surface and undisturbed gas. Simplifications of the

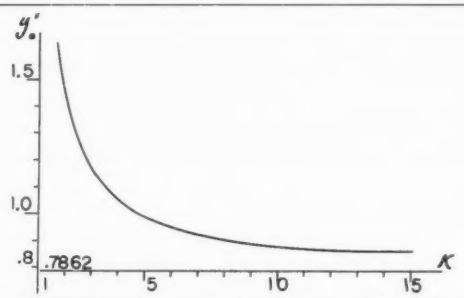

FIG. 2. Proper tip slope for optimum nose curves, unspecified tip radius ($S \ll 1$).

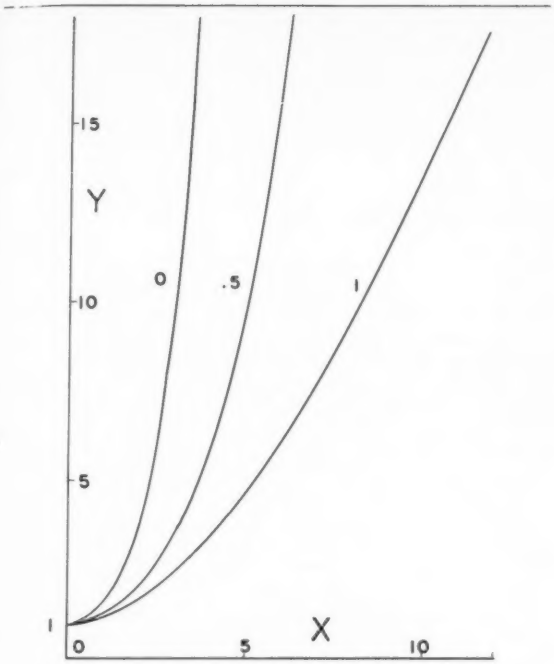

FIG. 3. Low-subsonic optimum nose curves, $k < 1$.

drag formula were obtained at hypersonic as well as low-subsonic extremes.

To minimize the drag on a nose of specified length and base radius, the ordinary method of calculus of variations was found to be inadequate. A generalized approach was developed accordingly in Part (2), and the specification of end conditions discussed at length.

In Part (3), the technique developed in Part (2) was applied to the two extreme cases considered in Part (1) for an axially symmetric body in free-molecule flow. The optimum nose curve solutions in both cases were obtained in parametric presentation, and their analytic behavior was discussed in detail.

Results of the present investigation indicate that in all cases an optimum nose in free-molecule flow requires a flat tip. This alarming conclusion has its counterpart in continuum flow at the hypersonic extreme,[16, 17] and is evidently a consequence of the corpuscular nature of the flow model adopted. The general shape of the nose curve for the hypersonic extreme is found to be independent of the temperature ratio and resembles a slender conventional ogive warhead with a flat tip. The shape for the low-subsonic extreme varies with temperature ratio T_r/T in the following manner: for a hot body the curve is convex; for a cold body, concave. Both shapes have flat tips. For a nose with specified length, tip and base radii, the solution exists within a restricted range only. Indeed, in the cases of hypersonic and low-subsonic hot body, with specified values of tip and base radii, there is a lower limit of nose length below which no solution can be found. Furthermore, by keeping the base radius fixed and letting the tip radius approach zero, the required nose length approaches infinity. In the low-subsonic cold-body case, the situation is reversed—i.e., there is an upper limit of nose length for specified tip and base radii, and on letting the tip radius approach zero, the admissible nose length also vanishes.

In Fig. 1, characteristic curves for $S \ll 1$ are plotted. The axis-crossing points represent the first end condition—i.e., give the proper tip slope for the unspecified-tip-radius problem; the negative slopes at crossing points represent the second end condition. The bottom curve ($k = \infty$) is identical with that for the hypersonic solution ($S \ll 1$).

In Fig. 2, the proper tip slopes for optimum nose curves ($S \ll 1$) Eq. (47), are plotted against k. It is interesting to note that the proper tip slope is a function of temperature ratio alone, it exists only for $k > 1$, and its value always lies below the critical value given by Eq. (44).

In Figs. 3 and 4 optimum nose curves for several values of k, ($S \ll 1$), are presented. It may be pointed out that there is a general tendency of shortening in nose length with decreasing temperature ratio, provided the base radius remains fixed. It may also be noted that at the low-subsonic extreme, the hot-body solution ($k > 1$) asymptotically approaches the hypersonic solution as the temperature ratio approaches infinity—i.e., takes on the shape of a slender conventional nose with flat tip; whereas the cold-body solution ($k < 1$) asymptotically approaches the minimal surface solution as temperature ratio approaches zero—i.e., (a) with prescribed tip radius, a catenoid; (b) with unspecified tip radius, a flat disc.

In order to facilitate access to the results of the present investigation, a tabulation of results has been constructed (see Table 1, following page).

REFERENCES

[1] Maxwell, J. C., *On the Conditions to be Satisfied by a Gas at the Surface of a Solid Body*, Scientific Papers, Vol. 2, p. 704.

[2] Epstein, P. S., *On the Resistence Experienced by Spheres in Their Motion Through Gases*, Phys. Rev., Vol. 23, p. 710, 1924.

[3] Millikan, R. A., *The General Law of Fall of a Small Spherical Body through a Gas, and Its Bearing upon the Nature of Molecular Reflection from Surfaces*, Phys. Rev., Vol. 22, p. 1, 1923.

[4] Tsien, H. S., *Superaerodynamics, Mechanics of Rarefied Gases*, Journal of the Aeronautical Sciences, Vol. 13, No. 12, pp. 653–664, December, 1946.

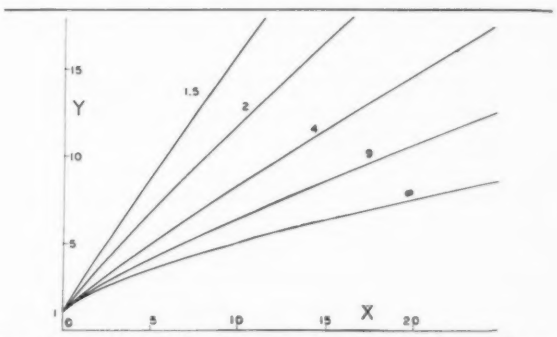

FIG. 4. Low-subsonic optimum nose curves, $k > 1$. (Curve $k = \infty$ is identical with hypersonic optimum nose curve)

TABLE 1
Minimum-Drag Nose-Curve Solutions for Free-Molecule Flow

	Hypersonic ($S \gg 1$)	Low Subsonic ($S \ll 1$)	
		$k > 1, \left(\sqrt{\frac{T_r}{T}} > \frac{2}{\pi}\right)$	$k < 1, \left(\sqrt{\frac{T_r}{T}} < \frac{2}{\pi}\right)$
Minimum Drag	Eq. (32) $0 < y' < \sqrt{2}$ $y'' < 0$	Eq. (42) $\frac{1}{\sqrt{k-1}} < y' < \sqrt{\frac{2k+1}{k-1}}$ $y'' < 0$	Eq. (42) $y'' > 0$
			Eq. (43) $x = 0, (y' = \infty)$
Proper y_0'*	0.7862, Eq. (37)	Eq. (47)	
Maximum Drag	Eq. (32) $\sqrt{2} < y' < \infty$ $y'' > 0$	Eq. (42) $\sqrt{\frac{2k+1}{k-1}} < y' < \infty$ $y'' > 0$	
	Eq. (33) $x = C$ $(y' = \infty)$	Eq. (43) $x = C$ $(y' = \infty)$	

* For unspecified y_0.

[5] Ashley, H., *Applications of the Theory of Free Molecule Flow to Aeronautics*, Journal of the Aeronautical Sciences, Vol. 16, No. 2, pp. 95–104, February 1949.

[6] Stalder, J. R., Goodwin, G., and Creager, M. O., *A Comparison of Theory and Experiment for High-Speed Free-Molecule Flow*, NACA Report 1032, 1951.

[7] Knudsen, M., *Die molekulare Wärmeleitung der Gase und der Akkommodationskoefficient*, Ann. Physik, Vol. 34, p. 593, 1911.

[8] Carter, W. J., *Optimum Nose Shapes for Missiles in the Superaerodynamic Region*, Journal of the Aeronautical Sciences, Vol. 24, No. 7, pp. 527–532, July, 1957.

[9] Kennard, E. H., *Kinetic Theory of Gases;* McGraw Hill Book Company, New York, 1938.

[10] Patterson, G. N., *Molecular Flow of Gases;* John Wiley and Sons, 1956.

[11] Tan, H. S., *On Optimum Nose Curves for Superaerodynamic Missiles*, Journal of the Aeronautical Sciences, Readers' Forum, Vol. 25, No. 4, pp. 263–264, April, 1958.

[12] Jeffreys, M., and Jeffreys, B. S., *Methods of Mathematical Physics;* Cambridge University Press, Cambridge, England, 1950.

[13] Courant, R., and Hilbert, D., *Methoden der mathematischen Physik;* Julius Springer, Berlin, 1937.

[14] Bliss, G. A., *Calculus of Variations;* Open Court, 1944.

[15] Tan, H. S., *On a Special Bolza Variational Problem*, to be published.

[16] Newton, Isaac, *Principia*, University of California Press, Berkeley, Calif., 1946.

[17] Eggers, A. J., Jr., Resnikoff, M. M., and Dennis, D. H., *Bodies of Revolution Having Minimum Drag at High Supersonic Airspeeds*, NACA Report 1306, 1957.

Advances in Aeronautical Science

Proceedings of the First International Congress of the Aeronautical Sciences, Madrid, 1958 (2 Vols.)

In these two volumes are published the 46 papers presented by the world's outstanding specialists in the field of aeronautics and astronautics at the First International Congress of the Aeronautical Sciences held in Madrid in September, 1958, under the leadership of Prof. Theodore von Kármán. Some 600 delegates from 25 countries, including an official delegation from the U.S.S.R., attended, and the meeting was so successful that it was decided to hold similar congresses at 2-year intervals in future.

The volumes have a full author and subject index and number 1,200 pages. The *Proceedings*, edited by Th. von Kármán, A. M. Ballantyne, H. Blenk, R. R. Dexter, M. Roy, and H. L. Dryden, are of special interest to aerodynamicists, aeronautical engineers, rocketry research workers, and propulsion engineers.

The *Proceedings* (price, $30.00) may be obtained by writing to: *Sales Director, Pergamon Press, Inc., 122 East 55 St., New York 22, N.Y.*

Further Developments of New Methods in Heat-Flow Analysis†

M. A. BIOT*

Cornell Aeronautical Laboratory, Inc.

SUMMARY

Lagrangian methods in heat-flow problems and transport phenomena were introduced by the writer in some previous work. The present paper develops further one particular aspect of the method,—i.e., the elimination of "ignorable coordinates." This is accomplished by a special choice of generalized coordinates, each of which is constituted by an arbitrary temperature distribution and an "associated flow field." The latter is a vector field which is derived from the corresponding scalar field by a variational method. The procedure is valid for a certain class of nonlinear problems, provided we replace the temperature by the heat content as the unknown. It is shown that for normal coordinates derivation of the associated flow field is immediate. The use of normal coordinates and their associated flow fields is illustrated by an example. Introduction of Dirac functions and associated flow fields yields a procedure which constitutes a generalization of the classical formulation by Green's functions and integral equations. This is illustrated by application to one-dimensional problems of heating of a homogeneous or composite slab and directly verified by classical methods in the Appendix.

(1) INTRODUCTION

IN A PREVIOUS PUBLICATION[1] we have introduced new methods in heat-flow analysis. These methods have a two-fold basis; first, a new formulation of the thermodynamics of irreversible processes, and, second, the application of Lagrangian techniques to the mathematical analysis itself. The earlier developments were carried out in references 2, 3, and 4. We have recently reviewed in more detail in reference 5 the basic thermodynamic concepts and principles.

The formulation of dissipative phenomena into a variational language can be achieved in many ways.‡ The particular method which we have chosen is different from the classical variational approaches. It appears to be the most general and fits into a unified thermodynamic theory embracing a large category of physical phenomena, which leads to equations of the same type as in Lagrangian mechanics. A particularly useful concept which has been introduced is the *generalized thermodynamic force by a principle of virtual work*. In the case of thermal problems this results in a representation of the physical system by means of a vectorial flow field and to the use of a generalized thermal force to represent the externally applied temperatures. It also leads to new methods of numerical analysis of considerable advantage from the standpoint of simplicity and accuracy.

Our purpose here is to further develop one aspect of the theory which was only briefly discussed in reference 1. Heat flow may be separated into one part which represents the temperature field and another which is divergence-free and has no effect on the temperature and which we have referred to as "ignorable" in analogy with the coordinates of the same name in classical dynamics. We have also previously shown that these ignorable coordinates may be uncoupled from those representing the temperature alone, thereby reducing appreciably the number of unknown variables in the equations.

The present paper discusses and introduces additional properties of those generalized coordinates which are automatically uncoupled with the ignorable coordinates. In particular, this is achieved by choosing for each generalized coordinate a certain spatial temperature configuration of normalized amplitude and associating with it a certain vector field which we have referred to as the "associated flow field." The two fields are tied to each other and represent one simple generalized coordinate. In order to determine a particular coordinate we first choose a certain temperature configuration. The associated vector field is then derived from this temperature distribution by a variational method, using a principle of minimum dissipation. In a nonlinear problem we must choose a heat content configuration instead of a temperature field. Having thus determined a set of generalized coordinates, we are in a position to establish the Lagrangian differential equations which yield the time history of the system. Attention is called to the fact that the calculation is performed in steps. The first involves the evaluation of the associated flow field, and the second the evaluation of the Lagrangian equations. Each of these steps makes use only of variational methods and do not involve any spatial differentiation of the approximate field distribution adopted as generalized coordinates. This results in improved accuracy since none of the steps involve differentiation while the integrals used in evaluating the Lagrangian equations represent an averaging process over volumes or surfaces. The procedure is in contrast with classical variational methods which require the evaluation of the temperature gradient. The separation of the calculation into two successive steps with a concurrent reduction in the number of unknowns

Received July 2, 1958.

† This paper is based on Cornell Aero. Lab. Report SA-987-S-5, May, 1958.

* Consultant.

‡ Other variational formulations of heat conduction have also been proposed by Rosen[6] and by Chambers.[7] In contrast to our approach, they do not introduce the flow field and use expressions containing the temperature gradient. The relations are purely formal, and conservation of energy is not preserved.

greatly facilitates the numerical work without sacrifice in accuracy.

In reference 1 we have treated some one-dimensional problems by a method equivalent to the use of an associated flow field. These examples did not require the development of a formal theory because, in the particular problems treated, the flow field was already determined uniquely by the temperature distribution from the equation of conservation of thermal energy. This simplification, of course, is only applicable in certain exceptional cases and does not hold for problems in two or three dimensions. Of particular interest is the relation of the method of associated fields to the classical Green's function formulation. We will show that the latter may be derived as a very particular case of the present procedure. The introduction of associated flow fields along with a Dirac function representation of the temperature leads to integral equations which are shown to be equivalent to a Green's function method. In this formulation Green's function does not appear in its classical form but as an integral of the scalar product of two associated flow fields. By the same token we obtain a new procedure for the evaluation of Green's functions by approximate variational methods.

In Section (2) we have reviewed the fundamental equation derived in the previous work. We also indicated how these equations may be applied to the case where the thermal system contains distributed internal heat sources. This is of importance even in problems which do not involve physical sources, because they may sometimes be reduced mathematically to equivalent problems with such sources which may then be solved more easily. Section (3) discusses a general method of eliminating the ignorable coordinates by the use of a flow potential. This is carried one step further in Section (4) which develops the concept of the associated flow field as a practical method of eliminating the ignorable coordinates. Variational methods for the determination of the associated flow field directly as a vector field are discussed.

In Section (5) it is shown how the associated flow field is immediately derived without further calculation for the case of normal coordinates. An example of normal coordinates is discussed in Sections (6) and (7) for the two-dimensional problem of a flat cylinder of double wedge cross-section. It is also shown that formulation of a problem with normal coordinates requires only a knowledge of the temperature distribution of each coordinate, the corresponding eigenvalue (i.e., the relaxation constant), and the normal component of the associated flow field at the boundary. Sections (8) and (9) establish integral equations and Green's function methods as a particular case of the method of associated flow fields. Section (9) illustrates the significance of the general formulation on the particular example of the one-dimensional problem of heating of a slab across the thickness. The expression for the Green's function which follows immediately from the application of the concept of associated flow fields is verified by classical methods in the Appendix. Finally, in Section (10) it is shown that the method of associated flow fields may be extended to include problems where the surface heat-transfer coefficient is a function of time.

Attention is called to the general applicability of the present results to problems other than heat transfer. The methods are directly applicable to a large class of transport phenomena obeying the same type of equations of both linear and nonlinear character. In this category we may list the problems of diffusion of solutions in chemical engineering, mass diffusion of thermal neutrons in nuclear reactors, and fluid flow through porous media as encountered in problems of petroleum engineering.

(2) Outline of the General Theory

Let us first recall some of the general results which were derived in an earlier publication.[1] We represented the thermal field by the heat flow vector field.

$$\boldsymbol{H} = \boldsymbol{H}(q_1\, q_2 \ldots q_n\, x\, y\, z\, t) \tag{2.1}$$

This may be considered as a parametric vector field. The field depends on the coordinates x, y, z, the time t, and n unknown parameters $q_1\, q_2 \ldots q_n$. These parameters may be considered as generalized coordinates. The thermal problem consists in determining how these generalized coordinates must vary as a function of time in order to represent the actual heat flow phenomenon.

The theory was developed for the very general case of linear and nonlinear physical properties—i.e., the heat capacity, thermal conductivity, and heat-transfer coefficients may be functions of the temperatures, the coordinates, and the time.

We have shown that the equations for the unknowns q_i are

$$(\partial V/\partial q_i) + (\partial D/\partial \dot{q}_i) = Q_i \tag{2.2}$$

They are n differential equations involving the time derivatives $\dot{q}_i$. The function V of q_i was referred to as the thermal potential and the function D of q_i and $\dot{q}_i$ as the dissipation function. The vector Q_i is the generalized thermal force.

The thermal potential is defined as the volume integral

$$V = \iiint_\tau F d\tau \tag{2.3}$$

where

$$F = \int_0^\theta c\theta d\theta \tag{2.4}$$

with c the heat capacity per unit volume and θ the temperature. The heat capacity may be a function of the coordinates and the temperature. The thermal potential V is a function of the flow field $\boldsymbol{H}$ by the relation expressing the conservation of energy—i.e.,

$$\int_0^\theta c\, d\theta = -\operatorname{div} \boldsymbol{H} \tag{2.5}$$

The dissipation function is defined† as

$$D = \frac{1}{2}\iiint_{\tau}\frac{1}{k}\left(\frac{\partial H}{\partial t}\right)^2 d\tau + \frac{1}{2}\iint_{S}\frac{1}{K}\left(\frac{\partial H_n}{\partial t}\right)^2 dS \quad (2.6)$$

an expression which refers to the volume τ and the heat-transfer properties of the boundary S. The symbol H_n refers to the normal component at the boundary taken positive outward. Since D is independent of the sign of H_n we may take it as positive either *inward* or *outward*. However for the sake of uniformity the subscript n will refer to the positive outward direction. The thermal conductivity k in the volume τ may be a function of the temperature and the coordinates. The surface heat-transfer coefficient is denoted by K and may also be a function of the coordinates, the time, and the temperature. As shown in reference 1, a similar expression may also be written if we wish to take care of surface radiation.

Finally, we define a generalized thermal force Q_i by a method of virtual work. If θ_a denotes the external temperature applied outside of the heat-transfer layer at the surface we write

$$Q_i\delta q_i = \iint_S \theta_a \delta H_{(n)} dS \quad (2.7)$$

where $\delta H_{(n)}$ is the variation due to δq_i alone of the normal component of the heat flow vector at the boundary S, its sign being positive *inward*. We see that expression (2.7) is equivalent to the virtual work at the boundary by the external temperature θ_a on the virtual heat flow $\delta H_{(n)}$. We use the subscript (n) to indicate that the normal component is taken positive inward in contrast to H_n which is positive outward as indicated above. The value of Q_i may be written

$$Q_i = \iint_S \theta_a[\partial H_{(n)}/\partial q_i]/dS \quad (2.8)$$

If the surface heat transfer is through an aerodynamic boundary layer the temperature θ_a is the so-called adiabatic temperature of the layer.

In the particular case of a linear system—i.e., if its properties are independent of the temperature—the thermal potential becomes

$$V = (1/2)\iiint c\theta^2 d\tau \quad (2.9)$$

and relation (2.5) is replaced by

$$c\theta = -\text{div } \boldsymbol{H} \quad (2.10)$$

In the present developments we shall be concerned primarily with systems which are linear and whose properties are also independent of time. Furthermore we shall represent the flow field linearly in terms of the variables, q_i, by

$$\boldsymbol{H} = \sum^{i} \boldsymbol{H}_i q_i \quad (2.11)$$

where

$$\boldsymbol{H}_i = \boldsymbol{H}_i(x\ y\ z) \quad (2.12)$$

are fixed configuration flow fields. In this case the thermal potential and dissipation functions are

$$\left.\begin{aligned} V &= (1/2)\sum^{ij} a_{ij}q_iq_j \\ D &= (1/2)\sum^{ij} b_{ij}\dot{q}_i\dot{q}_j \end{aligned}\right\} \quad (2.13)$$

with constant coefficients a_{ij} and b_{ij}.

The above equations do not include the case where heat is generated inside the body. The heat conduction equation in this case becomes

$$\text{div } (k \text{ grad } \theta) = c(\partial\theta/\partial t) - w \quad (2.14)$$

where w is the heat produced per unit time and per unit volume. In many engineering problems such as those involving electric heating and nuclear reactors internal heat generation must be taken into account. The equations above may be used in this case provided we replace Eq. (2.5) by

$$\int_0^t w\,dt - \int_0^\theta c\,d\theta = \text{div } \boldsymbol{H} \quad (2.15)$$

This procedure is valid for both the linear and nonlinear problem. That Eqs. (2.15) and (2.2) lead to the correct formulation of the heat flow problem when there is internal heat generation may be verified by proceeding exactly as in Sections (3) and (8) of reference 1. In this case, a particular method of formulation of the general equations for the thermal coordinates is obtained by putting

$$\int_0^t w\,dt = \text{div } \boldsymbol{H}^* \quad (2.16)$$

$$\int_0^\theta c\,d\theta = -\text{div } \boldsymbol{H}^+ \quad (2.17)$$

with

$$\boldsymbol{H} = \boldsymbol{H}^+ + \boldsymbol{H}^* \quad (2.18)$$

The field $\boldsymbol{H}^*$ is *any field* satisfying relation (2.16). Once chosen it is a given function of $x\ y\ z\ t$. The unknown portion of the field

$$\boldsymbol{H}^+ = \boldsymbol{H}^+(q_1\ q_2 \ldots q_n\ x\ y\ z\ t) \quad (2.19)$$

is a function of the unknown generalized coordinates. The temperature is defined in terms of $\boldsymbol{H}^+$ by relation (2.17). The differential equations for q_i are the same as Eq. (2.2) above, with a thermal potential (2.3), a dissipation function

$$D = (1/2)\iiint_{\tau}(1/k)\,[(\partial\boldsymbol{H}^+/\partial t) + (\partial\boldsymbol{H}^*/\partial t)]^2 dt + (1/2)\iint_S (1/K)\,[(\partial H_n{}^+/\partial t) + (\partial H_n{}^*/\partial t)]^2\,dS \quad (2.20)$$

and a thermal force

$$Q_i = \iint_S \theta_a(\partial H_{(n)}{}^+/\partial q_i)dS \quad (2.21)$$

† We are assuming here an isotropic material. The more general case of anisotropic media was developed in detail in reference 1.

The introduction of heat sources in the problem may also result from a purely formal viewpoint in a *linear* physical problem in which there are no actual heat sources. This arises if we consider the heat conduction equation (2.14) with $w = 0$ and put

$$\theta = \theta^+ + \theta^* \tag{2.22}$$

where θ^* is the *steady-state* temperature distribution which would occur under the particular instantaneous external temperatures applied to the systems at any given time. This temperature satisfies the equation

$$\text{div } (k \text{ grad } \theta^*) = 0 \tag{2.23}$$

and the instantaneous boundary conditions at time t. Since we are dealing with a linear problem, the temperature θ^+ then satisfies the equation

$$\text{div } (k \text{ grad } \theta^+) = c(\partial\theta^+/\partial t) + c(\partial\theta^*/\partial t) \tag{2.24}$$

The field θ^+ corresponds to the case *where the externally applied temperature θ_a is zero*, with heat sources

$$w = -c(\partial\theta^*/\partial t) \tag{2.25}$$

which are given functions of time, distributed throughout the body. We therefore apply relations (2.16) and (2.17). In the present case they become

$$c\theta^* = -\text{div } \boldsymbol{H}^* \tag{2.26}$$

$$c\theta^+ = -\text{div } \boldsymbol{H}^+ \tag{2.27}$$

where $\boldsymbol{H}^*$ is any particular field satisfying relation (2.26). The differential equations for the field $\boldsymbol{H}^+$ are then,

$$(\partial V/\partial q_i) + (\partial D/\partial \dot{q}_i) = 0 \tag{2.28}$$

with the thermal potential

$$V = (1/2) \iiint c\theta^{+2} d\tau \tag{2.29}$$

and a dissipation function given by Eq. (2.20).

We have already discussed in reference 1 the calculation of a transient thermal field by separation into an instantaneous steady state and a remainder. A further example of such separation will also be considered hereafter [see Section (7)].

(3) The Concept of Flow Potential

We shall now discuss a particular aspect of the general method which was already briefly touched upon in reference 1 and greatly simplifies its application. The particular procedure we have in mind results from the representation of the flow field as the sum of two fields with different properties. We introduce a scalar field

$$\psi = \psi(q_1 \ldots q_n \; x \; y \; z \; t) \tag{3.1}$$

which is a function of the generalized coordinates q_i, the space coordinates x, y, z, and which may or may not contain the time explicitly. We shall refer to ψ as the flow potential. We write the heat flow field as

$$\boldsymbol{H} = -k \text{ grad } \psi + \boldsymbol{F} \tag{3.2}$$

where $\boldsymbol{F}$ is a vector field

$$\boldsymbol{F} = \boldsymbol{F}(f_1 \ldots f_s) \tag{3.3}$$

which is a function of s generalized coordinates f_s and chosen such that it is divergence free,

$$\text{div } \boldsymbol{F} = 0 \tag{3.4}$$

The total flow field $\boldsymbol{H}$ is thus a function of $n + s$ coordinates q_i and f_i. The temperature θ is then given by ψ alone—i.e.,

$$c\theta = \text{div } (k \text{ grad } \psi) \tag{3.5}$$

We shall first assume that the heat capacity $c(x, y, z)$ and the thermal conductivity $k(x, y, z)$ are either constant or functions of the coordinates but are independent of the time or the temperature. For the time being, the surface heat-transfer coefficient $K(x, y, z)$ is assumed to be either a constant or a function of the location only. The more general case is examined in Section (10). The possibility of including the case of a time- and temperature-dependent heat-transfer coefficient has an important bearing on problems of aerodynamic heating for variable velocity boundary layers. The case where c and k are temperature-dependent will be briefly discussed at the end of this section.

The reason for splitting up the field into two parts as in Eq. (3.2) is that for many problems we are interested in the temperature distribution only, and not in the heat flow. Now $\boldsymbol{F}$, being a divergence-free field, does not contribute to the temperature. Hence, somehow the problem would be simplified if we could ignore this field and find equations which involve only ψ. In other words, we are interested in *decoupling* the two fields ψ and $\boldsymbol{F}$.

We will show that this can be done by choosing ψ in an appropriate way. Consider first the thermal potential

$$V = (1/2) \iiint c\theta^2 d\tau \tag{3.6}$$

The value of θ is determined by Eq. (3.5). Hence, the thermal potential does not contain $\boldsymbol{F}$ and depends only on the coordinates q_i. This is also true if heat is generated internally, in which case we must use Eq. (2.15). Next, consider the dissipation function

$$D = (1/2) \iiint_\tau (1/k)(\partial \boldsymbol{H}/\partial t)^2 d\tau + (1/2) \iint_S (1/K)(\partial H_n/\partial t)^2 dS \tag{3.7}$$

From Eq. (3.2) we derive

$$\partial \boldsymbol{H}/\partial t = -k \text{ grad } \dot{\psi} + (\partial \boldsymbol{F}/\partial t) \tag{3.8}$$

$$\partial H_n/\partial t = -k \text{ grad}_n \dot{\psi} + (\partial F_n/\partial t) \tag{3.9}$$

Where $\text{grad}_n \dot{\psi}$ and $\partial F_n/\partial t$ are the normal components at the boundary of the vectors grad $\dot{\psi}$ and $\partial \boldsymbol{F}/\partial t$. As pointed out above, we may choose the positive direction of these normal components as we please. In conformity with our previous choice, the subscript n denotes the normal component taken positive outward. Substituting expressions (3.8) and (3.9) in the dissipa-

tion function (3.7), we may write it as the sum of three terms:

$$D = D_\theta + D_{\theta f} + D_f \tag{3.10}$$

where

$$D_\theta = (1/2) \iiint_\tau k(\text{grad } \psi)^2 d\tau + (1/2) \iint_S (k^2/K)\ (\text{grad}_n\ \psi)^2 dS$$

$$D_{\theta f} = -\iiint_\tau (\text{grad } \psi)\ (\partial \boldsymbol{F}/\partial t) d\tau - \iint_S (k/K)\ (\text{grad}_n\ \psi)\ (\partial F_n/\partial t) dS$$

$$D_f = (1/2) \iiint_\tau (1/k)\ (\partial \boldsymbol{F}/\partial t)^2 d\tau + (1/2) \iint_S (1/K)(\partial F_n/\partial t)^2\ dS$$

The coupling terms between q_i and f_i are contained in $D_{\theta f}$. Let us therefore attempt to find conditions under which this term vanishes. Note that because $\boldsymbol{F}$ is divergence-free—i.e., satisfies relation (3.4)—we may write

$$\text{div}[\psi \cdot (\partial \boldsymbol{F}/\partial t)] = (\text{grad } \psi) \cdot (\partial \boldsymbol{F}/\partial t) \tag{3.11}$$

Applying the divergence theorem (also called Green's formula), we derive

$$\iiint_\tau (\text{grad } \psi) \cdot (\partial \boldsymbol{F}/\partial t) d\tau = \iint_S \psi (\partial F_n/\partial t) dS \tag{3.12}$$

Substituting Eq. (3.12) in the expression of $D_{\theta f}$, we find

$$D_{\theta f} = -\iint_S [\psi + (k/K)\text{grad}_n\ \psi](\partial F_n/\partial t) dS \tag{3.13}$$

This expression will vanish if ψ is chosen so that on the boundary it satisfies

$$\psi + (k/K)\ \text{grad}_n \psi = 0 \tag{3.14}$$

If the surface heat-transfer coefficient is a function of time, this is a differential relation involving the time. If K is independent of time, this condition reduces to

$$K\psi + k\ \text{grad}_n \psi = C_P \tag{3.15}$$

where C_P depends only on the location on the surface. In particular, we may put $C_P = 0$; hence,

$$K\psi + k\ \text{grad}_n \psi = 0 \tag{3.16}$$

If we choose the flow potential ψ to satisfy these boundary conditions, then V and D_θ depend only on the n coordinates q_i and we may write the n equations

$$(\partial V/\partial q_i) + (\partial D_\theta/\partial \dot{q}_i) = Q_i \tag{3.17}$$

with the thermal forces

$$Q_i = \iint_S \theta_n k (\partial/\partial q_i)\ (\text{grad}_n\ \psi) dS \tag{3.18}$$

The other equations for the coordinates f_i,

$$\partial D_f/\partial \dot{f}_i = 0 \tag{3.19}$$

do not enter into the picture as far as the temperature field is concerned, and are relevant only if we wish to determine the amount of heat flow. As pointed out in reference 1, the coordinates may be called "ignorable coordinates" in analogy with the similar case in dynamics when such coordinates appear only in the expression for the kinetic energy. For instance, in a free elastic solid, the ignorable coordinates are those corresponding to rigid translations and rotations. They are irrelevant if we are interested only in the strains.

If the thermal field contains surfaces of discontinuity for the conductivity k we may still use a flow potential ψ, which will have the same properties as above provided both ψ and the component of k grad ψ normal to the surface of discontinuity be continuous across this surface. Since ψ is continuous along the surface of discontinuity this implies a refraction of the flow lines across the surface.

We have assumed until now that c, k, are independent of the temperature. If c is temperature-dependent, the method is applicable, except that Eq. (3.5) must be replaced by

$$h(\theta) = \int_0^\theta c\ d\theta = \text{div}\ (k\ \text{grad}\ \psi) \tag{3.20}$$

If k is also temperature-dependent, but independent of the coordinates, it is well known that the problem may be reduced to one with a constant value for k (see reference 1). Finally, the method may be extended to the case of anisotropic media for the case where the conductivity is temperature-independent.

(4) Temperature Fields and Their Associated Flow Fields as Generalized Coordinates

In the particular case of a system with physical properties independent of the temperature and the time, the quantities c, k, and K are functions only of the coordinates. The flow potential may then conveniently be represented by

$$\psi = \sum^i \psi_i(x\ y\ z) q_i \tag{4.1}$$

The corresponding temperature field is

$$\theta = \sum^i \theta_i(x\ y\ z) q_i \tag{4.2}$$

and the corresponding flow field is

$$\boldsymbol{H} = \sum^i \boldsymbol{\Theta}_i\ (x\ y\ z) q_i \tag{4.3}$$

with

$$\theta_i = (1/c)\ \text{div}\ (k\ \text{grad}\ \psi_i) \tag{4.4}$$

$$\boldsymbol{\Theta}_i = -k\ \text{grad}\ \psi_i \tag{4.5}$$

In addition, for the field to be uncoupled with the ignorable coordinates each function ψ_i must satisfy the boundary condition

$$K\psi_i + k\ \text{grad}_n \psi_i = 0 \tag{4.6}$$

This result was already established in reference 1 and is also a consequence of the more general relations (3.14) derived above.

The point of importance which we shall now discuss is the fact that Eq. (4.4) and the boundary condition (4.6) completely define the flow potential ψ_i when θ_i is given. The function ψ_i is simply the steady-state temperature for heat sources of intensity $-c\theta_i$ per unit volume and per unit time distributed throughout the system while the external temperature is maintained zero. The field $\boldsymbol{\Theta}_i$ is also completely determined by θ_i. It is the steady rate of heat flow established in this system of sources. We shall call $\boldsymbol{\Theta}_i$ the associated flow field for the fixed temperature configuration θ_i. Note that because of the minus sign the sources $-c\theta_i$ may be considered as heat sink of magnitude $c\theta_i$.

In practice, it will generally be much easier to choose a number of temperature configurations θ_i as approximations to the problem rather than choosing suitable approximations for ψ_i. The thermal problem can then be formulated completely if we first calculate the flow fields $\boldsymbol{\Theta}_i$ associated with each temperature configuration. Each scalar field θ_i and its associated vector field $\boldsymbol{\Theta}_i$ defines a generalized coordinate q_i. Now the calculation of the associated flow field may be accomplished by approximate methods, and, particularly, by variational methods. Since ψ_i represents the steady-state temperature due to the sources, there are numerous approximate methods available for its calculation. In particular, we may use a variational method by putting equal to zero the variation of

$$I = \iiint_\tau [(1/2)k(\text{grad } \psi_i)^2 + c\theta_i\psi_i]d\tau + (1/2)\iint_S K\psi_i^2 dS \quad (4.7)$$

where ψ_i is the quantity to be varied and θ_i is given. This leads to Eq. (4.4) with the boundary condition (4.6).

Actually, of course, we are not interested in the scalar ψ_i but in the associated field $\boldsymbol{\Theta}_i$, as given by relation (4.5). Since this involves the calculation of the gradient of ψ_i it is more accurate to use the variational method, to calculate the vector field $\boldsymbol{\Theta}_i$ directly. This can be done by minimizing the dissipation function

$$D' = (1/2)\iiint_\tau (1/k)\boldsymbol{\Theta}_i^2 d\tau + (1/2)\iint_S (1/K)\,[\boldsymbol{\Theta}_i]_n^2\, dS \quad (4.8)\dagger$$

for variations of $\boldsymbol{\Theta}_i$ which satisfy the constraint

$$\text{div } \boldsymbol{\Theta}_i = -c\theta_i \quad (4.9)$$

This may be derived by adapting to the particular case of steady sources the considerations of Section (2) above, and the general variational principles as formulated in references 1 and 2. The steady-state source is $w = -c\theta_i$ and the rate of heat flow is $\partial \boldsymbol{H}/\partial t = \boldsymbol{\Theta}_i$.

† The subscript n indicates the component of $\boldsymbol{\Theta}_i$ normal to the surface S and taken positive outward.

This procedure of minimizing expression (4.8) for D' under the constraint (4.9) may also be derived directly by introducing a Lagrangian multiplier λ. It is then equivalent to putting equal to zero the variations of

$$D'' = \iiint_\tau [(1/2k)\boldsymbol{\Theta}_i^2 + \lambda(\text{div } \boldsymbol{\Theta}_i + c\theta_i)]d\tau + (1/2)\iint (1/K)\,[\boldsymbol{\Theta}_i]_n^2\, dS \quad (4.10)$$

We derive Euler's equations corresponding to this variational problem. These equations are, in the volume τ,

$$(1/k)\boldsymbol{\Theta}_i - \text{grad } \lambda = 0 \quad (4.11)$$

and at the boundary,

$$\lambda + (1/K)\,[\boldsymbol{\Theta}_i]_n = 0 \quad (4.12)$$

Taking into account the constraint (4.9), these equations lead to

$$\text{div } [k \text{ grad } \lambda] = -c\theta_i \quad (4.13)$$

$$\lambda + (k/K)\,\text{grad}_n\lambda = 0 \quad (4.14)$$

Eqs. (4.11), (4.13), and (4.14) are identical with those defining $\boldsymbol{\Theta}_i$ in terms of θ_i. The Lagrangian multiplier λ plays the role of $-\psi_i$.

An alternate procedure which may generally be more convenient is to put

$$\boldsymbol{\Theta}_i = \boldsymbol{F}_i + \boldsymbol{\Theta}_i' \quad (4.15)$$

where $\boldsymbol{\Theta}_i'$ is *any field* satisfying the relation

$$\text{div } \boldsymbol{\Theta}_i' = -c\theta_i \quad (4.16)$$

The field $\boldsymbol{F}_i$ is the variable to be varied under the condition

$$\text{div } \boldsymbol{F}_i = 0 \quad (4.17)$$

The variation of

$$D = (1/2)\iiint_\tau (1/k)\,(\boldsymbol{F}_i + \boldsymbol{\Theta}_i')^2 d\tau + (1/2)\iint_S (1/K)\,[\boldsymbol{F}_i + \boldsymbol{\Theta}_i']_n^2\, dS \quad (4.18)$$

is then made to vanish under the constraint (4.17).

It is important to note that, in practice, we do not require the calculation of the scalar field ψ_i. Once the thermal coordinate θ_i has been chosen, its associated vector field $\boldsymbol{\Theta}_i$ is determined directly, and is the only additional field required to define the generalized coordinate.

In Section (2) we have considered the case where there are internal heat sources. It was found that we could separate the flow field into two parts $\boldsymbol{H}^*$ and $\boldsymbol{H}^+$ satisfying relations (2.16) and (2.17). These relations for a linear problem become

$$\int_0^t w\, dt = \text{div } \boldsymbol{H}^* \quad (4.19)$$

$$c\theta = -\text{div } \boldsymbol{H}^+ \quad (4.20)$$

The field $\boldsymbol{H}^*$ is any field satisfying the first equation.

The concept of the associated flow field may also be used in this case by considering as above the representations

$$\theta = \sum^{i} \theta_i q_i \tag{4.21}$$

$$\boldsymbol{H}^{+} = \sum \boldsymbol{\Theta}_i{}^{+} q_i \tag{4.22}$$

The field $\boldsymbol{\Theta}_i{}^{+}$ is associated with the temperature θ_i by the relations

$$\theta_i = (1/c) \operatorname{div} (k \operatorname{grad} \psi_i{}^{+}) \tag{4.23}$$

$$\boldsymbol{\Theta}_i{}^{+} = -k \operatorname{grad} \psi_i{}^{+} \tag{4.24}$$

and the boundary condition

$$K\psi_i{}^{+} + k \operatorname{grad}_n \psi_i{}^{+} = 0 \tag{4.25}$$

The dissipation function is expressed in terms of a total flow field

$$\boldsymbol{H} = \boldsymbol{H}^{*} + \boldsymbol{H}^{+} + \boldsymbol{F} \tag{4.26}$$

where $\boldsymbol{F}$ satisfies the relation

$$\operatorname{div} \boldsymbol{F} = 0 \tag{4.27}$$

We may consider that $\boldsymbol{F}$ contains the arbitrary portion of the divergence-free field which may be added to $\bar{H}^{*}$. Repeating the argument of the previous sections and taking into account Eqs. (4.24) and (4.25) we see that in the dissipation functions the fields $\boldsymbol{F}$ and $\bar{H}^{+}$ are uncoupled. Hence, if we are interested only in the temperature θ, we may use for the dissipation function

$$D = (1/2) \iiint_{\tau} (1/k) \left[(\partial \boldsymbol{H}^{*}/\partial b) + (\partial \boldsymbol{H}^{+}/\partial t)\right]^2 d\tau + (1/2) \iint_{S} (1/K) \left[(\partial \boldsymbol{H}^{*}/\partial t) + (\partial \boldsymbol{H}^{+}/\partial t)\right]^2 dS \tag{4.28}$$

For the same reason as just mentioned, addition of a divergence-free field to $\boldsymbol{H}^{*}$ introduces no new coupling between $\boldsymbol{H}^{*}$ and $\boldsymbol{H}^{+}$. We need of course write only those terms which include q_i; hence, we put

$$D = (1/2) \iiint_{\tau} (1/k) \left(\sum^{i} \boldsymbol{\Theta}_i{}^{+} \dot{q}_i\right)^2 d\tau + (1/2) \iint_{S} (1/K) \left[\sum^{i} (\boldsymbol{\Theta}_i{}^{+})_n \dot{q}_i\right]^2 dS + \iiint_{\tau} (1/k) (\partial \boldsymbol{H}^{*}/\partial t) \left(\sum^{i} \boldsymbol{\Theta}_i{}^{+} \dot{q}_i\right) d\tau + \iint_{S} (1/K) (\partial H_n{}^{+}/\partial t) \sum^{i} [\boldsymbol{\Theta}_i{}^{+}]_n q_i dS \tag{4.29}$$

The same procedure will be used when the temperature field is separated into an instantaneous steady state θ^{*} and a remainder θ^{+}. As pointed out above, this amounts to distributing sources (2.25) throughout. Eqs. (4.19) and (4.20) are simply replaced by Eqs. (2.26) and (2.27). The remainder temperature θ^{+} is then expanded into a sum of temperature configurations $\theta_i{}^{+}$ with associated fields

$$\theta^{+} = \sum^{i} \theta_i{}^{+} q_i, \qquad \boldsymbol{H}^{+} = \sum^{i} \boldsymbol{\Theta}_i{}^{+} q_i \tag{4.30}$$

The fields $\boldsymbol{\Theta}_i{}^{+}$ associated with each temperature configuration may be evaluated by a variational method as above. Hence, the equations for q_i for the field θ^{+} are then obtained from Eq. (2.28) using the dissipation function (4.29).

(5) The Associated Flow Field for Normal Coordinates

In many applications it is possible to determine readily the temperature fields corresponding to the thermal modes or normal coordinates. These thermal modes are decaying temperature distributions under boundary conditions of zero external temperature ($\theta_a = 0$). Systems where this concept applies are those for which the physical parameters c, k, and K depend only on the coordinates. The system may or may not include a surface layer for heat transfer.

These thermal modes may be used as normal coordinates to solve the problem of finding the temperature distribution when arbitrary external temperatures θ_a are applied at the surface. However, in order to do this we must calculate the corresponding thermal forces by a method of virtual work, and this implies the knowledge of the heat flow field associated with each thermal mode.

We will show that the flow field associated with each mode is immediately determined from the temperature distribution. Let us represent the flow field of each thermal mode by $\boldsymbol{\Theta}_s$ and its temperature field by θ_s. Since we are interested only in those modes associated with a temperature field, we introduce a flow potential ψ_s associated with $\boldsymbol{\Theta}_s$ and $\boldsymbol{\theta}_s$. From Eqs. (4.4) and (4.5) we derive

$$\boldsymbol{\Theta}_s = -k \operatorname{grad} \psi_s \tag{5.1}$$

$$\operatorname{div} (k \operatorname{grad} \psi_s) = c\theta_s \tag{5.2}$$

The boundary condition for ψ_s is given by Eq. (4.6)—i.e.,

$$K\psi_s + k \operatorname{grad}_n \psi_s = 0 \tag{5.3}$$

Eq. (5.2) together with Eq. (5.3) completely determines ψ_s when θ_s is given. In order to find ψ_s let us consider the temperature field. It satisfies the equation

$$\operatorname{div} (k \operatorname{grad} \theta) = c(\partial\theta/\partial t) \tag{5.4}$$

with the boundary condition

$$K\theta + k \operatorname{grad}_n \theta = 0 \tag{5.5}$$

Note that we are dealing here with a relaxation mode—i.e., a case where the temperature θ_a outside the surface layer is zero and the rate of heat transfer at the surface is measured by $K\theta$. A thermal mode is a solution of the type

$$\theta = \theta_s(x\ y\ z)e^{-\lambda_s t} \tag{5.6}$$

where θ_s is a fixed temperature field normalized in an arbitrary way. Eq. (5.4) and the boundary condition (5.5) become

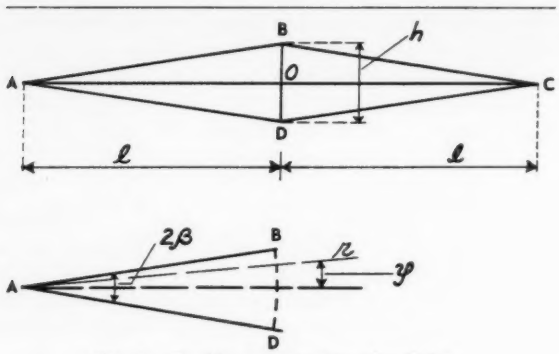

FIG. 1. Double wedge section of cylinder.

$$\text{div } (k \text{ grad } \theta_s) = -\lambda_s c\theta_s \tag{5.8}$$

$$K\theta_s + k \text{ grad}_n\theta_s = 0 \tag{5.9}$$

By putting $$\psi_s = -(1/\lambda_s)\theta_s \tag{5.10}$$

these equations may be written

$$\text{div } (k \text{ grad } \psi_s) = c\theta_s \tag{5.11}$$

$$K\psi_s + k \text{ grad}_n\psi_s = 0 \tag{5.12}$$

Hence, ψ_s as given by Eq. (5.10) is the unique solution of Eq. (5.2). The significance of this result lies in the fact that for every temperature field θ_s corresponding to a thermal mode, there exists a vector field

$$\mathbf{\Theta}_s = (k/\lambda_s)\text{grad } \theta_s \tag{5.13}$$

which represents the associated flow field. The scalar field θ_s and the associated vector field $\mathbf{\Theta}_s$ constitute a complete representation of the normal coordinate which corresponds to the eigenvalue λ_s. This concept and its practical usefulness are illustrated by the examples in Sections (6) and (7).

(6) Example of Normal Coordinates

Let us consider a flat cylindrical body of double wedge section ABCD (see Fig. 1). It is assumed that the body is homogeneous with constant heat capacity and thermal conductivity. The width of the body is $2l$ and the maximum thickness h. We shall evaluate the thermal modes in the cross section considered as a two-dimensional problem. The example will be restricted to the case of modes symmetrical with respect to AC and BD and to the case where there is no boundary layer—i.e., where the heat-transfer coefficient at the surface is infinite ($K = \infty$). The thermal modes then occur under conditions of constant temperature ($\theta = 0$) at the boundary of the solid.† We furthermore assume the thickness ratio h/l to be small so that the half portion ABD may be assimilated to a section of vertex angle,

$$2\beta = h/l \tag{6.1}$$

† It is clear that this assumption is not essential and that the use of normal coordinates applies quite generally to cases with a finite surface heat-transfer coefficient.

The temperature in the sector satisfies the heat conduction equation in polar coordinates r and φ with A as origin.

$$(\partial^2\theta/\partial r^2) + (1/r)(\partial\theta/\partial r) + (1/r^2)(\partial^2\theta/\partial\varphi^2) = (1/\kappa)(\partial\theta/\partial t) \tag{6.2}$$

The diffusivity is

$$\kappa = k/c \tag{6.3}$$

The boundary conditions for θ are

$$\left.\begin{aligned} \theta &= 0 \quad \text{for} \quad \varphi = \pm\beta \\ \partial\theta/\partial r &= 0 \quad \text{for} \quad r = l \end{aligned}\right\} \tag{6.4}$$

The arc of circle BD is assimilated to a straight line because β is assumed to be small. The thermal modes are solutions of the type

$$\theta = f(r)\cos(\nu\varphi)e^{-\lambda_s t} \tag{6.5}$$

Substitution in Eq. (5.4) yields

$$(d^2f/dr^2) + (1/r)(df/dr) + [(\lambda_s/\kappa) - (\nu^2/r^2)]f = 0 \tag{6.6}$$

Solutions of this equation which remain finite are

$$f = J_\nu(r\sqrt{\lambda_s/\kappa}) \tag{6.7}$$

This may be written

$$f = J_\nu[\alpha_s(r/l)] \tag{6.8}$$

with $$\alpha_s = l\sqrt{\lambda_s/\kappa} \tag{6.9}$$

The first boundary condition (6.4) is satisfied if we put

$$\nu = (\pi/\beta)[m + (1/2)] \qquad (m = 0, 1, 2 \ldots) \tag{6.10}$$

and the second boundary condition is

$$J_\nu'(\alpha_s) = 0$$

with $$J_\nu'(x) = dJ_\nu(x)/dx \tag{6.11}$$

Eq. (6.11) has an infinite number of roots α_s which may be evaluated numerically by interpolation from tables of Bessel functions. We may write λ_s in terms of α_s

$$\lambda_s = \kappa(\alpha_s^2/l^2) \tag{6.12}$$

The thermal modes are therefore

$$\theta = J_\nu[\alpha_s(r/l)]\cos(\nu\varphi)e^{-\lambda_s t} \tag{6.13}$$

There is a double infinity of modes attached to the roots α so that the subscript s has the significance of a double index. We write the thermal modes as

$$\theta = \theta_S e^{-\lambda_s t} \tag{6.14}$$

with $$\theta_S = J_\nu[\alpha_s(r/l)]\cos\nu\varphi \tag{6.15}$$

Any thermal distribution in the sector may be represented by a superposition of thermal modes

$$\theta = \sum^{s} \theta_s q_s \tag{6.16}$$

where q_s are generalized coordinates. As we have shown in the previous section the corresponding expansion for the heat flow field is

$$H = \sum^{s} \Theta_s q_s \tag{6.17}$$

where Θ_s is the flow field associated with the temperature distribution θ_s. It is given by

$$\Theta_s = (k/\lambda_s) \text{ grad } \theta_s \tag{6.18}$$

The thermal potential and the dissipation function are readily expressed in terms of the normal coordinates. In reference 1 we have formulated the orthogonality properties of the thermal modes. Because of these properties all cross products vanish in the expressions for V and D. The thermal potential is

$$V = (1/2) \sum^{s} a_s q_s^2 \tag{6.19}$$

with

$$a_s = (1/2)c \iint \theta_s^2 dx\, dy \tag{6.20}$$

The surface integral is extended to the area ABC of the sector. Similarly, the dissipation function is written

$$D = (1/2) \sum^{s} b_s \dot{q}_s^2 \tag{6.21}$$

with

$$b_s = (1/2)\ (k/\lambda_s^2) \iint (\text{grad } \theta_s)^2 dx\, dy \tag{6.22}$$

However, *this integral need not be evaluated* if we know a_s and λ_s. This can be shown readily by writing the differential equations satisfied by the thermal modes in terms of the normal coordinates q_s. Since the boundary temperature is zero the thermal force Q_s vanishes, and the general differential equation (2.2) becomes

$$(\partial V/\partial q_s) + (\partial D/\partial \dot{q}_s) = 0 \tag{6.23}$$

or

$$a_s q_s + b_s \dot{q}_s = 0 \tag{6.24}$$

The solutions of these equations are the thermal modes,

$$q_s = C_s e^{-\lambda_s t} \tag{6.25}$$

with

$$\lambda_s = a_s/b_s \tag{6.26}$$

hence,

$$b_s = a_s/\lambda_s \tag{6.27}$$

The dissipation function may therefore be written

$$D = (1/2) \sum^{\pi} (a_s/\lambda_s) \dot{q}_s^2 \tag{6.28}$$

with a_s equal to the integral (6.20).

(7) Application of Normal Coordinates

With a knowledge of the normal coordinates we may immediately express the temperature field caused by an arbitrary time-dependent distribution of the external temperature, θ_a, at the surface. We shall again consider the example of the previous section with infinite surface heat-transfer coefficient ($K = \infty$) and the same symmetric distribution of temperature with respect to AC. In addition, we shall also assume that the external temperature distribution is also symmetric with respect to BD. Because of the assumed symmetry the temperature field need be evaluated only in the sector ABO. Since $K = \infty$, the external temperature θ_a is identical with the temperature at the solid boundary.

The temperature is represented in terms of normal coordinates by the series (6.16). With each normal coordinate is associated a flow field Θ_s given by Eq. (3.18). The thermal potential V and dissipation function D are expressions (6.19) and (6.28) with coefficients a_s defined by Eq. (6.20). The differential equations for the normal coordinates q_s are

$$a_s q_s + (a_s/\lambda_s)\dot{q}_s = Q_s \tag{7.1}$$

where Q_s is the generalized force associated with q_s. It is defined in terms of the normal component $[\Theta_s]_{(n)}$ of the associated flow field at the boundary by applying Eq. (2.8). We find†

$$Q_s = \iint_S \theta_a [\Theta_s]_{(n)} dS \tag{7.2}$$

In the present example, since we consider only the sector ABO, the thermal force is

$$Q_s = -(k/\lambda_s) \int_0^l (\theta_a/r)\ (\partial\theta_s/\partial\varphi)_{\varphi=\beta}\, dr \tag{7.3}$$

or

$$Q_s = (-1)^m (k\nu/\lambda_s) \int_0^l (\theta_a/r) J_\nu[\alpha_s(r/l)]\, dr$$

The coefficients a_s defined by Eq. (6.20) are

$$a_s = (1/2c) \int_0^l dr \int_0^\beta r J_\nu^2[\alpha_s(r/l)] \cos^2 \nu\varphi\, d\varphi$$

$$a_s = (\beta l^2/8c)\ [1 - (\nu^2/\alpha_s^2)] J_\nu^2(\alpha_s) \tag{7.4}‡$$

The differential equations (7.1) determine q_s as a function of time. These values of q_s substituted in the series (6.16) determine the transient temperature field. It will be noticed that the temperature field as represented by the series is always zero right at the boundary, and therefore cannot represent the imposed boundary temperature. Nevertheless, it does represent correctly the temperature distribution inside the boundary. If, for instance, we impose a constant temperature θ_a on this boundary, the field will be represented by a series which has a constant value inside the boundary but whose value drops to zero if we are close enough to the boundary. This is a feature of nonuniform convergence already encountered in one-dimensional examples in references 1 and 4. There are advantages and disadvantages in expressing the temperature field by a series such as (6.16). The advantage is, of course, the orthogonality that results in the absence of coupling between the coordinates q_s. A disadvantage is the fact that the final distribution of temperature under equilibrium conditions is represented by a series. As was pointed out in reference 1, one way of avoiding this disadvantage is to split up the temperature field into two parts. Let us apply this method to the present example. Consider the solutions of the equations

† The subscript (n) denotes the normal component taken positive inward.

‡ This result may be obtained by making use of integral expressions originally derived by E. C. J. Lommel (see reference 8).

$$a_s q_s^* = Q_s \tag{7.5}$$

The q_s^* represent the equilibrium temperature distribution reached under instantaneous boundary temperatures θ_a considered as independent of time. It represents a temperature field

$$\theta^* = \sum^{s} \theta_s q_s^* \tag{7.6}$$

which may be evaluated directly by solving Laplace's equation

$$(\partial^2\theta^*/\partial x^2) + (\partial^2\theta^*/\partial y^2) = 0 \tag{7.7}$$

under the instantaneous boundary condition θ_a for the temperature. We then put

$$\theta = \theta^+ + \theta^* \tag{7.8}$$

with

$$\theta^+ = \sum^{s} \theta_s q_s^+ \tag{7.9}$$

$$q_s = q_s^+ + q_s^* \tag{7.10}$$

Substituting in Eqs. (7.1) and taking into account relation (7.5) gives the differential equation for q_s^+

$$q_s^+ + (1/\lambda_s)\dot{q}_s^+ = -(1/\lambda_s)\dot{q}_s^* \tag{7.11}$$

Now from Eq. (7.5) we may also write

$$-(1/\lambda_s)\dot{q}_s^* = -(\dot{Q}_s/\lambda_s a_s) \tag{7.12}$$

The time derivative $\dot{Q}_s$ is found by calculating the initial work of the time derivative $\dot{\theta}_a$ of the boundary temperature.

(8) Integral Equations Derived From Associated Flow Fields—Relation to Green's Function

In Section (4) we have shown how temperature fields and their associated flow fields may be used as generalized coordinates in the formulations of heat flow problems. We shall now examine a particular case of this type of formulation which leads to integral equations in complete generality for all linear thermal systems with time-independent parameters. This formulation amounts to a generalization of the Green's function method and at the same time yields a new procedure for the approximate evaluation of this generalized Green's function itself.

We go back to Eq. (4.2), which represents the thermal field as

$$\theta = \sum^{i} \theta_i(x\ y\ z) q_i \tag{8.1}$$

where θ_i are fixed scalar distributions and q_i generalized coordinates. An interesting application of this representation arises if we write Eq. (8.1) in the form

$$\theta = \int \delta(\xi - x)\theta(x)dx \tag{8.2}$$

where $\delta(\xi - x)$ plays the role of the configuration θ_i, $\theta(x)dx$ represents the generalized coordinates q_i, and the summation is replaced by an integral. We have abbreviated the notation by writing $\theta(x)$ for $\theta(x\ y\ z)$. By a similar abbreviation the integral is a volume integral over $x\ y\ z$. The distribution $\delta(\xi - x)$ is written for $\delta(\xi - x, \eta - y, \zeta - z)$ and represents the spatial Dirac function equal to zero at any point except $\xi = x$, $\eta = y$, $\zeta = z$, and such that its volume integral over $\xi\eta\zeta$ is unity. By the property of Dirac functions, Eq. (8.2) is equivalent to stating that $\theta = \theta(\xi)$; i.e., the continuous set of unknown local temperatures constitute the generalized coordinates of the problem.

The flow field $\boldsymbol{\Theta}(\xi, x)$ associated with the temperature $\delta(\xi - x)$ is determined by the general procedure outlined above in Section (4). We solve the equation

$$\text{div } (k \text{ grad } \psi) = c\delta(\xi - x) \tag{8.3}$$

where

$$\psi = \psi(\xi, x) \tag{8.4}$$

with the boundary condition

$$K\psi + k \text{ grad}_n \psi = 0 \tag{8.5}$$

The gradients and all partial derivations are taken with respect to $\xi\ \eta\ \zeta$. The right-hand side of Eq. (8.3) represents a concentrated heat sink of magnitude c at point $x\ y\ z$ and ψ is the corresponding temperature field. The flow field associated with $\delta(\xi - x)$ is

$$\boldsymbol{\Theta}(\xi, x) = -k \text{ grad } \psi(\xi, x) \tag{8.6}$$

We have also indicated in Section (5) how $\boldsymbol{\Theta}$ could be evaluated by an approximate variational procedure. Eq. (4.3) for the total flow field becomes the volume integral

$$\boldsymbol{H} = \int \boldsymbol{\Theta}(\xi, x)\theta(x)dx \tag{8.7}$$

In order to obtain the general equations for the thermal field we must construct the thermal potential V and the dissipation function D. The first is written immediately as

$$V = (1/2) \int c\theta^2 dx \tag{8.8}$$

The second is found by writing first

$$(\partial \boldsymbol{H}/\partial t)^2 = \iint \boldsymbol{\Theta}(\xi, x') \cdot \boldsymbol{\Theta}(\xi, x)\dot{\theta}(x')\dot{\theta}(x)dx'dx \tag{8.9}$$

We easily derive

$$D = (1/2) \int \gamma(x', x)\dot{\theta}(x')\dot{\theta}(x)dx'dx \tag{8.10}$$

with

$$\gamma(x', x) = \int [1/k(\xi)]\boldsymbol{\Theta}(\xi, x')\boldsymbol{\Theta}(\xi, x)d\xi + \int (1/K)\Theta_n(\xi, x')\Theta_n(\xi, x)dS \tag{8.11}$$

The second integral is a surface integral over the boundary where $\Theta_n(\xi, x)$ represents the normal component of $\boldsymbol{\Theta}(\xi, x)$ at a point ξ of the boundary. Finally the generalized force $Q(x)$ is obtained by considering the virtual work of the applied external temperature θ_a on the heat flow $\delta H_{(n)}$ at the boundary for a variation $\delta\theta(x)$. We find

$$Q(x)\delta\theta(x) = \int_S \theta_a \delta H_{(n)} dS = \int_S \theta_a \Theta_{(n)}(\xi, x)\delta\theta(x)dS \tag{8.12}$$

The normal component $\Theta_{(n)}$ is taken positive inward. We derive

$$Q(x, t) = \int_S \theta_a(\xi, t)\Theta_{(n)}(\xi, x)dS \qquad (8.13)$$

We have written $Q(x, t)$ and $\theta_a(\xi, t)$ instead of $Q(x)$ and θ_a to indicate explicitly that these quantities are functions of both the coordinates and the time.

The final equations for the temperature field are obtained by using the concept of partial derivative with respect to $\theta(x)dx$ and $\dot{\theta}(x)dx$ as if they were coordinates q_i.† We find

$$c\theta(x, t) + \int \gamma(x', x)\dot{\theta}(x', t)dx' = Q(x, t) \qquad (8.14)$$

Again we write $\theta(x, t)$ instead of $\theta(x)$ to indicate explicitly that it is also an unknown function of time. This is an integral equation for the unknown temperature $\theta(x, t)$.

The particular form of this equation recalls immediately that obtained by the classical Green's function method.[10] In fact, it is shown in the Appendix that this equation in the case of well defined boundaries may also be derived by Green's function techniques. The derivation, however, is more elaborate. Actually, Eq. (8.14) achieves results which go substantially beyond the classical approach:

(1) The integral equation is eatablished directly and very simply as a particular application of general thermodynamic principles.

(2) It is formulated in a very general way and is applicable to any thermal system and boundary conditions, no matter how intricate, provided it is linear and with time-independent parameters.

(3) The kernel $\gamma(x', x)$ is expressed in terms of the integrated product of associated flow fields which themselves may be evaluated by approximate variational procedures as indicated above in Section (4). In this process, conservation of energy is preserved and rough approximations may be used because of the averaging effect of the integration in evaluating expression (8.11) for $\gamma(x', x)$.

It will be noted that Eq. (8.14) *gives directly the steady-state temperature field if the applied external temperature θ_a is independent of time.* Putting $\dot{\theta} = 0$ we may write Eq. (8.14) as

$$c\theta(x) = Q(x) \qquad (8.15)$$

This may also be looked upon as a consequence of reciprocity theorems for the influence coefficients relating steady temperature to heat flow, in direct analogy with Maxwell's theorem of the theory of elasticity.

An alternate formulation of Eq. (8.14) results from the introduction of an instantaneous steady-state temperature as already mentioned in reference 1 and in Sections (2), (4), and (7) above. This temperature field $\theta^*(x, t)$ is given in terms of $\theta_a(x, t)$ by

$$c\theta^*(x, t) = Q(x, t) = \int_S \theta_a(x, t)\Theta_{(n)}(\xi, x)dS \qquad (8.16)$$

† This is done currently in theoretical physics (see, for instance, reference 9). We could also follow the procedure introduced by this writer in reference 4—i.e., replace D by an operational invariant and use the variational principle directly.

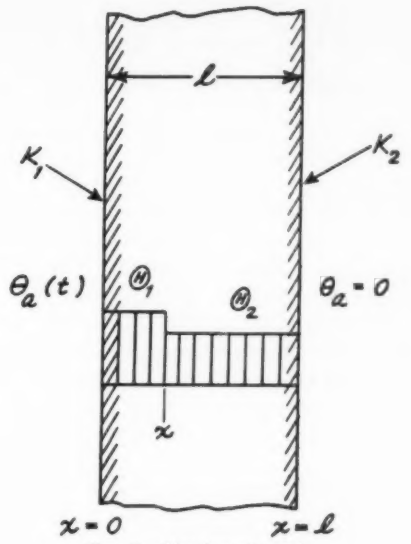

FIG. 2. Heating of a slab.

It is the temperature field which would be obtained if the instantaneous boundary temperature θ_a at time t were maintained constant. If we now write the actual temperature as

$$\theta(x, t) = \theta^+(x, t) + \theta^*(x, t) \qquad (8.17)$$

Eq. (8.14) becomes

$$c\theta^+(x, t) + \int \gamma(x', x)\dot{\theta}^+(x', t)dx' = \int \gamma(x', x)\dot{\theta}^*(x', t)dx' \qquad (8.18)$$

The temperature θ^+ results from subjecting the same thermal system to a new thermal force equal to the right-hand side of Eq. (8.18).

This is obviously an easier equation to solve if the temperatures vary slowly. Needless to say, since Eq. (8.18) is of the same form as the original, the process of splitting the temperature into an instantaneous steady state and remainder may be repeated, leading to an iterative solution of the problem.

(9) One-Dimensional Problems Formulated by Means of Associated Flow Fields

The treatment of a one-dimensional problem by the use of associated flow fields is given here as an illustration. Its main purpose is to familiarize the reader with the nature of the method and concepts. Furthermore, it also serves to outline the approximate method of numerical solution of the integral equation.

We shall consider the particular case of a slab of thickness l with constant values of k and c. One face at $x = 0$ has a heat-transfer coefficient K_1, and the other face at $x = l$ a heat-transfer coefficient K_2 (see Fig. 2). The outside temperature at $x = 0$ is a given function of time, $\theta_a(t)$, while the outside temperature at $x = l$ is zero. Consider the temperature $\theta(x, t)$ at point x and time t. The associated flow field corresponds to a concentrated heat sink in the plane of abscissa x while the temperature outside of the slab is maintained at

zero on *both sides*. Corresponding to Eq. (8.2) we have now the representation of the temperature field as

$$\theta(\xi) = \int \delta(\xi - x)\theta(x)dx \tag{9.1}$$

which is formally the same except that now $\delta(\xi - x)$ represents a one-dimensional Dirac function.

Corresponding to Eq. (8.3) the intensity of the heat sink is c per unit area of the slab cross section. The associated flow field is the heat flow which would flow into the sink from both sides of the slab under a steady-state condition. The flow field is uniform on each side of point x with values which are inversely proportional to the flow resistance on each side of the sink. Denoting by Θ_1 and Θ_2 the flow coming into the sink on each side, respectively, we have the two equations

$$\Theta_1 + \Theta_2 = c \tag{9.2}$$

$$\Theta_1[(1/K_1) + (x/k)] = \Theta_2\{(1/K_2) + [(l - x)/k]\} \tag{9.3}$$

The second equation states that the temperature drop between the sink and the region outside the slab is the same on both sides of the sink. Solving for Θ_1 and Θ_2 yields the flow field associated with the temperature $\delta(\xi - x)$. It is a discontinuous function

$$\Theta(\xi, x) = \Theta_1(x) \quad \text{for} \quad \xi < x \tag{9.4}$$

$$\Theta(\xi, x) = -\Theta_2(x) \quad \text{for} \quad \xi > x \tag{9.5}$$

with

$$\Theta_1(x) = \{c/[(1/K_1) + (1/K_2) + (l/k)]\} \times \{(1/K_2) + [(l - x)/k]\} \tag{9.6}$$

$$\Theta_2(x) = \{c/[(1/K_1) + (1/K_2) + (l/k)]\} \times [(1/K_1) + (x/k)] \tag{9.7}$$

The thermal force Q is

$$Q(x, t) = \theta_a(t)\Theta(0, x) \tag{9.8}$$

or

$$Q(x, t) = \theta_a(t)\Theta_1(x) \tag{9.9}$$

This is a function of the coordinate x and the time t. The kernel $\gamma(x', x)$ is found by applying Eq. (8.11)

$$\gamma(x', x) = (1/k)\int_0^l \Theta(\xi, x')\Theta(\xi, x)d\xi + (1/K_1)\Theta_1(x')\Theta_1(x) + (1/K_2)\Theta_2(x')\Theta_2(x) \tag{9.10}$$

The integral in this expression is readily evaluated. Taking into account relations (9.2) and (9.3), the result may be simplified to

$$\left.\begin{aligned}\gamma(x', x) &= c[(x/k) + (1/K_1)]\Theta_1(x') \quad \text{for} \quad x < x' \\ \gamma(x', x) &= c\{[(l - x)/k] + (1/K_2)\}\Theta_2(x') \quad \text{for} \quad x > x'\end{aligned}\right\} \tag{9.11}$$

This may be recognized as the Green's function of the one-dimensional problem—i.e., it is proportional to the temperature distribution due to a source at point x'. That this should be so is, of course, a consequence of the general proof in the Appendix. Obviously, in one-dimensional problems we could introduce Green's function directly instead of going through the process of calculating first the associated flow field $\Theta(\xi, x)$, and the above derivation is intended only as an illustration. However, as pointed out above, the introduction of the associated flow field provides an approximate method of evaluation of Green's function for the more complex two- and three-dimensional problems.

The integral equation for the temperature is

$$c\theta(x, t) + \int_0^l \gamma(x', x)\dot{\theta}(x', t)dx' = \theta_a(t)\Theta_1(x) \tag{9.12}$$

This equation is reduced to a system of linear differential equations if we divide the interval of integration into a certain number of segments, the dividing points being at abscissas x_i. We put

$$\theta_i = \theta(x_i, t) \tag{9.13}$$

We may then write the matrix approximation

$$\int_0^l \gamma(x', x_i)\dot{\theta}(x', t)dx' = [b_{ij}]\ [\dot{\theta}_j] \tag{9.14}$$

If the intervals Δx are equal and in even number the relation (9.14) may be obtained by Simpson's rule—i.e., we may write

$$[b_{ij}] = [S]\ [\Gamma]\Delta x \tag{9.15}$$

The matrix $[\Gamma]$ is made up of elements

$$[\Gamma] = [\gamma(x_j, x_i)] \tag{9.16}$$

and $[S]$ is a diagonal matrix which yields Simpson's method of integration

$$[S] = \frac{1}{3}\begin{bmatrix} 1 & & & & & & \\ & 4 & & & & & \\ & & 2 & & & 0 & \\ & & & 4 & & & \\ & & & & \cdot & & \\ & & & & & \cdot & \\ & & & & & & \cdot \\ & & 0 & & & 4 & \\ & & & & & & 1 \end{bmatrix} \tag{9.17}$$

The integral equation (9.12) then reduces to a system of linear differential equations with a finite number of unknown temperatures θ_i. This system is

$$c\theta_i + \sum^j b_{ij}\dot{\theta}_j = \theta_a(t)\Theta_1(x_i) \tag{9.18}$$

The system may be conveniently solved by normal coordinates because the homogeneous systems obtained by putting $\theta_a = 0$ is in a form which can be readily used for the computation of the thermal modes by iteration starting with the mode of longest relaxation time.

It should be noted that a division of the domain in equal intervals Δx is not the best. We may just as easily take a few smaller intervals near to the surface at which the temperature is applied, and larger intervals elsewhere. The essence of the procedure remains unchanged, but we have allowed for a more accurate representation of the temperature in the region where a

higher resolution is required. Such a procedure coupled with the present formulation and the use of Simpson's rule should yield a very high accuracy with a relatively small number of unknowns.

As pointed out in the general treatment [see Section (8)], the steady-state temperature distribution results immediately from Eqs. (9.12) and (9.5) in explicit form without any further solution. Assuming θ_a independent of time and putting $\dot{\theta} = 0$ in Eq. (9.12) we find

$$\theta(x) = \theta_a \frac{(1/K_2) + [(l - x)/k]}{(1/K_1) + (1/K_2) + (l/k)} \tag{9.19}$$

which, as can be verified, is the steady-state temperature under the prescribed boundary conditions. The method is also easily applied to the case of an inhomogeneous or composite slab. In this case the thermal conductivity is a function of the abscissa. Eq. (9.3) is replaced by

$$\Theta_1\left[\frac{1}{K_1} + \int_0^x \frac{d\xi}{k(\xi)}\right] = \Theta_2\left[\frac{1}{K_2} + \int_x^l \frac{d\xi}{k(\xi)}\right] \tag{9.20}$$

The factor $1/k$ in expression (9.10) for $\gamma(x\ x')$ must remain under the integral sign. We then proceed exactly as in the case of the homogeneous slab.

(10) The Associated Field for the Case of Time-Dependent Surface Heat-Transfer Coefficients

In the above treatment of associated fields we have assumed that the surface heat-transfer coefficient K may be a function of the coordinates but is independent of the time. We will now show explicitly that the concept of associated field applies also to the more general case where K is also a function of time. In this case, the associated field will generally be a function of time and the corresponding differential equations will have time-dependent coefficients.

In order to show this, let us consider separately the dissipation function for the solid volume τ. This dissipation function is written

$$D_\tau = (1/2) \iiint_\tau (1/k)\ (\partial \boldsymbol{H}/\partial t)^2 d\tau \tag{10.1}$$

The differential equation of the thermal system may be written in terms of this dissipation function as

$$(\partial V/\partial q_i) + (\partial D_\tau/\partial \dot{q}_i) = Q_i' \tag{10.2}$$

where Q_i' is now the thermal force due to the temperatures θ' at the solid boundary—i.e.,

$$Q_i' = \iint_S \theta' [\partial H_{(n)}/\partial t] dS \tag{10.3}$$

This is the same expression as Eq. (2.8), in which the external temperature θ_a is replaced by θ'.

If the surface heat-transfer coefficient is denoted by K, we may write

$$\partial H_{(n)}/\partial t = K(\theta_a - \theta') \tag{10.4}$$

solving for θ' and substituting in the expression for Q_i', Eqs. (10.2) are written

$$(\partial V/\partial q_i) + (\partial D_\tau/\partial \dot{q}_i) + \iint_S (1/K)\ [\partial H_{(n)}/\partial t]\ [\partial H_{(n)}/\partial q_i] dS = Q_i \tag{10.5}$$

with $$Q_i = \iint_S \theta_a [\partial H_{(n)}/\partial q_i] dS$$

These equations are obviously valid if K is a function of both time and location.

Consider now a field represented as

$$\boldsymbol{H} = \sum^{i} \boldsymbol{\Theta}_i q_i + \sum^{j} \boldsymbol{F}_j f_j \tag{10.6}$$

As before, we have split the field into two parts. One part is divergence-free—i.e.,

$$\operatorname{div} \boldsymbol{F}_j = 0 \tag{10.7}$$

with the corresponding ignorable coordinates written as f_j instead of q_i. The other part yields a temperature distribution by the relations

$$\operatorname{div} \boldsymbol{\Theta}_i = -c\theta_i \tag{10.8}$$

The temperature field is then

$$\theta = \sum^{i} \theta_i q_i \tag{10.9}$$

Looking at Eqs. (10.5) it is seen that the coupling terms between the coordinates q_i and f_j are

$$b_{ij}' = \iiint_\tau (1/k) \boldsymbol{F}_j \boldsymbol{\Theta}_i d\tau + \iint_S (1/K) F_{jn} \Theta_{in} dS \tag{10.10}$$

We denote by F_{jn} and Θ_{in} the components of $\boldsymbol{F}_j$ and $\boldsymbol{\Theta}_i$ taken positive outward. Changing from inward to outward components does not affect the result since it amounts to a double change of sign in expression (10.5). We now consider that $\boldsymbol{\Theta}_i$ is derived from a flow potential ψ_i

$$\boldsymbol{\Theta}_i = -k \operatorname{grad} \psi_i \tag{10.11}$$

This does not restrict the generality since the total flow field itself is derived from a flow potential. We substitute expression (10.11) for $\boldsymbol{\Theta}_i$ in the volume integral of relation (10.10) and integrate by parts. Taking into account the property that $\boldsymbol{F}_j$ is divergence-free—i.e., satisfies relation (10.7)—we find

$$b_{ij}' = -\iint_S F_{jn} [\psi_i + (k/K) \operatorname{grad}_n \psi_i] dS = 0 \tag{10.12}$$

This expression vanishes if we choose the flow potentials ψ_i such that they satisfy the condition

$$K\psi_i + k \operatorname{grad}_n \psi_i = 0 \tag{10.13}$$

at the boundary. On the other hand, combining Eqs. (10.8) and (10.11) we derive

$$\operatorname{div} (k \operatorname{grad} \psi_i) = c\theta_i \tag{10.14}$$

Hence, ψ_i is completely determined from the temper-

ature field θ_i by this last equation and the boundary condition (10.13). The flow potential ψ_i is the steady-state temperature generated by distributed sinks $c\theta_i$, under conditions of zero outside temperature. Although this is a steady-state problem, we must remember that the boundary condition (10.13) is variable since K is a function of time. In other words, we are dealing here with a succession of instantaneous steady states. Although the distribution of heat sinks is independent of time, the flow potential ψ_i and the associated flow fields $\mathbf{\Theta}_i$ will be functions of time. This may be expressed explicitly by writing

$$\left.\begin{aligned} \theta &= \sum^{i} \theta_i(x, y, \xi) q_i \\ \boldsymbol{H} &= \sum^{i} \Theta_i(x, y, z, t) q_i \end{aligned}\right\} \qquad (10.15)$$

With these associated flow fields the problem may be formulated by Eqs. (2.2) with only the non-ignorable coordinates q_i appearing in the equations. The coefficients of $\dot{q}_i$ in the differential equations will now be functions of time.

As in the previous case discussed in Section (4), the method is applicable to the nonlinear case where the heat capacity is temperature-dependent. It is also, of course, valid for anisotropic media as can be easily verified by repeating the derivation for this case.

Of practical importance is the applicability to this case of the variational methods already outlined in Section (4) for the evaluation of the associated field. Again we do not need to calculate the flow potential ψ_i, but the vector field $\mathbf{\Theta}_i$ may be derived directly from the temperature θ_i by a variational method. The variational formulation expresses a principle of minimum dissipation for the flow field generated by the prescribed distribution of heat sinks. We must call attention to the fact that, although the minimizing flow field is a steady-state flow, it is a continuous succession of steady states due to the time dependence of the surface heat-transfer properties.

It is, of course, not necessary to express the temperature as a linear function of q_i. The method is therefore applicable to the case where the temperature field is described by the more general function $\theta(x, y, z, t, q_i)$. Furthermore, the surface heat-transfer coefficients may also be a function of the surface temperature. In this case, the associated flow field contains the surface temperature and the time explicitly.

Appendix

A direct verification of Eq. (8.14) and of the identity of $\gamma(x', x)$ with Green's function is obtained as follows. Let us write the following well-known identities:

$$\int_\tau W \operatorname{div}(k \operatorname{grad} U) d\tau + \int_\tau k \operatorname{grad} W \operatorname{grad} U d\tau = \int_S k W \operatorname{grad}_n U dS \qquad (A\text{-}1)$$

$$\int_\tau U \operatorname{div}(k \operatorname{grad} W) d\tau + \int_\tau k \operatorname{grad} U \operatorname{grad} W d\tau = \int_S kU \operatorname{grad}_n W dS \qquad (A\text{-}2)$$

and Green's theorem derived by writing the difference of the above identities

$$\int_\tau [W \operatorname{div}(k \operatorname{grad} U) - U \operatorname{div}(k \operatorname{grad} W)] d\tau = \int_S k(W \operatorname{grad}_n U - U \operatorname{grad}_n W) dS \qquad (A\text{-}3)$$

The left side integral is extended over the volume τ with the volume element $d\tau$ and the surface integrals over the boundary S of this volume. The symbol grad_n denotes the normal component of the gradient taken positive outward.

Consider now a Green's function $g(x', x)$ defined by the equation

$$\operatorname{div}(k \operatorname{grad} g) = c\delta(x' - x) \qquad (A\text{-}4)$$

with the boundary condition

$$Kg + k \operatorname{grad}_n g = 0 \qquad (A\text{-}5)$$

Dirac's function is represented by $\delta(x' - x)$. For abbreviation, x stands for $x\ y\ z$ and x' for $x'y'z'$. The differential operators act on the coordinates $x'y'z'$ so that g represents the temperature due to a steady heat sink of magnitude c located at $x\ y\ z$. Consider also a transient thermal problem with a temperature θ satisfying the equations

$$\operatorname{div}(k \operatorname{grad} \theta) = c(\partial\theta/\partial t) \qquad (A\text{-}6)$$

and the boundary condition

$$K(\theta - \theta_a) + k \operatorname{grad}_n \theta = 0 \qquad (A\text{-}7)$$

Let us now substitute

$$U = g, \qquad W = \theta \qquad (A\text{-}8)$$

into relation (A-3). We find

$$\int_\tau [\theta \operatorname{div}(k \operatorname{grad} g) - g \operatorname{div}(k \operatorname{grad} \theta)] dx' = \int_S k(\theta \operatorname{grad}_n g - g \operatorname{grad}_n \theta) dS \qquad (A\text{-}9)$$

The volume element $dx'dy'dz'$ is written as dx'. Taking into account Eqs. (A-4) and (A-6), the volume integral may be written

$$\int_\tau [\theta \operatorname{div}(k \operatorname{grad} g) - g \operatorname{div}(k \operatorname{grad} \theta)] dx' = c\theta(x) - \int_\tau cg(x', x) [\partial\theta(x')/\partial t] dx' \qquad (A\text{-}10)$$

Taking into account Eqs. (A-5) and (A-7), the surface integral becomes

$$\int_S k(\theta \operatorname{grad}_n g - g \operatorname{grad}_n \theta) dS = \int_S \theta_a k \operatorname{grad}_n g \, dS = Q(x, t) \qquad (A\text{-}11)$$

We have put this expression equal to $Q(x, t)$ because it coincides with the definition (8.13) of the same quantity in the text. In fact, we may write

$$\left.\begin{aligned} \boldsymbol{\Theta} &= -k \text{ grad } g(x', x) \\ \text{and} \qquad \Theta_{(n)} &= k \text{ grad}_n g(x', x) \end{aligned}\right\} \tag{A-12}$$

where $\Theta_{(n)}$ denotes the normal component of the boundary flow directed positively inward. Hence,

$$Q(x, t) = \int_S \theta_a(t)\Theta_{(n)}(x, x')dS \tag{A-13}$$

We remember that x' plays the role of the variable in the integration and x that of a parameter. Combining Eqs. (A-9), (A-10), and (A-11) we derive

$$c\theta(x) - \int_\tau cg(x', x)\dot{\theta}(x')dx' = Q(x, t) \tag{A-14}$$

Comparing this with Eq. (8.14), we see that $-cg(x', x)$ plays the role of $\gamma(x', x)$.

That these quantities are actually identical may be verified directly by applying either one of the identities (A-1) and (A-2). Let us consider again the scalar field $g(x', x)$ defined by (A-4) and (A-5) replacing x' by the coordinate ξ (an abbreviation for $\xi\ n\ \zeta$). In this case, ξ plays the role of the running coordinates and x that of parameters representing the location of the source. Let us consider two such functions, $g(\xi, x)$ and $g(\xi, x')$, and put

$$W = g(\xi, x), \quad U = q(\xi, x') \tag{A-15}$$

Applying identity (A-1) we find

$$\int_\tau g(\xi, x) \text{ div } [k \text{ grad } g(\xi, x')]d\tau + \int_\tau k \text{ grad } g(\xi, x) \text{ grad } g(\xi, x')d\tau = \int_S kg(x, \xi) \text{ grad}_n g(\xi, x')dS \tag{A-16}$$

We write

$$\left.\begin{aligned} \boldsymbol{\Theta}(\xi, x) &= -k \text{ grad } g(\xi, x) \\ \boldsymbol{\Theta}(\xi, x') &= -k \text{ grad } g(\xi, x') \end{aligned}\right\} \tag{A-17}$$

$$\left.\begin{aligned} \Theta_n(\xi, x) &= -k \text{ grad}_n (\xi, x) \\ \Theta_n(\xi, x') &= -k \text{ grad}_n (\xi, x') \end{aligned}\right\} \tag{A-18}$$

Furthermore we utilize Eqs. (A-4) and (A-5), applying the first one to $g(\xi, x')$ and the second one to $g(\xi, x)$.

$$\left.\begin{aligned} \text{div } [k \text{ grad } g(\xi, x')] &= c\delta(\xi, x') \\ Kg(\xi, x) + k \text{ grad}_n g(\xi, x) &= 0 \end{aligned}\right\} \tag{A-19}$$

Introducing these expressions in the volume and surface integrals of Eq. (A-16), we derive

$$cg(x', x) = -\int_\tau \frac{1}{k} \boldsymbol{\Theta}_n(x', \xi)\boldsymbol{\Theta}_n(x, \xi)\, d\tau - \int_S \frac{1}{K} \Theta_n(x', \xi)\, \Theta_n(x, \xi)dS \tag{A-20}$$

Comparing this with expression (8.11), we conclude

$$\gamma(x', x) = -cg(x', x) \tag{A-21}$$

thereby establishing the identity of this function with the classical Green's function type defined by Eqs. (A-4) and (A-5).

References

[1] Biot, M. A., *New Methods in Heat Flow Analysis with Application to Flight Structures*, Cornell Aeronautical Laboratory Report No. SA-987-S-3, May, 1956; see also, Journal of the Aeronautical Sciences, Vol. 24, No. 12, pp. 857–873, December, 1957.

[2] Biot, M. A., *Variational Methods in Irreversible Thermodynamics with Application to Viscoelasticity*, The Physical Review, Vol. 97, No. 6, pp. 1463–1479, March 15, 1955.

[3] Biot, M. A., *Theory of Stress-Strain Relations in Anisotropic Viscoelasticity and Relaxation Phenomena*, J. Appl. Phys., Vol. 25, No. 11, pp. 1385–1391, November, 1954.

[4] Biot, M. A., *Thermoelasticity and Irreversible Thermodynamics*, J. Appl. Phys., Vol. 27, No. 3, pp. 240–253, March, 1956.

[5] Biot, M. A., *Linear Thermodynamics and the Mechanics of Solids*, Cornell Aeronautical Laboratory Report April, 1958; Proceedings, Third U.S. National Congress of Applied Mechanics, ASME, June, 1958.

[6] Rosen, P., *On Variational Principles for Irreversible Processes*, J. Chem. Phys., Vol. 21, No. 7, pp. 1220–1221, July, 1953.

[7] Chambers, L. C., *A Variational Principle for the Conduction of Heat*, Quart. J. Mech. & Appl. Math., Vol. 9, Part 2, pp. 234–235, June, 1956.

[8] McLachlan, N. W., *Bessel Functions for Engineers*, University Press, New York, 1934.

[9] Goldstein, H., *Classical Mechanics*, Chapter XI, Addison-Wesley Press, Inc., Reading, Mass., 1951.

[10] Carslaw, H. S., and Jaeger, J. C., *Conduction of Heat in Solids* Oxford, Clarendon Press, London, England, 1948.

An Authorized Binding for Journal of the Aero/Space Sciences

Arrangements have been made by the Institute of the Aeronautical Sciences for members and subscribers to have their Journals bound carefully and economically. Simply write for details to:

Publisher's Authorized Bindery Service, 5809 West Division St., Chicago 51, Ill.

Readers' Forum

BRIEF REPORTS of investigations in the aeronautical sciences and discussions of papers published in the JOURNAL are presented in this special department. Entries must be restricted to a maximum of 1,300 words or the equivalent of one JOURNAL page including formulas and illustrations. Publication is completed as soon as possible after receipt of the material. The Editorial Committee does not hold itself responsible for the opinions expressed by the correspondents.

Contents

The Kutta Condition and the Condition for Minimum Drag ..... ROBERT T. JONES 382

Author's Reply ..... H. YOSHIHARA 383

Forebody Drag Characteristics of an Ogive Cylinder ..... W. T. STRIKE AND JACK D. WHITFIELD 383

Steady-State Surface Temperatures in Dissociated High-Speed Gas Flows ..... DANIEL E. ROSNER 384

Jet Flap Thrust Recovery ..... WILLIAM M. FOLEY AND ELLIOTT G. REID 385

An Unusual Aerodynamic Stagnation-Temperature Effect ..... IRVIN GLASSMAN AND JAMES E. A. JOHN 387

Influence of Shock-Wave Attenuation by Boundary-Layer Growth on Contact-Surface Motion in a Shock Tube ..... JAN ROSCISZEWSKI 388

Hydraulic Analogy for Two-Dimensional and One-Dimensional Flows ..... W. H. T. LOH 389

Equations of Thin Toroidal Shells ..... T. AU 391

Reduction of Strain Rosettes in the Flastic Range ..... C. S. ADES 392

Errata—"On the Generalized Prandtl Relation" ..... S. M. RAMACHANDRA 393

The Yield Strength of Beams in Pure Bending ..... ROBERT M. RIVELLO 393

Accumulative Fatigue Damage Caused by Random Loading ..... H. C. SCHJELDERUP 394

On Hypersonic Similarity for Nozzles ..... MARTIN H. BLOOM 395

Pressure Distributions for a Two-Dimensional Blunt-Nosed Body at Different Angles of Attack ..... ANTONIO FERRI AND VICTOR ZAKKAY 395

On the Continuity of the Schmidt Number at the Interface Between the Laminar Sublayer and the Outer Turbulent Region ..... NATHAN NESS 396

A Comparison of Several Approximate Theories of Melting Ablation ..... GEORGE W. SUTTON 397

The Elastic-Plastic Bending of an Eccentrically Loaded Sandwich Column ..... WILLIAM E. BOYCE 398

The Effect of Helium Injection at an Axially Symmetric Stagnation Point ..... H. HOSHIZAKI AND H. J. SMITH 399

The Kutta Condition and the Condition for Minimum Drag

Robert T. Jones

National Aeronautics and Space Administration, Ames Research Center, Moffett Field, Calif.

December 8, 1958

IN A RECENT COMMUNICATION, Yoshihara and Strand[1] concluded that the conditions for minimum drag in lifting surface theory are not valid for wings with singular edge forces. Such edge forces are normally incorporated in the surface integral for drag by a limiting process. In reference 1, however, the edge forces are given a separate expression in the form of a line integral taken around the edge. The line integral is then added to the expression for the direct drag, but is omitted in the expression of the interference drag—i.e., in the Ursell-Ward relation. This inconsistency evidently leads to the erroneous conclusion.

The selection of a distribution of lift by the condition of minimum drag does not, in general, agree with the selection imposed by the Kutta condition. The latter condition merely selects a flow as being physically probable in a viscous fluid.

With plan forms pointed at the front or rear the optimum distributions of lift do, in fact, require suction peaks at either the leading or trailing edges. Thus, in the case of a slender triangular wing moving base foremost, such a peak appears along the trailing edge and a component of the minimum drag appears as a downstream edge force. Figure 1 illustrates two methods by which this singular mathematical model might be interpreted in a practical sense. (In actual practice boundary-layer control might be employed.) Clearly, our consideration of the sharp edge and the limiting process is only an effort to simplify the formulas. If the limiting calculation produced a result different from that obtained by integrating the nearby smooth pressure distributions, then we would find it difficult to attribute any physical significance to the result.

Contributors Please Note

Readers' Forum items must be confined to the equivalent of one page in the *Journal*. Contributions that exceed this limit will be returned to the authors for condensation and rewrite. To avoid inconvenience and delay, please adhere to the following specifications:

(1) Five, double-spaced, typewritten, manuscript pages ($8\frac{1}{2}$ by 11 in.), including wide margins, formulas, and headings, equal one printed page.

(2) For every illustration, deduct at least one-half or as much as one manuscript page, depending on the size of the illustration.

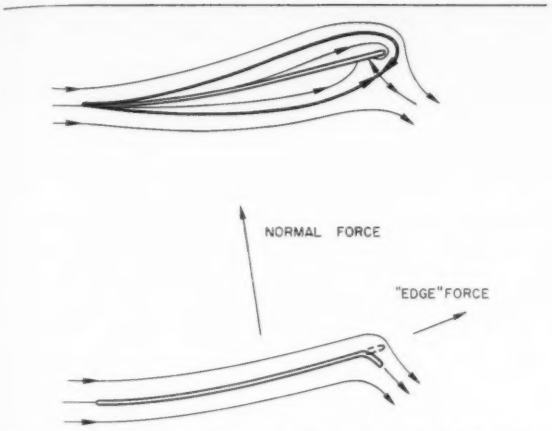

FIG. 1. Alternative interpretations of a trailing-edge singularity.

It is interesting to note that the optimum distribution of lift over the reversed triangular wing is not given by the writer's slender wing theory, since the latter theory is concerned with the magnitude of the lift as determined by the Kuta condition. For the optimum lift distribution we have to return to Munk's original airship theory.

REFERENCE

[1] Yoshihara, Hideo, and Strand, Torstein, *On Jones' Criterion for Optimum Lifting Wings*, Journal of the Aero/Space Sciences, Vol. 25, No. 9, p. 600, September, 1958.

Author's Reply

H. Yoshihara
Aerodynamics Group Engineer, Convair, A Division of General Dynamics Corp., San Diego, Calif.
February 9, 1959

IN THE DERIVATION of the Jones criterion of minimum drag using the calculus of variations,[1, 2] use was made of the Ursell-Ward reciprocal flow relations. In this relation certain interference terms between the edge suction forces in the forward and reverse flows arise when the Kutta condition is not imposed. When the combined downwash is constant, it is found that these interference forces just cancel the edge suction force term in the variational procedure on which our conclusions were based in reference 2, thus justifying Jones' comments above. On the other hand, if the Kutta condition is imposed in the forward and reverse flows in the Ursell-Ward relation, these interference forces will vanish, and it is found that Jones' criterion follows, but *only* if the edge suction forces are kept invariant in the variation at the zero value required by the Kutta condition in both the forward and reverse flows. Thus, it is seen that Jones' criterion is a requirement for the minimal drag either when one has a constrained optimum, where edge forces are not allowed, or when one has a more general optimum, where no restrictions are placed on the edge condition.

The optimal drag can be computed using the combined flow method of Graham.[3] A salient feature of this method is the use of Jones' criterion as a boundary condition. Since the latter condition was found to be applicable under various edge conditions, it would follow that if there is a multiplicity of optimum wing warps possible, they must all have the same drag. Of primary interest is that warp which yields zero edge forces. Here the Kutta condition will be fulfilled at the trailing edge, and the requirements of finite pressures would minimize violations of the linear theory and separation effects at the leading edge.

The existence of optimum wings without edge forces may be conjectured by considering the direct variational procedure of superimposing a family of basic wing warps each having finite pressures at the edges. A minimizing sequence of these basic warps can then be constructed by ordinary calculus.

REFERENCES

[1] Sedney, R., *On Jones' Criterion for Thin Wings of Minimum Drag*, Readers' Forum, Journal of the Aeronautical Sciences, Vol. 21, No. 9, pp. 639, 640, September, 1954.

[2] Yoshihara, H., and Strand, T., *On Jones' Criterion for Optimum Lifting Wings*, Readers' Forum, Journal of the Aero/Space Sciences, Vol. 25, No. 9, p. 600, September, 1958.

[3] Graham, E., *The Calculation of Minimum Supersonic Drag by Solution of an Equivalent Two-Dimensional Potential Problem*, Douglas Aircraft Report No. SM-22666, December, 1956.

Forebody Drag Characteristics of an Ogive Cylinder

W. T. Strike and Jack D. Whitfield
*Gas Dynamics Facility, ARO, Inc., Tullahoma, Tenn.**
December 19, 1958

EXPERIMENTAL LAMINAR skin-friction data have been obtained which show an increase with Mach Number due to the pressure gradients influences on the ogive cylinder tested. This trend, of course, is directly opposite to the flat-plate case; however, theoretical values are shown to agree very well with the data.

Inviscid pressure distributions on the ogive cylinder can be obtained by means of the second-order shock expansion analysis described by Syvertson and Dennis.[1] W. Mangler[2] provides the method required to transform an axisymmetric flow into a corresponding two-dimensional flow (or the converse transformation) for analytical purposes.

The laminar boundary-layer characteristics of the equivalent two-dimensional body with pressure gradient then can be theoretically estimated by means of Low's analysis.[3] Once the displacement thickness has been estimated, an effective correction to the original body shape can be made, via Mangler's transformation, and a revised pressure distribution obtained. This revised pressure distribution then can be used to obtain a more accurate estimate of the boundary-layer characteristics. A second such iteration as this was made for Mach Number 4, but resulted in a negligible correction to the boundary-layer displacement thickness.

* Contract Operator, USAF Arnold Engineering Development Center, Air Research and Development Command, Tullahoma, Tenn.

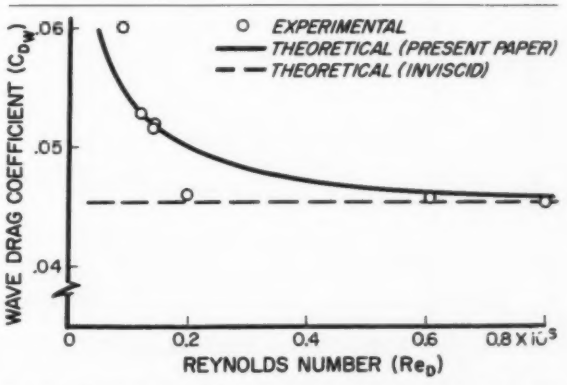

FIG. 1. Wave-drag coefficient as a function of Reynolds Number for a 20-caliber tangent ogive, $M_\infty = 4.0$

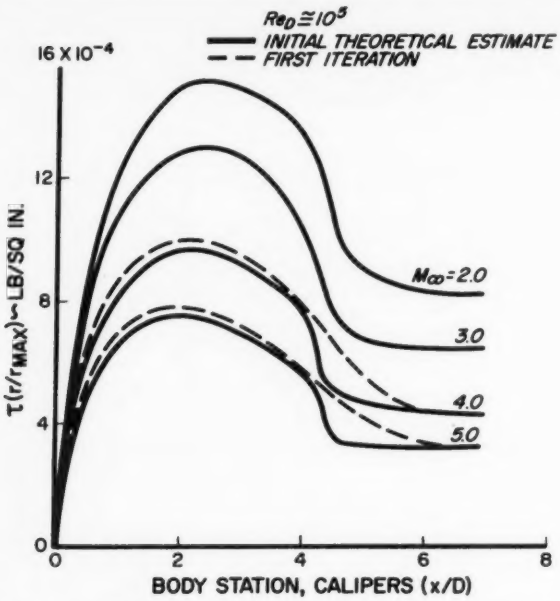

FIG. 2. Relative local shear stress on a 20-caliber tangent ogive-cylinder.

The variation of pressure distribution, and hence wave drag, with Reynolds Number can be estimated by the above procedure. The theoretical wave-drag coefficient, C_{D_W}, based on maximum frontal area, is presented as a function of Reynolds Number and compared with experimental data in Fig. 1. Although the inaccuracies of these experimental data do not permit an accurate confirmation of the theoretical wave drag, the relative trend is established.

The local shear stresses obtained from the theoretical estimates are presented in Fig. 2. The total or average skin-friction coefficient, based on wetted surface area, as obtained from a graphical integration of Fig. 2, is presented as a function of Mach Number for the ogival nose and the ogive cylinder in Fig. 3 and compared with theoretical flat-plate values.[4] The ogive cylinder case is compared to the experimental data.

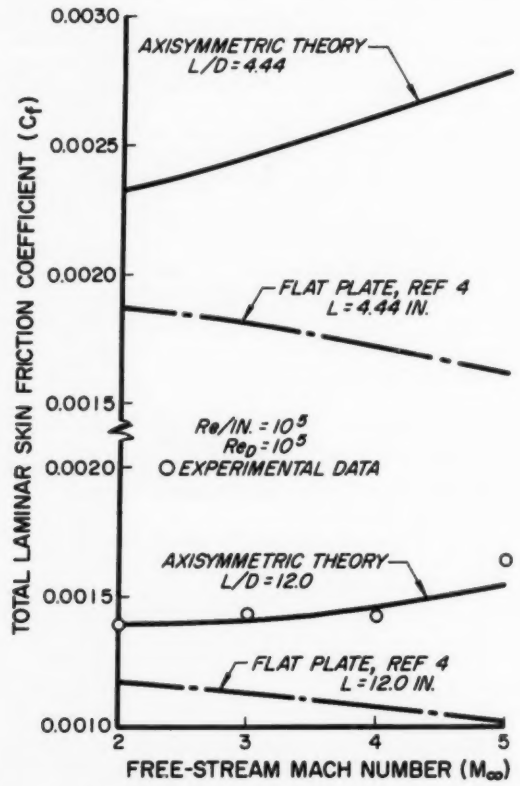

FIG. 3. Total laminar skin-friction coefficients for a 20-caliber tangent ogive (L/D = 4.444) and a 20-caliber tangent ogive-cylinder (L/D = 12).

REFERENCES

[1] Syvertson, Clarence A., and Dennis, Davis H., *A Second Order Shock Expansion Method Applicable to Bodies of Revolution Near Zero Lift*, NACA TN 3527, 1956.

[2] Mangler, W., *Compressible Boundary Layers on Bodies of Revolution*, ATI No. 28063, June, 1946.

[3] Low, George M., *Simplified Method for Calculation of Compressible Laminar Boundary Layer with Arbitrary Free-Stream Pressure Gradient*, NACA TN 2531, October, 1951.

[4] Van Driest, E. R., *Investigation of Laminar Boundary Layer in Compressible Fluids Using the Crocco Method*, NACA TN 2597, 1952.

Steady-State Surface Temperatures in Dissociated High-Speed Gas Flows*

Daniel E. Rosner
AeroChem Research Laboratories, Inc., Princeton, N.J.
December 8, 1958

BESIDES VISCOUS DISSIPATION, exothermic surface recombination of atoms contributes to the steady-state wall temperature assumed by a body immersed in a dissociated supersonic stream. The flat plate has recently been treated from a laminar boundary-layer point of view by Vaulin[1] in a highly condensed paper. For the "chemically-frozen," "diffusion-controlled" case Vaulin gives the ratio of surface to free-stream temperature as

$$T_w/T_e = 1 + [(\gamma - 1)/2]M^2(Pr_\lambda)^{1/2} + (\alpha_e Q/\bar{c}_p T_e)(Le)^{2/3} \quad (1)$$

subject to the assumptions that the Prandtl and Lewis Numbers are constant, as are the density-viscosity product and the frozen specific heat $\bar{c}_p$ of the mixture. Here M and α_e are the free stream Mach Number and degree of dissociation (it is implicitly assumed that $\alpha \ll 1$), Q is the heat release of the recombination reaction, and radiation from the surface is neglected.

Since this result can also be obtained from an elementary similitude approach (Frank-Kamenetsky), it is readily generalized to cases that are neither "diffusion-controlled" nor "reaction-rate controlled." Furthermore, the effects of radiation and secondary transport phenomena, such as thermal diffusion, can be assessed. The form of these extensions is indicated here, together with the implication of results of this type, with respect to recent observations[2] on small catalytic probes in supersonic nonequilibrium dissociated streams.

We consider first the case of arbitrary surface catalytic activity in the absence of radiation, thermal diffusion, etc. Now the atom concentration, or "degree of dissociation" α_w at the insulated wall is no longer necessarily small compared to the free-stream value α_e, and a catalytic rate constant k_w, peculiar to the atom/surface combination, enters the problem. In the simplest instances, the heterogeneous kinetics will be described by a first-order law of the form

$$\dot{R}_w = k_w \rho_w \alpha_w \quad (2)$$

where k_w usually depends upon T_w. If Nu_D represents the local Nusselt Number for diffusion, then in the steady-state $\dot{R}_w$ must

* This research was supported by the U.S. Air Force through the Air Force Office of Scientific Research of the Air Research and Development Command under Contract No. AF 49(638)-300.

also be given by

$$\dot{R}_w = Nu_D(D_{12}\rho)^* \{(\alpha_e - \alpha_w)/x\} \quad (3)$$

The asterisk refers to evaluation at a suitable "reference temperature." As to the energetics, at the steady-state value of T_w the product $Q\dot{R}_w$ must balance the rate $\dot{q}_\lambda$ of heat convected away from the hot surface. In the supersonic case $\dot{q}_\lambda$ may be written in terms of the local Nusselt Number Nu_λ for heat transfer

$$\dot{q}_\lambda = Nu_\lambda\lambda^*\left[\left(T_w - T_e\right\{1 + [(\gamma - 1)/2]M^2Pr_\lambda^{1/2}\}\right)/x\right] \quad (4)$$

where λ^* represents the "frozen" thermal conductivity of the mixture. Following Frank-Kamenetsky,[3] from low-speed similitude theory and solutions to the boundary-layer equations, Nusselt Numbers can ordinarily be written in the separable form[4]

$$Nu_\lambda = C(Re_x)^m (Pr_\lambda)^n \quad (5a)$$

$$Nu_D = C(Re_x)^m (Pr_D)^n \quad (5b)$$

where, in the approximations to be considered, the constant C and the exponents m and n of the Reynolds and Prandtl Numbers are the same for both heat and mass transfer. Here Pr_D is the "Prandtl Number for diffusion," more conventionally known as the Schmidt Number; thus, $Le = Pr_\lambda/Pr_D$. Introducing Eqs. (5a) and (5b) into the energy balance and eliminating the "nonobservable" or "intermediate" concentration α_w we obtain

$$T_w/T_e = 1 + [(\gamma - 1)/2]M^2(Pr_\lambda)^{1/2} + (\alpha_eQ/\bar{c}_pT_e)(Le)^{1-n}\{\mathcal{C}/(1 + \mathcal{C})\} \quad (6)$$

where $\mathcal{C}$ is the modified "catalytic parameter"

$$\mathcal{C} \equiv k_w\rho_w \{(Nu_D)(D_{12}\rho)^*/x\}^{-1} \quad (7)$$

A parameter of this form appears in all viscous flow problems involving the coupling of convection, diffusion, and surface reactions[5, 6] and can be interpreted[5] as the ratio of a characteristic diffusion time to a reaction time characteristic of the surface activity. To be consistent with the recovery factor $(Pr_\lambda)^{1/2}$ in Eq. (4), for the flat plate case $m = 1/2$ and $n \sim 1/3$ so that Le in Eq. (6) is raised to the 2/3 power.

While the catalytic parameter $\mathcal{C}$ itself depends upon the surface temperature, Eq. (6) has been written in this form to illustrate the two important limiting cases. When $\mathcal{C} \to \infty$, we approach Vaulin's "diffusion-controlled" result [Eq. (1)]. This condition is always approached far downstream on catalytic surfaces.[5, 6] On the other hand, for $\mathcal{C} \ll 1$ the surface reaction contribution becomes linear in $\mathcal{C}$ and we enter the "kinetic regime." For example, this would be realized at some finite station x along a noncatalytic surface if it became catalytic thereafter. In the limit $\mathcal{C} \to 0$ no surface reaction takes place and we obtain the well-known gasdynamic result for the laminar recovery temperature in a supersonic stream. Steady-state values of T_w for arbitrary values of $\mathcal{C}$ lie between these two extremes. Lastly, it should be observed that the catalytic parameter affects the result for the surface temperature in the same manner as in Goulard's recent extension[7] of the stagnation point heat-transfer problem to the case of highly cooled walls of arbitrary catalytic activity. However, this is not at all surprising.

The above approach is currently being applied at this laboratory to interpret equilibrium probe temperatures in terms of the free-stream atom concentration. For example, using small wires or spheres, one deals with perimeter-mean quantities and bases the significant global Nusselt Numbers on probe diameter. The low-speed result is of the form of Eq. (6) with the Mach Number term absent. With a suitable choice of "driving force" and reference quantities this same result should be experimentally applicable to the supersonic case, as in hot wire anemometry.[8] Correction factors to quantitatively account for radiation and secondary transport processes can readily be obtained by the introduction of additional terms in the basic energy balance. A correction factor accounting for thermal diffusion and the diffusion thermo-effect is discussed in reference 3 in connection with the low-speed catalytic oxidation problem. For atom recombination at hot surfaces, we remark that the correction for thermal diffusion dominates its conjugate effect and enters the problem through a "Lewis Number for thermal diffusion." Furthermore, since the thermal diffusion coefficient for atoms is expected to differ in sign from the ordinary binary diffusion coefficient,[9] thermal diffusion will tend to increase T_w over that given by Eq. (6). Radiation, of course, tends to lower T_w by an amount depending on the emissivity of the surface.

To fix ideas, the implications of the relations given above are discussed in terms of the limiting case $\mathcal{C} \to \infty$ (diffusional regime) in the absence of thermal diffusion and radiation. By way of analogy, it is interesting to note that $(Le)^{1-n}$ plays the role of a "recovery factor" for surface reactions. Thus, if $\alpha_eQ/\bar{c}_p$ is interpreted as the temperature rise which would result from adiabatic recombination (AR) in the gas phase, the probe temperature can *exceed* $T_{AR}{}^0$ if $Le > 1$ and $n < 1$. This is no more a violation of the principle of energy conservation than the fact that the adiabatic wall temperature can *exceed* the stagnation temperature T^0 of a chemically inert supersonic stream[10] if $Pr_\lambda > 1$. In fact, preliminary experimental evidence[8] indicates that for atom-molecule mixtures produced in a glow discharge, one must invoke Lewis Numbers exceeding 1.4 to account for observed probe temperatures in a supersonic "low-temperature" discharge tunnel.

Finally, it should be observed that the overall heterogeneous kinetics will fail to be adequately represented by Eq. (2) when the surface is hot enough to cause the dissociation[11, 12] of an appreciable number of incident molecules.

References

[1] Vaulin, E. P., *Steady Temperature of a Plane Plate in a Reacting Gas Flow*, Soviet Phys. Doklady, Vol. 2, No. 2, pp. 187–191, March–April, 1957.

[2] Rosner, D. E., and Calcote, H. F., *Generation of Supersonic Dissociated and Ionized Non-Equilibrium Streams*, AeroChem Research Laboratories, TM-10, ASTIA Doc. No. 207 590, October, 1958.

[3] Frank-Kamenetsky, D. A., *Diffusion and Heat Exchange in Chemical Kinetics*, translated by N. Thon; Princeton University Press, Princeton, N.J., 1955.

[4] Eckert, E. R. G., *Introduction to the Transfer of Heat and Mass;* McGraw-Hill Book Company, New York, 1950.

[5] Rosner, D. E., *Chemically Frozen Boundary Layers with Surface Reaction*, Princeton University Aeronautical Engineering Report No. 419, March, 1958.

[6] Chambré, P. L., and Acrivos, A., *On Chemical Surface Reactions in Laminary Boundary Layer Flows*, J. Appl. Phys., Vol. 27, No. 11, pp. 1322–1328, November, 1956.

[7] Goulard, R., *On Catalytic Recombination Rates in Hypersonic Stagnation Heat Transfer*, Jet Propulsion, Vol. 28, No. 11, pp. 737–745, November, 1958.

[8] Kovasznay, L. S. G., and Tornmarck, S. I. A., *Heat Loss of Hot Wires in Supersonic Flow*, The Johns Hopkins University, Bumblebee Report No. 127, June, 1950.

[9] Scala, S. M., and Baulknight, C. W., *Transport and Thermodynamic Properties in a Hypersonic Laminar Boundary Layer*, General Electric Company, Missile and Ordnance Systems Department, TIS No. 58SD232 (Aerophysics Research Memo No. 10).

[10] Emmons, H. W., and Brainerd, J. G., *Temperature Effects in a Laminar Compressible-Fluid Boundary Layer Along a Flat Plate*, J. Appl. Mech., Vol. 8, No. 3, pp. 105–110, September, 1941.

[11] Scala, S. M., *Hypersonic Heat Transfer to Surfaces Having Finite Catalytic Efficiency*, General Electric Company, M.O.S.D. 57SD646, (Aerophysics Research Memo No. 4), July, 1957.

[12] Rosner, D. E., *Boundary Conditions for the Flow of a Multicomponent Gas*, Jet Propulsion, Vol. 28, No. 8, Part 1, pp. 555–556, August, 1958.

Jet Flap Thrust Recovery

William M. Foley and Elliott G. Reid

Graduate Student, and Professor of Aerodynamics, Respectively, Stanford University, Stanford, Calif.*

January 6, 1959

THIS RÉSUMÉ of one segment of a Convair-sponsored investigation just completed at Stanford University has been prepared for immediate publication to avoid delay in announce-

* Now Engineer, Research Department, United Aircraft Corporation.

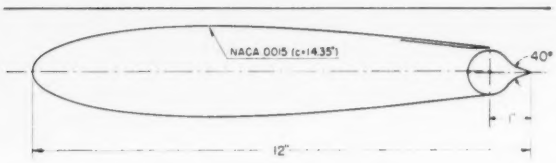

FIG. 1. Model profile.

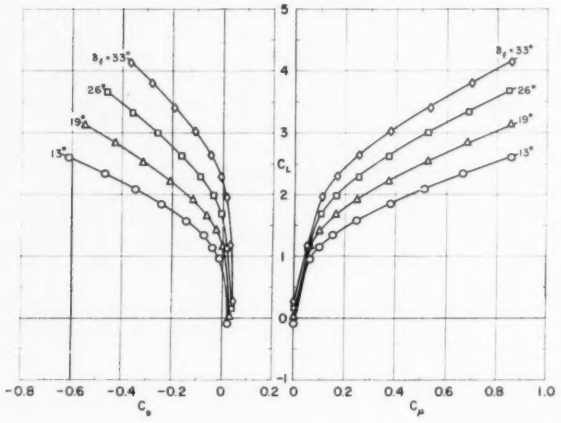

FIG. 2. Test results.

ment of the significant finding that substantially complete thrust recovery has been obtained in two-dimensional-flow tests of a jet flap wing.

The purpose of the experiments described herein was to confirm or disprove the widely disputed theoretical prediction that the oblique discharge of air from such a wing should result in an upstream thrust of magnitude equal to that of the total jet momentum reaction, rather than that of its streamwise component.[1] Toward that end, parallel vertical walls were installed in the open throat of the 7.5 ft. diameter Stanford wind tunnel to enable determination of the air forces experienced in two-dimensional flow by a jet flap wing model of 12 in. chord and 24 in. span.

The model was suspended from the overhead aerodynamic balance by rigid members housed within the vertical walls. Circular apertures of 14.1 in. diameter were cut in the inner wall plates to accommodate flush, plane, circular discs of 14.0 in. diameter which were fastened to the ends of the wing. (No effort was made to determine or correct for the drag of these discs.) The interior of the model, whose profile is shown in Fig. 1, served as a plenum chamber from which the jet sheet issued through a full-span slot of $0.0047c$ width. Compressed air was supplied to the plenum chamber through ducts incorporated in the supporting members, and tare forces due to the pressure and flow of compressed air were eliminated by the adjustment of movable duct elements.

Preliminary and auxiliary experiments consisted in determination of the value of dC_D/dC_L^2 which characterized the wind tunnel installation and in the measurement of jet reactions in the absence of wind. The value $dC_D/dC_L^2 = 0.0243$ was established by measuring wing forces at various angles of attack with the slot sealed and flap undeflected. Static jet reactions measured at various flap settings and jet velocities ranged from 0.91 to 0.94 of those calculated from pressure-temperature-mass-flow data and these forces were found to be inclined at about 25° to the flap's plane of symmetry—i.e., they were nearly parallel to the rearmost upper surface element of the flap profile.

The definitive force tests were carried out at a wind speed of 70 ft. per sec.—to enable the attainment of substantial values of C_μ with a compressor of limited capacity. They consisted in varying the jet velocity over a wide range at each of four flap settings while the wing angle of attack remained fixed at 0°. The results are shown in Fig. 2—in connection with which it is noted that δ_f = flap angle, $C_\mu = M/qS$, and M = *calculated* momentum flux.

Preliminary analysis of these data began with examination of the variations of C_D with C_μ at constant values of C_L. As may be seen in Fig. 3, these variations proved to be not only linear but also characterized by nearly identical rates—i.e., lines of slope -0.94 were found to closely approximate the variations of C_D with C_μ at all values of C_L. Thus, Fig. 3 clearly indicates that a large and substantially uniform percentage of the calculated jet reaction was transformed into upsteam thrust when the flap angle and jet velocity were so adjusted as to maintain C_L at fixed values.

Consideration of Fig. 3 suggested that the unequal vertical distances between the parallel lines which correspond to increasing values of C_L might reflect nothing more than differences between the corresponding coefficients of drag due to lift. To test this hypothesis, *all* of the experimentally determined values of C_D were reduced by the amounts $0.0243\ C_L^2$ and the resulting values were plotted against C_μ.

The result of thus reducing and replotting the basic data of Fig. 2 is shown in Fig. 4. There it will be seen that all data points lie on—or very close to—a single straight line of slope -0.94. Since the basic data represent the results of large variations of δ_f, θ_f (jet discharge angle), C_μ, and C_L, the unique

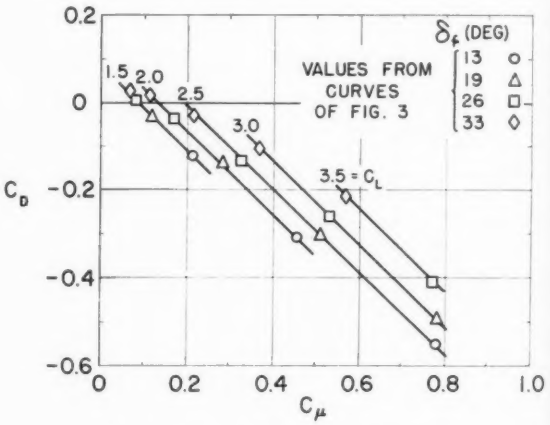

FIG. 3. Drag variation at constant lift.

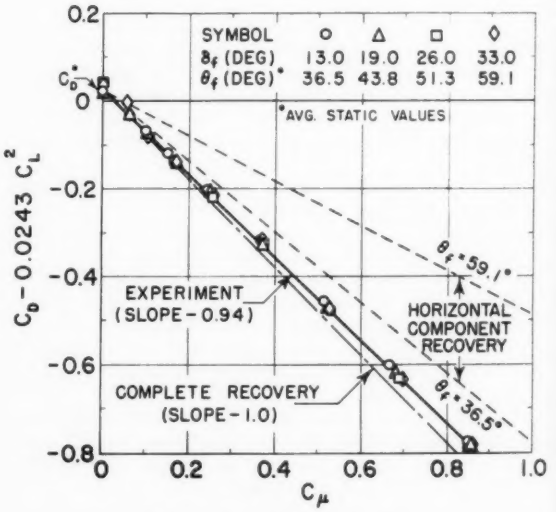

FIG. 4. Residual drag vs. C_μ.

linear relationship illustrated in Fig. 4 shows that substantially complete and uniform thrust recovery was attained under all of the operating conditions which prevailed during these tests. In fact, the magnitude of the thrust recovered appears to be almost exactly equal to that of the total reaction which would have been measured—at the same momentum flux—under conditions of static discharge.

The incompatibility of the concept of "horizontal component recovery" with the results of these experiments is also shown in Fig. 4. Broken lines have been drawn to show how that component of C_D which is not due to lift would vary with C_μ if only the horizontal component of the jet reaction were recovered as thrust. (The broken lines define values of $C_D^* - C_\mu \cos \theta_f$). It is quite evident that the experimental results exhibit no evidence of such dependence upon jet discharge angle.

REFERENCE

[1] Davidson, I. M., *The Jet Flap*, J. R.Ae.S., Vol. 60, No. 541, pp. 25–41, January, 1956.

An Unusual Aerodynamic Stagnation-Temperature Effect†

Irvin Glassman* and James E. A. John**
Princeton University, Princeton, N.J.

December 19, 1958

IN A PROGRAM concerned with the mixing of compressible jets with quiescent air, experimental measurements were obtained in which stagnation temperatures along the centerline of the jet ($T_c°$) were greater than either the uniform initial stagnation temperature of the jet ($T_1°$) or the ambient temperature (T_a). This effect was most evident when the initial Mach Number was the greatest and when the ratio $T_1°/T_a$ was at a minimum (unity for the actual experimental cases).

The experiments were performed with two axially symmetric nozzles. One, a Mach 2.6 nozzle designed for shock-free parallel flow,[1] and another, a subsonic nozzle operated so that exit Mach Numbers of 0.97 and 0.68 were obtained. Both nozzles were designed with large exit diameters (2.55 in.) in order to minimize boundary-layer effects. The stagnation temperatures were measured with probes modeled after a Pratt and Whitney design[2] which gave recovery factors better than 95 per cent. The actual experimental rake consisted of six stagnation-pressure and five stagnation-temperature probes alternated with each other; details of the experimental facility are described elsewhere.[1]

The high-stagnation-temperature effect was first noticed during experimentation with the $M = 2.6$ nozzle and heated air ($T_1°/T_a > 1$). In this case, as in the others to be discussed, the stagnation temperature of the nozzle air stream could be varied so that a specified $T_1°/T_a$ ratio could be obtained. All instrumentation was checked thoroughly to establish that the effects measured were real.

Fig. 1 shows the $M = 2.6$ results (the U_c/U_1 results for the $M_1 = 2.6$, $T_1°/T_a = 1$, case are from reference 3) plotted in the form of the centerline decay as a function of the distance downstream from the nozzle, X. One immediately notices that the high-stagnation-temperature effect increases with a decrease in $T_1°/T_a$ ratio and begins near the end of the velocity potential core. Stagnation temperatures approximately 8 per cent greater than the initial stagnation temperature are indicated. (Only cursory checks of energy conversation could be made, for unfortunately the apparatus had to be disassembled before extensive measurements could be taken. Although these checks were inconclusive, the authors believe the data to be worthwhile reporting.) This increase is equivalent to about 42°F. for the $T_1°/T_a = 1$ case ($T_a = 530$°R.).

Since the temperature-ratio range covered is more significant, the results shown in Figs. 2 and 3 for the $M_1 = 0.97$ and 0.68 tests are even more interesting (the results for the $M_1 = 0.97$

† This study was part of a larger program in supersonic and subsonic mixing carried out at Princeton University from 1951–1956. The program was sponsored by Project SQUID, which is supported by the Office of Naval Research under Contract N6-ori-105, T.O. III, NR-098-038. Reproduction in full or part is permitted for any use of the United States Government. The advice given during the course of this study by Prof. L. Crocco is gratefully acknowledged.

* Assistant Professor, Department of Aeronautical Engineering.

** Formerly, Assistant-in-Research, Department of Aeronautical Engineering. Now, Research Engineer, Air Reduction Co., Murray Hill, N.J.

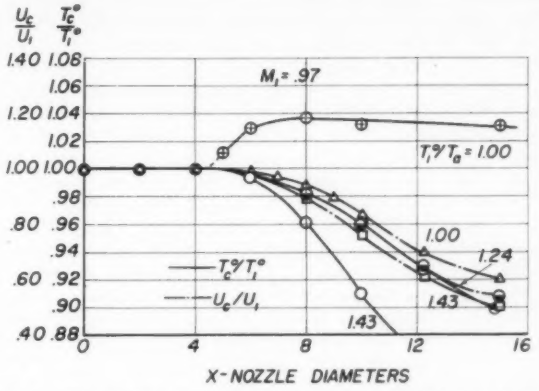

FIG. 2. Centerline stagnation temperature and velocity variation for a Mach 0.97 jet mixing with quiescent air.

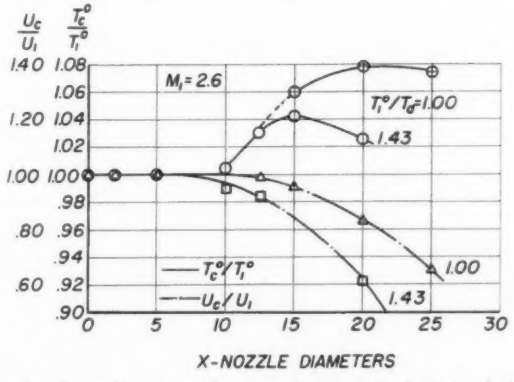

FIG. 1. Centerline stagnation temperature and velocity variation for a Mach 2.6 jet mixing with quiescent air.

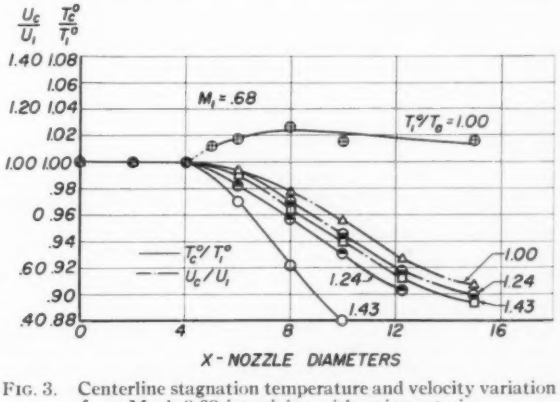

FIG. 3. Centerline stagnation temperature and velocity variation for a Mach 0.68 jet mixing with quiescent air.

and 0.68, $T_1°/T_a = 1.25$ and 1.47, cases are from reference 1). One recognizes that, for the temperature ratios $T_1°/T_a = 1.43$ and 1.24, "normal" centerline decay curves are obtained. But, for the case initially isoenergetic ($T_1°/T_a = 1$) an "unusual" centerline decay curve is obtained. Again, in Figs. 2 and 3 one is able to relate the start of an appreciable rise in stagnation temperature to a position near the end of the velocity potential core.

The effect noticed appears to be contrary to what is known about compressible heat transfer and cannot be explained from such considerations. However, similar effects[5] have been explained qualitatively by Ackeret[6] in a theory based upon a nonsteady potential-flow analysis. If the stagnation-temperature probe acts as a resonance tube, then the effects obtained in this study are similar to those found by Sprenger[7] and the actual existence of unusually high stagnation temperatures at points in the flow field is in doubt. But it is interesting to note that such effects could exist in stagnation-temperature probes.

References

[1] Warren, W. R., Jr., *An Experimental and Analytical Investigation of Compressible Free Jets*, Ph.D. Thesis, Dept. of Aero. Engrg., Princeton University, 1957.

[2] Eber, G. R., *Physical Measurements in Gas Dynamics and Combustion*, Vol. IX, "High Speed Aerodynamics and Jet Propulsion," p. 192, Princeton University Press, 1954.

[3] Pitkin, E. T., and Glassman, I., *Experimental Mixing Profiles of a Mach 2.6 Free Jet*, Journal of the Aero/Space Sciences, Vol. 25, No. 12, pp. 791–793, December, 1958.

[4] Corrsin, S., and Uberoi, M. S., *Further Experiments on Flow and Heat Transfer in a Heated Turbulent Air Jet*, NACA TN 1863, 1949.

[5] Ryan, L. R., *Experiments on Aerodynamic Cooling*, Mitteilung Nr. 18, des Instituts für Aerodynamik ETH, Zürich, 1951.

[6] Ackeret, J., *Über die Temperaturverteilung hinter angeströmten Zylindern*, Mitteilung Nr. 21 des Instituts für Aerodynamik ETH, Zürich, 1954.

[7] Sprenger, H., *Über thermische Effekte in Resonanzröhren*, Mitteilung Nr. 21 des Instituts für Aerodynamik ETH, Zürich, 1954.

Influence of Shock-Wave Attenuation by Boundary-Layer Growth on Contact-Surface Motion in a Shock Tube

Jan Rosciszewski
Katedra Aerodynamiki, Politechnika Warszawska, Warsaw, Poland

January 6, 1959

Symbols

a	= velocity of sound
a_0	= velocity of sound on the front of a shock wave
k	= c_p/c_v
i_0	= $(V^2/2) + [k/(k-1)]\,(p/\rho)$ = stagnation enthalpy
r	= $[a/(k-1)] + (V/2)$
C_{fw}	= skin-friction coefficient
d_0	= duct diameter
s	= $[a/(k-1)] - (V/2)$
t	= time
u	= variable velocity in cross section
x	= coordinate measured along tube axes
A_0	= duct cross-section area
C_α, C_β	= constant values along each α, β characteristics
E	= $(V^2/2) + [1/(k-1)]\,(p/\rho)$
S	= specific entropy
U	= velocity of shock-wave propagation
V	= velocity of flow outside of boundary layer
α, β	= coordinates measured along characteristics of first and second family, respectively
δ	= boundary-layer thickness
δ_{ij}	= $\int_0^\delta [1 - (\rho^i u^j/\bar{\rho}^i V^j)]\,dy$
$\delta^* = \delta_{11}$	= displacement thickness
γ	= element of shock line
ϵ	= with subscript r, V, U, etc., small disturbance of corresponding value
ξ	= $U°t - x$ coordinate measured from shock wave
ξ_α, ξ_β	= ξ coordinate measured from a point of intersection shock line with α and β characteristics, respectively

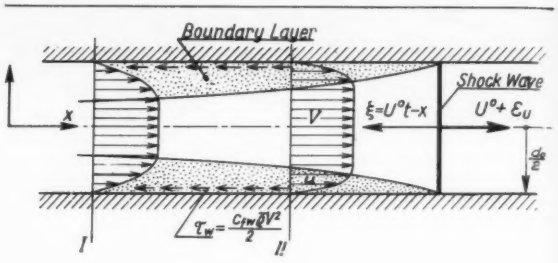

FIG. 1.

q_w	= heat flow per unity of time and wall area
ρ	= variable density in cross section
$\bar{\rho}$	= density outside of the boundary layer
D/Dt	= $(\partial/\partial t) + V(\partial/\partial x)$
$d/d\gamma$	= $(\partial/\partial t) + U(\partial/\partial x)$
Superscript o	= values corresponding to ideal shock tube flow

BELOW IS DISCUSSED a problem of contact-surface acceleration in shock tube, observed experimentally by Glass and Patterson.[1]

The method of a small parameter is applied to equations governing nonsteady, nonisentropic flow behind the shock wave.[2, 3] These equations can be written in the generalized form

$$\partial r/\partial\alpha \equiv (\partial r/\partial t) + (V + a)(\partial r/\partial x) = F_1(V, a, \xi) + [a/2c_p(k-1)]\,(\partial S/\partial\alpha) \quad (1)$$

$$\partial s/\partial\beta \equiv (\partial s/\partial t) + (V - a)(\partial s/\partial x) = F_2(V, a, \xi) + [a/2c_p(k-1)]\,(\partial S/\partial\beta) \quad (2)$$

Writing three laws of mechanics, we shall calculate coefficients $F_{1,2}$ representing a boundary-layer influence on shock tube flow.

We assumed that $\delta/d_0 \ll 1$ and that all boundary-layer parameters calculated as for a shock motion over a flat plate depend on distance from shock wave $\xi = U°t - x$ only.[4]

Conservation of Mass

For the control volume, see Fig. 1,

$$\left[\iint_{A_0} \rho u dA\right]_I - \left[\iint_{A_0} \rho u dA\right]_{II} = \partial/\partial t \left\{\int_{x_I}^{x_{II}} \left[\iint_{A_0} \rho dA\right] dx\right\}$$

Taking into account $\iint_{A_0} \rho u dA = (A_0 - \pi d_0\delta^*)\bar{\rho}V$, etc.,

we get for $x_{II} \to x_I$

$$(D\bar{\rho}/Dt) + \bar{\rho}(\partial V/\partial x) = (4\bar{\rho}/d_0)[V(\partial\delta^*/\partial x) + (\partial\delta_{10}/\partial t)] = -(4\bar{\rho}/d_0)[V(d\delta^*/d\xi) - U(d\delta_{10}/d\xi)] \quad (3)$$

Momentum Equation

Assuming pressure to be constant in this and the preceding section, we have (see Fig. 1)

$$A_0(p_I - p_{II}) - \pi d_0 \int_{x_I}^{x_{II}} \bar{\rho}(V^2/2)C_{fw}dx = \left[\iint_{A_0} \rho u^2 dA\right]_{II} - \left[\iint_{A_0} \rho u^2 dA\right]_I + (\partial/\partial t)\left\{\int_{x_I}^{x_{II}} \left[\iint_{A_0} \rho u dA\right] dx\right\}$$

Using Eq. (3), we get for $x_{II} \to x_I$

$$(DV/Dt) + (1/\bar{\rho})(\partial p/\partial x) = -(2C_{fw}V^2/d_0) + (4V^2/d_0)[d(\delta^* - \delta_{12})/d\xi] - (4VU/d_0)[d(\delta_{10} - \delta^*)/d\xi] \quad (4)$$

Energy Equation

$$\left[\iint_{A_0} i_0\rho u dA\right]_{II} - \left[\iint_{A_0} i_0\rho u dA\right]_I + (\partial/\partial t)\left\{\int_{x_I}^{x_{II}} \left[\iint_{A_0} \rho E dA\right] dx\right\} = -\pi d_0 \int_{x_I}^{x_{II}} q\,dx$$

Using Eqs. (3), (4) we get for $x_{II} \to x_I$

$$(1/c_p)(DS/Dt) - \{[2(k-1)V^2]/d_0a^2\}\left([(U/V)+2]\,(d\delta_{12}/d\xi) - (d\delta_{13}/d\xi) + C_{fw} + (U/V)\{1-[2/(k-1)]\,(a^2/V^2)\}\times (d\delta_{10}/d\xi) - \{2(U/V)+1-[2/(k-1)]\,(a^2/V^2)\}\,(d\delta^*/d\xi) - [2/(k-1)]\,(a^2/V^2)\,(d\delta_{01}/d\xi)\right) - [4q_w(k-1)/\bar{\rho}d_0a^2] \quad (5)$$

From Eqs. (3)–(5) we get

$$F_{12}(\xi) = [2V^2/d_0]\left(\{\pm 1 \pm (U/V) - (k-1)\,(U/a) - [(k-1)/2]\,(V/a)\}\,(d\delta^*/d\xi) + \{[(k-1)/2]\,(U/a) + [(k-1)/a]\,V \mp 1\}\,(d\delta_{12}/d\xi) \mp (C_{fw}/2)\,[1 \mp (k-1)\,(V/a)] + (U/V)\{[(k-1)/2]\,(V/a) \mp 1\}\,(d\delta_{10}/d\xi) - (a/V)\,(d\delta_{01}/d\xi)\{[(k-1)/2](V/a)\}(d\delta_{13}/d\xi) - [q_w(k-1)/\bar{\rho}aV^2]\right) \quad (6)$$

Expressing all parameters in Eqs. (1), (2), and (6) as $r = r^\circ + \epsilon_r$, $V = V^\circ + \epsilon_V$ etc., where $\epsilon_r \ll r^\circ$, $\epsilon_V \ll V^\circ$ etc., and changing variables: $\xi = U^\circ t - x$ and $\tau = t$, we get

$$\frac{\partial\{\epsilon_r - [a^\circ\epsilon_S/2(k-1)C_p]\}}{\partial\alpha} \equiv \frac{\partial\left(\epsilon_r - \{a^\circ\epsilon_S/[2(k-1)c_p]\}\right)}{\partial\tau} + (U^\circ - V^\circ - a^\circ)\,\frac{\partial\left(\epsilon_r - \{a^\circ\epsilon_S/[2(k-1)c_p]\}\right)}{\partial\xi} = F_1(\xi)$$

$$\frac{\partial\left(\epsilon_s - \{a^\circ\epsilon_S/[2(k-1)c_p]\}\right)}{\partial\beta} \equiv \frac{\partial\left(\epsilon_s - \{a^\circ\epsilon_S/[2(k-1)c_p]\}\right)}{\partial\tau} + (U^\circ - V^\circ + a^\circ)\,\frac{\partial\left(\epsilon_s - \{a^\circ\epsilon_S/[2(k-1)c_p]\}\right)}{\partial\xi} = F_2(\xi)$$

These equations give two families of straight α and β characteristics; viz.,

$$x = (V^\circ + a^\circ)t + x_{0\alpha}, \quad x = (V^\circ - a^\circ)t + x_{0\beta} \quad (7)$$

Along every characteristic of these families we have the following relations:

$$\epsilon_r - \{a^\circ/[2(k-1)]\}\,(\epsilon_S/c_p) = [1/(U^\circ - V^\circ - a^\circ)]\int_0^{\xi_\alpha} F_1(\xi)d\xi + C_\alpha(x_{0\alpha}) \equiv \Phi(\xi_\alpha) + C_\alpha \quad (8)$$

$$\epsilon_s - [a^\circ/2(k-1)]\,(\epsilon_S/c_p) = [1/(U^\circ - V^\circ + a^\circ)]\times \int_0^{\xi_\beta} F_2(\xi)d\xi + C_\beta\,(X_{0\beta}) \equiv \psi(\xi_\beta) + C_\beta \quad (9)$$

Using the conservation laws of mechanics along the shock wave and after development in a Maclaurin's series, we have[3]

$$\epsilon_r = K(U^\circ)\epsilon_U, \quad \epsilon_s = H(U^\circ)\epsilon_U, \quad \epsilon_S/c_p = E(U^\circ)\epsilon_U \quad (10)$$

Applying Eqs. (8) and (9) to points on shock line and taking into account that for $\xi_\alpha = 0$ $\Phi(\xi_\alpha) = 0$, and for $\xi_\beta = 0$ $\psi(\xi_\beta) = 0$, we get

$$P\epsilon_U \equiv \{K - [E/2(k-1)]\}\,\epsilon_U = C_\alpha(x_{0\alpha}) \quad (11)$$

$$R\epsilon_U \equiv \{H - [E/2(k-1)]\}\,\epsilon_U = C_\beta(x_{0\beta}) \quad (12)$$

where $P/R = C_\alpha/C_\beta > 0$. We arbitrarily choose point C on the contact line ($x = V^\circ t$). For points A and C (they lie on the same characteristic α), we have (Fig. 2) $C_{\alpha A} = C_{\alpha C}$, and similar for B and C: $C_{\beta B} = C_{\beta C}$.

For point $C(\xi_{\alpha C} \gg \xi_{\beta C})$ we have from Eqs. (8), (9), (11), and (12)

$$\epsilon_{VC} = \epsilon_{rC} - \epsilon_{sC} = \Phi(\epsilon_{\alpha,C}) - \psi(\xi_{\beta C}) + C_{\alpha C}(X_{0\alpha}) - C_{\beta C}(X_{0\beta}) \equiv \Omega(\xi_C) + P\epsilon_{UA} - R\epsilon_{UB} \quad (13)$$

In accordance with Eqs. (6), (8), and (9), calculations on the basis of reference 4 give* $\Omega(\xi_C) = \Phi(\xi_{\alpha C}) - \psi(\xi_{\beta C}) > 0$ and $d\Omega/d\xi > 0$ for $\xi_C > 0$. Taking the derivative in the direction of contact line, we get, after simple geometrical considerations,

$$D\epsilon_V/Dt = (U^\circ - V^\circ)\,(d\Omega/d\xi) + P(d\epsilon_U/d\gamma)_A\,[a^\circ/(V^\circ + a^\circ - U^\circ)]\sqrt{(a_0^2 - V^{\circ 2})/[a_0^2 - (V^\circ + a^\circ)^2]} - R[a^\circ/(U^\circ - V^\circ + a^\circ)]\sqrt{(a_0^2 + V^{\circ 2})/[a_0^2 + (V^\circ + a^\circ)^2]}\,(d\epsilon_U/d\gamma)_B \quad (14)$$

where γ is an element of arc measured along the shock line.

If we assume zero acceleration of the contact surface, $D\epsilon_V/Dt = 0$, we see [since $(U^\circ - V^\circ)\,(d\Omega/d\xi) > 0$] by the assumption that ϵ_U is a monotonic function of γ that $d\epsilon_U/d\gamma < 0$. Conversely, if we take $d\epsilon_U/d\gamma = 0$, we get a positive value of $D\epsilon_V/Dt$.

For certain values of $d\epsilon_U/d\gamma < 0$, we can then have positive values of $D\epsilon_V/Dt$, which means that the contact surface can be accelerated by attenuated shock wave. The value $d\Omega/d\xi$ is larger for a turbulent boundary layer than for a laminar one. Transition from laminar to turbulent flow in the boundary layer has the tendency to increase acceleration of the contact surface.

To obtain the value of ϵ_U or ϵ_V, it is necessary to take into consideration gas motion on the left side of the contact surface. Because of the nonsteady boundary layer in the rarefaction wave region and for partially hot and cold boundary layers it is more complicated.

* For a turbulent boundary layer, this value is greater than for a laminar one.

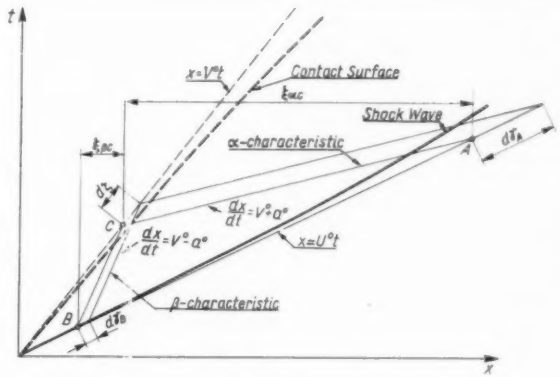

FIG. 2.

REFERENCES

[1] Glass, I., and Patterson, G. N., *Theoretical and Experimental Study of Shock-Tube Flows*, Journal of the Aeronautical Sciences, Vol. 22, No 2, pp. 73–100, February, 1955.

[2] Rudinger, G., *Wave Diagrams for Nonsteady Flow in Ducts;* D. Van Nostrand Co., Princeton, N.J., 1955.

[3] Rosciszewski, J., *Propagation of Shock Wave in Ducts of Nonuniform Cross-Section*, Ph.D. thesis, to be published.

[4] Mirels, H., *The Wall Boundary Layer Behind A Moving Shock Wave*, Symposium on Boundary Layer Research, edited by H. Görtler; Springer Verlag, Berlin, 1958.

Hydraulic Analogy for Two-Dimensional and One-Dimensional Flows

W. H. T. Loh
Chance Vought Aircraft, Inc., Dallas, Texas

December 24, 1958

SYMBOLS

a	=	local speed of sound
C_P	=	specific heat at constant pressure
C_V	=	specific heat at constant volume
C	=	constant or wave propagation speed
g	=	gravitational constant
h	=	local water depth
K	=	ratio of specific heats = C_P/C_V
l	=	some characteristic length
n	=	exponent in relation $z = C\,y^n$
p	=	local pressure
t	=	time or some characteristic time
T	=	local temperature
u	=	local velocity in x direction

x, y, z = rectangular coordinates, x in flow direction, y in vertical direction, and z in horizontal direction
ρ = local density
ξ = a function of x, which represents the displacement of the plane disturbed by the wave motion

Subscripts and Superscript

a = air flow
w = water flow
o = undisturbed condition or the initial equilibrium condition.
$'$ = prime is used to represent the nondimensional quantity of the parameter; such as $\rho' = \rho/\rho_0$, $p' = p/p_0$ etc., except u', t', x' are defined as u/a_0 or u/c_0, t/t_a or t/t_w, x/l_a or x/l_w, respectively.

THE ANALOGY comes from similarities of the basic flow equations. In two-dimensional steady flow, the equations of continuity, momentum, and energy were found by many authors (e.g., see references 1–4) to be identical in mathematical forms for irrotational flow of an isentropic perfect gas of specific-heat ratio 2.0 and flow of incompressible frictionless water in an open horizontal channel of rectangular cross section. They are

	Gas Flow	Water Flow
Continuity:	$u'(\partial\rho'/\partial x') + \rho'(\partial u'/\partial x') + v'(\partial\rho'/\partial y') + \rho'(\partial v'/\partial y') = 0$	$u'(\partial h'/\partial x') + h'(\partial u'/\partial x') + v'(\partial h'/\partial y') + h'(\partial v'/\partial y') = 0$
Momentum:	$u'(\partial u'/\partial x') + v'(\partial v'/\partial x') = -[1/(K-1)] \times (\partial p'^{[(K-1)/K]}/\partial x')$	$u'(\partial u'/\partial x') + v'(\partial v'/\partial x') = -(\partial h'/\partial x')$
	$u'(\partial u'/\partial y') + v'(\partial v'/\partial y') = -[1/(K-1)] \times (\partial p'^{[(K-1)/K]}/\partial y')$	$u'(\partial u'/\partial y') + v'(\partial v'/\partial y') = -(\partial h'/\partial y')$
Energy:	$u^2/u_{max}^2 = 1 - (T/T_0)$	$u^2/u_{max}^2 = 1 - (h/h_0)$

Comparison of the corresponding equations shows the following analogous terms:

Gas Flow			Water Flow	
Density ratio	$\rho'\ (=\rho/\rho_0)$	=	Water depth ratio	$h'\ (=h/h_0)$
Pressure ratio	$p'^{[(K-1)/K]}\ (=p^{[(K-1)/K]}/p_0)$	=	Water depth ratio	$h'\ (=h/h_0)$
Temperature ratio	$T'\ (=T/T_0)$	=	Water depth ratio	$h'\ (=h/h_0)$
Velocity of sound	$a\ [=\sqrt{K(p/\rho)}]$	$\sim$	Wave velocity	$C\ (=\sqrt{gh})$
Mach Number	$u'\ (=u/a_0)$	=	Froude Number	$u'\ (=u/C_0)$

The condition which must be satisfied by the momentum equation is

$$1/(K-1) = 1$$

The last condition requires that the water flow can only be comparable to the flow of a fictitious gas having a ratio of specific heats $K = 2.0$.* Although there is no such gas found in nature, the hydraulic analogy has been found very useful in a qualitative manner for the study of two-dimensional subsonic and supersonic flows.

Instead of using two-dimensional flow equations, the one-dimensional unsteady flow equations were examined early in 1944 by the writer, under the guidance of Prof. E. S. Taylor of M.I.T., and the results were reported later in reference 5. It was found then that they are identical in mathematical forms for a flow of an irrotational isentropic perfect gas of specific-heat ratio of any value, say K, and a flow of an incompressible frictionless water in an open horizontal channel of a cross section described by the expression $z = Cy^n$.

Similar results were also obtained independently at a later date by Probstein and Hudson.[5] Shapiro described literally the writer's results in references 7 and 8 and gave the writer's work as the reference in reference 8. Following the writer's early approach in one-dimensional unsteady flow, Szebehely and Whicker generalized the hydraulic-analogy analysis to apply to the external steady-flow case.[9] For internal flows, Schweitzer applied the writer's findings to a research study in exhaust dynamics in references 10 and 11. References 9, 10, and 11 all mentioned the writer's work and listed it in their references. Although the work has been drawn or applied by several authors, it has never been published. It is the suggestion of W. R. Sears that a Readers' Forum note be written to publish these equations for people who are interested in the one-dimensional unsteady-flow hydraulic analogy. Therefore, these equations are being summarized here:

	Gas Flow	Water Flow
Continuity:	$u'(\partial\rho'/\partial x') + \rho'(\partial u'/\partial x') + (l_c/a_0t_a)(\partial\rho'/\partial t') = 0$	$u'(\partial h'^{n+1}/\partial x') + h'^{n+1}(\partial u'/\partial x') + [l_w/\sqrt{gh_0/(n+1)}\ t_w](\partial h'^{n+1}/\partial t') = 0$
Momentum:	$(\partial u'/\partial t') + (a_0t_a/l_a)u'(\partial u'/\partial x') = -(a_0t_a/l_a) \times [1/(K-1)](\partial p'^{[(K-1)/K]}/\partial x')$	$(\partial u'/\partial t') + [\sqrt{gh_0/(n+1)}t_w/l_w]\ u'(\partial u'/\partial x') = -[\sqrt{gh_0/(n+1)}t_w/l_w](n+1)(\partial h'/\partial x')$
Energy:	$(\partial T'/\partial t') + (a_0t_a/l_a)u'(\partial T'/\partial x') + (K-1)p'[\partial(1/\rho')/\partial t'] + (K-1)(a_0t_0/l_a)p'u'[\partial(1/\rho')/\partial x'] = 0$	$(\partial h'/\partial t') + [\sqrt{gh_0/(n+1)}t_w/l_w]u'(\partial h'/\partial x') + [1/(n+1)]h'^{n+2}[\partial(1/h'^{n+1})/\partial t'] + [1/(n+1)] \times [\sqrt{gh_0/(n+1)}t_w/l_w]h'^{n+2}\ u'[\partial(1/h'^{n+1})/\partial x'] = 0$

Wave equations, shown below, naturally will follow the similarities of the basic equations of continuity, momentum, and energy. However, for those who are interested in one-dimensional longitudinal plane waves traveling in a duct (for gas) or in a channel (for water) these results might as well be added here for easy reference:

Gas Flow	Water Flow
$\partial^2\xi/\partial t^2 = -(1/K)a_0^2(\partial/\partial x)\ [(p/p_0) - 1]$	$\partial^2\xi/\partial t^2 = -[(n+1)/(n+2)]\ [gh_0/(n+1)] \times (\partial/\partial x)[(h/h_0)^{n+2} - 1]$
$\partial^2\xi/\partial t^2 = a_0^2(\partial^2\xi/\partial x^2)$	$\partial^2\xi/\partial t^2 = [gh_0/(n+1)]\ (\partial^2\xi/\partial x^2)$
$(\partial^2/\partial t^2)\ [(p/p_0) - 1] = a_0^2(\partial^2/\partial x^2)\ [(p/p_0) - 1]$	$(\partial^2/\partial t^2)\ [(h/h_0)^{n+2} - 1] = [gh_0/(n+1)] \times (\partial^2/\partial x^2)[(h/h_0)^{n+2} - 1]$
$(\partial^2/\partial t^2)\ [(\rho/\rho_0) - 1] = a_0^2(\partial^2/\partial x^2)\ [(\rho/\rho_0) - 1]$	$(\partial^2/\partial t^2)\ [(h/h_0)^{n+1} - 1] = [gh_0/(n+1)] \times (\partial^2/\partial x^2)\ [(h/h_0)^{n+1} - 1]$

* Similar results hold for two-dimensional unsteady flows.

The corresponding expressions for velocity of sound in gas and velocity of propagation of long gravity waves in water are as follows:

$$a = \sqrt{K(p/\rho)} = \sqrt{KRT} \qquad C = \sqrt{gh/(n+1)}$$
$$a_0 = \sqrt{K(p_0/\rho_0)} = \sqrt{KRT_0} \qquad C_0 = \sqrt{gh_0/(n+1)}$$

Comparison of these equations shows the following analogous terms:

Gas Flow		Water Flow
Local speed of sound		Local speed of wave propagation
$a = \sqrt{KRT}$	$\sim$	$C = \sqrt{gh/(n+1)}$
Local Mach Number		Local Froude Number
$M = u/a$	=	$M = u/c$
Local density ratio		Local water depth ratio
(ρ/ρ_0)	=	$(h/h_0)^{n+1}$
Local pressure ratio		Local water depth ratio
(p/p_0)	=	$(h/h_0)^{n+2}$
Local temperature ratio		Local water depth ratio
(T/T_0)	=	(h/h_0)
Flow analogous number		Flow analogous number
$(a_0 l_a/l_a)$	=	$[\sqrt{gh_0/(n+1)}\,t_w/l_w]$
Function of gas specific heat ratio		Function of channel cross-sectional exponent
$[1/(K-1)]$	=	$(n+1)$

The last condition is the one the water channel must possess in order to represent a gas flow of desired specific-heat ratio K.

For ordinary gasdynamics problems, the following cross sections are useful:

(1) Parabolic	$n = 1.5$	$K = 1.4$
(2) Triangular	$n = 1.0$	$K = 1.5$
(3) Rectangular	$n = 0$	$K = 2.0$

The velocity in a water channel can be made as small as one thousandth or less of that occurring in a gas stream, according to the analogous relationship

$$\text{Velocity of sound} = \sqrt{K(P/\rho)} \sim \text{Wave velocity} = \sqrt{gh/(n+1)}$$

The time scale can correspondingly be lengthened. This makes the hydraulic analogy a relatively easy way to observe and study transient effects in gasdynamics. The slow motion can even be seen by the human eye. This feature is particularly useful for the study of unsteady flow in ducts.

References

[1] Preiswerk, E., *Application of the Methods of Gas Dynamics to Water Flows With Free Surfaces*, NACA TM-934 and 935.

[2] Ippen, A. T., and Knapp, R. T., *Study of High Velocity Flow in Curved Channels of Rectangular Crossection*, Trans. Amer. Geoph. Union, 1936.

[3] Riabouchinsky, D., *Sur l'Analogie Hydraulique des Mouvements d'un Fluide Compressible*, Compt. Rend. de l'Acad. des Sciences, 195, 998–999, 1932.

[4] von Kármán, T., *Eine praktische Anwendung der Analogie zwischen Überschallströmung in Gasen und uberkritescher Strömung in offenen Gerinnen*, ZAMM, pp. 49–56, January 18, 1938.

[5] Loh, W. H. T., *A Study of the Dynamics of the Induction and Exhaust Systems of a Four Stroke Engine by a Hydraulic Analogy*, ScD. Thesis, M.I.T., 1946.

[6] Probstein, R. F., and Hudson, G. E., *A Water Analogue of the Isentropic Flow of Compressible Gases Which Have Arbitrary Ratios of Specific Heats*, Project SQUID Report No. NYU-20-R, August, 1948.

[7] Shapiro, A. H., and Malavard, L., *Analogue Methods in Physical Measurements in Gas Dynamics and Combustion*, "High Speed Aerodynamics and Jet Propulsion," Vol. IX, pp. 309–321, Princeton University Press, 1954.

[8] Shapiro, A. H., *An Appraisal of the Hydraulic Analogue to Gas Dynamics*, Massachusetts Institute of Technology Meteor Report 34, 1949.

[9] Szebehely, V. G., and Whicker, L. F., *Generalization and Improvement of the Hydraulic Analogy*, pp. 893–901, Proc. 1st U.S. Nat'l. Congress Applied Mech. (1951), Edwards Brothers, Inc., Ann Arbor, 1952.

[10] Schweitzer, P. H., *Research In Exhaust Manifolds*, Trans. ASME, Vol. 74, No. 4, pp. 517–528, May, 1952.

[11] Schweitzer, P. H., and Tsu, T. C., *Improving Engine Performance by Exhaust Pipe Tuning*, ONR Report, 1951.

Equations for Thin Toroidal Shells

T. Au

Associate Professor of Civil Engineering, Carnegie Institute of Technology, Pittsburgh, Pa.

January 6, 1959

Symbols

- ϕ = angle between the axis of revolution and the normal to middle surface at a point of the shell, measured along the meridian
- r_m = radius of curvature of the meridian
- r_c = circumferential radius
- A = angle through which the tangent to a meridian at a point of the shell rotates during the deformation
- U = product of meridional shear and circumferential radius
- E = Young's modulus of elasticity
- μ = Poisson' ratio
- t = thickness of the shell
- D = flexural rigidity, $Et^3/12(1-\mu^2)$
- P = uniform internal pressure
- K = meridional radius of the toroidal knuckle in Fig. 1
- λ = a dimensionless ratio, such that λK is the distance from the axis of revolution to the center of the generating circle of the toroidal knuckle in Fig. 1

IN THE ANALYSIS of thin elastic shells of revolution having constant radius of curvature along the meridian, the fundamental equations of equilibrium and deformation based on Love-Meissner's assumptions can be reduced to two simultaneous differential equations of second order. With notations given and the Meissner differential operator $L(x)$ for any variable x defined as:

$$L(x) = (d/d\phi)\,[(r_c \sin\phi)\,(dx/d\phi)/r_m]/r_m \sin\phi - (x\cot^2\phi)/r_c$$

the system of equations for case of shells of constant thickness can be expressed as follows:[1]

$$L(A) - \mu A/r_m = U/D \tag{1a}$$

$$L(U) + \mu U/r_m = -EtA + f(\phi) \tag{1b}$$

in which $f(\phi)$ depends only on the shape of the shell and the magnitude of the load.

The first-order terms in Eqs. (1a) and (1b) can be eliminated by the introduction of two new variables. In the cases of conical and spherical shells, such reduction leads to rather simple results.[2] For the portion of a toroidal shell which serves as the knuckle of a toriconical or torispherical head of a pressure vessel, similar results can be obtained.

Referring to the torodial shell in Fig. 1, which has constant

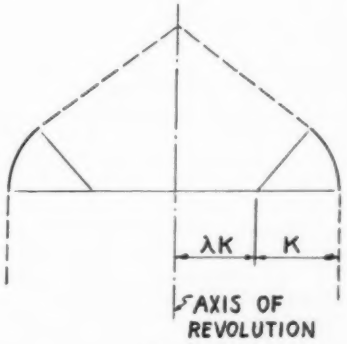

FIG. 1.

meridional radius and thickness, and is subjected to uniform internal pressure, Eqs. (1a) and (1b) become

$$L(A) - \mu A/K = U/D \tag{2a}$$

$$L(U) + \mu U/K = -EtA + f(\phi) \tag{2b}$$

for which

$$L(x) = [(d^2x/d\phi^2)(1 + \lambda \csc \phi) + (dx/d\phi)(\cot \phi) - x(\cot \phi \cos \phi)/(\lambda + \sin \phi)]/K$$

and

$$f(\phi) = \lambda PK(\cos \phi)(\lambda + \sin \phi)(\sin \phi - 2\lambda)/2 \sin^4 \phi$$

By introducing two variables η and ζ which are related to A and U respectively, as follows:

$$\eta = (AD/K^2)(\lambda + \sin \phi)^{1/2}$$
$$\zeta = (U/K)(\lambda + \sin \phi)^{1/2}$$

Eqs. (2) can be reduced to

$$[a(\phi)](d^2\eta/d\phi^2) - [b(\phi) + \mu]\eta = \zeta \tag{3a}$$

$$[a(\phi)](d^2\zeta/d\phi^2) - [b(\phi) - \mu]\zeta = c(\phi) - 12(1 - \mu^2)(K/t)^2 \eta \tag{3b}$$

in which

$$a(\phi) = 1 + \lambda \csc \phi$$
$$b(\phi) = [a(\phi)/4(\lambda + \sin \phi)^2](3 - 2\lambda \sin \phi - 5 \sin^2 \phi)$$
$$c(\phi) = [f(\phi)](\lambda + \sin \phi)^{1/2}$$

Numerical solution of Eqs. (3a) and (3b) can readily be obtained by finite difference method for given boundary conditions.

References

[1] Pöschl, T., *Berechnung von Behältern*, p. 63, Julius Springer, Berlin, 1926.

[2] Pasternak, P., *Die praktische Berechnung biegefester Kugelschalen, kreisrunder Fundamentplatten auf elastischer Bettung und kreiszylindrischer Wandungen in gegenseitiger monolither Verbindung*, Zeit. Mathematik und Mechanik, Vol. 6, p. 1, 1926.

Reduction of Strain Rosettes in the Plastic Range

C. S. Ades

Head of Structures Development, Airframe Equipment Section, Bendix Products Division, Bendix Aviation Corporation, South Bend, Ind.

January 12, 1959

ALTHOUGH much has been written on the reduction of strain rosettes, the writer has never known a method which applies in both the elastic and plastic ranges of the material. The following is offered as a solution to this problem. Since the calculations involved can get rather lengthy, the method is set up so that it can be readily programed for a digital computer.

The method makes use of what is often called the deformation theory.[1] The maximum and minimum principal strains are determined from the gage readings, as usual. Since we are involved with a biaxial strain condition, an equivalent intensity of strain, e_i, is determined by substituting the principal strains into an equation derived by use of the distortion energy principle. The corresponding intensity of stress, σ_i, is determined from the stress-strain curve for the material, and the modulus is taken equal to σ_i/e_i. Obviously, if σ_i and e_i are within the proportional limit of the material, their ratio will be the initial or Young's modulus, while, if they are above the proportional limit, their ratio will be the secant modulus. Whichever is obtained, however, is used in the equations for determining the principal stresses. The equations and steps necessary to reduce the gage readings to principal stresses are given below.

Let us assume that R_1, R_2, and R_3 are the three gage readings obtained from an SR-4 rectangular rosette strain gage. The corrected strains are given by the following:

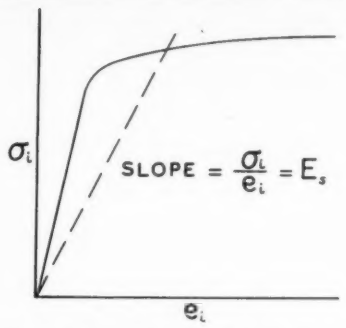

FIG. 1. Illustration showing typical stress-strain curve and method of obtaining secant modulus, E_s.

$$\epsilon_1 = R_1 - (1/b)R_2$$
$$\epsilon_2 = 1.02R_2 - (1/b)(R_1 + R_3)$$
$$\epsilon_3 = R_3 - (1/b)R_1$$

The correction factor b is furnished with the gages. The principal strains are determined from the following:[2]

$$A = (\epsilon_1 + \epsilon_3)/2, \quad B = 1/2\sqrt{(\epsilon_1 - \epsilon_3)^2 + (2\epsilon_2 - \epsilon_1 - \epsilon_3)^2},$$
$$\epsilon_{max} = A + B, \quad \epsilon_{min} = A - B$$

The angle that ϵ_{max} makes with R_1 is given by the following:

$$\tan 2\phi = (2\epsilon_2 - \epsilon_1 - \epsilon_3)/(\epsilon_1 - \epsilon_3)$$

When positive, the angle is measured clockwise from R_1. The intensity of strain is then computed by the use of the following:

$$e_i = (1/1 - \mu^2) \times \sqrt{(1 - \mu + \mu^2)(\epsilon_{max}^2 + \epsilon_{min}^2 - \epsilon_{max}\epsilon_{min}) + 3\mu\epsilon_{max}\epsilon_{min}}$$

This equation is the same as that used in the deformation theory, except that Poisson's ratio, μ, is left in it as a variable and not taken equal to 1/2, the value generally used in the plastic range. As a first assumption, let $\mu = \mu_{PL}$, the elastic range value of μ. If $e_i \leq \epsilon_{PL}$, the proportional limit strain, then the values for μ and e_i are correct; but, if $e_i > \epsilon_{PL}$, a new value for μ, as follows, is computed.[3]

$$\mu = \{1 - [(1 + \delta)/(1 + e_i)]^{1/2}\}/e_i$$

where

$$\delta = (1 + \epsilon_{PL})(1 - \mu_{PL}\epsilon_{PL})^2 - 1$$

Since the values of μ and e_i are assumed interdependent, the calculation of each must be repeated until sufficient accuracy is obtained. The writer knows of no definite proof that the value of μ is dependent only on the intensity of strain, but it appears to be as good an assumption as can be made at the present time. Also, it is consistent with the philosophy that the plastic condition is determined by the value of e_i. Once we have the value of e_i, the modulus can be obtained from the stress-strain curve, as shown in Fig. 1.

In accordance with the deformation theory but still considering μ variable, the equations for the principal stresses are as follows:

$$\sigma_{max} = E_s(\epsilon_{max} + \mu\epsilon_{min})/(1 - \mu^2)$$
$$\sigma_{min} = E_s(\epsilon_{min} + \mu\epsilon_{max})/(1 - \mu^2)$$

Substituting in these the values given above for ϵ_{max} and ϵ_{min}, we arrive at the equations for determining the maximum and the minimum stresses:

$$A'' = AE_s/(1 - \mu), \quad B'' = BE_s/(1 + \mu)$$
$$\sigma_{max} = A'' + B''$$
$$\sigma_{min} = A'' - B''$$
$$\tau_{max} = \text{maximum shear stress} = (\sigma_{max} - \sigma_{min})/2$$

Once the computer program is prepared, the following information must be read into the computer in order to obtain a solution: R_1, R_2, R_3, b, μ_{PL}, ϵ_{PL}, and the stress-strain curve for the material. The information read out should include the value of σ_i. Experi-

ments, particularly on ductile materials, have shown that this value is more significant than the principal stresses in determining the state of stress acting at a point in a body.

REFERENCES

[1] Stowell, E. Z., *A Unified Theory of Plastic Buckling of Columns and Plates*, NACA Report No. 898, 1948.

[2] Hetényi, M., *Handbook of Experimental Stress Analysis*, pp. 390–437; John Wiley and Sons, Inc., New York, 1954.

[3] Stang, A. H., Greenspan, M., and Newman, S. B., *Poisson's Ratio of Some Structural Alloys for Large Strains*, J. Res., U.S. National Bureau of Standards, Vol. 37, pp. 211–221, October, 1946.

Errata—"On the Generalized Prandtl Relation"

S. M. Ramachandra

Lecturer, Department of Aeronautical Engineering, Indian Institute of Science, Bangalore, India

January 14, 1959

PERMIT ME to point out an error which appeared in the above-mentioned Readers' Forum note by Prof. Rudi S. Ong, page 209, in the March, 1958, issue of this journal.

The Eqs. (5) in the note should read

$$n_t = (\partial\phi/\partial t)/[(\partial\phi/\partial t)^2 + g^{\lambda\mu}(\partial\phi/\partial x^\lambda)(\partial\phi/\partial x^\mu)]^{1/2}$$

$$n_\lambda = (\partial\phi/\partial x^\lambda)/[(\partial\phi/\partial t)^2 + g^{\lambda\mu}(\partial\phi/\partial x^\lambda)(\partial\phi/\partial x^\mu)]^{1/2}$$

The equation preceding Eq. (9) on page 210 should read

$$[(\partial\phi/\partial t) + (\partial\phi/\partial x^\mu)v_1{}^\mu]\rho_1\bar{\nu}_\lambda + c^2\bar{\rho}(\partial\phi/\partial x^\lambda) = 0$$

instead of

$$\rho_1\bar{\nu}_\lambda[(\partial\phi/\partial t) + v_1{}^\mu(\partial\phi/\partial x^\mu) + c^2\bar{\rho}(\partial\phi/\partial x^\lambda)] = 0$$

The Yield Strength of Beams in Pure Bending

Robert M. Rivello

Associate Professor of Aeronautical Engineering, University of Maryland, College Park, Md.

January 13, 1959

IN THE ANALYSIS of beams subjected to pure bending, the classical assumption that plane sections remain plane is usually retained even though the stresses exceed the proportional limit of the material.[1] Such an assumption leads to a linear strain distribution for an initially straight beam. In the design of aircraft structures, specifications usually require that the stresses within the structure shall not exceed the yield stress when it is subjected to limit loads. The maximum strain for this case is equal to $0.002 + \sigma_y/E$ (Fig. 1) and the assumption of a linear

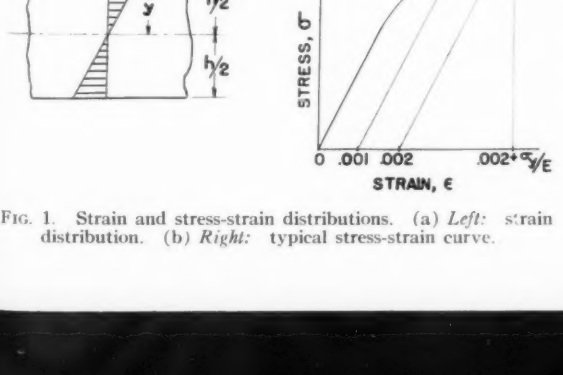

FIG. 1. Strain and stress-strain distributions. (a) *Left:* strain distribution. (b) *Right:* typical stress-strain curve.

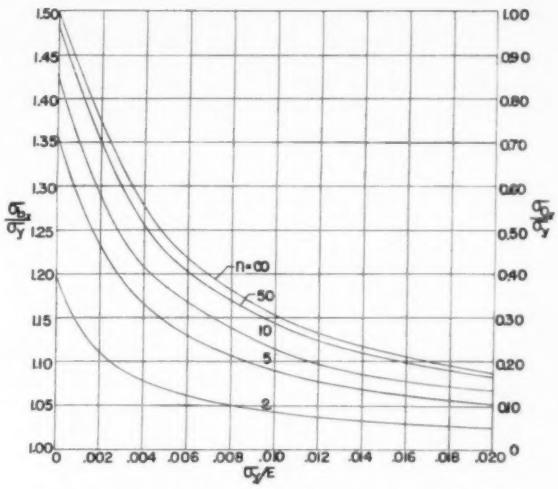

FIG. 2. Variation of σ_{by}/σ_y and σ_{oy}/σ_y with n and σ_y/E.

strain distribution then leads to the result

$$\epsilon = [0.002 + (\sigma_y/E)]2y/h \tag{1}$$

The bending stress for any fiber may be found from the stress-strain curve for the corresponding strain at the fiber.

The bending stresses are related to the applied bending moment by the equilibrium condition

$$M = \int_A \sigma y dA \tag{2}$$

where the integral extends over the area of the cross section. It is customary to solve Eq. (2) by a numerical integration, using the actual stress-strain curve of the material. It is the purpose of this note to present a less time-consuming method for determining the yield strength of beams by using the Hill parameters[2] for the stress-strain curve in combination with the Cozzone method[3] for plastic bending.

For stresses up to and slightly beyond the yield stress, it is possible to accurately represent the stress-strain curve by the Hill equation[2]

$$\epsilon = (\sigma/E) + 0.002(\sigma/\sigma_y)^n \tag{3}$$

where n is a shape parameter of the stress-strain curve (see Fig. 1) given by

$$n = 0.301/\log(\sigma_y/\sigma_1) \tag{4}$$

By equating Eqs. (1) and (3), substituting into Eq. (2), and changing the variable of integration to stress, the following integral is obtained for the yield moment M_y of a rectangular beam of width b and height h

$$M_y = \{bh^2/2[0.002 + (\sigma_y/E)]^2\} \times \int_0^{\sigma_y} [(\sigma/E) + 0.002n(\sigma/\sigma_y)^n][(\sigma/E) + 0.002(\sigma/\sigma_y)^n]d\sigma \tag{5}$$

Integrating gives

$$M_y = \{bh^2/2[0.002 + (\sigma_y/E)]^2\}\{(\sigma_y{}^3/3E^2) + [0.002(n+1) \div (n+2)](\sigma_y{}^2/E) + [0.002^2n/(2n+1)]\sigma_y\} \tag{6}$$

The yield moment is related to the bending yield modulus by the defining equation for σ_{by}

$$M_y = \sigma_{by}I/c \tag{7}$$

where in this case c equals $h/2$.

Equating Eqs. (6) and (7) gives the following result for the rectangular beam:

$$\sigma_{by}/\sigma_y = \{3/[0.002 + (\sigma_y/E)]^2\}\{[0.002^2n/(2n+1)] + [0.002(n+1)/(n+2)](\sigma_y/E) + (1/3)(\sigma_y/E)^2\} \tag{8}$$

Eq. (8) is plotted in Fig. 2 for a range of the Hill parameters which should cover all practical problems.

Equations for the bending yield modulus become very complicated for cross sections other than rectangular if the Hill stress-strain relation is used with Eq. (2). A simple approximate solution for sections symmetrical about the axis normal to the plane of the bending moment may be obtained by using the Cozzone method for plastic bending.[3] Cozzone has shown that if a trapezoidal stress distribution having a minimum stress σ_0 and a maximum stress σ_m is substituted for the true distribution the moment of the stress distribution is given by

$$M = 2Q\sigma_0 + (I/c)(\sigma_m - \sigma_0) \tag{9}$$

and the bending modulus is then given by

$$\sigma_b = \sigma_m + \sigma_0[(2Qc/I) - 1] \tag{10}$$

The criteria for the selection of σ_0 is that the trapezoidal distribution shall produce the same moment as the true distribution on the actual cross section. Cozzone found, however, that the value of σ_0 determined for a rectangular cross section could be used for other sections with very little error.

Solving Eq. (9) for the case of a rectangular cross section with the maximum stress equal to the yield stress gives

$$\sigma_{0y}/\sigma_y = 2[(6M_y/bh^2\sigma_y) - 1] \tag{11}$$

where σ_{0y} is the value of σ_0 to be used for the bending yield modulus. By using Eqs. (6) and (8)

$$\sigma_{0y}/\sigma_y = 2[(\sigma_{by}/\sigma_y) - 1] \tag{12}$$

Eq. (12) is given in Fig. 2 where the right-hand margin applies. The following bending yield modulus is then found from Eq. (10) for sections symmetrical about an axis perpendicular to the plane of bending

$$\sigma_{by} = \sigma_y + \sigma_{0y}[(2Qc/I) - 1] \tag{13}$$

References

[1] Timoshenko, S. P., *Strength of Materials, Part II, Advanced Theory and Problems*, 2nd Ed., pp. 362–371; D. Van Nostrand Co., Inc., New York, 1941.

[2] Hill, H. N., *Determination of Stress-Strain Relations from "Offset" Yield Strength Values*, NACA TN 927, 1944.

[3] Cozzone, F. P., *Bending Strength in the Plastic Range*, Journal of the Aeronautical Sciences, Vol. 10, No. 5, pp. 137–151, May, 1943.

Accumulative Fatigue Damage Caused by Random Loading

H. C. Schjelderup

Design Specialist, Douglas Aircraft Company, Inc., Long Beach, Calif.

January 14, 1959

Symbols

N_1	= number of cycles of stress S_1 to failure, (an abscissa of the SN diagram)
N_g	= total number of cycles of stress for failure for fluctuating stress amplitude history
$\alpha_i = n_i/N_G$	= percentage of cycles of stress Si
S_1	= peak stress amplitude
S_i	= stress amplitude
$\bar{S}$	= the root mean square stress amplitude
d	= an exponent related to the material
$\sigma i = Si/\bar{S}$	= a dimensionless stress ratio
$P(\sigma)$	= the probability density distribution of peak stress amplitudes
$P_R(\sigma) = \sigma e^{-\sigma^2/2}$	= the Rayleigh distribution of peak stress amplitudes
$K = (1/\sigma_1)^d$	= a constant dependent upon the choice of peak stress S_1

THE PROBLEM of fatigue damage associated to structural vibrations caused by jet noise has been discussed by various authors.[1, 2, 3] All have based their analysis on Miner's hypothesis of cumulative fatigue damage and a Rayleigh[4] distribution of peaks. Differences in results have been mainly caused by treatment of the basic fatigue curve.

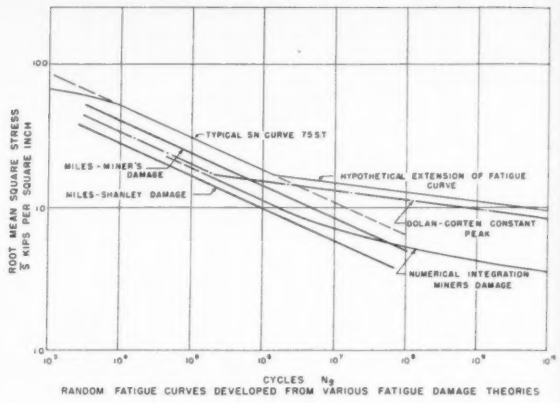

RANDOM FATIGUE CURVES DEVELOPED FROM VARIOUS FATIGUE DAMAGE THEORIES

FIG. 1.

Dolan and Corten[5] have hypothesized a refinement to the accumulative-damage concept which weighs the damage at various stress levels in terms of the peak stress [Eq. (1)]

$$N_g = \frac{N_1}{\sum_1^n \alpha_i (Si/S_1)^d} \tag{1}$$

Eq. (1) may be reformed in terms of the ratio of stress to root-mean-square stress as Eq. (2)

$$N_g = N_1/K\sum_1^n \alpha_i(\sigma_i)^d, \quad Si \leq S_1 \tag{2}$$

If the probability-density distribution of peak stress amplitudes is given by a function $P(\sigma)$ and noting $\alpha(\sigma) = P(\sigma)d\sigma$, Eq. (2) may be rewritten

$$N_g = (N_1/K)\left[1\Big/\int_0^{\sigma_1} P(\sigma)\sigma^d d\sigma\right] \tag{3}$$

This integration must be restricted to a finite peak value or the Dolan-Corten concept of damage is unusable. Then, regardless of the choice of $\bar{S}$, if a maximum peak value σ_1 is fixed and the probability distribution does not change, Eq. (3) will take the form

$$N_g = N_1/C \tag{4}$$

The implication of Eq. (4) is that the ratio of life of a structure undergoing random vibration to that undergoing sinusoidal vibration at a peak stress equal to the root-mean-square stress of the random vibration is constant.

Miles, on the other hand, showed, using Miner's damage theory, that for equivalent life, the ratio of sinusoidal to random stress is constant. However, if the experimental fatigue curve is used rather than the power approximation, this ratio becomes dependent upon the structural life.

Expressed graphically, the comparative results are shown in Fig. 1. Since the constants for Dolan-Corten accumulative-damage theory are unknown, the position of the curve expressed by Eq. (4) is arbitrary.

Of interest is the fact that if the power approximation to the fatigue curve is used, then the Dolan-Corten hypothesis of damage yields identical results to hypothesis of Miner or Shanley, dependent upon the choice of peak factor. On the other hand, if the experimental fatigue curve is followed, the Dolan-Corten theory yields results that contradict the numerical application of Miner's theory. This difference is attributed partially to the choice of a constant peak factor.

A conclusion would be that the simple application of the Dolan-Corten hypothesis of cumulative-fatigue damage to the random vibration problem is not sufficient, and a statistical consideration of the most probable peak must be included in order to yield more realistic results. For this reason one may become discouraged as to the possibility of improving the theoretical treat-

ment of the problem in the regime of fatigue damage and thus concentrate on experimental verification or development of the "random fatigue curve."

References

[1] Miles, John W., *On Structural Fatigue Under Random Loading*, Journal of the Aeronautical Sciences, Vol. 21, No. 11, pp. 753–762, November, 1954.

[2] Head, A. K., and Hooke, F. N., *Random Noise Fatigue Testing*, International Conference on the Fatigue of Metals, Session 3, Paper 9, London, September, 1956.

[3] Schjelderup, H. C., and Karnesky, A., *A Combined Analytical and Experimental Approach to AIF*, 25th Shock and Vibration Bulletin, Part II, December, 1957.

[4] Lord Rayleigh, *Theory of Sound*, 2nd Ed., Vol. 1, p. 40; Dover Publications, New York, 1954.

[5] Corten, H. T., and Dolan, T. J., *Cumulative Fatigue Damage*, International Conference on the Fatigue of Metals, Session 3, Paper 2, London, September, 1956.

On Hypersonic Similarity for Nozzles*

Martin H. Bloom

Professor of Aeronautical Engineering, Polytechnic Institute of Brooklyn, Freeport, N.Y.

January 20, 1959

Symbols

K = $M_\infty \tau$ or $\sqrt{M_\infty^2 - 1}\,\tau$
L = axial length from throat to test section
M_∞ = uniform test section Mach Number
R = test section radius
x = axial coordinate
y = radial or normal (top) coordinate
γ = ratio of specific heats
η = y/R, $\eta_w(\xi)$ value of η on solid surface
ξ = x/L
τ = ratio R/L

Subscripts

1 = the known flow
2 = the unknown flow to be determined by comparison with the known flow

It is of interest to note that Tsien's hypersonic similarity theory for potential flow[1] has a realm of applicability in two-dimensional and axially-symmetric nozzle flow. For this purpose, the result may be stated as follows:

For two nozzles with the same dimensionless contour $\eta_w(\xi)$ and the same K, the dimensionless perturbation variables are similar at corresponding points (same ξ, η), provided that the usual hypersonic similarity restrictions are met—that is, $\tau \ll 1$, $K = 0(1)$ at least, and equal values of γ. The Van Dyke extension to the supersonic regime follows the redefinition: $K = \sqrt{M_\infty^2 - 1}\,\tau$, and replacement of M_∞^2 by $M_\infty^2 - 1$ everywhere.

Although the similarity principle cannot be expected to be valid in the supersonic regime of either nozzle, this regime occupies a small part of the total length of a hypersonic nozzle. Approximately then, the ratio of length-to-test section diameter varies as the test Mach Number for hypersonic nozzles.

To determine the supersonic portion of the flow field accurately, the method of characteristics may be employed, continuing upstream from the hypersonic to the sonic region. However, it is especially straightforward to derive this part of the field if the known nozzle is started by means of a source flow[2,3] in which the flow properties are constant along circular arcs measured from a reference center. In this case, the Mach Number at the lower bound of the hypersonic region in the unknown nozzle may simply be matched to the equal value of a source flow whose solution can readily be obtained. The arc of a circle on which the Mach Number is constant in the known flow will remain a circular arc of constant (but different) Mach Number in the similar flow to the hypersonic approximation [see Eq. (1)].

Letting subscripts 1 and 2 denote the "known" and "unknown" flows to be related, within the hypersonic approximation at corresponding points:

$$M_1^2 - M_2^2 = M_{\infty 1}^2 - M_{\infty 2}^2 \qquad (1)$$

indicating that when $M_{\infty 1} > M_{\infty 2}$, $M_1 > M_2$. Thus, when $M_{\infty 1} > M_{\infty 2}$, the entire unknown hypersonic field lies within the corresponding hypersonic known field. When $M_{\infty 1} < M_{\infty 2}$, the known hypersonic field may correspond only to part of the unknown hypersonic field. As a result, it may not be possible to determine the remainder of the unknown hypersonic field by similarity laws. This is true particularly when $M_{\infty 1} \ll M_{\infty 2}$, since M_2 may be high while the corresponding M_1 already is low. On the other hand, when $M_{\infty 1} \gg M_{\infty 2}$, only a small portion of the known field corresponds to the entire unknown field; therefore, a high degree of accuracy in the known field may be required to produce satisfactory accuracy in the unknown field.

* This work was done in connection with USAF, AEDC Contract AF 40(600)-732.

References

[1] Tsien, H. S., *Similarity Laws of Hypersonic Flows*, J. Math. & Phys. Vol. 25, No. 3, pp. 247–251, 1946. Also, Shapiro, A. H., *Compressible Fluid Flow*, Vol. 2, p. 747; Ronald Press Co., New York, 1953.

[2] Cresci, R. J., *Tabulation of Coordinates for Hypersonic Axisymmetric Nozzles. Part I—Analysis and Coordinates for Test Section Mach Numbers of 8, 12 and 20*, WADC TN 58-300, AD 204 213, October, 1958.

[3] Landsbaum, E. M., *Contour Nozzles*, American Rocket Society, Preprint 734-58 (presented at ARS Annual Meeting, November, 1958).

Pressure Distributions for a Two-Dimensional Blunt-Nosed Body at Different Angles of Attack*

Antonio Ferri and Victor Zakkay

Professor of Aeronautical Engineering, and Research Associate, Respectively, Polytechnic Institute of Brooklyn, Freeport, N.Y.

January 15, 1959

The problem of the flow field in the region of the detached shock in hypersonic flow is of interest for practical applications. Most of the work performed until now on this problem has been related to the study of symmetrical boundary conditions. When the curvature of the body is nearly constant throughout the elliptic region, the Newtonian flow approximation is sufficiently accurate for practical applications. However, the shape of the body in the region of the sonic velocity has very large influence on all the flow field. An interesting experiment indicating the importance of the boundary conditions near the

* This research was supported by the U.S. Air Force through the Air Force Office of Scientific Research, Air Research and Development Command, under Contract AF 49(638)-217, Project No. 1750.

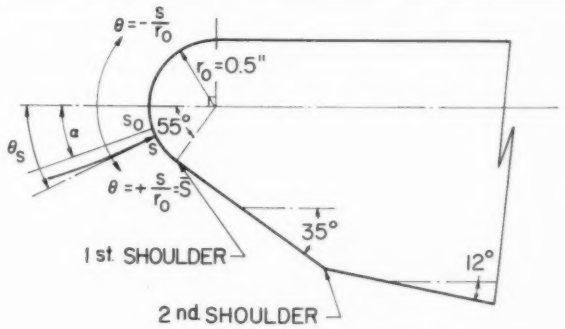

Fig. 1. Body geometry.

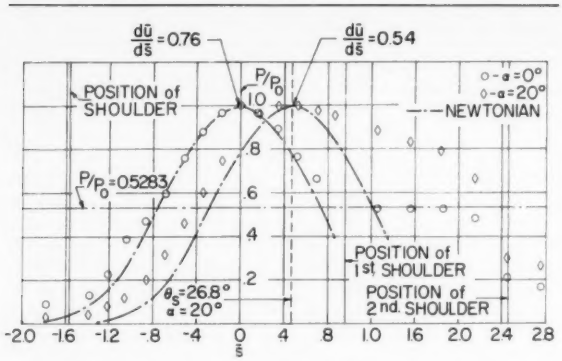

FIG. 2. Pressure distribution at $\alpha = 0°$ and 20°.

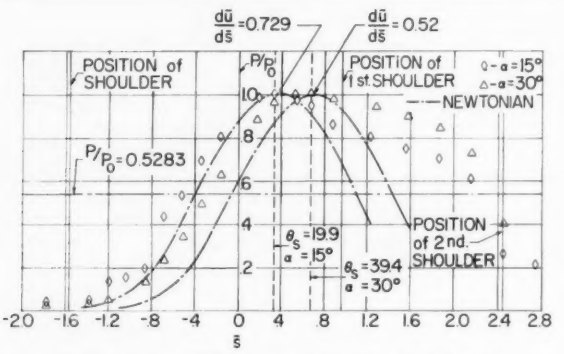

FIG. 3. Pressure distribution at $\alpha = 15°$ and 30°.

sonic line has been performed at the Polytechnic Institute of Brooklyn at Mach Number of 6.0. The detailed results of this investigation have been reported in references 1 and 2. In this note only, few of the more interesting points will be presented.

We consider a two dimensional body having a circular nose, as shown in Fig. 1. The circular part of the nose is extended for an angle of 145°; therefore, at appropriate values of the angle of attack of the body, it is possible to perform tests where the elliptic region is limited to the circular part of the body and the sonic points are on the circular part, or, it is possible to move one sonic point outside of the circular region. In the second case, the flow at the nose is not symmetrical, and the stagnation point is not on the radial line parallel to the free-stream direction. The flow at the nose has an antisymmetrical part which is equivalent to the presence of circulation.

Results of the measured pressure distribution for $\alpha = 0$ corresponding to the first case, and $\alpha = 15°$, 20°, and 30° corresponding to the second case, are shown in Figs. 2 and 3 and are compared with the modified Newtonian pressure distribution. The velocity gradient at the stagnation point for both cases is:

$$(d\bar{u}/d\bar{s})_{\alpha=30°} = 0.52, \quad (d\bar{u}/d\bar{s})_{\alpha=0} = 0.76$$

where $\bar{u} = u/\sqrt{\bar{h}_s}$, h_s = stagnation enthalpy, and $\bar{s} = s/r_0$.

This variation of stagnation velocity gradient corresponds to a reduction of heat transfer at the stagnation point of the order of 21 per cent[3] that could be obtained in a symmetrical Newtonian flow by increasing the radius of curvature of the order of 21 per cent.

REFERENCES

[1] Ferri, A., *A Review of Some Recent Developments in Hypersonic Flow*, WADC TN 58-230, September, 1958.

[2] Zakkay, V., and Fields, A., *Pressure Distribution on a Two-Dimensional Blunt-Nosed Body at Various Angles of Attack*, Polytechnic Institute of Brooklyn, PIBAL Report No. 461, October, 1958.

[3] Fay, J. A., and Riddell, F. R., *Theory of Stagnation Point Heat Transfer in Dissociated Air*, Journal of the Aeronautical Sciences, Vol. 25, No. 2, pp. 73–85, 121, February, 1958.

On the Continuity of the Schmidt Number at the Interface Between the Laminar Sublayer and the Outer Turbulent Region†

Nathan Ness*
Specialist, Missiles and Space Vehicles Department, General Electric Company, Philadelphia, Pa.
January 21, 1959

AN ACCEPTED METHOD for analyzing turbulent boundary layers and one which has provided useful results in the past is to divide the flow regime normal to the body surface into two regions—namely, into a laminar sublayer adjacent to the body surface and into a fully turbulent outer region. These two regions are tied together at their mutual interface by imposing continuity of the dependent variables, continuity of shear, continuity of energy transfer, and, in the case of diffusion processes, continuity of mass diffusion. It is then usually assumed that the laminar and turbulent Schmidt and Prandtl Numbers are constant and not necessarily equal respectively to each other.

It is the intent of this note to demonstrate that if a more rigorous analysis is imposed—that is, if the laminar Schmidt Number is permitted to vary through the sublayer—the magnitude of the turbulent Schmidt Number, still considered constant, cannot be arbitrarily assumed.

This conclusion was obtained during the analysis of the binary mixture turbulent boundary layer. The solution proceeded along the classical lines of dividing the flow regime into two regions, as mentioned above; analogies between skin friction and mass diffusion, and between skin friction and heat transfer were then derived by considering all variations of the dependent variables in the streamwise direction negligible. (The details are contained in reference 1).

Calculations were performed for the injection of helium into an air boundary layer. It has been shown[2] that, over a wide range of temperature (500°R. < T < 3,500°R.), the Schmidt Number may be considered a function of concentration only. For a helium-air mixture, the Schmidt Number-concentration dependence is closely approximated by the quadratic:[2]

$$Sc = \alpha_0 + \alpha_1 C_1 + \alpha_2 C_1^2 \qquad (1)$$

† Based on work performed under the auspices of the USAF Ballistic Missiles Division, Contract No. AF 04(645)-24.

* The author would like to acknowledge the helpful discussions with Dr. J. B. Fanucci and the assistance of Mrs. Gladys Smookler in performing the calculations.

Fig.1 VARIATION OF C_{1_a} WITH C_{1_w} FOR CONSTANT VALUES OF THE PARAMETER ζ

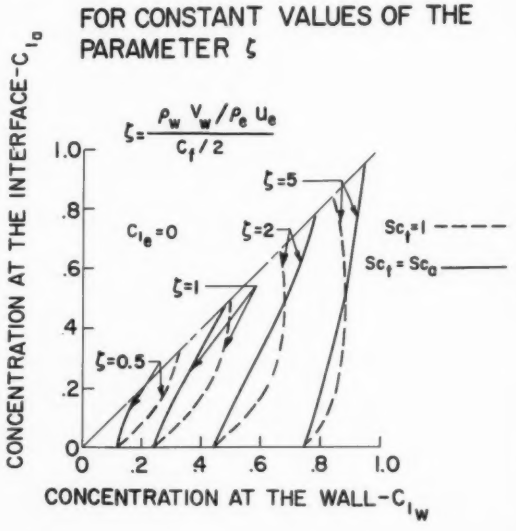

where Sc is the Schmidt Number in the laminar region, α_i (i = 0, 1, 2) are constants and $C_1 = \rho_1/\rho$ is the mass fraction of the injected specie; ρ is the density.

With the aid of Eq. (1), the conservation of specie equation in the laminar sublayer can be integrated in closed form to give the following relationship between the concentration and the velocity:[1]

$$1 + \zeta(u/u_e) = [(C_1 + A)/(C_{1w} + A)]^{\omega_1} \times [(C_1 + B)/(C_{1w} + B)]^{\omega_2} [(1 - C_1)/(1 - C_{1w})]^{\omega_3} \quad (2)$$

where $\zeta = (\rho_w v_w/\rho_e u_e)/(C_f/2)$; $\rho_w v_w$ is the mass flux at the wall, $\rho_e u_e$ is the mass flux at the outer edge of the boundary layer and C_f is the local skin-friction coefficient. A, B, and ω_i (i = 1, 2, 3) in Eq. (2) are constants dependent only on the coefficients α_i in Eq. (1); u is the convective velocity in the streamwise direction while v is the convective velocity normal to the body surface.

The conservation-of-specie equation in the turbulent region is also integrated in closed form assuming the turbulent Schmidt Number Sc_t constant. The relationship between the concentration and the velocity then is:[1]

$$(1 - \bar{C}_1)/(1 - C_{1a}) = [(1 + \zeta\bar{u}/u_e)/(1 + \zeta u_a/u_e)]^{Sc_t} \quad (3)$$

where the subscript a refers to the interface, and the bar over a symbol represents a time-averaged quantity.

Eqs. (2) and (3) may be combined, after the former is evaluated at the interface and the latter at the outer edge of the boundary layer, by the elimination of u_a/u_e to give:

$$[(C_{1_a} + A)/(C_{1_w} + A)]^{\omega_1} [(C_{1_a} + B)/(C_{1_w} + B)]^{\omega_2} \times [(1 - C_{1_a})/(1 - C_{1_w})]^{\omega_3} - (1 + \zeta) \times [(1 - C_{1a})/(1 - C_{1_e})]^{1/Sc_t} = 0 \quad (4)$$

This equation relates the concentration at the interface to the concentration at the wall and at the edge of the boundary layer. Its solution is shown in Fig. 1 for constant values of the parameter ζ when $Sc_t = 1$ (the value usually assumed) and when $Sc_t = Sc_a$. It is noted that the assumption of a turbulent Schmidt Number of unity throughout the analysis results in a double-valued curve when $\zeta > 1$.

It can be shown[1] that this inconsistency can be eliminated by either of two methods: (1) the value of the turbulent Schmidt Number may be maintained at a fixed constant outside the range of variation of the laminar Schmidt Number. (For a helium-air mixture, the laminar Schmidt Number varies between 0.22 and 1.68[2]). Or, what is more logical, (2) continuity of the Schmidt Number at the interface can be imposed.

References

[1] Ness, N., *An Improved Reynolds Analogy for a Binary Mixture-Turbulent Boundary Layer*, Aerophysics Laboratory Operation TM 94, MSV Dept., General Electric Company, October 16, 1958.

[2] Carlson, W. O., *Engineering Relationships for Binary Gas Mixture Transport Properties*, Aerophysics Laboratory Operation TM 64, MSV Dept., General Electric Company, December 9, 1957.

A Comparison of Several Approximate Theories of Melting Ablation

George W. Sutton

Missile and Space Vehicle Department, General Electric Company, Philadelphia, Pa.

January 21, 1959

Symbols

- c_p = specific heat of liquid
- K = thermal conductivity of liquid
- T = temperature
- y = coordinate normal to surface
- ρ = density
- $\mu(T)$ = viscosity of liquid
- η = efficiency
- β = inviscid velocity gradient at stagnation point
- τ = shear stress

Table 1
Properties of Glass

K	$= 3.42 \times 10^{-3}$ B.t.u./ft. sec. °F.
c_p	= 0.29 B.t.u./lb. °F.
ρ	= 131 lb./ft.^{3}
μ	$= 0.0672 \exp(8{,}720/T)^{1.612}$

Table 2
Boundary Conditions

T_i	= 4,000°F. $= T^*$
T_∞	= 0°F.
v_i	$= 0$, $u_\infty = 0$
τ	$= 5 \times 10^{-5} x\,[2\mu_i\rho_l\beta^2]^{1/2}$
ρ_e/ρ_l	$= 9.5 \times 10^{-6}$

Subscripts

- i = interface between gaseous boundary layer and liquid
- l = liquid
- ∞ = $y \to \infty$
- e = edge of gaseous boundary layer

Because the similarity analysis for melting ablation[1, 2] requires numerical integration, several approximate theories have been developed[3–6] which are applicable to viscous melts of large Prandtl Number, where the convective terms in the streamwise momentum equation, and streamwise temperature gradients may be neglected. (Near a stagnation point, it has been rigorously demonstrated that the convective terms are negligible for a liquid having high viscosity.[7])

In this note, numerical results obtained from these approximate theories are compared to the results obtained from similarity solutions at an axially symmetric stagnation point, where the similarity solution is exact, for a glass with the properties listed in Table 1. This glass has no definite melting point, hence neither the Lees[3] nor the Roberts[6] analysis strictly applies. In all cases, the same interface temperature, shear stress, and pressure gradient was chosen (see Table 2). The heat flux, $K(\partial T/\partial y)_i$, required to cause the gas-liquid interface temperature to be 4,000°F.; the melting rate, v_∞; and the efficiency of the condensed phase, given by:

$$\eta = K(\partial T/\partial y)_i/[\rho_l c_p v_\infty (T_i - T_\infty)] \quad (1)$$

are compared between all theories. A value of η less than unity indicates that some of the melt is swept downstream before reaching T_i.

Theories Which Neglect Pressure Gradients

To perform the calculations for the Lees and Roberts theories, a melting temperature of 3,127°F. was chosen because this causes the material efficiency, as calculated from Lees' theory, to agree with that obtained from the similarity solution. The results are shown in Table 3. It is seen that the agreement between Lees' and Roberts' methods is excellent, which is probably due to the resemblance between the two methods. In Table 3 are also shown the results of numerical integration of the similarity equations, neglecting pressure gradient, which indicate that these approximate theories result in melting rates which are about 25 per cent too high for the same gas-liquid interface temperature.

Table 3
Solutions with $\rho_e = 0$

	Melting rate, $-10^4 \dfrac{v_\infty}{[2\mu_i\beta/\rho_l]^{1/2}}$	Heating rate, $-10^2 \dfrac{K(\partial T/\partial y)_i}{KT^*[2\rho_l\beta/\mu_i]^{1/2}}$	Efficiency, η
Lees	3.539	6.170	0.9127
Roberts	3.555	6.269	0.9233
Bethe & Adams	3.500	6.685	1.0000
Carrier	3.493	4.990	0.7479
Similarity	2.871	5.005	0.9127

TABLE 4
Solutions with $\rho_e/\rho_l = 9.5 \times 10^{-5}$

	Melting rate, $-10^4 \frac{v_\infty}{[2\mu_i\beta/\rho_l]^{1/2}}$	Heating rate, $-10^2 \frac{K(\partial T/\partial y)_i}{KT_i^*[2\rho_l\beta/\mu_i]^{1/2}}$	Efficiency, η
Bethe & Adams	5.600	10.696	1.0000
Carrier	5.043	7.875	0.8176
Similarity	4.475	7.567	0.8853
Lew & Fanucci	3.916	6.720	0.8984

THEORIES WHICH INCLUDE PRESSURE GRADIENTS

Instead of assuming the velocity profile,[3,5] Bethe and Adams[4] assumed that the temperature profile is exponential, and then integrated the momentum equation in an approximate manner. However, they chose a material efficiency, η, equal to unity. Carrier[5] has improved their analysis by a repeated integration of the energy equation. Both of these theories are compared to the results of a similarity analysis in Table 4. Melting and heating rates in the absence of pressure gradient, as calculated from these two theories, are shown in Table 3. The agreement with the similarity analysis is poorer than when pressure gradient is included.

Roberts[6] also presented an integral technique. No calculations were performed using this method, but Lew and Fanucci[8] have independently developed a more general integral technique which agrees well with the similar solution.

DISCUSSION

For the material chosen and the same interface temperature, all approximate theories yield heating and melting rates which are too large, although Carrier's analysis appears to be the most accurate. For a material which only melts, these errors are not significant. In practice,[2] usually $K(\partial T/\partial y_i)$ is given, and one calculates T_i, in which case all approximate theories yield values of T_i which are too small. This error is significant only if $T_e \sim T_i$, since $K(\partial T/\partial y)_i \backsim T_e - T_i$; or when calculating the amount of melt which vaporizes, since the vaporization rate is a very strong function of T_i.

REFERENCES

[1] Sutton, G. W., *The Hydrodynamics and Heat Conduction of a Melting Surface*, Journal of the Aeronautical Sciences, Vol. 25, No. 1, pp. 29–32, January, 1958.

[2] Scala, S. M., and Sutton, G. W., *The Two-Phase Laminar Boundary Layer —A Study of Surface Melting*, Proc. of the 1958 Heat Transfer and Fluid Mechanics Institute, pp. 231–240; Standford University Press, Calif., 1958.

[3] Lees, L., *Similarity Parameters for Surface Melting of a Blunt-Nosed Body in a High Velocity Gas Stream*, presented at the Fluid Mechanics Div. Mtg. of the Amer. Phys. Soc., November, 24, 1958, San Diego, Calif..

[4] Bethe, H. H., and Adams, M. C., *A Theory for the Ablation of Glassy Materials*, AVCO Research Laboratory Research Report No. 38, November, 1958. See also this issue, p. 321.

[5] Carrier, G., *Aerodynamic Heat Transfer to a Melting Body*, Space Technology Laboratories Report No. GM-TM-0165-00268, August, 1958.

[6] Roberts, L., *On the Melting of a Semi-Infinite Body of Ice Placed in a Hot Stream of Air*, J. Fluid Mech., Vol. 4, Part 5, pp. 505–528, September, 1958.

[7] Tellep, D., personal communication.

[8] Lew, H. G., and Fanucci, J., *Ablation of Melting Surfaces*, to be published.

The Elastic-Plastic Bending of an Eccentrically Loaded Sandwich Column

William E. Boyce
Assistant Professor of Mathematics, Rensselaer Polytechnic Institute, Troy, N.Y.

February 9, 1959

AN EARLIER PAPER[1] dealt with the plastic behavior of a straight sandwich column loaded by eccentric forces parallel to the axis of the column. In order to isolate the nonconservative aspects of the problem, the column was assumed to be made of a rigid plastic material exhibiting linear strain-hardening. The present note extends the analysis to include elastic effects, and assesses their importance.

Consider a uniform, simply supported sandwich column of length $2l$. The states of stress and strain can be described by the stresses σ_u, σ_e and the strains ϵ_u, ϵ_e in the upper and lower flanges; they are related by the equations

$$\dot{\sigma}_u = E\dot{\epsilon}_u, \quad \dot{\sigma}_e = E\dot{\epsilon}_e \tag{1}$$

in the elastic range, and

$$\dot{\sigma}_u = C\dot{\epsilon}_u, \quad \dot{\sigma}_e = C\dot{\epsilon}_e \tag{2}$$

in the plastic range. Here E and C are the elastic and plastic moduli, respectively, and dots indicate time derivatives. Integration for compressive loads leads to

$$\sigma_u = E\epsilon_u, \quad \sigma_e = E\epsilon_e \tag{3}$$

in the elastic range; and, as long as no element unloads,

$$\sigma_u + \sigma_0 = C\epsilon_u + (C/E)\sigma_0, \quad \sigma_e + \sigma_0 = C\epsilon_e + (C/E)\sigma_0 \tag{4}$$

in the plastic range. Alternatively, the stress state can be represented by the bending moment M and the axial force N;

$$M = TDH(\sigma_e - \sigma_u), \quad N = TD(\sigma_e + \sigma_u) \tag{5}$$

where T and D are, respectively, the thickness and width of the flanges, and H their distance from the centerline. Similarly, the extension ϵ and curvature κ of the centerline are given by

$$\epsilon = (\epsilon_e + \epsilon_u)/2, \quad \kappa = (\epsilon_e - \epsilon_u)/2H \tag{6}$$

Let the column be loaded by compressive forces of magnitude P, parallel to the axis of the column, a distance e from it, and applied nearer the upper flange. Then, if W denotes the transverse displacement, positive downwards, equilibrium considerations imply that at every point of the column,

$$M = P(e + W), \quad N = -P \tag{7}$$

It follows from Eqs. (5) and (7) that

$$\left.\begin{aligned} \sigma_u &= -(P/2TD)\,[1 + (e/H) + (W/H)] \\ \sigma_e &= -(P/2TD)\,[1 - (e/H) - (W/H)] \end{aligned}\right\} \tag{8}$$

Finally, κ is given by

$$\kappa = -(\partial^2 W/\partial x^2) \tag{9}$$

For small values of P, both flanges remain elastic. However, at a load P_1, a plastic zone will form at the center of the upper flange. Later, plastic zones will also form in the lower flange, beginning at the ends, since the bending displacement tends to reduce the compressive stress elsewhere in the lower flange. These plastic zones will spread as P increases until, eventually, if the eccentricity e is small, both flanges become entirely plastic at a load P_2. If loading is continued, the displacement will ultimately become so large (say, at a load P_3) that stress reversal takes place in the lower flange—i.e., the applied load tends to stretch this flange, rather than to compress it, as before. While in principle the analysis could be continued, the occurrence of stress reversal is frequently a convenient indication that the column has reached its limit of serviceability. On the other hand, for larger eccentricities the column may experience stress reversal before becoming fully plastic.

Further investigation shows that, for $e/H \ll 1$, the loads P_1 and P_2 are close together. Hence, almost the complete load displacement curve can be obtained by a combination of fully elastic and fully plastic analyses, which are relatively simple to carry out. The much more difficult elastic-plastic analysis furnishes little additional information.

When the column is entirely elastic, Eq. (3) may be substituted into Eqs. (5), giving

$$M/H = TDE(\epsilon_e - \epsilon_u) = 2TDHE\kappa = -2TDHE(\partial^2 W/\partial x^2) \tag{10}$$

The first equilibrium equation then leads to

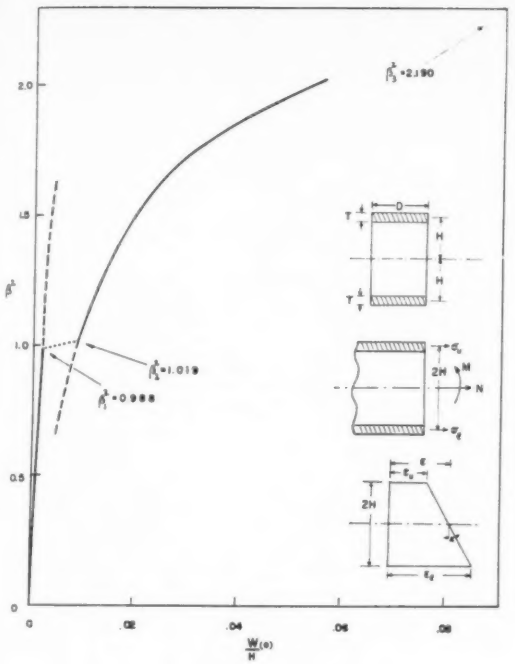

FIG. 1.

$$(W/H)'' + (C/E)\beta^2(W/H) = -(C/E)\beta^2 e/H \qquad (11)$$

where primes denote differentiation with respect to x/l, and

$$\beta^2 = Pl^2/2CTDH^2 \qquad (12)$$

The solution of Eq. (11), subject to the boundary conditions

$$W(\pm l) = 0 \qquad (13)$$

is $$W/H = (e/H)\left\{[\cos\sqrt{C/E}\,\beta(x/l)/\cos\sqrt{C/E}\,\beta] - 1\right\} \qquad (14)$$

The load β_1 marking the end of the elastic regime is determined by setting $\sigma_u = -\sigma_0$ at $x = 0$. This gives

$$(\alpha - \beta_1^2)\cos\sqrt{C/E}\,\beta_1 - (e/H)\beta_1^2 = 0 \qquad (15)$$

where $\alpha = \sigma_0 l^2/CH^2$.

Later, when the column is entirely plastic, Eqs. (4) may be substituted into Eqs. (5), and thence into Eqs. (7), so that

$$(W/H)'' + \beta^2(W/H) = -\beta^2(e/H) \qquad (16)$$

is the differential equation defining W/H in the plastic range. The solution, again subject to Eq. (13), is

$$W/H = (e/H)\left\{[\cos\beta(x/l)/\cos\beta] - 1\right\} \qquad (17)$$

The load β_2 signaling the beginning of fully plastic flow satisfies

$$(\beta_2^2 - \alpha)\cos\beta_2 - (e/H)\beta_2^2 = 0 \qquad (18)$$

which results from setting $\sigma_e = -\sigma_0$ at $x = 0$ (the last point of the lower flange to become plastic), and substituting W/H from Eq. (17) into Eq. (8). Finally, the load β_3 producing stress reversal at the center of the lower flange is found by setting $d\sigma_c/d\beta = 0$ there, or

$$\cos\beta_3 - (e/H)\left[1 + (1/2)\beta_3\tan\beta_3\right] = 0 \qquad (19)$$

It is noteworthy that Eqs. (16)–(19) are independent of E, and only Eq. (18) involves α. Hence, the load at which a column becomes fully plastic is independent of its elastic properties, and the later behavior of the column is independent of the yield stress as well. This observation justifies the reverse reasoning by which the fully plastic displacement function was used to find the load at which fully plastic flow starts.

Passing to the limit as $e/H \to 0$, it is evident from Eq. (17) that instability occurs when $\beta = \pi/2$; this is the tangent modulus load of the classical theory.

Fig. 1 contains a plot of load versus maximum displacement. The solid curves are computed from Eqs. (14) and (17) with β_1, β_2, and β_3 calculated from Eqs. (15), (18), and (19), using $e/H = 0.01$, $\alpha = 1$, and $C/E = 1/3$. The dashed extensions indicate the nature of the load displacement curves beyond the range required for the given values of the parameters. The dotted curve represents the elastic-plastic regime for the given column, and its exact determination would require a lengthy analysis, involving the matching of separate elastic and plastic solutions in each flange across moving internal boundaries. Since for a given column the load displacement curve must always be monotone increasing and continuous on physical grounds, and since the end points of the elastic-plastic portion have already been found, it seems superfluous to carry out the complete elastic-plastic analysis as long as this regime is of short duration.

REFERENCE

[1] Boyce, William E., *The Plastic Bending of an Eccentrically Loaded Column*, Journal of the Aeronautical Sciences, Vol. 24, No. 5, pp. 332–338, 367, May, 1957.

The Effect of Helium Injection at an Axially Symmetric Stagnation Point

H. Hoshizaki and H. J. Smith
Missile and Space Division, Lockheed Aircraft Corporation, Sunnyvale, Calif.

January 30, 1959

SYMBOLS

C = constant
C_{p_i} = foreign gas specific heat
$f(0)$ = injection rate parameter = $-(\dot{m}_i/2\sqrt{\beta\rho_e\mu_e})$
$\dot{m}_i$ = injection mass rate
p = pressure
$\dot{q}$ = net heat transfer rate
$\dot{q}_0$ = zero mass injection heat-transfer rate
$\dot{q}_c$ = conductive heat-transfer rate
T = temperature
u = velocity
W = foreign gas mass concentration
β = velocity gradient at edge of boundary layer = du_e/dx
η = Blasius similarity variable = $y\sqrt{\beta/\nu_e}$

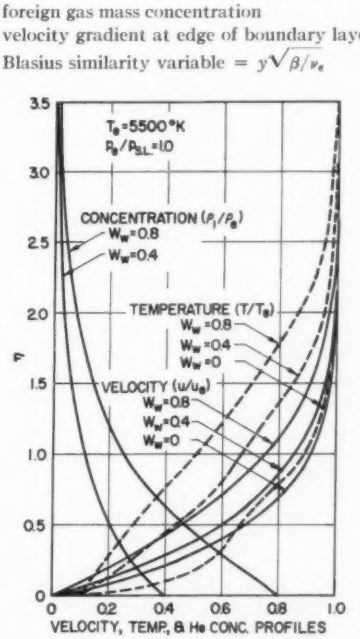

FIG. 1. Boundary-layer profiles.

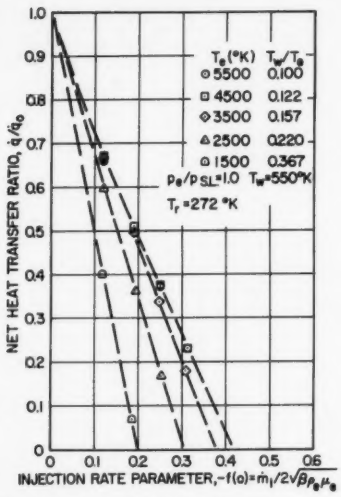

FIG. 2. Reduction of net heat-transfer rate due to helium injection.

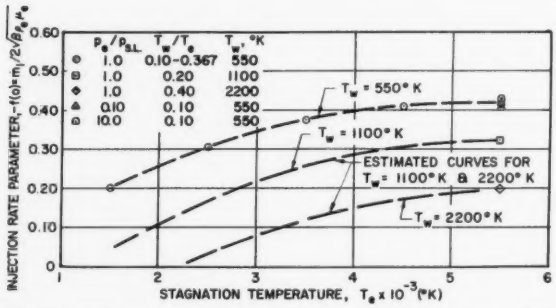
INJECTION RATE PARAMETER, $-f(0)=\dot{m}_1/2\sqrt{\beta\rho_e\mu_e}$
STAGNATION TEMPERATURE, $T_e \times 10^{-3}$(°K)
p_e/p_{SL} T_w/T_e T_w, °K
1.0 0.10-0.367 550
1.0 0.20 1100
1.0 0.40 2200
0.10 0.10 550
10.0 0.10 550
T_w = 550° K
T_w = 1100° K
ESTIMATED CURVES FOR T_w = 1100° K & 2200° K
T_w = 2200° K

FIG. 3. Helium injection rate necessary to maintain a specified wall temperature.

ρ = mixture density
ρ_1 = helium density
μ = mixture dynamic viscosity
ν = mixture kinematic viscosity

Subscripts

e = edge conditions
r = reservoir
s.l. = sea level
w = wall

AN EFFECTIVE MEANS of protecting the surface of a hypersonic re-entry vehicle is to inject small quantities of a lightweight gas into the boundary layer through a porous wall. This process, which is known as mass-transfer cooling, protects the surface in two ways. First of all, as the injected gas or coolant passes from the reservoir through the wall to the surface, a considerable quantity of heat is absorbed as its temperature is raised from the reservoir temperature to the wall surface temperature. Characteristically, lightweight gases have relatively high specific heats.

Secondly, the transfer of mass and enthalpy by convection and diffusion normal to the surface alters the characteristics of the boundary layer in such a manner as to reduce the temperature gradient at the wall, and, hence, the conductive heat transfer at the wall. This is sometimes referred to as the blowing effect.

In reference 1, a detailed analysis has been made of the effect of injecting helium into the boundary layer in the vicinity of an axially symmetric stagnation point. For simplicity, the boundary layer was considered to be a "binary mixture" of helium and dissociated air. The diffusion and recombination of oxygen and nitrogen atoms was neglected although the thermal and transport properties used for air are thermodynamic equilibrium values. The fluid properties of the mixture were computed as functions of temperature and helium concentration from the results of reference 2.

Numerical solutions to the binary mixture boundary-layer equations were obtained by the method of successive approximations. Typical velocity, temperature, and helium concentration profiles are presented in Fig. 1. The concentration of helium at wall, W_w, which is used as a parameter in Fig. 1, is related to the injection rate parameter $f(0)$. By imposing the physical restriction that the air mass rate at the wall vanishes, it can be shown that

$$f(0) = CW_w/2(1 - W_w) \tag{1}$$

The reduction in the net heat-transfer rate due to mass injection is shown in Fig. 2. The net heat-transfer rate can be shown to be equal to the difference between the conductive heat rate and the rate at which the coolant "enthalpy rise" is transported away.

$$\dot{q} = \dot{q}_c - \dot{m}_1 c_{p_1}(T_w - T_r) \tag{2}$$

Note that substantial reductions in net heat-transfer rates are possible with moderate mass injection rates. As an example, under peak heating conditions for typical satellite re-entry, $-f(0) = 0.30$ corresponds approximately to a mass injection rate of a few hundredths of a lb./sec. ft.[2]

In order to maintain a constant wall temperature, the net heat transfer to the wall must, of course, be zero. Hence, the injection rates necessary to maintain a specific wall temperature are given by the points where the net heat-transfer curves intercept the abscissa. These equilibrium values of the injection rate parameter are presented in Fig. 3 along with some additional data. Once the body shape and trajectory are known, the helium injection rate necessary to maintain a given wall temperature can be obtained from Fig. 3.

REFERENCES

[1] Hoshizaki, H., and Smith, H. J., *Axi-Symmetric Stagnation Point Mass-Transfer Cooling*, LMSD 48379, December 17, 1958.

[2] Carlson, W. O., and Schneider, P. J., *Transport Properties for Binary Gas Mixtures*, University of Minnesota, A. F. Tech. Rept., No 7, Minneapolis, Minn., January, 1956.

Change of Address

Since the Post Office Department does not as a rule forward magazines to forwarding addresses, it is important that the Institute be notified of changes in address 30 days in advance of publishing date to ensure receipt of every issue of the JOURNAL and AERO/SPACE ENGINEERING.

Notices should be printed legibly and sent directly to:

Subscription Department
Institute of the Aeronautical Sciences, Inc.
2 East 64th Street, New York 21, N.Y.

REQUIREMENTS *for* CONTRIBUTIONS
to the publications of the
INSTITUTE *of the* AERONAUTICAL SCIENCES

The Institute of the Aeronautical Sciences invites both members and nonmembers from any country to submit papers for publication in the JOURNAL OF THE AERO/SPACE SCIENCES and AERO/SPACE ENGINEERING. The Institute, following the practice of other societies, does not pay for contributions.

The following directions for the preparation of papers, if followed by authors, will save correspondence, avoid the return of papers for changes, minimize the work of preparation for the printer, and save the expense due to the charges made for "author's corrections."

MANUSCRIPTS: The original typewritten copy of the paper is desired. **To expedite review, an additional copy of both the manuscript and figures should be submitted.** The manuscript must be double or triple spaced on one side of white paper sheets, consecutively numbered. There should be wide margins to allow for the marking of directions to the printer. Correcting, changing, or adding to papers after they are in type is costly. It is, therefore, imperative that papers submitted be in final form. Typographical errors may be corrected on proofs, but if authors wish to add material, they may do so at their own expense. In mailing, drawings may be rolled, but manuscripts should be sent flat. Send by first-class mail (register if you wish for your own protection) to the Editorial Office, Institute of the Aeronautical Sciences, 2 East 64th Street, New York 21, N.Y. All manuscripts will be examined by the Editorial Committee and by the Editor. Authors will be advised as promptly as possible whether the paper is acceptable for publication.

TITLES: The title of the paper should be brief. The name and initials of the author should be written as he prefers. The use of the full name of an author is advocated because of the frequent duplication of initials and surnames which sometimes makes it difficult to establish the identity of the author. This is particularly important for large annual indexing and abstracting services. All titles and degrees or honors are omitted. The name of the organization with which the author is associated should be placed after his name on a separate line. The date on which the paper is received will be inserted by the Editor. The author's title or position should be indicated in a footnote.

SUMMARIES OR ABSTRACTS: An abstract to be printed at the beginning should accompany each article. It should be adequate as an *index* and as a *summary*. It should contain a statement of major conclusions reached, since summaries in many cases constitute the only source of information used in compiling scientific reference indexes. Abstracts printed in other journals, especially foreign, in most cases consist of summaries from printed papers. The summary should explain as adequately as possible the major conclusions to a nonspecialist in the subject and should contain from 100 to 300 words, depending on the length of the paper.

SUBHEADINGS: Subheadings should be inserted by the author at frequent intervals. The work of editorial preparation will be simplified by the author's provision of many subheadings.

MATTER USUALLY DELETED: Photographs or illustrations of little technical interest and not showing advances in general practice. Too detailed tabular matter (general results of such tables may be included in the text). Lengthy descriptions of materials or processes or of preliminary experiments or theories that preceded final results; salient features only are of interest.

REFERENCES: References should be numbered consecutively and grouped together at the end of the manuscript, with only the corresponding number being mentioned in the text. The arrangement should be as follows. For books: [1]Durand, W. F., *Aerodynamic Theory*, 1st Ed., Vol. 1, p. 23; Julius Springer, Berlin, 1934. For magazines: [1]England, C. R., Crawford, A. B., and Mumford, W. W., *Some Results of a Study of Ultra-Short-Wave Transmission Phenomenon*, Proc. IRE, Vol. 20, No. 12, pp. 481–482, March, 1933. Please give author, title, edition, volume, number, page, publisher, and place and date of publication as indicated. Omission of one required fact causes much extra editorial work and possible inaccuracies.

ILLUSTRATIONS: Illustrations should accompany manuscripts, and each should always be referred to in the text by number. Drawings or graphs should not be larger than 12 × 16 inches, and must be made with jet black India ink on white paper or tracing cloth, the latter being preferred. *Do not use typewriter for lettering.* The smallest lettering on 8 × 10 inch figures should be no less than $^1/_4$ inch high. Cross-section paper (white with black lines) may be used, but it should not have more than 4 lines per inch. If finer ruled paper is used, the major division lines should be drawn in with black ink, omitting the finer divisions. In the case of finely ruled paper, only blue-lined paper can be accepted. *Tracing paper and blueprints* are not acceptable. Lettering and all markings must be large enough to be readable after reduction to single-column width ($3^5/_{16}$ in.). Mail rolled or flat; never fold. Drawings that cannot be reproduced (including pencil drawings) will be returned to the author for redrawing, thus delaying publication of the paper. Photographs should be distinct and show clear black and white contrasts. They must be on glossy white paper. Avoid round and oval photographs.

CAPTIONS AND LEGENDS: Legends or captions must accompany each drawing or photograph submitted. If written on the drawing or photograph, they should be placed below and well outside the part to be reproduced. Each table should have a caption such as Table 1, Table 2, Table 3, etc. Captions should be complete in themselves so as to make the data intelligible to the reader without reference to the text. A duplicate list of captions for figures should be included as the last page of the manuscript. Use "Fig. 1" (not Figure 1), "Figs. 3 and 4," etc., in both the text and the numbering of illustrations. In the text, "Eq. (1)" or "Eqs. (1) and (2)" is used, not "Equation (1)." In captions, legends, and in table headings, write all words in full; do not abbreviate, except for "Fig." and "Eq."

MATHEMATICAL WORK: Formulas may be typewritten or carefully written in pen and ink, the writing to be large enough so that it can be marked for the printer. Considerable space for marking should be allowed above and below all equations. All complicated equations should be repeated on separate sheets with plenty of space left for marking. The solidus should be used for simple fractions appearing within the text. Make all expressions clear to the typesetter. Greek letters used in formulas should be clearly designated by name in the margin of the manuscript. The difference between capital and lower-case letters should be clearly distinguished and care taken to avoid cohfusion between zero (0) and the letter (o), between the numeral (one), and the letter (ell) and the prime (′), between alpha and a, kappa and k, u and mu, v and nu, n and eta. All subscripts and exponents should be clearly distinguished. Avoid complicated exponents and subscripts. Dots and bars over letters or mathematical expressions should also be avoided. When it is necessary to repeat a complicated expression, it should be represented by some convenient symbol.

SYMBOLS AND ABBREVIATIONS: The symbols recommended in the American Standard Association "Letter Symbols for Aeronautical Sciences," ASA Y10.7—1954, should be used wherever practicable. All symbols should be clearly written and carefully checked. Standard abbreviations should be used, and it should be noted that most abbreviations are lower case, such as m.p.h., b.m.e.p., i.h.p., b.hp., hp., etc.

CORPORATE MEMBERS

OF THE

INSTITUTE OF THE AERONAUTICAL SCIENCES

AC SPARK PLUG DIVISION, GENERAL MOTORS CORPORATION
ACADEMY OF AERONAUTICS
ADAMS RITE MANUFACTURING COMPANY
AEROJET-GENERAL CORPORATION
AEROLAB DEVELOPMENT COMPANY
AERONCA MANUFACTURING CORPORATION
AERONUTRONIC SYSTEMS, INC.
AEROQUIP CORPORATION
AGAWAM AIRCRAFT PRODUCTS, INC.
ALLIED RESEARCH ASSOCIATES, INC.
ALLISON DIVISION, GENERAL MOTORS CORPORATION
ALUMINUM COMPANY OF AMERICA
AMERICAN AIRLINES, INC.
AMERICAN BOSCH ARMA CORPORATION
AMERICAN NON-GRAN BRONZE COMPANY
AMERICAN STEEL & WIRE DIVISION, UNITED STATES STEEL CORPORATION
AMOCO CHEMICALS CORPORATION
AMPHENOL-BORG ELECTRONICS CORPORATION
ANDERSON, GREENWOOD & CO.
ARDE ASSOCIATES
ASSOCIATED AVIATION UNDERWRITERS
AVCO RESEARCH LABORATORY
AVIEN, INC.
AVRO AIRCRAFT LIMITED
BAKER STEEL & TUBE COMPANY
BEECH AIRCRAFT CORPORATION
BELL AIRCRAFT CORPORATION
BENDIX AVIATION CORPORATION
BOEING AIRPLANE COMPANY
BOOZ, ALLEN & HAMILTON
THE BRISTOL AEROPLANE COMPANY (U.S.A.) INC.
BULOVA RESEARCH AND DEVELOPMENT LABORATORIES, INC.
CANADAIR, LTD.
THE CESSNA AIRCRAFT COMPANY
CHANCE VOUGHT AIRCRAFT, INCORPORATED
THE CHASE MANHATTAN BANK
CHICAGO AERIAL INDUSTRIES, INC.
THE CLEVELAND PNEUMATIC INDUSTRIES, INC.
CONSOLIDATED CONTROLS CORPORATION
CONTINENTAL MOTORS CORPORATION
CORNELL AERONAUTICAL LABORATORY, INC.
CURTISS-WRIGHT CORPORATION
DANIEL, MANN, JOHNSON, & MENDENHALL
THE DECKER CORPORATION
DEL MAR ENGINEERING LABORATORIES
DELCO-REMY DIVISION, GENERAL MOTORS CORPORATION
DOAK AIRCRAFT COMPANY, INC.
DOUGLAS AIRCRAFT COMPANY, INC.
DZUS FASTENER COMPANY, INC.
EASTERN AIR LINES, INC.
EATON MANUFACTURING COMPANY
EDO CORPORATION
ELASTIC STOP NUT CORPORATION OF AMERICA
ELECTROL INCORPORATED
ENGINEERING SUPERVISION COMPANY
ESSO STANDARD OIL COMPANY
FAIRCHILD CAMERA AND INSTRUMENT CORPORATION
FAIRCHILD ENGINE AND AIRPLANE CORPORATION
THE FIRESTONE TIRE & RUBBER COMPANY
THE GARRETT CORPORATION
GENERAL DYNAMICS CORPORATION
GENERAL ELECTRIC COMPANY
GENERAL PRECISION EQUIPMENT CORPORATION
G. M. GIANNINI & CO., INC.
GIANNINI PLASMADYNE CORPORATION
THE B. F. GOODRICH COMPANY
GOODYEAR AIRCRAFT CORPORATION
GRUMMAN AIRCRAFT ENGINEERING CORPORATION
HYDRO-AIRE, INC.
INSURANCE COMPANY OF NORTH AMERICA COMPANIES
INTERNATIONAL BUSINESS MACHINES CORPORATION
THE INTERNATIONAL NICKEL COMPANY, INC.
ITT LABORATORIES, DIVISION OF INTERNATIONAL TELEPHONE AND TELEGRAPH CORPORATION
JANITROL AIRCRAFT DIVISION, SURFACE COMBUSTION CORPORATION
JOHNS-MANVILLE SALES CORPORATION
EARLE M. JORGENSEN CO.
WALTER KIDDE & COMPANY, INC.
KOLLSMAN INSTRUMENT CORPORATION
LAVELLE AIRCRAFT CORPORATION
LEAR, INCORPORATED
C. W. LEMMERMAN, INC.
LIBRASCOPE, INCORPORATED
THE LIQUIDOMETER CORPORATION
LOCKHEED AIRCRAFT CORPORATION
LOEWY-HYDROPRESS DIVISION OF BALDWIN-LIMA-HAMILTON CORPORATION
LONGINES-WITTNAUER WATCH COMPANY, INC.
MARQUARDT AIRCRAFT COMPANY
THE MARTIN COMPANY
MARTIN STEEL PRODUCTS CORPORATION
McDONNELL AIRCRAFT CORPORATION
MELETRON CORPORATION
MID-CONTINENT MANUFACTURING, INC.
MINNEAPOLIS-HONEYWELL REGULATOR COMPANY
NATIONAL CREDIT OFFICE, INC.
NORTH AMERICAN AVIATION, INC.
NORTHROP CORPORATION
NUCLEAR DEVELOPMENT CORPORATION OF AMERICA
PAN AMERICAN WORLD AIRWAYS, INC.
THE RALPH M. PARSONS COMPANY
PESCO PRODUCTS DIVISION, BORG-WARNER CORPORATION
PHILLIPS PETROLEUM COMPANY
PIASECKI AIRCRAFT CORPORATION
RADIO CORPORATION OF AMERICA DEFENSE ELECTRONIC PRODUCTS
REPUBLIC AVIATION CORPORATION
ROHR AIRCRAFT CORPORATION
PAUL ROSENBERG ASSOCIATES
RYAN AERONAUTICAL COMPANY
SANDBERG-SERRELL CORPORATION
SHAFER BEARING DIVISION, CHAIN BELT COMPANY
SHELL OIL COMPANY
SIMMONDS AEROCESSORIES, INC.
SOCONY MOBIL OIL COMPANY, INC.
SOLAR AIRCRAFT COMPANY
SOUTHWEST PRODUCTS CO.
SPACE TECHNOLOGY LABORATORIES, INC.
R. DIXON SPEAS ASSOCIATES
SPERRY GYROSCOPE COMPANY DIVISION OF SPERRY RAND CORPORATION
STANDARD OIL COMPANY OF CALIFORNIA
STANDARD OIL COMPANY (INDIANA)
STANDARD-THOMSON CORPORATION CLIFFORD MANUFACTURING DIVISION
STANLEY AVIATION CORPORATION
THIOKOL CHEMICAL CORPORATION
THOMPSON RAMO WOOLDRIDGE INC.
TRANS WORLD AIRLINES, INC.
TURBO PRODUCTS, INC.
UNION CARBIDE CORPORATION
UNITED AIR LINES, INC.
UNITED AIRCRAFT CORPORATION
UNITED STATES AVIATION UNDERWRITERS, INC.
VARD, INC.
VERTOL AIRCRAFT CORPORATION
VITRO CORPORATION OF AMERICA
WESTERN GEAR CORPORATION
WESTINGHOUSE ELECTRIC CORPORATION
WESTON INSTRUMENTS DIVISION OF DAYSTROM, INC.
WYMAN-GORDON COMPANY
YOUNG RADIATOR COMPANY